A Computational Investigation of the Mechanism of CB1954 Reduction by *E.coli* Nitroreductase

By

Andrew Joseph Christofferson

UNIVERSITY OF BIRMINGHAM

A thesis submitted to
The University of Birmingham
For the degree of
DOCTOR OF PHILOSOPHY

School of Chemistry
The University of Birmingham
November 2009

Abstract

The flavoenzyme NTR (nitroreductase nfsB from *Escherichia coli*) and the prodrug CB1954 (5-[aziridin-1-yl]-2,4-dinitrobenzamide) have been found to be a good potential combination for virus-directed enzyme prodrug therapy (VDEPT). However, wild-type NTR has poor kinetics and binding with CB1954, and the mechanism for the reduction of CB1954 by NTR is poorly understood.

The aim of this work has been to investigate, using quantum mechanical computational methods, the potential underlying reaction mechanisms so as to identify the order of electron and proton transfers, and source of the protons, that make up the initial reduction step. Additionally, molecular mechanics and molecular dynamics have been used to examine the nature of the active site of the wild-type enzyme, as well as several mutants, and determine possible binding modes of the substrate. Finally, ONIOM calculations were utilised to examine substrate orientations and electronic states at a quantum mechanical level with key active site amino acids present at a molecular mechanics level.

Calculations with the MPW1PW91 density functional and 6-31G** basis set yielded a single gas phase transition state geometry for the hydride transfer from the FMN (flavin mononucleotide) cofactor of NTR to a nitro group of CB1954. Additionally, three reaction profiles were generated which suggest that in the gas phase, the reduction proceeds by electron transfer from FMN, proton transfer , then second proton transfer and electron transfer concerted with N-O bond breaking, regardless of the source (FMN or solution) or order of the protons.

Molecular mechanics calculations with the FF03 force field found a binding mode with the amide group of CB1954 bound in the active site of NTR—an orientation ideally suited for an electron transfer mechanism.

Acknowledgements

For starters, I would like to thank my supervisor, Dr. John Wilkie. I know it's obligatory to thank your supervisor, but I truly am grateful to him for giving me the opportunity to work on this project, as well as all the support, advice, and encouragement he's given me throughout my time here in England.

I would also like to thank our collaborators Dr. Eva Hyde, Dr. Peter Searle, and Dr. Scott White, and their respective research groups.

I'd like to thank Professor Roy Johnston for sorting out funding for me, as otherwise I wouldn't have been able to come here in the first place.

The friends I've made since I've been here and who have helped me so much along the way are too numerous to mention individually, and I won't even try (for fear of accidentally leaving someone out) but I would particularly like to thank Dr. Damian John Richard Johnson, aka Captain Chair, for his friendship and support. I'd also like to especially thank the members of the Hannon group for putting up with me drinking their coffee every day, and for teaching me Italian. Of course I'd like to thank the other members of my group, the members of Richard Tuckett's group, and certain members of Trevor Rayment's group, who shared my office with me.

Finally, I'd like to thank my friends and family back in America (and elsewhere in the world) who have been so supportive of me during my time here.

So thanks, cheers, gracias, grazie, merci, danka, obrigado, asante sana, etc. to everyone.

Andy

Contents

Chapter 1
Introduction

This chapter introduces the concept of virus-directed enzyme prodrug therapy (VDEPT), and why the enzyme NTR and prodrug CB1954 are a good potential combination for VDEPT.

Additionally, the motivation for a computational approach to the determination of the binding and reaction mechanism for the reduction of CB1954 by NTR is outlined.

1.1 Virus-Directed Enzyme Prodrug Therapy (VDEPT)

Cancer kills approximately 7 million people worldwide each year[1]. To date, a wide variety of methods and approaches to treating cancer have been studied, and although many treatments are highly effective against tumour cells *in vitro*, their use in human patients is limited due to their toxicity.

Virus-Directed Enzyme Prodrug Therapy (VDEPT) is a gene therapy approach to cancer treatment aimed at overcoming this obstacle. In VDEPT, a virus, in this case CTL102, a replication-defective adenovirus[2], is genetically modified to carry the genes for a specific enzyme not found within normal human cells—an expression cassette. When the virus is injected directly into a tumour, the tumour cells are directed to synthesise the enzyme, causing the expression of the enzyme within the cancer cells. The patient is then given an inactive, non-toxic prodrug, which reacts with the enzyme within the cancer cells to produce a cytotoxic compound that kills the cells[2,3]. Advantages of this particular virus are effective gene transfer to a wide variety of cells, independence of cell replication status, and effectiveness with cells resistant to cis-platin and other forms of treatment[3]. Additionally, this particular virus has been shown to have no observable dose-limiting toxicity, and no detectable presence outside the tumour 24 hours after injection[2].

In order for a particular enzyme/prodrug combination to be considered, certain criteria must be met. First, both the enzyme and the prodrug must be non-toxic by themselves, and ideally the activated prodrug should have a short half-life. The activated prodrug should be

able to diffuse into neighbouring cancer cells and destroy them, even if they were not infected by the modified virus. This is known as the bystander effect[2].

It has been found that the prodrug CB1954 (5-(aziridin-1-yl)-2,4-dinitrobenzamide) and the flavoenzyme nitroreductase (NTR) from *E. coli* are a good potential combination for VDEPT[4-7]. This enzyme/prodrug combination has already reached the clinical trial stage[8,9], and while it has clearly demonstrated a certain degree of effectiveness, improvements are desired. Using computation to investigate the catalytic mechanism of NTR and determine possible binding modes of CB1954 will allow us to identify mutations for NTR that may improve the efficiency of the NTR/CB1954 combination.

1.2 CB1954 (5-(aziridin-1-yl)-2,4-dinitrobenzamide)

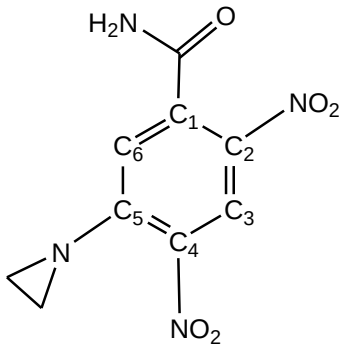

Figure 1.1: 5-(aziridin-1-yl)-2,4-dinitrobenzamide (CB1954).

CB1954 (Figure 1.1) has several qualities that make it an excellent potential prodrug for VDEPT. As a prodrug, it has been found to be non-toxic at therapeutic levels when administered intravenously[2]. This lack of toxicity can largely be attributed to the fact that the prodrug is not easily activated by enzymes normally found in the human body. While it has been found to be activated by rat DT-diaphorase[10,11], it is a poor substrate for the

analogous human DT-diaphorase[12]. Additionally, in its activated form it can diffuse through the cell membrane from virus-infected cells into neighbouring tumour cells, and kill these cells as well, even if the activating enzyme is not present (the bystander effect)[13]. In contrast to other anti-tumour agents, this diffusion is not limited to gap junctions, further increasing its utility[13,14].

The prodrug is activated by an enzyme-initiated reduction of a nitro group to a hydroxylamine. The 4-nitro hydroxylamine derivative then reacts with acetylthioesters naturally found in the cell to form an N-acetoxy derivative[5]. The initial conversion from a strongly electron-withdrawing nitro group to an electron-donating hydroxylamine effectively acts as a 'switch' to convert the relatively harmless prodrug into a strongly cytotoxic compound.

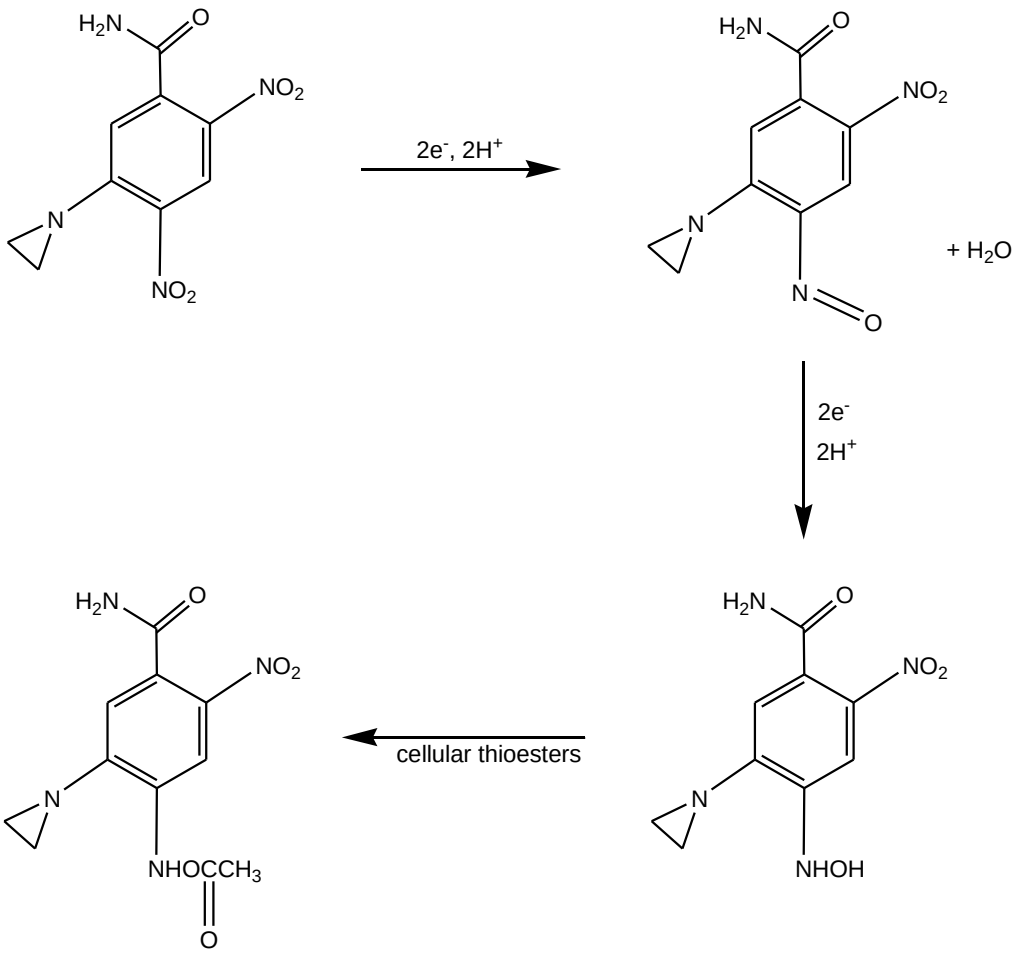

Figure 1.2: Activation of CB1954 via the 4-nitro reduction[6]. The 2-nitro reduction terminates at the hydroxylamine.

This activated compound is highly cytotoxic, and causes DNA-DNA interstrand crosslinks to form within the cancer cells. These crosslinks are poorly repaired, and cause cell death in both dividing and non-dividing cells. While the 4-nitro derivative acts as a bifunctional alkylating agent and is vastly more cytotoxic[6], the 2-nitro derivative has been observed to have a greater bystander effect *in vivo*[15]. An advantage of CB1945 is that cells are killed independently of the cell cycle, whereas with some other potential prodrug candidates only replicating cells are destroyed[3,14].

1.3 Nitroreductase (NTR)

Figure 1.3: *E. coli* nitroreductase NfsB (NTR) from the 1YKI crystal structure[16] (oxidised form, ligand not shown). The protein backbone is shown in green, while the two FMN cofactors are shown in purple.

Wild-type *E. coli* nitroreductase (Figure 1.3), encoded by the *nfs*B gene, was initially identified as a target for antibiotics such as nitrofurazone and nitrofurantoin[16]. Although its actual function within the bacteria has yet to be discovered, it is known to reduce a wide range of nitroaromatics and quinones. Expression of NTR in the bacteria is induced by the MarA protein during oxidative stress, so it may function as a general 2-electron reductant to limit free radical formation.

The enzyme exists as a dimer, with a large dimer interface, and each of the identical subunits contains 217 amino acids and an FMN (flavin mononucleotide) cofactor. NTR has two active sites, each formed at the dimer interface by residues from both subunits. The

protein itself has a relatively rigid structure and primarily acts as a framework for the reaction between FMN and the substrate. In *Enterobacter cloaccae* nitroreductase, an enzyme with 88% sequence homology and similar function, the only difference between the oxidised and reduced states of the enzyme is an increase in the butterfly angle of FMN from 16 to 25 degrees[17].

NTR is referred to as an "oxygen-insensitive" enzyme, because the reduced form does not easily give up one electron to molecular oxygen to form the semiquone radical[18,19]. Thus two-election oxidation and reduction is observed, but one-electron oxidation or reduction is not. This may be due to the nature of the amino acids surrounding FMN and their tendency to not stabilize the semiquinone state of the bound flavin[17].

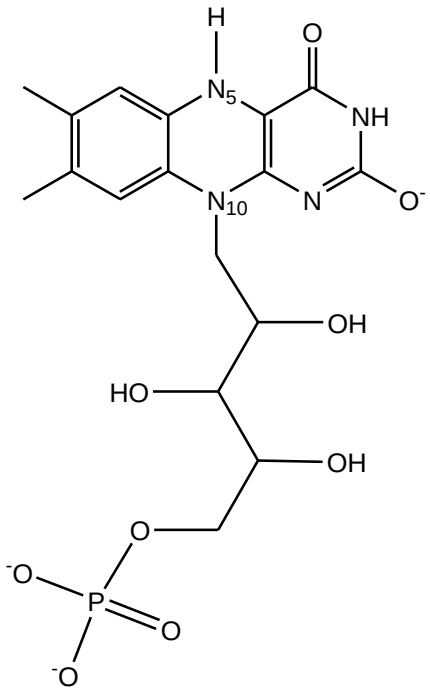

Figure 1.4: The *re* face of the reduced form of FMN.

The FMN cofactor is tightly—but not covalently—bound, with only the *re* face accessible. Several key amino acids are important for FMN binding: Ser12 and Arg10 of one subunit, and Lys205 and Arg207 of the opposite subunit, all interact with the phosphate group, with Ser12 having an additional hydrogen bond to the ribityl tail[20]. Val145 and Tyr144 have hydrophobic interactions with the dimethylbenzoide ring[21]. Lys74 and Gly166 each have one hydrogen bond to FMN, while Lys14, Asn71, and Glu165 all have up to two.

Many, but not all, of these interactions are highly conserved within a family of analogous-function flavoproteins, and may have a key effect on the redox potential of FMN[21].

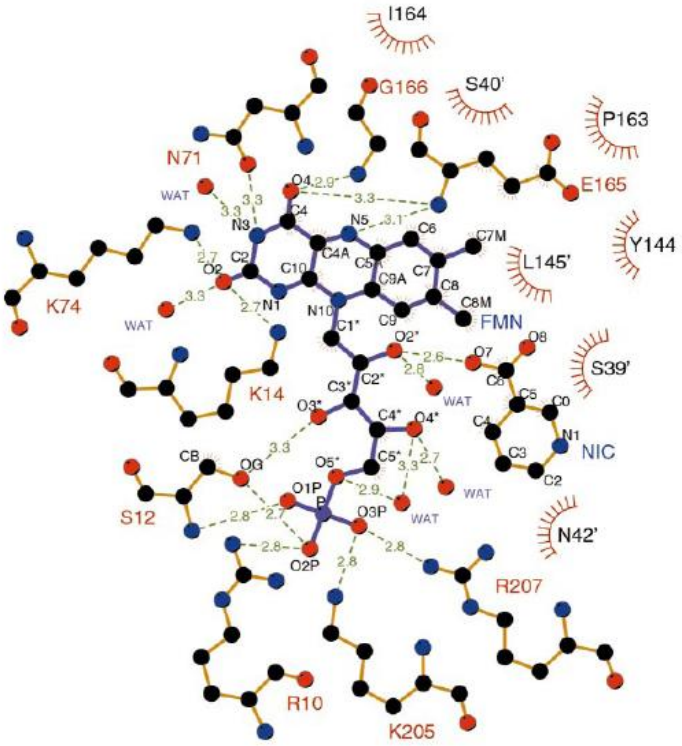

Figure 1.5: The interactions between FMN and the amino acids of the NTR active site, with bound nicotinic acid[20]. NTR is in the oxidised state. Hydrogen bonds are shown in green, and van der Waals interactions in red. Figure taken from Lovering *et al.* (2001) *J. Mol. Biol*, **309**, p208.

A comparison of enzymes within the flavoprotein family that includes NTR can yield some clues as to which residues are important for FMN and substrate binding, and why. There are five regions which are highly conserved within the family for FMN binding: Arg207 and Lys205 for the phosphate group, Leu145 and Tyr144 to interact with the dimethylbenzoide ring, Glu165 and Gly166 to donate hydrogen bonds to N5 and O4, residues 10-13 and 39-41 to interact with the ribityl chain, and residues 72-75 to donate hydrogen bonds to the pyrimidine ring[21]. Gly166 is absolutely conserved among the family, possibly because a larger side-chain could interfere with substrate binding[17]. Although the proline itself is not necessarily conserved, the backbone carbonyl of Pro163—an electron-rich group—interacts with the π system of the isoalloxazine ring[17]. Lys14 and Asn71 are not precisely conserved within the family, but other proteins have residues of analogous functionality, such as Arg and Gln respectively. These subtle changes may modulate both the redox potential of FMN, as well as substrate binding. Lys14 in particular may act to help stabilize the negative charge that develops on N1 as FMN is reduced[22].

The donation of a hydrogen bond from the backbone of Glu165 to N5 of FMN is conserved not just within this family of flavoproteins, but in a much broader group of flavoenzymes with a wide variety of structures and functions. Among this larger group, it is found that the angle between the hydrogen bond donor, N5 and N10 consistently falls within a range of 116 to 170 degrees[23]. The angle in NTR is 156.3 degrees[20]. It is thought that this hydrogen bond increases the oxidative power of FMN[24].

Steady-state kinetics studies have shown that the enzyme reacts via a ping-pong bi-bi mechanism[16]. First, NAD(P)H binds to the enzyme and donates two electrons to the FMN cofactor. $NAD(P)^+$ is then released, allowing the opportunity for the substrate to bind to the

active site of the reduced enzyme and thereby be reduced itself[21]. The active site cannot accommodate NAD(P)H and a second substrate simultaneously.

As stated previously, NTR has a broad substrate range. Although it reduces both nitroaromatics and quinones, it has been observed to reduce quinones faster[25,26]. The primary feature of aromatic substrate binding appears to be hydrophobic ring stacking, with the substrate sandwiched between the FMN ring system and the Phe124 residue at a distance of approximately 3.5 Å from each[20]. An example of this can bee seen in the 1ICR crystal structure[20], obtained from the RCSB Protein Data Bank[27,28], which shows nicotinic acid bound to NTR, and provides a good example of aromatic substrate binding. The lack of many other consistent interactions between the substrate and protein may explain both NTR's broad substrate range, and its affinity for aromatic substrates.

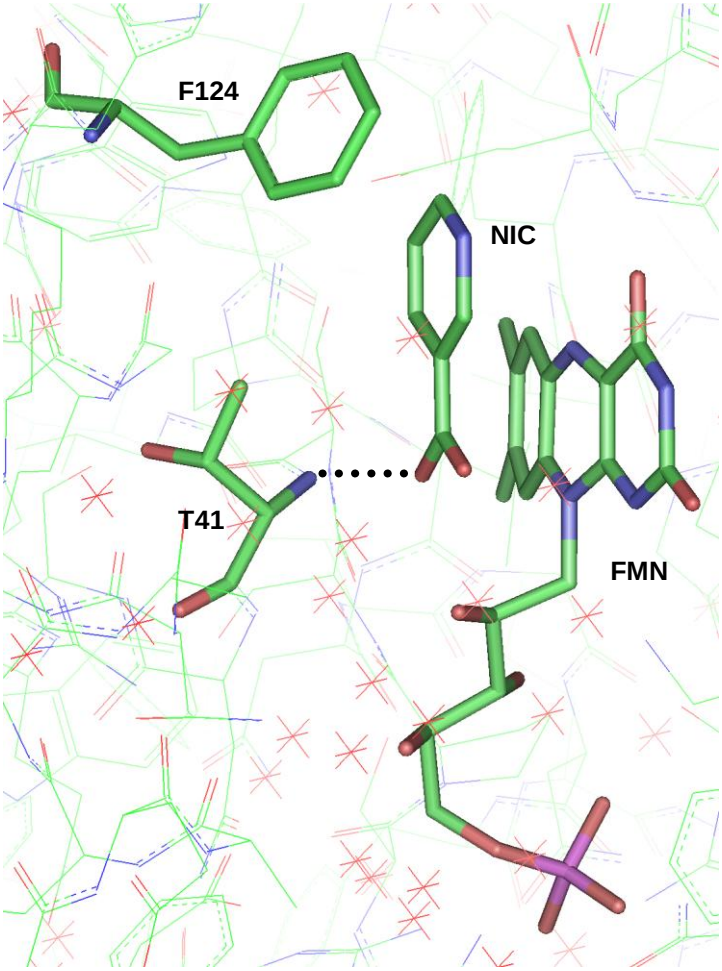

Figure 1.6: Nicotinic acid (NIC) bound to oxidised NTR from the 1ICR crystal structure[20].

Nicotinic acid is an NADH analogue and its binding in the active site can yield some clues as to how NADH and other substrates bind to the enzyme in its oxidised state. In a study of a broad range of flavoenzymes, it was found that the site of oxidative attack on the substrate is consistently found at a distance of 3.5 angstroms from N5, with a substrate-N5-N10 angle of 96-117 degrees[23]. For nicotinic acid, the C4 carbon was found at a distance of 3.4 angstroms, with an angle of 101 degrees[20]. C4 is the site of oxidative attack on NADH, which confirms that nicotinic acid is a good analogue for NADH.

As with most aromatic ligands, nicotinic acid binds in a hydrophobic sandwich between FMN and Phe124. Additionally, the carboxyl group has a hydrogen bond to the

backbone of the Thr41 residue[20]. This hydrogen bond is also seen with other ligands, such as nitrofurazone and acetate, in the oxidised state of the enzyme. Acetate and acetamide are only found bound in the active site in the oxidised state of the enzyme, implying that amides and carboxylic acid groups may bind preferentially in the oxidized state of the enzyme[16].

There is a large change in electron distribution in FMN upon reduction[29]. In free flavin, the pKa on N5 changes from 8.5 in the oxidised state (where all three rings are aromatic) to 6.8 in the reduced state (where only the outer two rings are aromatic)[16]. This change in electron distribution may explain differences in binding between the oxidised and reduced enzyme.

The flavoenzyme pentaerythritol tetranitrate reductase has also been reported to have different binding properties for the oxidised and reduced states of the enzyme[30].

1.4 The NTR/CB1954 Combination

NTR may reduce either of the two nitro groups on CB1954, but not both groups of the same molecule. With wild-type NTR, both hydroxylamine species are formed in equal proportions and at the same rate, despite the fact that radiochemical reduction of CB1954 strongly favours the 4-nitro product[31].

As NTR requires NADH or NADPH in order to reduce the nitro group, no extracellular activation occurs, and cell death is limited to cells infected with the genetically modified virus, and those neighbouring cells which are killed via the bystander effect[2].

The bystander effect has a profound influence on the efficacy of VDEPT. Experimental results from human trials have shown that there is a significant reduction in

tumour size, and a corresponding improvement in patient survival rate, when only 5% of tumour cells were observed to express the enzyme[9].

Unfortunately, there is a competing metabolic process that deactivates the cytotoxic molecule, limiting the range of the bystander effect. What this process is exactly is currently unknown, but it does undoubtedly interfere with the efficacy of the bystander effect.

The primary limitations of the NTR/CB1954 combination are a low affinity of NTR for the prodrug, and a slow reaction rate. CB1954 is not a natural substrate of nitroreductase, and so does not naturally bind well to the enzyme. As a result, a low yield of activated prodrug is observed[6]. Additionally, kinetic studies have shown that the reduction of the nitro group by the enzyme to the nitroso intermediate is the rate-limiting step[16]. Attempts have been made to mutate the enzyme in order to improve yield, as well as modulate the ratio of 4-nitro and 2-nitro reduction, but only moderate progress has been made so far[32]. This is primarily due to the fact that the exact mechanism for the reduction of the prodrug by NTR is unknown.

Directed mutation of the enzyme is generally limited to two or three amino acids per protein. Without knowing the actual mechanism of the reaction, it is difficult to predict what mutations will result in greater activation of the prodrug. Although six amino acids most likely to affect enzyme activity have been identified experimentally, approximately 10^{11} mutant proteins would have to be made in order to test all possible amino acid combinations[32]. Computational investigation of the NTR reaction mechanism could provide the knowledge required to focus the mutation efforts on the amino acid substitution combinations that will most likely provide improved enzyme activity.

1.5 Possible NTR/CB1954 Reaction Mechanisms

It is has been determined that the nitro group of CB1954 is reduced to a hydroxylamine via two successive 2-electron transfers[6]. Although the reduction of the nitro group to the unstable nitroso intermediate must be performed by the enzyme, it is not necessary for nitroreductase to be involved in the reduction of the nitroso intermediate to hydroxylamine, as the nitroso may be directly reduced by NAD(P)H in solution[16]. Therefore, the focus of this research is on the enzyme-catalysed reduction of the 4-nitro group of CB1954 to a nitroso group.

The overall reduction from nitro to nitroso requires the addition of two protons and two electrons, and while the electrons must come from the FMN cofactor of NTR and at least one of the protons must come from solution, the source of the other proton may be FMN or solution.

Hydride transfer is considered to be the concerted transfer of one proton and two electrons from the same source—in this case the FMN. The addition of the proton from solution (for the total of two protons and two electrons) may occur either before or after this hydride transfer. There are two possible acceptors of the hydride: the nitrogen of the nitro group, or one of the oxygens. While hydride transfer to nitrogen requires additional rearrangement in order to form the nitroso, the electropositive nature of the nitrogen makes it worth considering as a potential acceptor for the negative hydride ion.

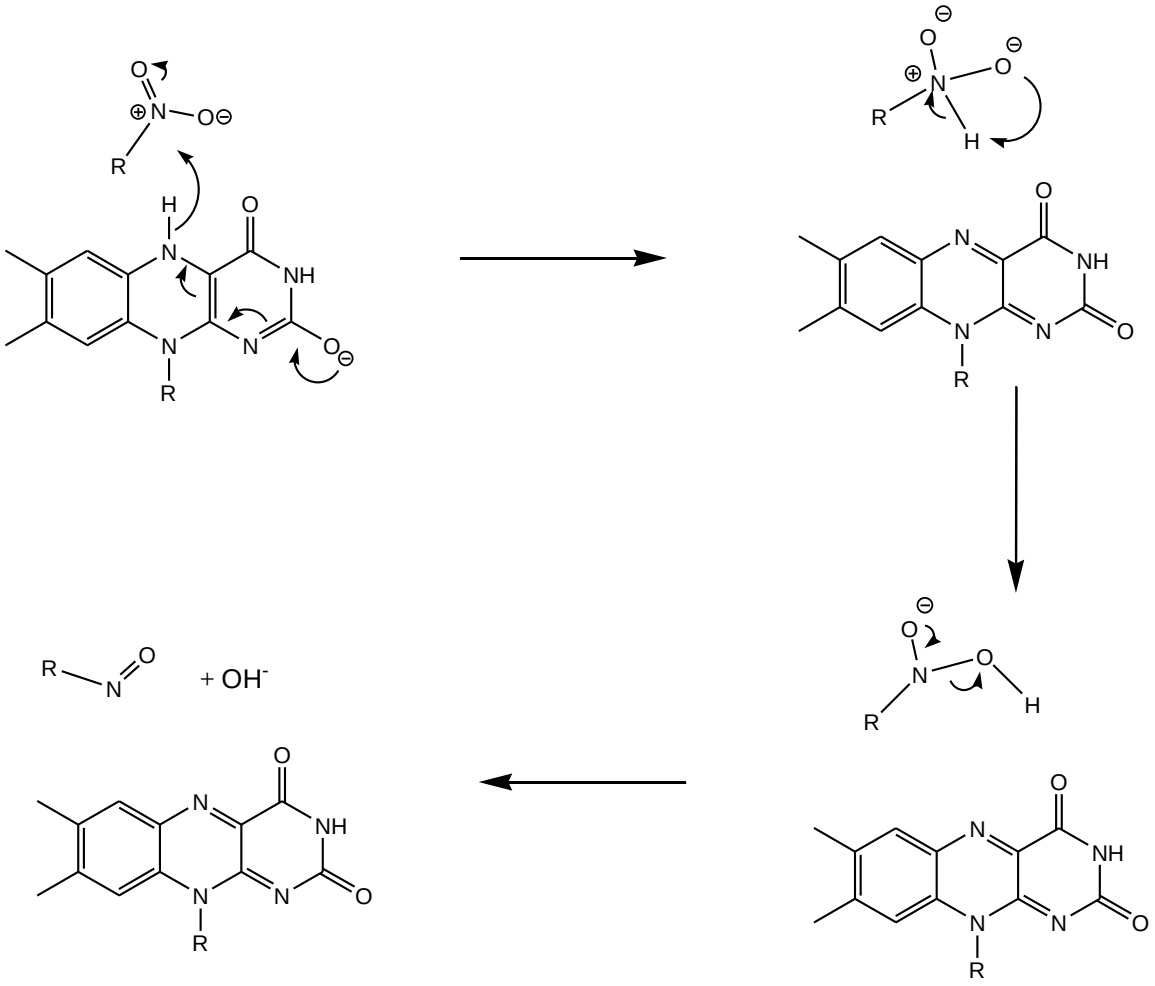

Figure 1.7: Possible hydride transfer mechanisms for the reduction of a nitro group to a nitroso by FMN[33].

Hydride transfer requires that either the nitrogen or one of the oxygen atoms of the nitro group comes within van der Waals contact of HN5 of FMN. Electron transfer (where both electrons come from FMN but both protons come from solution) only requires that some part of CB1954 is within van der Waals contact of some part of the π-system of FMN while the nitro group is exposed to solution, as both the HOMO of FMN and LUMO of CB1954 are delocalised across much of their respective molecules.

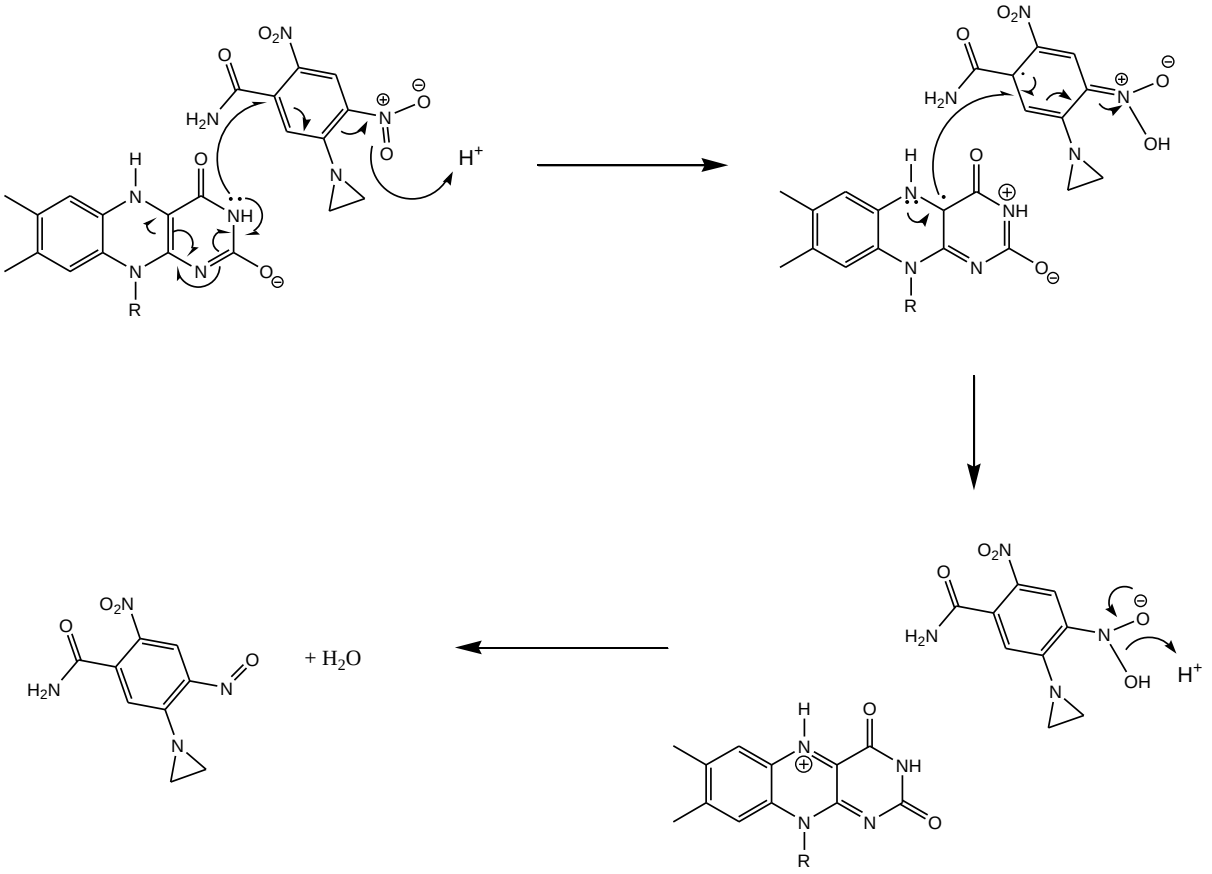

Figure 1.8: Possible electron transfer mechanism for the reduction of the 4-nitro group of CB1954 by FMN[33].

There is empirical evidence that argues for both hydride transfer and electron transfer. FMN has been observed to undergo both one-electron and two-electron transfers as a cofactor in other enzymes[34]. Although it is difficult to prove true hydride transfer experimentally, if a

two-electron transfer is followed immediately by a proton transfer from the FMN, this is essentially the same as a hydride transfer, termed "net hydride transfer" in this thesis. The initial reduction of FMN by NAD(P)H is believed to occur via hydride transfer[20,23].

For the electron transfer mechanism to be viable, FMN must donate two electrons to CB1954, then lose the N5 proton to solution before it can be reduced again by NAD(P)H. The pKa of the oxidised, protonated FMN is 0.2[34], which allows for this possibility.

The X-ray crystal structures of NTR provide ambiguous information about the reaction mechanism. The 1YKI crystal structure[16] appears to show nitrofuran, an antibiotic, bound to the enzyme active site with the amide group over N5 of FMN, and the nitro group exposed to solution—a position most ideally suited for electron transfer. However, both the enzyme and nitrofurazone are present in their oxidised forms[16]. Other crystal structures apparently show CB1954 bound to the active site of the enzyme with the either the 2-nitro or 4-nitro group over N5 of FMN[35], but because of the symmetrical nature of the prodrug (each group has exactly 23 electrons), it is nearly impossible to definitively determine the orientation of the molecule in an X-ray crystal structure, while others have raised doubts over whether this structure shows CB1954 bound at all[36].

1.6 Knowledge-Based Design of NTR Mutants

Knowledge of the exact reaction mechanism is critical, as it will help determine what amino acids should be mutated in order to increase activity. If NTR is found to reduce via hydride transfer, the enzyme should be mutated in such a way as to maximise the binding of CB1954 in an orientation that favours the reduction of the 4-nitro group. But if the

mechanism is in fact electron transfer, it may be more beneficial to mutate the enzyme in a way that modifies the redox potential of FMN.

There are, however, several limitations to enzyme mutation. Because the active site is comprised of residues from both subunits, it is possible that even mutation of only one or two amino acids could affect the dimer formation of the protein. Additionally, it is possible that changes that improve the binding and reactivity of CB1954 may interfere with the first step of the reaction—the reduction of NTR by NAD(P)H.

Initially, nine residues in the active site of NTR surrounding FMN that could have an effect on catalysis or substrate binding were identified for single mutation: Ser40, Thr41, Tyr68, Phe70, Asn71, Gly120, Phe124, Glu165, and Gly166[32]. For each position, all possible amino acid substitutions were generated and cloned into the *E. coli* bacteria. The clones were replicated on agar, and CB1954 was administered in order to determine the effect of the amino acid substitution on the reaction with the prodrug, as a decrease in bacterial growth correlates to an improvement in prodrug reduction. Of the nine potential residues, only Gly166 was found to be essential for prodrug reduction. Additionally, no significant improvements were found with any mutation of Glu165 or Gly120[32].

The best single mutants were found at Phe124, with fifteen amino acid substitutions yielding increased sensitivity to CB1954. The large hydrophobic side-chain of phenylalanine likely imposes restrictions in binding in the wild-type enzyme, and various studies have shown that mutations at this residue may be key in modulating substrate specificity[32,37].

Additional improvements were found by mutating Ser40 to residues with small side-chains such as glycine and alanine. Thr41 had improvements with residues with long hydrophobic groups, polar groups, or glycine. Tyr68 had improvements with glycine or asparagine. Phe70 had several residue substitutions with improvement, possibly due to its

location near the opening of the active site, where mutations could allow greater access to the active site, as well as reduce the difficulty of product release. Finally, Asn71 had improvements primarily with polar residues such as serine[32].

Kinetic parameters for wild-type NTR and the best mutants with both CB1954 and nitrofurazone were determined in order to give a more quantitative comparison of the mutants' efficacy. All substrate parameters were determined to be independent of NAD(P)H concentration[38]. Although the global turnover rate (k_{cat}) and global binding constant (K_m) for wild-type NTR and CB1954 could not be determined due to the limited solubility of the prodrug, the specificity constant (k_{cat}/K_m) measured at lower concentrations is still valid, because the overall reaction rate is determined by k_{cat}/K_m at low concentrations, and the concentration of CB1954 required for gene therapy applications is much lower than the solubility limit[39].

All of the single mutants except for the Asn71 to serine (N71S) showed both an improvement over wild-type, and an improvement in selectivity over nitrofurazone. This selectivity is important, as there are many potential competitors and inhibitors *in vivo*. The N71S mutant did show improvement over wild-type with CB1954, but greater improvement with nitrofurazone[39]. Crystal structures of the mutant show that the hydrogen bond from the asparagine side-chain to FMN is lost due to the shorter side-chain of the serine, but a conserved water molecule provides a hydrogen-bonding chain from the serine side-chain to FMN. It is believed that this mutation affects the redox potential of FMN, rather than substrate binding, as the improvements in the specificity constant for CB1954 and nitrofurazone are similar[39].

For the Thr41 to lysine (T41L) and Tyr68 to glycine (Y68G) mutants, the improvement in the specificity constant came from an increase in k_{cat}, while the K_m values remained largely the same as wild-type. For all of the other mutants, the effect was reversed—improvements in k_{cat}/K_m arose from a decrease in K_m, while there was little change in k_{cat}. Additionally, the T41L mutant showed a preference for the 4-nitro reduction over the 2-nitro by a 3:1 ratio[39]. Because none of these mutations have an appreciable effect on nitrofurazone, it is believed that improvements are due to interactions with the substrate, rather than a modulation of the redox potential of FMN[39].

All four of the mutants at Phe124 exhibited different k_{cat}/K_m values, suggesting that each mutant had a different affect on the substrate. Of the four, asparagine (F124N) had the best specificity constant and the greatest selectivity for CB1954.

Several single-mutation crystal structures have been determined, both for the holoenzyme and with bound nicotinate. Regardless of the presence or absence of substrate, all mutants were found to be structurally similar to wild-type NTR. Although there was naturally some variation in side-chain orientation, there was very little difference in backbone conformation, demonstrating that single mutations have little effect on protein folding or structure[39].

Further kinetic work was done on the best single, double and triple mutants, using both CB1954 and nitrofurazone as substrates[40]. The best double mutant was found to be a combination of the Thr41 to leucine and Asn71 to serine single mutants (T41L/N71S). The best triple mutant was a combination of Thr41 to glutamine, Asn71 to serine, and Phe124 to threonine (T41Q/N71S/F124T)[41].

Protein	k_{cat} s^{-1}	$K_{mCB1954}$ μM	$k_{cat}/K_{mCB1954}$ $\mu M^{-1} s^{-1}$
Wild-type	140 ± 32	17200 ± 4800	0.007
F124N	95 ± 7	3081 ± 465	0.031 ± 0.006
T41L/N71S	153 ± 8	216 ± 33	0.71 ± 0.08
T41Q/N71S/F124T	181 ± 7	569 ± 45	0.318 ± 0.016

Table 1.1: Kinetic parameters for the reduction of CB1954 by wild-type NTR and the best single, double, and triple mutants[40].

Protein	k_{cat} s^{-1}	$K_{mNitrofurazone}$ μM	$k_{cat}/K_{mNitrofurazone}$ $\mu M^{-1} s^{-1}$
Wild-type	225 ± 34	1850 ± 400	0.15 ± 0.02
F124N	110 ± 12	972 ± 208	0.11 ± 0.01
T41L/N71S	103 ± 8	237 ± 39	0.38 ±0.03
T41Q/N71S/F124T	142 ± 21	1039 ± 261	0.137 ± 0.02

Table 1.2: Kinetic parameters for the reduction of nitrofurazone by wild-type NTR and the best single, double, and triple mutants[40].

This data shows that there is very little improvement in turnover rate with the mutations for either CB1954 or nitrofurazone. The fact that k_{cat} values for the two substrates are rather similar also implies that the rate-limiting step may be independent of the redox reaction, and may in fact be product release. Additionally, the greatest improvements in substrate specificity come from improvements in binding, which implies that binding may be key to enzyme efficiency. It was also found that the T41L/N71S mutant reduces the 4-nitro group exclusively[40], while the triple mutant has no selectivity for either nitro group.

While random mutation of select amino acids has resulted in a 100-fold improvement in specificity for CB1954, the sheer number of possible combinations of residue mutations makes it difficult to produce further improvements without knowing more about the reaction mechanism of NTR and in particular, how the substrate binds.

1.7 Substrate Binding in NTR and Other Enzymes

The possible binding orientations of CB1954 in the active site of NTR will largely determine what reaction mechanism is allowed for the reduction of a nitro group by the enzyme. Therefore it is useful to look at how various substrates bind to NTR, as well as other enzymes which also reduce CB1954.

1.7.1 Dicoumarol and NTR

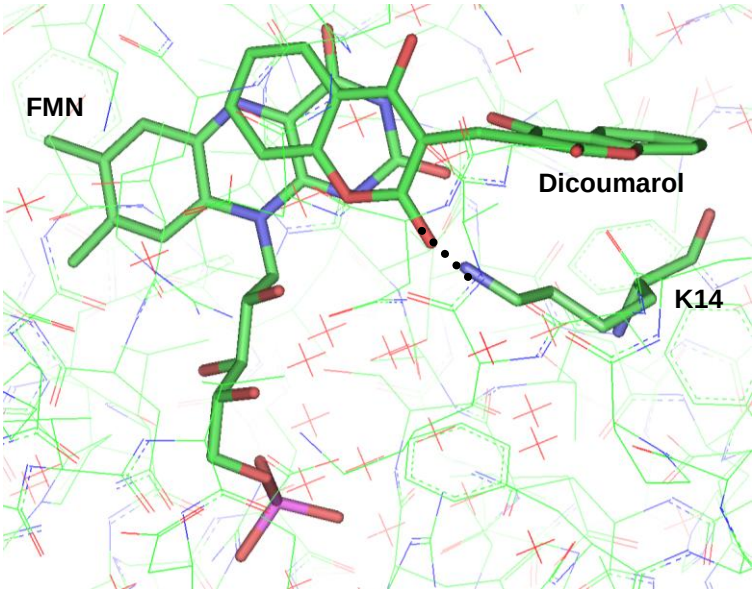

Figure 1.9: Dicoumarol bound to reduced NTR from the 1OOQ crystal structure[35].

Dicoumarol is a known specific, irreversible inhibitor of NTR[35]. The crystal structure of dicoumarol bound to reduced NTR primarily shows ring stacking interactions between dicoumarol and FMN, although there is one hydrogen bond from a keto oxygen to Lys14.

1.7.2 Acetate and NTR

Acetate (CH_3COO^-) is part of the buffer solution for many enzyme crystallisations, and because of its relatively high concentration, it is often found in the active site of the enzyme. Like nicotinic acid, it is found bound over FMN, with a single hydrogen bond to the Thr41 backbone. An example of this may be seen in the 1YLR crystal structure[16].

1.7.3 Nitrofurazone and NTR

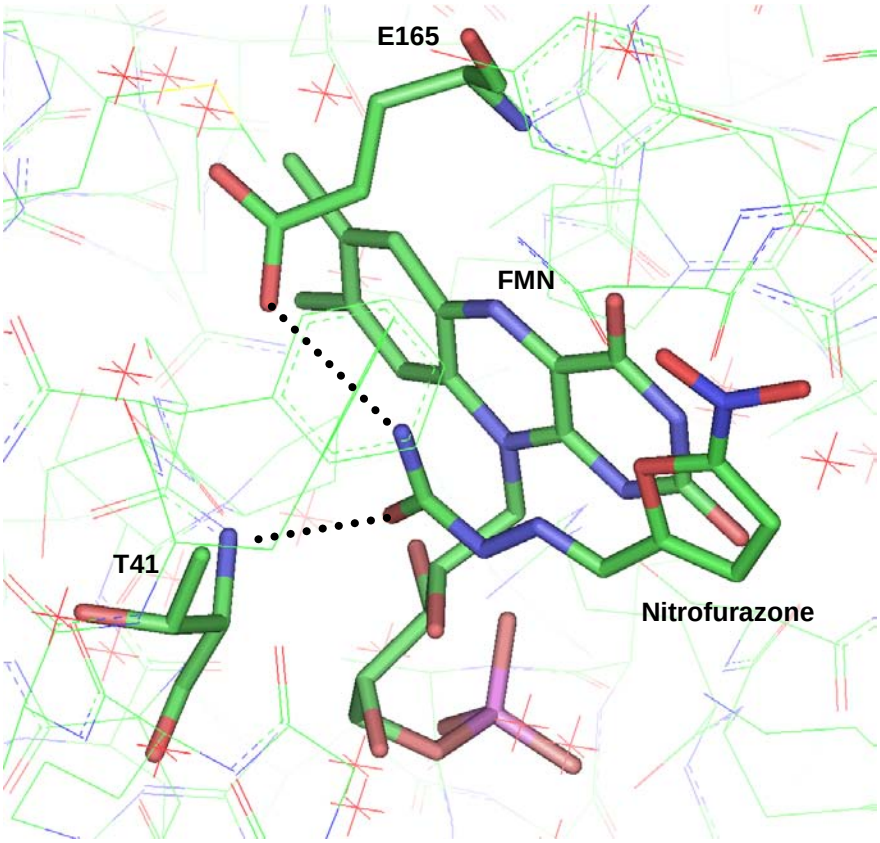

Figure 1.10: Nitrofurazone bound to oxidised NTR from the 1YKI crystal structure[16].

Like nicotinic acid and acetate, nitrofurazone has a hydrogen bond from a carbonyl oxygen to the Thr41 backbone. There is an additional hydrogen bond from the nitrofurazone amide group to the Glu165 side-chain. This may in fact represent an amide binding pocket, which would allow compounds with amide groups to bind within van der Waals contact of FMN, allowing the redox reaction to take place. As mentioned in Section 1.5, nitrofurazone is bound with the amide group over FMN and the nitro group exposed to solution—ideal for electron transfer and prohibitive for hydride transfer—but both NTR and nitrofurazone are present in their oxidised form.

1.7.4 CB1954 and NTR

The 1IDT crystal structure purports to show CB1954 bound to oxidised NTR in two different orientations: Active Site "A" (Figure 1.11) with the 2-nitro group close to N5 of FMN, and Active Site "B" (Figure 1.12) with the 4-nitro group close to N5 of FMN[35]. While this would explain why NTR produces 2-nitro and 4-nitro reduction products in equal proportions, it is unlikely that this supposition is valid, considering the fact that the two active sites are identical, and there is only one observed binding constant for CB1954 and other substrates[16,40].

There are several other problems with this crystal structure. The crystallisation was performed at pH 4.6, and CB1954 is very unstable below pH 6, with a half-life of minutes at best[42], but not long enough to form a complex. Additionally, it is very difficult to form a complex with any ligand when acetate is used as the buffer solution, as acetate tends to bind preferentially. One solution is to use a different buffer, e.g. citrate, then soak with the ligand of interest[36].

There are problems with the electron density refinement and interpretation as well. In the published structure, B factors remain constant down each side chain, instead of increasing with distance from the main chain. Also, published electron density maps are shown "edge on," which doesn't show the density for the ligand rings, with a very low contour level for the ligand. When the data was re-refined, after some phase bias removal it was found that there was only significant electron density for a small portion of the ligand, in the location where acetate has been determined to bind[16]. The rest of the ligand was positioned in noise[36]. It is also important to note that even if the ring position is correct, all of the groups on CB1954 have exactly 23 electrons, and are therefore indistinguishable at this resolution.

Still, this crystal structure does at least provide *possible* binding orientations for CB1954 bound to NTR in a manner suitable for hydride transfer, and no other crystal structures with CB1954 and NTR exist to date.

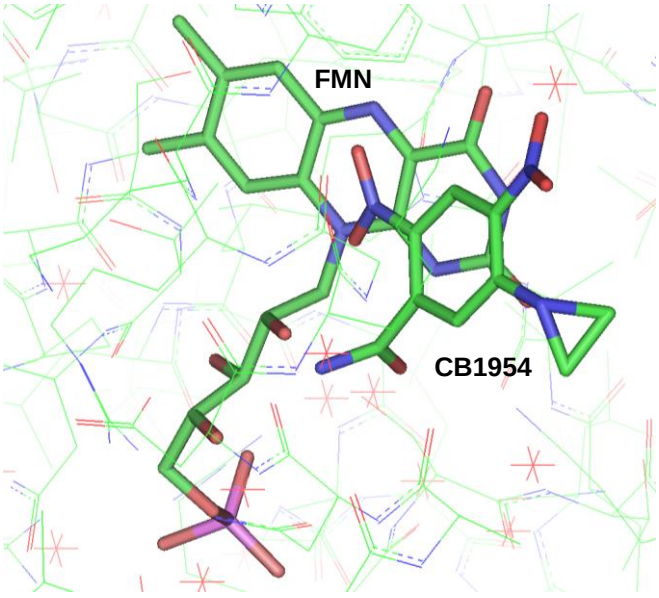

Figure 1.11: CB1954 bound to Active Site A of oxidised NTR from the 1IDT crystal structure[35].

The CB1954 in Active Site A has no hydrogen bonds to any amino acids or FMN.

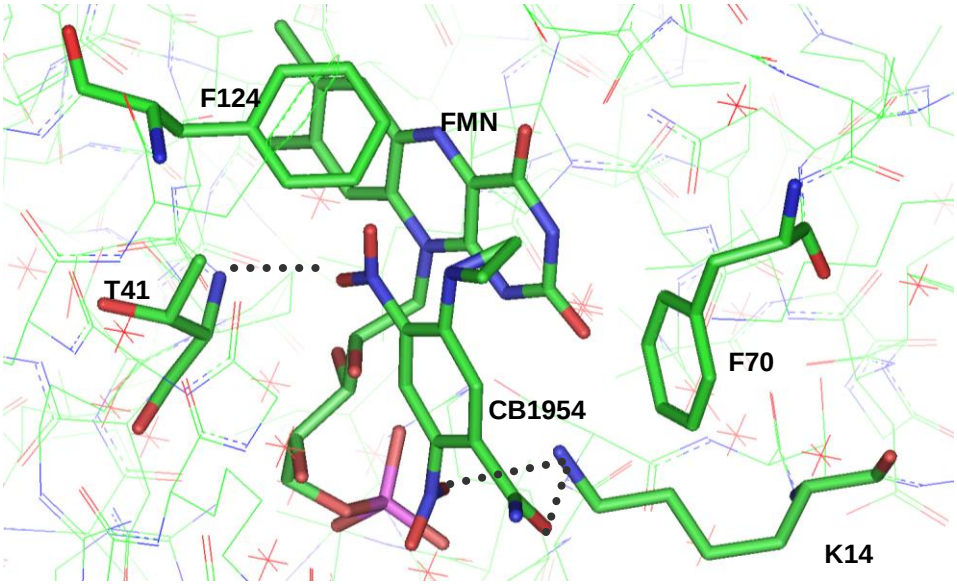

Figure 1.12: CB1954 bound to Active Site B of oxidised NTR from the 1IDT crystal structure[35].

Unlike Active Site A, there are several contacts between CB1954 and NTR in Active Site B. Both the amide and 2-nitro groups of CB1954 have hydrogen bonds with the Lys14 side-chain, and one oxygen of the 4-ntro group has a hydrogen bond with the Thr41 backbone. Additionally, the aziridine ring of CB1954 has hydrophobic contacts with both Phe124 and Phe70.

1.7.5 The Major Oxygen-Insensitive E. coli *Nitroreductase (NfsA)*

NfsA is a second *E. coli* nitroreductase capable of reducing both CB1954 and nitrofurazone. However, while NTR reduces the 2-nitro and 4-nitro groups of CB1954 in equal proportions, nfsA favours the 2-nitro reduction[43]. Unfortunately, no crystal structures are available that show any substrate bound to nfsA. It is interesting to note, however, that while there is only a 15% sequence similarity between NTR and nfsA[20], the 1F5V crystal

structure of unliganded nfsA[44] shows that the Ser41 backbone is in a nearly identical position to the Thr41 backbone of NTR relative to the FMN cofactor.

1.7.6 Menadione and Human Quinone Reductase Type 2 (NQO2)

Menadione, a quinone, is a known substrate of NTR. And while there is no crystal structure of menadione bound to NTR, the 2QR2 crystal structure[45] shows menadione bound to human quinone reductase type 2 (NQO2).

NQO2 is a flavoenzyme with an FAD cofactor, and like NTR reduces quinones and nitroaromatics[46]. While NQO2 utilises the *si* face of FAD, the binding of menadione may still yield some insights into how the substrate binds to NTR.

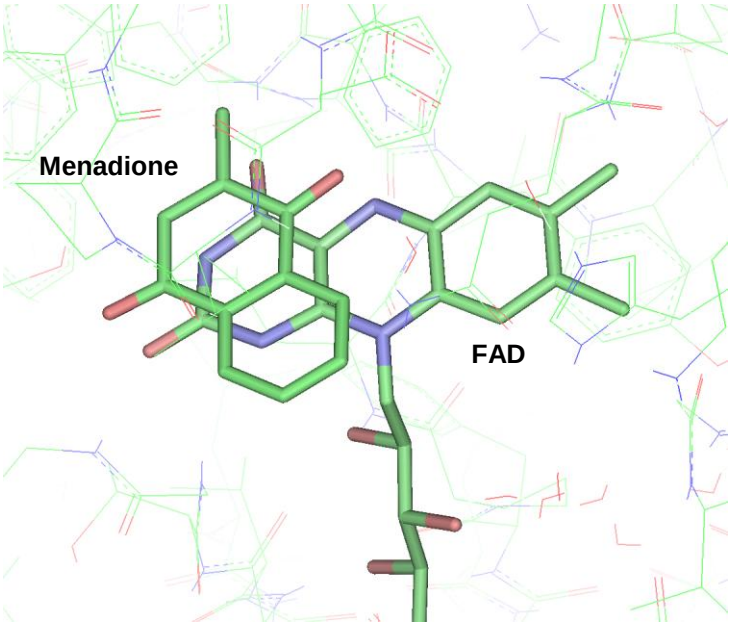

Figure 1.13: Menadione bound to NQO2 from the 2QR2 crystal structure[45]. The full structure of FAD is not shown.

The only contact between menadione and NQO2 is hydrophobic stacking between the substrate and FAD. The orientation of the keto oxygens indicates that the reaction mechanism in this case is almost certainly hydride transfer—with one oxygen obtaining the hydride from N5 of FAD, while the opposite oxygen, exposed to solution, may obtain a proton from solvent.

1.7.7 CB1954 and NQO2

Like Walker DT-Diaphorase, NQO2 reduces the 4-nitro group exclusively[47].

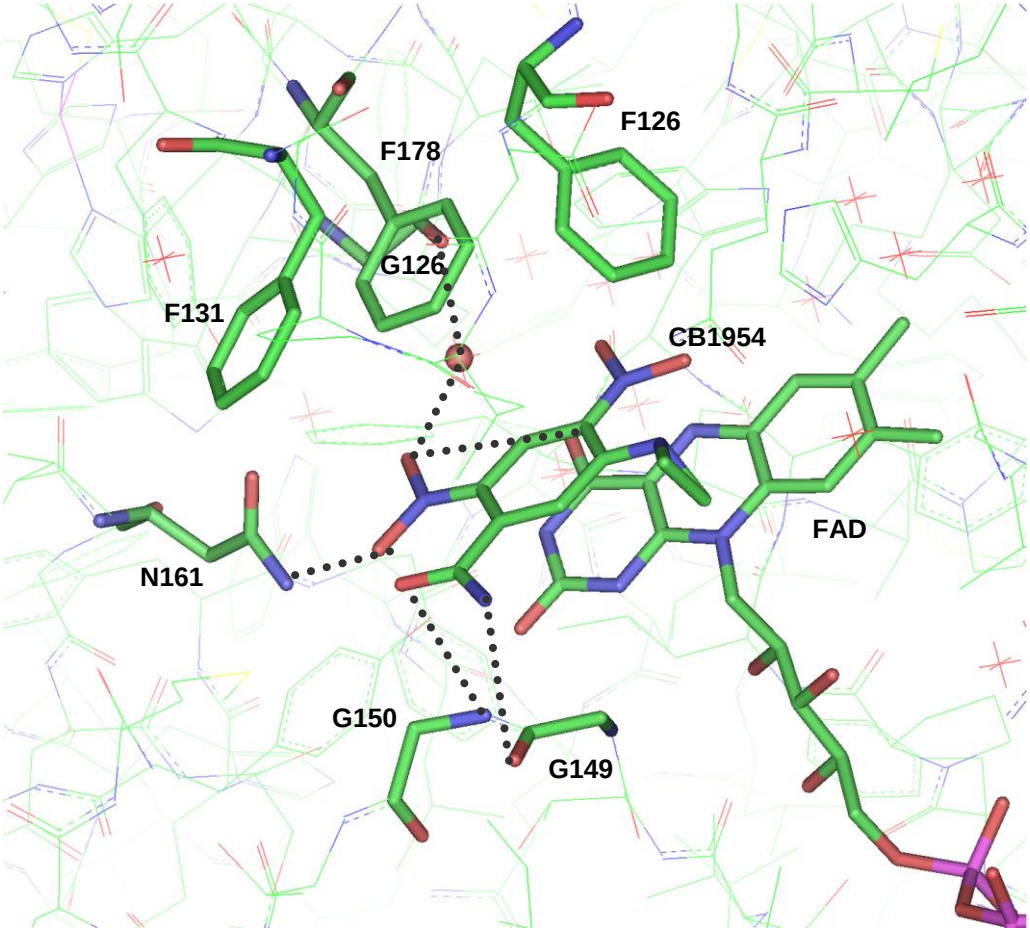

Figure 1.14: CB1954 bound to NQO2 from the 1ZX1 crystal structure[46]. The full structure of FAD is not shown.

CB1954 has several interactions with NQO2. Phe126, Phe131, and Phe178 all have hydrophobic interactions with the substrate. The amide group of CB1954 has hydrogen bonds with Gly149 and Gly150, while the 2-nitro group has hydrogen bonds with Asn161, O4 of FAD, and Gly174 through a water molecule.

Knowledge of how substrates bind to NTR, as well as how CB1954 and other substrates of NTR bind to other flavoenzymes, is helpful for finding the binding and reaction mechanism for CB1954 and NTR, but the fact that most crystal structures show the oxidised enzyme limits their relevance and utility somewhat. In order to examine substrate binding and reaction mechanisms for the reduced enzyme, a computational approach is required.

PDB Code (reference)	**Enzyme (oxidation state)**	**Ligand**	**Notes**
1OOQ[35]	NTR (red)	Dicoumarol	NTR uses *re* face of FMN cofactor
1YLR[16]	NTR (ox)	Acetate	
1YKI[16]	NTR (ox)	Nitrofurazone	
1IDT[35]	NTR (ox)	CB1954	Ligand may in fact be acetate
1F5V[44]	nfsA (ox)	-	nfsA favours 2-nitro reduction of CB1954
2QR2[45]	NQO2 (ox)	Menadione	NQO2 favours 4-nitro reduction of CB1954, uses *si* face of FAD cofactor
1ZX1[46]	NQO2 (ox)	CB1954	

Table 1.3: PDB codes of crystal structures of flavoproteins discussed in this work.

Chapter 2

Computational Methods

This chapter outlines the computational programs, underlying theories, and methodology utilised in determining the reaction mechanism and substrate binding for the CB1954/NTR combination.

2.1 Computational Methods

In order to determine reaction mechanisms and pathways for the reaction between FMN and CB1954, the quantum mechanical computational programs MOPAC 6.0[48] and Gaussian03[49] have been used. To study the reaction within the greater context of the actual protein, the molecular mechanics computational program AMBER 8[50,51], and the docking program Autodock 3.1[52] have been used.

2.2 Quantum Mechanical Methods[53,54]

Quantum Mechanical methods are primarily concerned with the interactions between electrons and nuclei. As such, they are not specifically concerned with bonds *per se*, but rather simply the arrangement of electrons and nuclei that gives the minimum energy. All quantum mechanical methods utilised in this work are based on the time-independent Schrödinger equation:

$$\hat{H}\Psi = E\Psi \tag{1}$$

where $\hat{H}$ is the Hamiltonian operator, which is comprised of five terms: the kinetic energy of the electrons, the kinetic energy of the nuclei, the interelectron repulsion, the internuclear repulsion, and the attraction of the electrons to the nuclei.

$$\hat{H} = T_e + T_N + V_{ee} + V_{NN} + V_{Ne} \tag{2}$$

Ψ is the wavefunction that describes the position of a particle (in this case an electron) in such a way that the probability density may be obtained from the integral of the square of the wavefunction. E is the corresponding energy of the electron. As it is impossible to solve the Schrödinger equation exactly for more than two interacting particles, in order to apply the equation to molecular systems some approximations must be used.

The first of these approximations to consider is the Born-Oppenheimer approximation[55], which argues that because the mass of the nuclei is so much greater than the mass of an electron, the electrons can adjust far more quickly to any nuclear movement. Therefore, the terms for electronic and nuclear motion in the electronic wavefunction can be separated, and the Schrödinger equation can be solved by considering the electrons to be moving in a fixed electrostatic field of the nuclei:

$$\Psi_{tot}(nuclei, electrons) = \Psi(electrons)\Psi(nuclei) \tag{3}$$

$$E_{tot} = E_{electrons} + E_{nuclei} \tag{4}$$

The Hamiltonian operator thus becomes:

$$\hat{H}_{el} = \sum_i h_i + U + \sum_{ij} \frac{1}{r_{ij}} \tag{5}$$

where $\hat{H}_{el}$ is known as the electronic Hamiltonian, and the three terms represent the kinetic energy of the electrons, the internuclear repulsion energy (a constant) and the interelectronic interaction (where i and j are electrons), respectively. In this sense, the molecule can be

described as a set of nuclei that moves over an electronic potential energy surface, and each electronic Hamiltonian is unique to a set of nuclear coordinates.

2.2.1 The Hartree-Fock Equation[53]

The Fock operator is a single-electron Hamiltonian operator that may be used to solve for an electron considered to be moving through a fixed field of nuclei and other electrons:

$$f_i(1) = \mathrm{H}^{core}(1) + \sum_{j=1}^{N} \{J_j(1) - K_j(1)\} \tag{6}$$

The H^{core} term describes the kinetic and potential energy of an electron in a fixed field of nuclei. The *J* term is the Coulomb operator, which corresponds to the electrostatic repulsion between a pair of electrons, and *K* is the exchange operator, which is related to the fact that electrons with the same spin tend to be found further away from each other.

In the Hartree-Fock equation, the Fock operator acts on the molecular orbital χ_i to give an eigenvalue for the orbital energy, ε_i, in exactly the same manner as the Hamiltonian operator acts on the wavefunction in the Schrödinger equation:

$$f_i \chi_i = \varepsilon_i \chi_i \tag{7}$$

The χ_i orbital functions are not true molecular orbitals. Rather, they are single-electron spin orbitals. Each single-electron orbital has a spatial function corresponding to the coordinates of the electron and a spin function that corresponds to its spin. In order to

describe an orbital that contains a pair of electrons, two single-electron orbitals with identical spatial functions but opposite spin functions are needed.

In order to obtain the molecular orbital functions, a linear combination of single-electron orbitals (LCAO-MO)[56-58] is used:

$$\chi_i = \sum c_{vi}\, \phi_v \tag{8}$$

The single-electron orbitals ϕ_v are known as basis functions. The combination of basis functions that can accommodate all of the electrons in a molecule is known as the basis set. Because the basis sets are fixed, the energies of the molecular orbitals depend solely on the variable set of atomic coefficients, c_{vi}. These coefficients effectively determine to what extent the corresponding basis functions are represented in the molecular orbital, and in that way the orbital shape and energy can be adjusted to find the optimal configuration.

The variation theorem[59] states that the energy obtained from an approximation to the true wavefunction will always be larger than the actual energy. Therefore, the Hartree-Fock equation may be solved by an iterative process known as the self-consistent field (SCF) approach[60,61]. First, a preliminary set of atomic coefficients are used to calculate the Coulomb and exchange terms in the Fock operator. The Hartree-Fock equation is then solved for a more appropriate set of atomic coefficients, which are used in the next iteration. The process continues until the value for the energy no longer decreases by a significant amount with respect to the previous iteration. This is the point at which the field is said to be self-consistent.

2.2.2 Basis Sets[53]

The Slater type orbital (STO) is a good model for the atomic orbital, but it is not useful in molecular orbital calculations because Slater functions, of the form $\exp(-\alpha r)$, are difficult, if not impossible, to evaluate for atomic orbitals on different nuclei. Therefore, one of the most common and effective methods of representing atomic orbitals is by using Gaussian type orbitals (GTOs), comprised of Gaussian functions. General Gaussian functions take the form $\exp(-\alpha r^2)$, and the product of two or more Gaussian functions is also a Gaussian function. Just as the molecular orbitals are linear combinations of single-electron orbitals, the single-electron orbitals are linear combinations of Gaussian functions.

The major shortcomings of using Gaussian functions are a tendency to underestimate long-range overlap between atoms, as well as charge and spin densities at the nucleus. However, this may be overcome somewhat by simply using a greater number of Gaussian functions. Three Gaussian functions, such as in the STO-3G basis set, is considered to be the minimum number of Gaussian functions required to adequately model a Slater orbital.

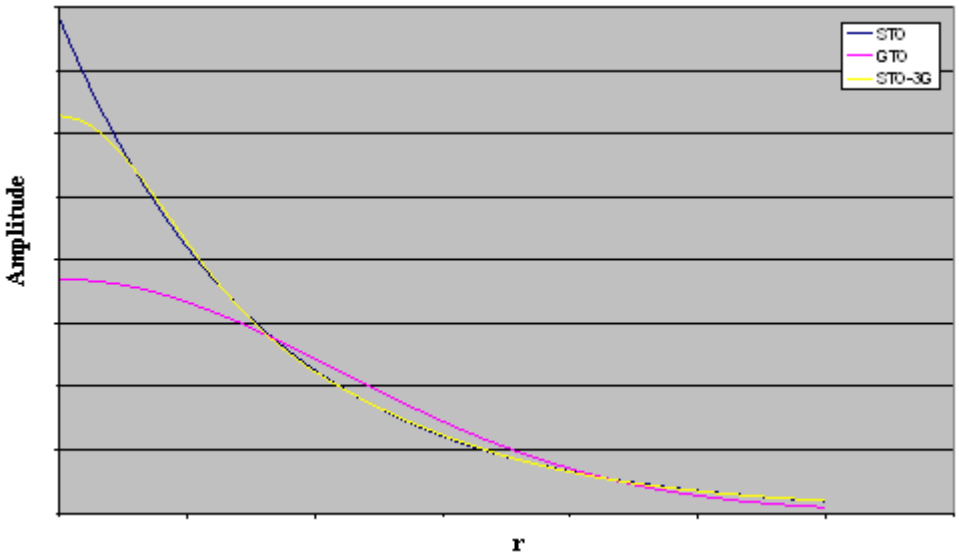

Figure 2.1: Comparison of Slater (blue) Gaussian (pink) and a linear combination of 3 Gaussian (yellow) functions for modelling atomic orbitals.

For all *ab initio* calculations performed, the 6-31g** basis set was used[62-72]. This basis set uses six Gaussian functions to describe the core orbitals, and four Gaussian functions (three contracted and one diffuse) to describe the valence orbitals. This basis set also includes polarisation functions, which are used to describe hybrid orbitals and the effects of nearby electrons.

2.2.3 Density Functional Theory (DFT)[53,54]

The key concept in density functional theory is that the energy of a system can be determined by the overall electronic density of that system. The energy can be described as a function of the electron density, ρ(r), by the following equation[73,74]:

$$E[\rho(r)] = \int V_{ext}(r)\rho(r)dr + E_{KE}[\rho(r)] + E_{H}[\rho(r)] + E_{XC}[\rho(r)] \quad (9)$$

where V_{ext} is the interactions of the electrons with an external potential (the nuclei), E_{KE} is the kinetic energy of the electrons, E_H is the electron-electron Coulombic energy, and E_{XC} is the exchange and correlation contribution.

DFT is often used as an alternative to Hartree-Fock. One of the primary advantages DFT has over Hartree-Fock is in calculating the exchange contribution. While the Hartree-Fock equation does have an exchange term, it treats all electrons as independent of each other, and does not take into account electron correlation.

Therefore, one solution is to use DFT within the local density approximation to obtain exchange and correlation terms that can be added to the Hartree-Fock functional.

For all *ab initio* calculations performed, the DFT/HF one parameter hybrid functional MPW1PW91 was used. This functional uses the modified Perdew-Wang MPW functional[75] for the DFT contribution to the exchange energy (in a linear combination with the HF exchange functional), and the Perdew-Wang 91 gradient-corrected DFT correlation functional PW91[76-80]. This functional was chosen because previous work with B3LYP and other related functionals resulted in severely distorted structures, or structures with unbound electrons[81].

2.2.4 Ab Initio vs. Semi-Empirical[53]

Ab initio calculations are those which use the full Hartree-Fock/Roothaan-Hall[60,61] calculation method, without ignoring or approximating any integrals or terms in the Hamiltonian operator. Although *ab initio* methods are often the most accurate, they are also quite computationally intensive.

Semi-Empirical methods involve the use of parameters for some integrals, or ignore some terms in the Hamiltonian entirely. Additionally, all core electrons are regarded as part of the nucleus, and only valence electrons are considered in the calculations. Parameters that are often used include dipole moments, molecular geometries, heats of formation, ionisation energy values, and atomic spectroscopic data.

Although ignoring and/or approximating terms in the Hamiltonian operator greatly increases the speed at which the calculations can be performed, a certain amount of accuracy is sacrificed.

For all semi-empirical calculations, the AM1 model was used[82]. In addition to the typical parameters associated with semi-empirical methods, the AM1 model attempts to increase accuracy by modifying core-core terms using Gaussian functions in order to better model non-bonding interactions.

All semi-empirical calculations were performed using MOPAC, while all *ab initio* calculations were performed using Gaussian03.

2.2.5 Setup and Implementation of Quantum Mechanics Calculations

While there are many different types of quantum mechanics calculations that may be performed, some general aspects of input file generation remain consistent for all quantum mechanics calculations.

2.2.5.1 Description of Coordinates

Two types of coordinate systems were implemented in this work: Z-matrix and Cartesian coordinates.

With a Z-matrix, the position of a given atom is defined according to its distance, angle, and dihedral with other specified atoms in the system. This is useful in circumstances where groups of atoms (individual molecules) are expected to move together, but problems may also arise, depending on how certain atoms are defined, as a small change in angle or dihedral for one atom may drastically affect the positions of other atoms defined by their relationship to that atom. Additionally, an angle of 180^{o} in the Z-matrix will cause the calculation to fail.

The Z-matrix coordinate system is especially useful when bond lengths, angles, and dihedrals of particular atoms are required to be frozen, while the remainder of the system is optimised.

Cartesian coordinates define atoms according to their three-dimensional distance (x, y, and z coordinates) from the origin. As such, the position of each atom is independent of the other atoms in the system. This has the advantage of keeping the movement of a single atom from affecting a larger portion of the system, but as all atoms are independent, the calculation may require more time to complete.

The Cartesian coordinate system is useful when atoms are required to be frozen, but the remainder of the system is optimised independently of its distance to, or angle with, the frozen atoms.

2.2.5.2 Single-Point and Optimisation Calculations

Determining the SCF energy of a particular geometry, with no change in the nuclear coordinates, is known as a single-point calculation. While many useful properties may be determined from a single-point calculation, the initial geometry is not necessarily the optimal one. In this case, a geometry optimisation must be performed.

Gaussian03 implements the Berny algorithm[83-87] for geometry optimisations. A Berny geometry optimisation begins with a guess of the second derivative matrix to determine initial force constants, and unless otherwise specified, force constants are updated for each subsequent step using the gradient information available from the steps performed in the optimisation.

For each step—each change in nuclear coordinates—an SCF optimisation is performed. Optimisation criteria (force and displacement) determine whether the program exits as a successful geometry optimisation, or an additional step is performed.

2.2.5.3 Charge and Multiplicity

For every quantum mechanics calculation, the overall charge of the entire system, and the overall multiplicity must be specified. Specifying the correct charge and multiplicity is important, as it among other things, determines whether Restricted Hartree-Fock (RHF) or Unrestricted Hartree-Fock (UHF) should be used.

RHF calculations treat all electrons as pairs—all molecular orbitals containing two electrons. As this is expected for many ground-state systems, all calculations specified as being in the singlet state were done using RHF, because the calculation is faster.

UHF calculations treat all electrons individually. While UHF may be used for ground-state calculations, it is considerably slower. However, in situations where there are unpaired electrons, such as systems in the doublet or triplet state, UHF must be used.

Gaussian03 calculations automatically output Mulliken charges[88], the partial atomic charges for a system. While Mulliken charges are not necessarily valid for individual atoms, as they do not take into account delocalisation and are dependent on the basis set used, they are useful for finding approximate molecular charges.

All Mulliken charges are listed in Appendix A.

2.2.5.4 Solvation

Gas-phase quantum mechanics calculations undeniably have their utility, but there are times when it is also useful to study a system in solution. The **SCRF=PCM** keyword specifies the calculation performed in the presence of solvent, utilising the polarisable continuum model (PCM)[89-101], with water as the default dielectric. Unfortunately, solvation calculations must be done as single-point calculations (due to hardware limitations), so a gas-phase optimisation typically precedes the solvation calculation.

By default, hydrogen atoms are enclosed in a sphere with the atom they are bonded to. For systems with hydrogens not bonded to any other atoms, the **RADII=UFF** keyword must be used, in order to model the hydrogen atoms explicitly.

2.3 Transition State Optimisations

Transition state optimisations are performed in order to find the energy and geometry of the transition state of the hydride transfer reaction—the concerted transfer of a proton and two electrons from N5 of FMN to an oxygen or nitrogen of one of the nitro groups of CB1954.

2.3.1 Preliminary Transition State Optimisations in MOPAC

The purpose of using MOPAC is to utilise semi-empirical methods to find approximate transition states for the hydride transfer reactions. Because semi-empirical calculations take so much less time than *ab initio* calculations, it is generally more efficient to

find approximate transition states at the semi-empirical level and then use the resulting geometries as input for *ab initio* calculations, rather than start from the beginning with *ab initio* calculations.

Additionally, because computation time directly corresponds to the number of atoms in a molecule, in order to further decrease computation time a truncated FMN, and nitrofuran in the place of CB1954, are used:

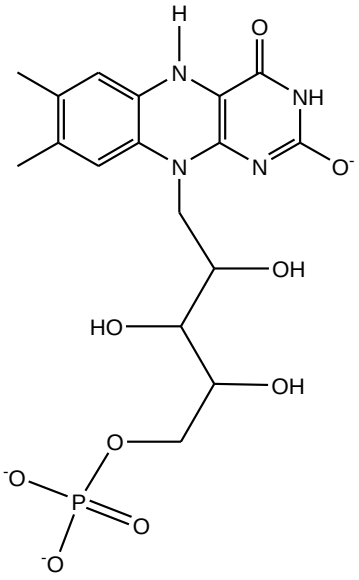

FMN (reduced)

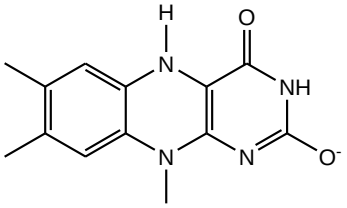

Truncated FMN used in calculations

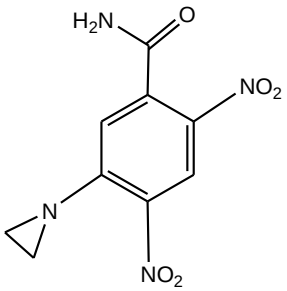

CB1954

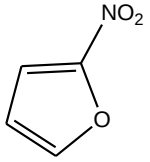

Nitrofuran

Figure 2.2: Cofactors and substrates used in calculations.

Although these changes will most certainly affect the electron distribution and partial charges of the relevant atoms, it is unlikely that it will affect the transition state optimisations to a significant degree.

The calculation for finding the preliminary transition state in MOPAC involves the **TS** keyword. This keyword is associated with the gradient of the reaction profile, and as such is used to modify the geometry in such a way as to approach a point where the gradient in the reaction profile is zero. Points on the reaction profile that have a gradient of zero are the reactants and products (minima), transition state (maximum), and any intermediates (local minima). Therefore, in order to find a transition state, the geometry must be such that the position on the reaction profile is between the points of inflection on either side of the transition state.

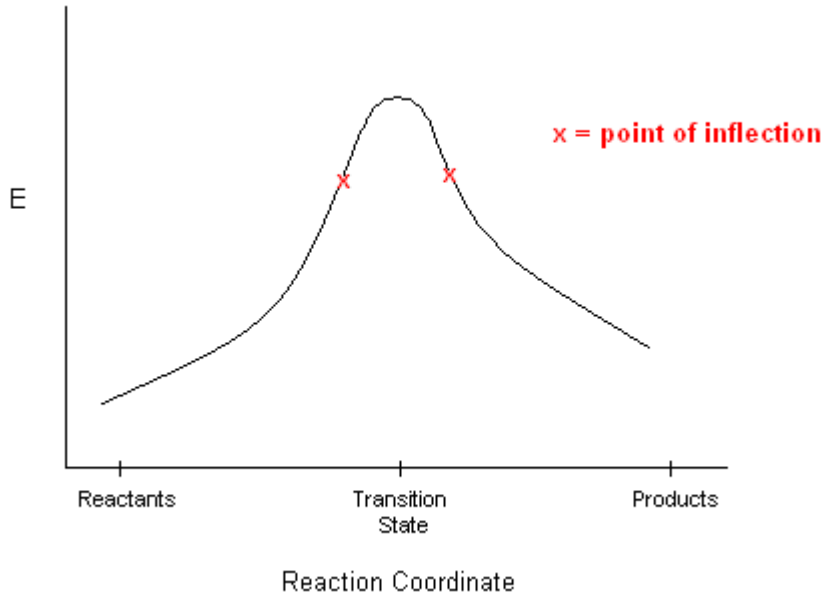

Figure 2.3: A reaction profile. Points of inflection are the points where the second derivative is zero.

In order to determine whether the result of a **TS** optimisation is truly a transition state, a frequency calculation must be done. At the geometry of the transition state, one vibrational frequency will be an imaginary number (negative eigenvalue). If only one of the frequencies is imaginary, then the structure is indeed at a transition state. In addition, decomposition of the negative eigenvalue will reveal bonds being made or broken in the transition state.

From the transition state, the products and reactants can be found using reaction path following. The intrinsic reaction coordinate (IRC)[102,103] is the path from the transition state to the products and to the reactants. Using the **IRC** keyword in MOPAC, the product and reactant geometries can be found from the transition state geometry, and thereby the activation enthalpy and reaction enthalpy as well. Unfortunately, these results are only accurate to within about five kcal/mol.

2.3.2 Transition State Optimisations in Gaussian03

Once the preliminary transition states are found at the AM1 level using MOPAC, these geometries can then be used as the input coordinates in Gaussian03 in order to determine more accurate transition state geometries and energies at the MPW1PW91/6-31G** level. The **Opt=TS** and **IRC** keywords in Gaussian03 have the same functions as in MOPAC, but a frequency calculation is not necessary as a transition state optimisation in Gaussian03 outputs all of the eigenvalues. In order to efficiently optimise transition states in Gausian03, it is necessary to calculate second derivatives at every step, using the **CalcAll** keyword, rather than using the default updating procedure.

As with MOPAC, in Gaussian03 the **IRC** keyword can be used to find the products and reactants, and thereby the activation barrier and energy of reaction.

2.3.3 Hydride Transfer Reaction Profiles

The overall reaction pathway for hydride transfer from FMN to CB1954 involves the net transfer of two protons and two electrons—two electrons and one proton (the hydride) from FMN, and one proton from solution. Using the reactant, product and transition state geometries from the transition state calculations, full reaction profiles can be determined.

This is done by freezing proton distances, and incrementally moving the protons sequentially from either N5 of FMN or hydroxonium (H_3O^+ to represent solution) to an oxygen or nitrogen of the nitro group on CB1954, and calculating the energy and molecular charge of two differing fixed electronic states (singlet for all electrons paired, triplet for two electrons unpaired). All other geometries in the system are allowed to optimise normally.

The reaction profiles determined are hydride first, followed by proton from solution; and proton from solution first, followed by hydride.

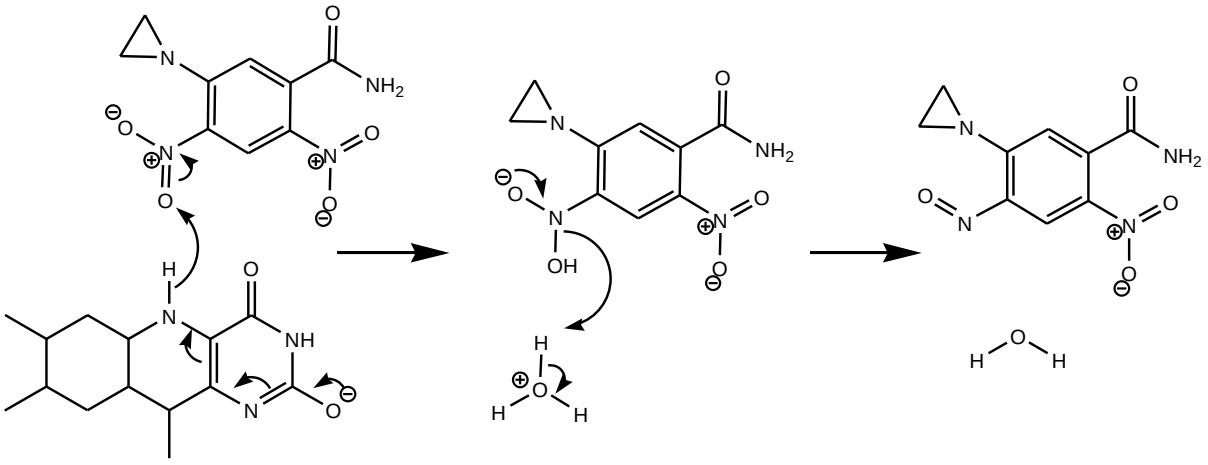

Figure 2.4: Reduction of the 4-nitro group of CB1954 by FMN via hydride transfer. In this mechanism the hydride from FMN is transferred first, followed by a proton from solution (represented by a hydroxonium ion).

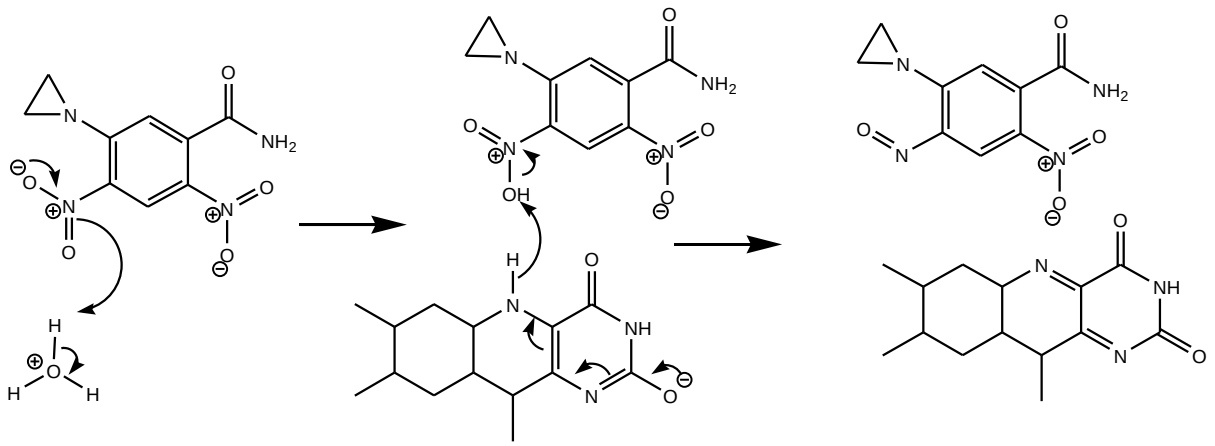

Figure 2.5: Reduction of the 4-nitro group of CB1954 by FMN via hydride transfer. In this mechanism a proton from solution (represented by a hydroxonium ion) is transferred first, followed by the hydride from FMN.

2.4 Electron Transfer Calculations

The calculations for finding electron transfer reaction mechanisms and pathways are quite different. First a configuration must be obtained that has the FMN and CB1954 in positions relative to each other that maximise the overlap of the HOMO on FMN and the LUMO on CB1954. A standard geometry optimisation is then performed on the ground state electron configuration in order to find the exact orientation of the two molecules that has the lowest energy. This is the reactant geometry. Then a geometry optimisation is done on the first excited (triplet) state. This is the product geometry (for the first electron transfer). Once the product and reactant geometries are obtained, the excited state energy at the reactants and ground state energy at the products can be determined, and the corresponding curves can be found. The point at which the adiabatic crossover is observed is the transition state.

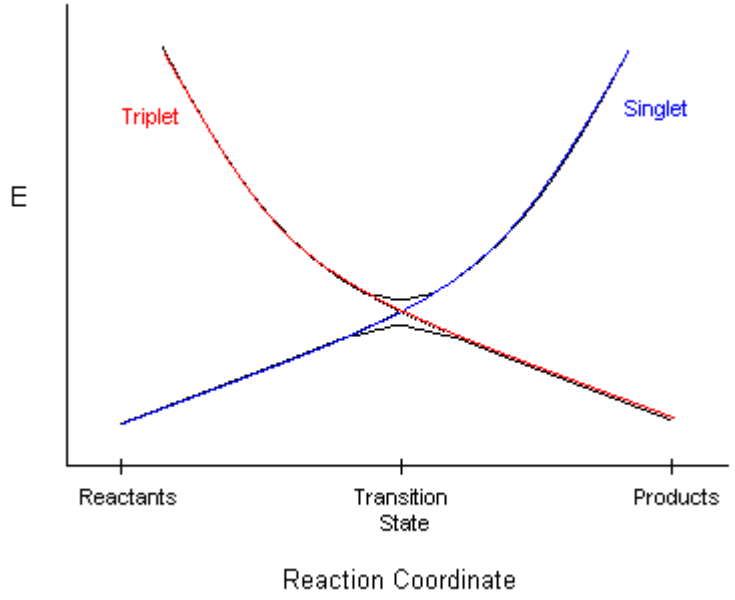

Figure 2.6: A reaction profile for electron transfer.

At the transition state there is a mixing of singlet and triplet electronic states. Because of this, the true energy of the transition state will always be lower than the energy of the pure singlet or triplet state. This is known as an avoided crossing, and the pure singlet or triplet state may be considered the upper limit of the true transition state energy.

2.4.1 Electron Transfer Profiles

The electron transfer reaction profiles are determined in a similar way to those for hydride transfer; by freezing proton distances, and incrementally moving the protons sequentially from hydroxonium ions (as both protons come from solution in the electron transfer mechanism) to an oxygen or nitrogen of the nitro group on CB1954, and calculating the energy and molecular charge for the singlet and triplet electronic states.

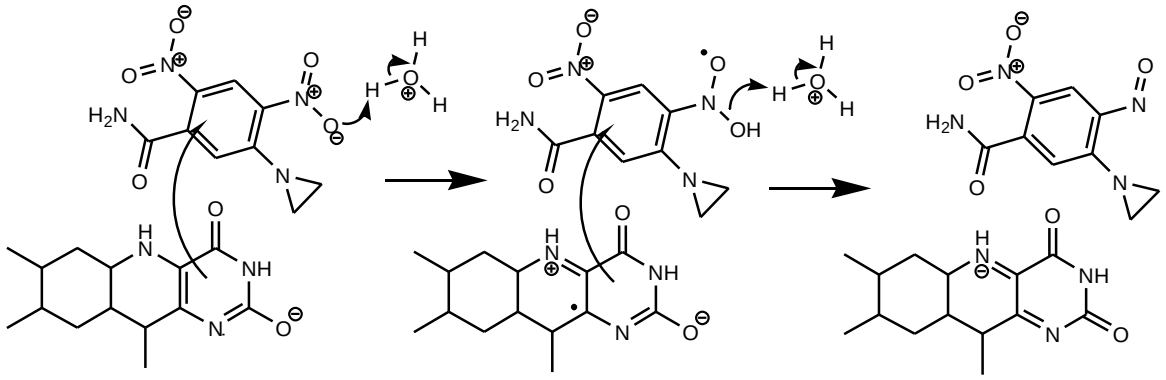

Figure 2.7: Electron transfer mechanism for the reduction of CB1954 by FMN. Hydroxonium ions represent solution.

2.4.2 CASSCF Calculations[53,54,104]

One drawback of the Born-Oppenheimer approximation is that it does not allow for mixing of electronic states. Therefore, in order to find the avoided crossing and true transition state energy and geometry, a different method must be used.

While Hartree-Fock calculations only deal with a single electron configuration, configuration interaction (CI) calculations add terms to the wavefunction to represent all possible electron configurations:

$$\Psi = c_0\Psi_0 + c_1\Psi_1 + c_2\Psi_2 + ... \quad (10)$$

where Ψ_0 is the wavefunction of the ground state, and Ψ_1, Ψ_2 etc. are wavefunctions of excited states, obtained by replacing occupied orbitals with virtual orbitals in the wavefunction. In a CI calculation, the coefficients of the wavefunctions (c_0, c_1, c_2 etc.), which determine the relative contribution of each wavefunction, are adjusted to minimise the energy

of the overall wavefunction. Thus the overall wavefunction may be considered to be the result of the interaction of all possible electron configurations.

Unfortunately, a full CI calculation on FMN and CB1954 would take more time and computer power than is currently available, so another approach is needed.

Complete Active Space Self-Consistent Field (CASSCF)[105] is a multiconfigurational approach which combines an SCF calculation with a CI calculation on the occupied and unoccupied orbitals of interest—in this case the HOMO of FMN and the LUMO of CB1954. The subset of orbitals involved in the CI calculation is known as the active space.

While a CASSCF calculation only performs a CI calculation on the active space, rather than all possible orbitals, it has the advantage of optimising both the coefficients of the wavefunctions, as well as the coefficients of the basis functions that make up the molecular orbitals, which a pure CI calculation does not do.

A CASSCF calculation typically involves two steps. The first step is a standard HF single point calculation, which is done in order to determine which orbitals should be in the active space. The second step is the CASSCF calculation itself, using the orbitals from the first step as input.

2.5 Molecular Mechanics

Molecular mechanics methods study molecules by looking at the "bonds" in a system. Because the total energy is calculated as a function of nuclear position only, the calculations are much simpler, and therefore may be performed on larger systems, such as proteins. All relevant information associated with bonding (for example length, angle, strength, partial charge, etc.) is derived from a predetermined 'force field,' which contains parameters for

atom types, depending on the local environment (surrounding atoms, bond order, hybridisation) the atom is in.

Although molecular mechanics calculations are faster and can be performed on larger systems than quantum mechanics calculations, it is impossible within simple molecular mechanics methods to form or break bonds, unless specific parameters are developed for the atoms involved in making and breaking bonds. As these parameters would differ for each system under investigation, this is generally not practical. Another drawback is that with molecular mechanics methods it is impossible to obtain any information on properties that are based on electron distribution.

However, despite these limitations, molecular mechanics methods are useful for looking at properties such as protein conformation and flexibility, the interactions between a protein and a ligand, hydrogen bonding, and solvent behaviour.

2.5.1 Force Fields[53]

There are a number of different force fields available, and what follows is a general outline for the AMBER force field[106] (the basic additive form from Cornell *et al.*)[107], which describes the potential energy of a system as a function of nuclear position in the following way:

$$PE = \sum_{bonds} f(r) + \sum_{angles} f(\theta) + \sum_{torsions} f(\phi) + \sum_{nonbonding} f(R_{ij}) \qquad (11)$$

Bond stretching is modelled by a simple harmonic oscillator, according to Hooke's law:

$$PE(r) = \sum_{bonds} k_r (r - r_{ref})^2 \tag{12}$$

where k_r is half the force constant and r_{ref} is the reference bond length. Bond angles are described in a similar way:

$$PE(\theta) = \sum_{angles} k_\theta (\theta - \theta_{ref})^2 \tag{13}$$

While bond lengths and angles are of course important, they tend to not vary much from the reference values as the force constants are comparatively large. Most of the variation in molecular structure and energy comes from torsions (dihedrals) and non-bonding interactions. The equation for dihedrals is expressed as a cosine series expansion, to reflect the fact that there are barriers to rotation around chemical bonds:

$$PE(\phi) = \sum_{dihedrals} \frac{V_n}{2} (1 + \cos[n\phi - \gamma]) \tag{14}$$

where n refers to the number of minima as the bond is rotated 360^o, V_n is a constant relating to the relative barriers to rotation, and γ is the phase factor, which determines the minimum value of the dihedral.

The non-bonding term actually represents two types of interactions: electrostatics and van der Waals forces. To calculate the electrostatics, all atoms are given a partial charge according to their atom type, and the energy is determined as a sum of interactions of point charges using Coulomb's law:

$$PE(R) = \sum_{i<j}^{atoms} \frac{q_i q_j}{\varepsilon R_{ij}} \tag{15}$$

where q_i and q_j are the partial charges of the atoms, R_{ij} is the distance between the atoms, and ε is the dielectric constant. Current AMBER force fields use a more complicated Ewald mesh approximation[53,108] for electrostatics in periodic systems.

A Lennard-Jones 6-12 term is used to model the van der Waals forces:

$$PE(R) = \sum_{i<j}^{atoms} \frac{A_{ij}}{R_{ij}^{12}} - \frac{B_{ij}}{R_{ij}^{6}} \tag{16}$$

where R_{ij} is the distance between the atoms, and A and B are constants relating to the repulsive (exchange) and attractive (dispersive London) forces, respectively. While the R^{-6} term for the attractive forces does have a theoretical basis, the R^{-12} term for the repulsive forces is simply used because it makes the calculations easier to perform.

Force fields are empirical; there is no underlying mathematical formula that perfectly generates all the necessary parameters for all situations. Instead, values are determined from experimental data, or in some cases, *ab initio* or semi-empirical quantum-mechanical calculations. The parameters for bonds, angles, dihedrals and non-bonding interactions are given by the atom types, according to the various molecular configurations studied. For

example, an sp^3 carbon is going to have different bond lengths, angles, dihedrals and partial charge than a carbon in a carboxyl group, and the atom types reflect this.

There is no single perfect force field for every possible application. Therefore the best approach is to choose a force field that was parameterised using molecules that most closely resemble the system to be studied, and as such contains atom types with appropriate parameters.

2.5.2 Docking

Autodock 3.1 is a molecular mechanics protein docking program that determines in what position and how well a particular ligand could bind to a protein.

As with any docking program, the protein structure may be obtained from X-ray crystallography data—in most cases from the RCSB Protein Data Bank[27,28]—or from a homology model[109]. Docking my also be performed on the output of a molecular mechanics or molecular dynamics calculation. Initially, water molecules and any other extraneous molecules are removed from the structure, and an appropriate force field is then applied. Next, a grid is set up around the active site.

Autodock 3.1 implements a Lamarckian Genetic Algorithm technique[52], which utilises a genetic algorithm for the global search, with a local search in each step to find energy minima. For each docking run, the ligand begins in a random position that is within the specified grid, but not necessarily entirely inside the active site. From there, its orientation with respect to the protein is incrementally adjusted until the optimal conformation is found.

Unfortunately, there are problems with this docking method. Firstly, because there is no flexibility allowed in the protein, there is no way to change the conformation of the protein if it is not in a configuration that can readily accept a particular ligand. While attempts have been made to incorporate flexibility into docking calculations[110], Autodock does not implement these methods. There is also an issue with K_i values.

K_i values are a measure of how strongly a ligand binds to a protein, where the smaller the K_i value, the stronger the binding. We have found that Autodock consistently overestimates the binding strength; while a strongly bound ligand in Autodock may have a K_i value between 10^{-10} and 10^{-12} M, this corresponds to an experimental value approximately between 10^{-5} and 10^{-6} M in most cases[111]. Although this means that K_i values determined by Autodock cannot realistically be compared to experimentally determined K_i values (or even values obtained from other docking programs), rankings of binding strength based on K_i values solely taken from Autodock are still valid.

The energy function used by Autodock[52] is as follows:

$$\Delta G = \Delta G_{vdw} + \Delta G_{hbond} + \Delta G_{elec} + \Delta G_{conform} + \Delta G_{tor} + \Delta G_{sol} \qquad (17)$$

where ΔG_{vdw} represents dispersion/repulsion, ΔG_{hbond} represents hydrogen bonding, ΔG_{elec} represents electrostatics, $\Delta G_{conform}$ represents deviation from covalent geometry, ΔG_{tor} represents restriction of internal rotors and global rotation and translation, and ΔG_{sol} represents desolvation upon binding and hydrophobic effect.

For all docking runs, the modified consistent force field CFF91[112,113] was used.

2.5.2.1 Setup and Implementation of Docking Runs

First, the protein structure in the form of a PDB file—including any cofactors but without ligands or water molecules—is loaded into a visualisation program such as InsightII[(114)], and if necessary hydrogen atoms are added. Next, atom types are assigned, and the protein is centred on the active site. The protein is then saved as a MOL2 file.

A similar procedure is done for the ligand that is to be docked with the protein, but in the case of the ligand, it is centred on the centre of mass. The ligand is saved as a MOL2 file as well, but must be converted to a PDBQS file. The PDBQS file gives information on the number of rotatable bonds in the system, which can be treated as non-rotatable during the calculation, if desired.

Autodock performs ten runs, and gives an output of K_i values, as well as the resulting orientations of the ligand with respect to the protein, which can be viewed in InsightII.

2.5.3 Molecular Mechanics Minimisations[(53)]

As stated previously, molecular mechanics is based on using force fields to determine the energy of a system as a function of the nuclear coordinates. The way in which the total potential energy varies as a function of the nuclear coordinates is known as the potential energy surface. The potential energy surface is multi-dimensional, and can have multiple maxima and minima. The purpose of a molecular mechanics minimisation calculation is to find the structure (configuration of nuclear coordinates) with the minimum energy.

Amber 8 is a package of molecular simulation programs and force fields specifically designed with the purpose of studying biomolecules. AMBER, which stands for Assisted

Model Building and Energy Refinement, uses the method of steepest descent[115,116] to find minima on the potential energy surface. While this method is one of the quickest and easiest, it has the disadvantage of only moving downhill on the potential energy surface, and as such will only find the nearest local potential energy minimum, which may not necessarily be the global minimum.

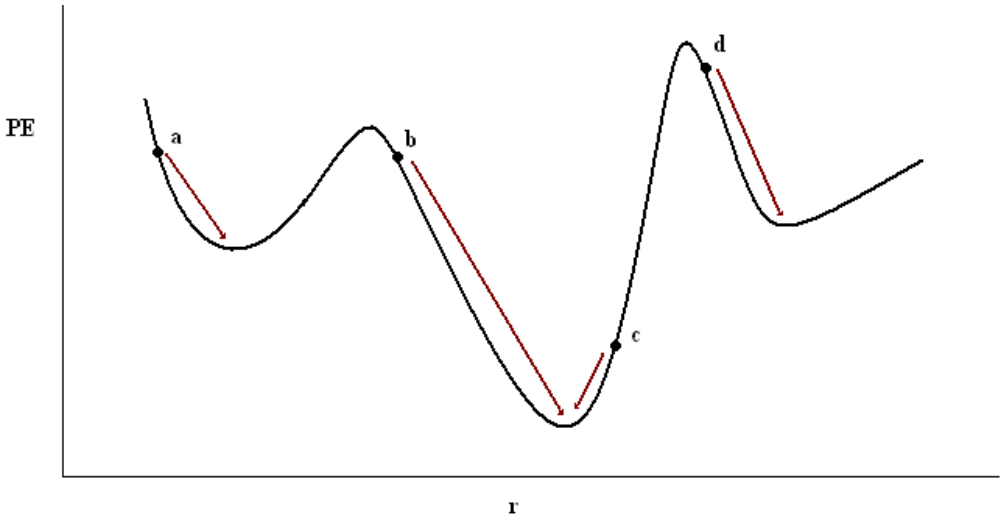

Figure 2.8: One-dimensional potential energy surface.

Figure 2.8 illustrates this. While the steepest descent method will find the global minimum for the set of initial nuclear coordinates designated by **b** or **c**, the coordinates designated by **a** or **d** will only minimise to local energy minima on the potential energy surface. Therefore, the initial geometry of the system is important. Initial geometries may be obtained from various sources, such as X-ray crystal structures, docking calculations, or molecular dynamics simulations.

Steepest descent methods can show oscillatory behaviour in long, narrow valleys of a potential energy surface. AMBER therefore uses steepest descent for 10 cycles, followed by the conjugate gradient method[117] (this is the default for AMBER 8, and the method used in this work).

2.5.3.1 Setup and Implementation of Molecular Mechanics Minimisations

Unlike the docking calculations, molecular mechanics minimisations require the ligand to be present in the PDB file. And while it is better if hydrogen atoms are not present on the protein, it is essential that they be added to the ligand and cofactor beforehand (which can be done in InsightII). Water molecules should not be present.

LEaP is the program, as part of the AMBER 8 package, that produces the *inprcd* (initial coordinates) and *prmtop* (parameters and topology) files for AMBER calculations. LEaP will add appropriate hydrogens to amino acids, but not to ligands or cofactors. It is also used to add a water box to the system in order to model solvent behaviour (discussed further in Section 2.5.4.2).

A force field must be specified for LEaP. For all calculations performed, the FF03 force field[118] was used to model the protein, and GAFF, the general AMBER force field[119], was used for ligands and cofactors. The FF03 force field utilises charges derived from quantum calculations, and a continuum dielectric to mimic solvent polarisation. The GAFF was designed to be compatible with any protein force field, and is used in conjunction with Antechamber and Parmchk to generate preparatory files for ligands and cofactors.

Antechamber and Parmchk are a pair of programs in the AMBER 8 package, used for generating parameter files for small molecules. For all calculations, the AM1-BCC charge method[120], which was designed to mimic HF/6-31G*, was used to determine atom types for the ligands and cofactors.

All prep files are given in Appendix B.

Sander is the program in the AMBER 8 package that actually performs the molecular mechanics calculations. For all molecular mechanics minimisations, a maximum of

10,000,000 cycles was specified, and two successive minimisations were performed to ensure that the minimum was actually reached, as there is a possibility that a single minimisation could terminate before the cut-off criteria are actually reached. Default AMBER 8 values were used for all other calculation parameters.

2.5.4 Molecular Dynamics[53,54]

Molecular dynamics is a molecular modelling method aimed at studying the behaviour of a system over time. This is done by integrating Newton's second law of motion:

$$F = ma \tag{18}$$

where F is the force acting on a particle, m is the mass of the particle, and a is the acceleration of the particle. Essentially, every atom in the system is given an initial, random velocity, and from this and the nuclear position forces are calculated, and over a short time step new positions and velocities are determined. In this manner a trajectory for the system is generated.

2.5.4.1 Timescale

In addition to its utility in determining the structure corresponding to the global energy minimum, molecular dynamics is useful for studying general features of protein movement and flexibility[111,121], the interactions between proteins and ligands[122], and hydrogen bonding/solvent interactions[123].

Because molecular dynamics looks at the changes in a system over time, it is important to know the timescale of conformational changes in a molecular system. The fastest movements—bond-angle vibrations—occur on a femtosecond timescale[124]. Small localized movements, such as the motions and rearrangements of amino acid side chains, occur on a picosecond timescale[125]. Small changes to protein structure, such as small loop movements and other reorientations of the protein backbone, can occur on a nanosecond timescale, while protein folding occurs on a scale of microseconds to milliseconds, or longer[126,127]. Ligand binding generally occurs on a microsecond-plus timescale[128]. While microsecond timescale molecular dynamics simulations have been performed using novel parallel-processor approaches[126], such a method was not feasible for this work, and as such the scope of this work has been limited to the nanosecond timescale. While this will not allow for the modelling of ligand binding from the starting point of free ligand in solution, it can show whether a ligand present in the active site at the start of the simulation is truly bound or not.

The choice of time step is important. Too large a time step, and the simulation will not be able to accurately model the system of interest; too small a time step, and it will simply take too much time to model a timescale of interest, due to the limitations of computing power available at present.

The time step must be at least an order of magnitude smaller than the fastest periodic motion if any reliable data is to be obtained from the MD run. As time step comparable with the time-period of the fastest motions leads to large inaccuracies arising from the approximations used to deal with forces that change constantly through the time step. Thus time-reversibility is lost, and conservation of energy/momentum is lost without this. For all molecular dynamics simulations in this work, a 2 femtosecond time step was used. This is

short enough to model the timescale of interest, but not too short for the simulation to be limited by the computer processing power currently available.

2.5.4.2 Periodic Boundary Conditions and Solvent Modelling

In order to accurately model how a protein behaves *in vivo*, the inclusion of bulk solvent in the system is necessary. Not only does this restrict the movement of the protein (as water would *in vivo*), but it also dampens long-range protein-protein interactions, and allows for the modelling of solvent-protein interactions, such as hydrogen bonds.

To model bulk solution perfectly, a nearly infinite amount of water molecules would be required; otherwise there is a possibility that the protein could reach the "edge" of the system and no longer be completely surrounded by solvent molecules. In order to avoid this, periodic boundary conditions are applied. Essentially, what this means is that the entire system is enclosed in a "box" (although it does not necessarily have to be a cube) and for every atom that moves outside the box, an image of the atom appears on the opposite side. In this manner the protein effectively interacts with an unlimited supply of water molecules. Ideally, the fewer water molecules in the system the better, as computation time increases as the number of atoms increases, but it is important that the dimensions of the box be such that the protein cannot interact with itself across the periodic boundary.

For all molecular mechanics and molecular dynamics simulations the TIP3P[(129)] water box was used, with a depth of 10 angstroms from the protein to the periodic boundary. This ensures that the protein cannot interact with itself across the periodic boundary, as the maximum cut-off used for non-bonded interactions is 8 angstroms (the AMBER default for

the Particle Mesh Ewald method). TIP3P is a 3-site model, with a point charge for each atom, and Lennard-Jones parameters for the oxygen.

2.5.4.3 Temperature and Equilibration

In order to accurately model a biological system, molecular dynamics simulations are run at 300K, which is approximately room temperature. This gives the system the appropriate energy, similar to what it would have *in vivo*. The weak-coupling algorithm[130] continually removes energy from the system in order to maintain a constant temperature.

Because the initial velocities assigned to the atoms in the first step of a molecular dynamics run are random, if the system is not properly minimised beforehand, the initial forces calculated could potentially be strong enough to denature the protein. Therefore, the first step in any molecular dynamics simulation is a molecular mechanics optimisation.

The TIP3P water box is a snapshot of room-temperature water at equilibrium. This does not, however, mean that the *system* is at equilibrium. Therefore, the second step in a molecular dynamics run is a 200ps equilibration run. This allows the water to equilibrate with the protein and any ligands or other molecules present, before the actual simulation run is performed. Specifically, the vibration energy is equilibrated so that it is evenly distributed across all vibrational modes

2.5.4.4 Setup and Implementation of Molecular Dynamics Runs

Sander has a variety of parameters and variables for molecular dynamics which can be modified according to what type of system is being studied, and what results are required.

As stated previously, every molecular dynamics run begins with a molecular mechanics minimisation. The output from a minimisation is then used as the input for a set of three molecular dynamics equilibration runs. Three dynamics runs are done for every molecular mechanics minimisation because initial velocities are assigned to atoms randomly, and there is a chance that the forces calculated from these velocities could cause the protein to denature, change to a non-productive conformation, or at the very least cause the ligand to be ejected from the active site. However, with three sets of different initial velocities, the results can be viewed with greater confidence if at least two of them are the same.

All molecular dynamics runs were performed with a 2fs time step, and a constant temperature of 300K. Bond lengths were constrained using the SHAKE algorithm[131], and bonding interactions were omitted for force evaluations. Energies were recorded every 200fs, and coordinates and velocities were recorded every 10ps for equilibration runs, and 50ps for all following runs. Default values were used for all other parameters.

Each dynamics run consists of a 200ps equilibration run, followed by ten 1ns runs, for a total of 10ns for evaluation.

2.6 Hybrid QM/MM (ONIOM)[54]

Hybrid QM/MM methods are a "best of both worlds" approach to molecular modelling. In hybrid QM/MM calculations, the portion of the system where bonds are being formed or broken, or where knowledge of electron distribution is important, quantum mechanical methods are employed. For the rest of the system, which may contribute electrostatic interactions, hydrogen bonding, or simply steric effects, molecular mechanics methods are used.

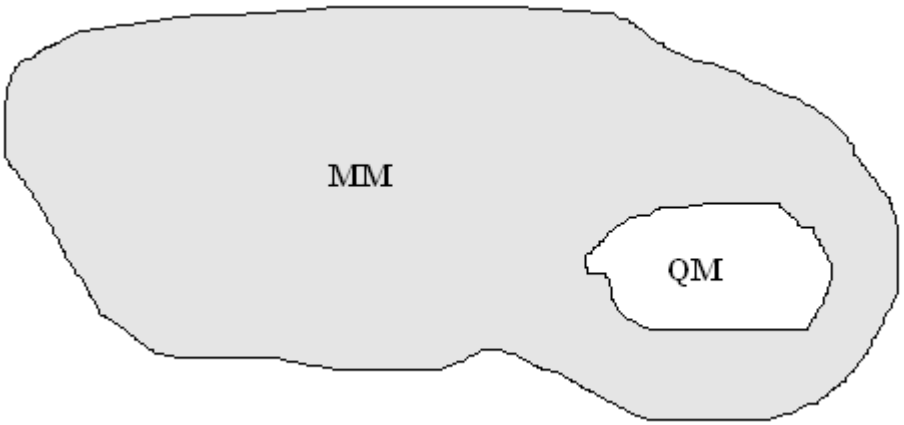

Figure 2.9: Hybrid QM/MM. Portions of the system which require information about electronic structure are studied at the QM level (white) while the remainder of the system is studied at the MM level (grey).

The simplest way to describe the Hamiltonian equation for hybrid QM/MM methods is as follows:

$$H_{complete} = H_{QM} + H_{MM} + H_{QM/MM} \quad (19)$$

where H_{QM} describes the interaction between atoms in the quantum mechanics section, H_{MM} describes the interaction between atoms in the molecular mechanics section, and $H_{QM/MM}$ describes the interactions between the atoms in the quantum mechanics section and atoms in the molecular mechanics section.

In an ONIOM[132-138] calculation, rather than having discrete QM and MM sections, there is a "real" system (all atoms present), and a "model" system, where the model system is a subset of the real system.

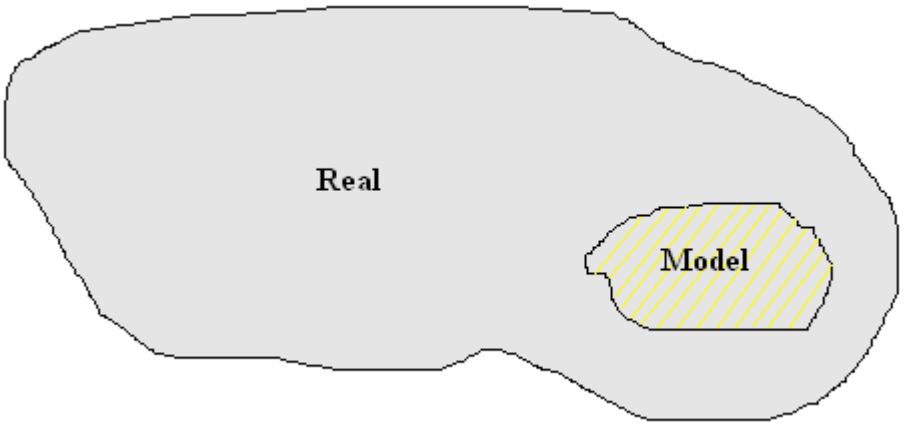

Figure 2.10: In an ONIOM calculation, a MM calculation is performed on the entire system—the "real" system (grey)—while a QM calculation is performed on the "model" system (yellow) and the MM energy for the "model" system is subtracted from the total energy.

In a two-layer ONIOM calculation (as shown in Figure 2.10), a molecular mechanics calculation is performed on the "real" system, and then the "model" system is subtracted from this. The partial charges from the "real – model" (molecular mechanics) system may then be incorporated into the Hamiltonian for the "model" (quantum mechanics) section (electrostatic embedding). This effectively models the electrostatic interactions between the quantum mechanics and molecular mechanics systems. In other words, the quantum mechanics wavefunction is polarised by the point charges from the molecular mechanics system. Alternatively, ONIOM calculations may be performed without electrostatic embedding which will allow only a steric effect of the real system on the model system.

There are a variety of other ways to perform ONIOM calculations, but the method described here was the one used for all of this work.

2.6.1 Setup and Implementation of ONIOM Calculations

The first step in an ONIOM calculation is to assign atom type. This is done in a similar method to the docking setup, using InsightII[114] and the cff91 force field[112,113]. Once the atom types are assigned, the system must be saved as a MOL2 file. This is then converted to a Gaussian03 input file (.com) with Cartesian coordinates using a file conversion program such as Babel[139]. The charges must be manually added from the MOL2 file to the Gaussian input file.

ONIOM calculations are performed in Gaussian03. For all calculations, the molecular mechanics section used the UFF[140] force field and the quantum mechanics section used the 6-31g** basis set[62-72] and the MPW1PW91 DFT functional[75-80].

Chapter 3

Hydride Transfer

This chapter describes the gas-phase quantum mechanics calculations utilised to study the possible hydride transfer mechanisms for the reaction between CB1954 and the FMN cofactor of NTR.

3.1 Hydride Transfer

As NTR itself is reduced by NAD(P)H via hydride transfer, it is logical to begin by looking at the reduction of CB1954 by NTR via hydride transfer as well. However, because of the inherent complexity of these calculations (two different nitro groups, multiple different possible orientations) preliminary calculations were performed using nitrofuran, which only has one nitro group, and no other ring substitutions. NTR is known to reduce a wide variety of nitrofurans, one of which is nitrofurazone[16].

3.2 Infinite Separation Calculations for Nitrofuran

All calculations take time, but one quick and easy method for getting a rough comparison of the two possible hydride transfer products—to the nitrogen of the nitro group, or one of the oxygens—is to take the FMN and nitrofuran separately and optimise the reactants and products of the hydride transfer for both molecules, and then sum their energies. This effectively gives the energy of reaction, treating the molecules as though they were at infinite separation.

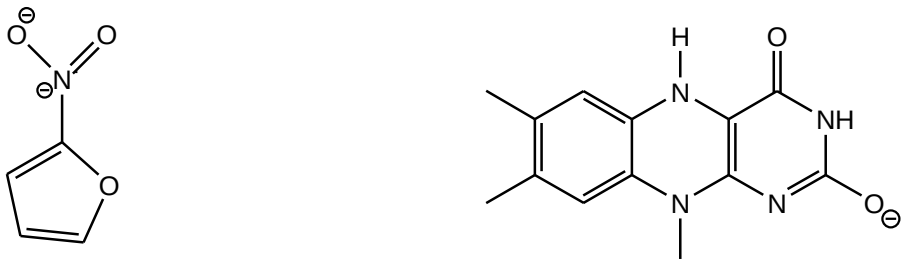

Figure 3.1: Infinite separation hydride transfer reactants.

Infinite separation calculations are much quicker because no bonds are actually being made or broken, and there are no interactions between the molecules. Unfortunately, they do not give any information about reaction barriers or molecular orientations. Still, they are useful as a basis for comparison, to see what effects molecular orientation and orbital overlap have on the energies of the reactions.

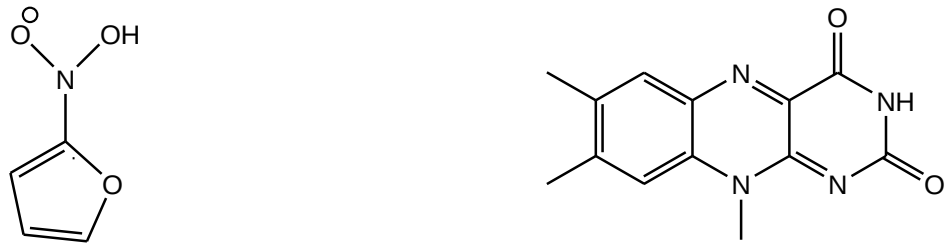

Figure 3.2: Infinite separation hydride transfer to oxygen products.

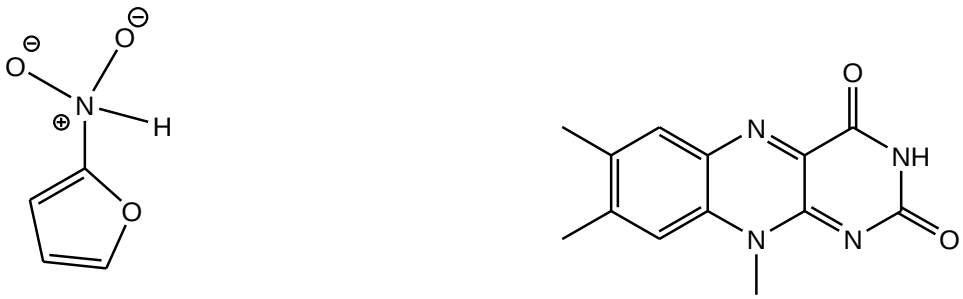

Figure 3.3: Infinite separation hydride transfer to nitrogen products.

Infinite separation calculations were performed in Gaussian03, which reports energies in units of Hartree. In order to make these numbers more meaningful, they were converted to kcal/mol with the energy of the reactants arbitrarily set to zero. One Hartree is equal to 627.509391 kcal/mol. Infinite separation calculations were performed at the MPW1PW91/6-31G** level.

3.2.1 Results of Nitrofuran Infinite Separation Calculations

MPW1PW91/6-31G**	Energy (Hartree)	Energy relative to reactants (kcal/mol)
Reactants	−1307.00937	0
Hydride transfer to nitrogen products	−1306.90434	65.87
Hydride transfer to oxygen products	−1306.93768	44.96

Table 3.1: Reactants and products of hydride transfer from reduced FMN to nitrofuran at infinite separation.

While these results most certainly do not tell the whole story, they do immediately provide two important pieces of information: in both cases hydride transfer at infinite separation is endothermic, and hydride transfer to oxygen is favoured over hydride transfer to nitrogen.

3.3 Preliminary Transition State Calculations for Nitrofuran

As discussed in Section 2.3.1, preliminary transition state calculations are done using MOPAC 6.0 and the semi-empirical AM1 model. In addition to the greater speed of finding transition states, MOPAC utilises a more flexible optimiser than Gaussian03—one that does not cause the calculation to fail should the number of negative eigenvalues change as the transition state is approached. MOPAC calculations were restricted to the singlet state, as with hydride transfer it is expected that all electrons will remain paired.

A variety of different orientations of nitrofuran with respect to FMN were tested, and a total of four transition state geometries were found; three for the hydride transfer to the oxygen of the nitro group, and one for the hydride transfer to the nitrogen of the nitro group.

Frequency calculations confirmed that they were indeed transition states, and IRC calculations were used to find the products and reactants.

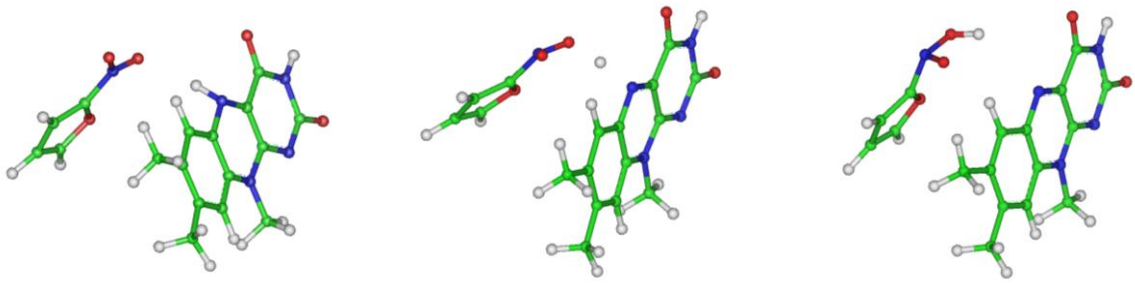

Figure 3.4: Reactant, transition state, and products geometries of the hydride transfer from FMN to an oxygen of the nitrofuran nitro group, Orientation A—nitrofuran ring overlapping FMN.

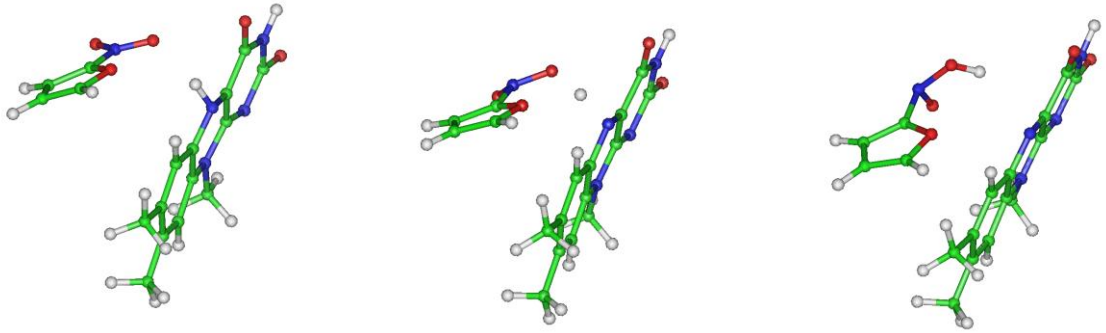

Figure 3.5: Reactant, transition state, and products geometries of the hydride transfer from FMN to an oxygen of the nitrofuran nitro group, Orientation B—nitrofuran ring rotated 90^{o} with respect to Orientation A.

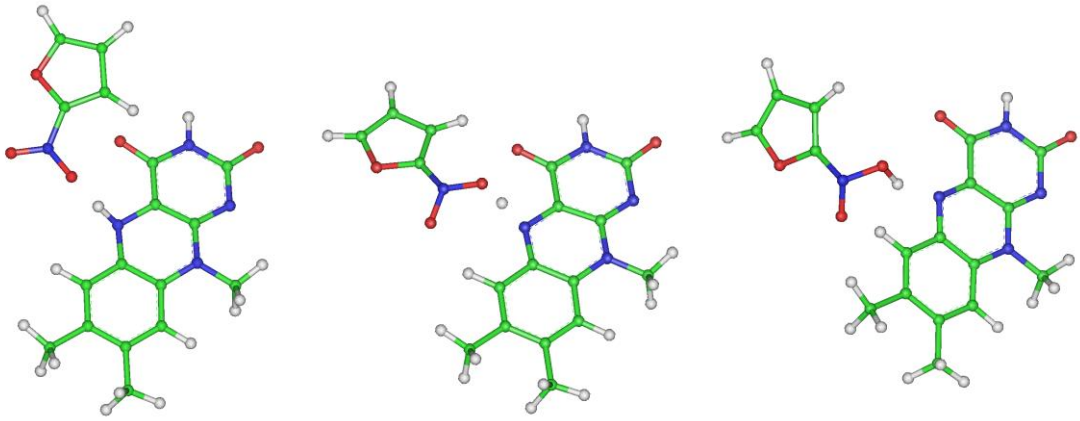

Figure 3.6: Reactant, transition state, and products geometries of the hydride transfer from FMN to an oxygen of the nitrofuran nitro group, Orientation C—nitrofuran ring rotated 180^{o} with respect to Orientation A.

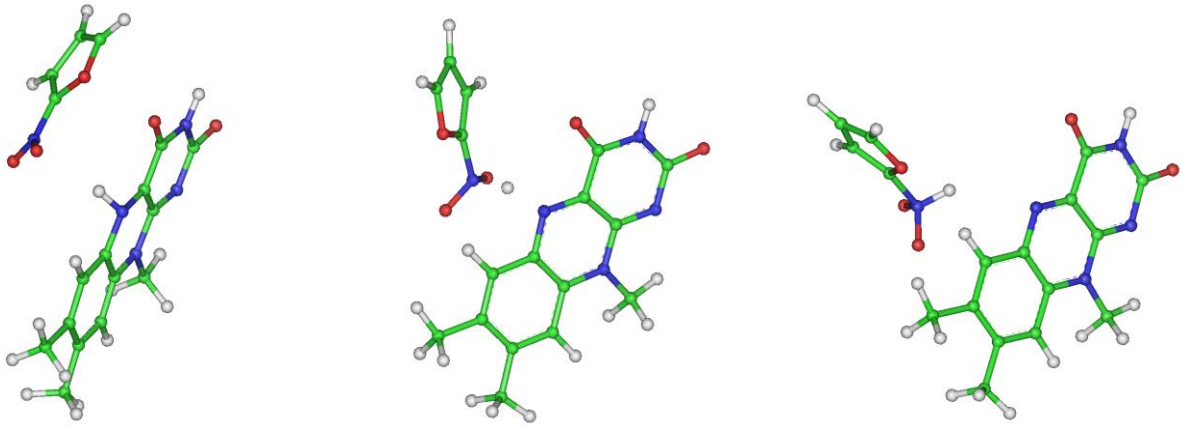

Figure 3.7: Reactant, transition state, and products geometries of the hydride transfer from FMN to the nitrogen of the nitrofuran nitro group (Orientation D in Table 3.2).

MOPAC 6.0 reports enthalpies in kcal/mol, and from the enthalpies of the products, reactants, and transition state, the activation enthalpy (transition state − reactants) and enthalpy of reaction (products − reactants) can be determined.

	Step	N_{FMN} – H distance (Å)	H – acceptor distance (Å)	Energy (kcal/mol)	Activation Enthalpy (kcal/mol)	Enthalpy of Reaction (kcal/mol)
A	react.	1.00	2.33	−36.27	44.98	6.23
	t.s.	1.33	1.23	8.71		
	prod.	2.82	0.97	−30.04		
B	react.	1.01	2.28	−34.55	43.94	6.02
	t.s.	1.32	1.24	9.39		
	prod.	2.73	0.97	−28.53		
C	react.	1.01	2.42	−39.81	45.97	10.27
	t.s.	1.37	1.20	6.16		
	prod.	2.95	0.97	−29.54		
D	react.	1.01	3.28	−36.11	59.42	43.07
	t.s.	1.48	1.29	23.31		
	prod.	2.77	1.06	6.96		

Table 3.2: Distance from hydride to donor (N5 of FMN) and acceptor (oxygen or nitrogen of the nitro group), AM1 energy, activation enthalpy and enthalpy of reaction of the four reaction orientations (Figures 3.4-3.7).

Based on the activation enthalpy and enthalpy of reaction results, it would appear that different orientations of the nitrofuran with respect to FMN do not affect the activation enthalpy or overall enthalpy of the reaction in any significant way. However, the activation enthalpy and enthalpy of reaction for the hydride transfer to nitrogen were significantly larger than any of the activation enthalpies found for a hydride transfer to an oxygen. This would indicate that, at least in the gas phase, hydride transfer to an oxygen of the nitro group is much more favourable than hydride transfer to the nitrogen of the nitro group. Additionally, enthalpies were substantially lower than the corresponding energies of reaction at infinite separation. While this may be in part due to a change in level of theory (semi-empirical vs *ab initio*), it is likely that intermolecular interactions also played a significant part—particularly for the transfer to oxygen.

These preliminary transition state geometries were inserted into the active site of the enzyme in order to determine what amino acids are most likely to affect substrate binding.

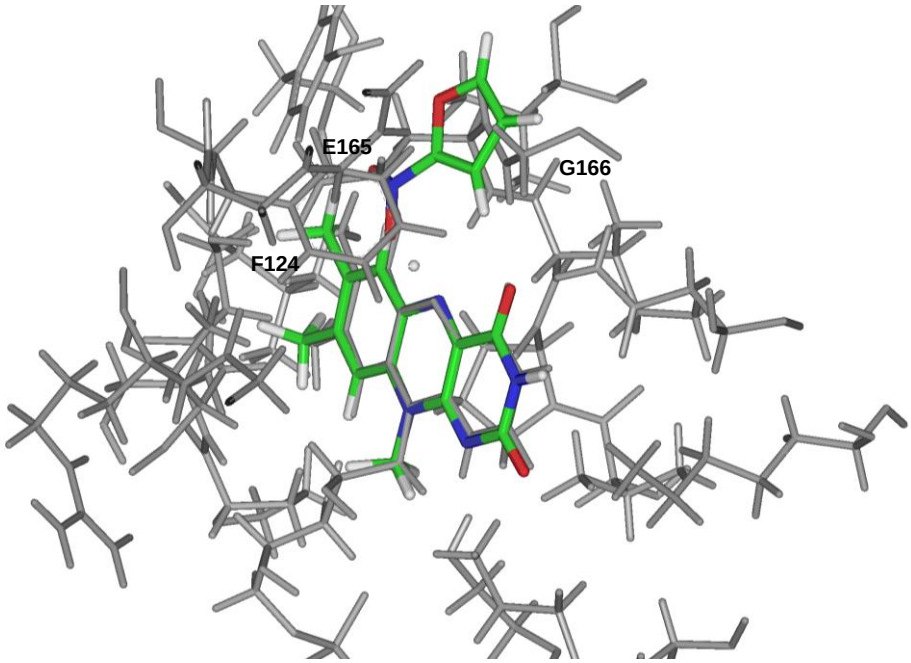

Figure 3.8: AM1 transition state for the hydride transfer to nitrofuran Orientation C superimposed in the active site of NTR from the 1YKI crystal structure[16].

Three amino acids were identified as most likely to interfere with substrate binding: Glu165, Gly166, and Phe124. Unfortunately, these three were actually three of the six amino acids already identified by the experimental group as either potential mutants, or critical to enzyme activity (see Section 1.6), and therefore no new information was obtained. However, these results do show that the information obtained by computational methods is in good agreement with those obtained from experiments.

3.4 Ab Initio *Transition State Calculations for Nitrofuran*

The orientations for the four transition states found at the AM1 level using MOPAC 6.0 were subsequently used in Gaussian03 at the MPW1PW91/6-31G** level in order to find more accurate energies and geometries. As with the semi-empirical calculations, all *ab initio* transition state calculations were performed in the singlet state, with RHF. Of the four, only orientation C ever reached a transition state.

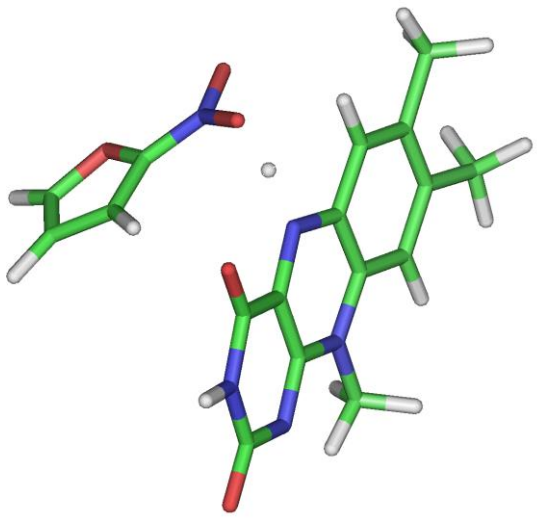

Figure 3.9: Nitrofuran transition state at the MPW1PW91/6-31G** level in Gaussian03.

As with the AM1 transition states, IRC calculations were used to confirm reactants and products. Additionally, Mulliken charges were used to determine the molecular charge of FMN and nitrofuran. Full Mulliken charges for all calculations are given in Appendix A.

Step	N_{FMN} – H distance (Å)	H – O_{nit} distance (Å)	Charge on FMN[a]	Charge on nitrofuran[a]	Energy[b] (kcal/mol)	Activation Energy (kcal/mol)	Reaction Energy (kcal/mol)
react.	1.01	2.48	−0.93	−0.07	0	21.11	17.62
t.s.	1.41	1.11	−0.89	−0.54	21.11		
prod.	2.19	0.98	−0.77	−0.23	17.62		

Table 3.3: Reactants, products and transition state for the hydride transfer from FMN to nitrofuran at the MPW1PW91/6-31G** level. [a] The partial charge for the hydrogen being transferred is included in the charge on FMN for the reactants and on nitrofuran for the products, but not included on either for the transition state. [b] Energy values are converted from Hartree to kcal/mol, with the value for reactants set to zero.

Compared to the semi-empirical transition states, the activation energy is about 20 kcal/mol less, but the reaction energy is about 10 kcal/mol greater. Additionally, the charges on the two molecules appear to show that this is not strictly hydride transfer, but rather no net transfer of charge accompanies the transfer of a proton, indicating that there must be a substantial overlap of orbitals across the two molecules.

3.5 Reaction Profile for Hydride Transfer to Nitrofuran

Hydride transfer transition state calculations in Gaussian03 at the MPW1PW91/6-31G** level make use of the RHF approach and are performed in the singlet state—all electrons paired—because the traditional view of hydride transfer is one proton and two electrons transferred simultaneously. This method has the advantage of making the calculations faster, but it may not necessarily model the true reaction pathway. The results

described in Section 3.4 do not sit comfortably with this idea of true hydride transfer. Though a transition state is observed for the H transfer, this is not accompanied by the transfer of a full negative charge as we might expect for true hydride transfer. In order to obtain a better idea of what the reaction pathway might be, a full reaction profile for the hydride transfer to nitrofuran has been determined, relaxing the requirement that all electrons remain paired.

Starting with the reactant geometry obtained from the Gaussian03 IRC calculation, the distance between the "hydride" and the N5 on FMN, and an oxygen of the nitro group on nitrofuran, are fixed, while all other geometric coordinates are allowed to optimise normally. For each subsequent step, the "hydride" is moved incrementally away from N5 of FMN, and towards the oxygen of nitrofuran, through the transition state geometry, and finishing with the product geometry. At each step geometries are optimised for both singlet and triplet (outermost two electrons unpaired) electronic states and the resulting energies recorded. This allows us to consider the possibility of separate proton and electron transfer.

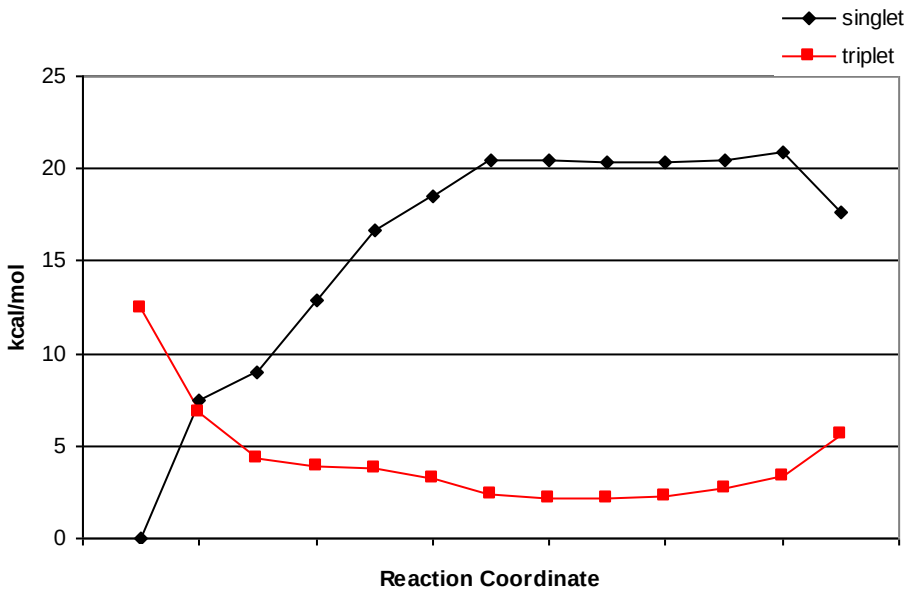

Figure 3.10: Reaction profile for the "hydride" transfer from FMN to an oxygen of the nitrofuran nitro group at the MPW1PW91/6-31G** level.

Figure 3.10 clearly shows that traditional hydride transfer is not the favoured mechanism for the reduction of nitrofuran by FMN in gas phase. While the singlet is undoubtedly lower in energy at the reactants, the triplet is lower in energy by approximately 15 kcal/mol at the hydride transfer transition state, and 12 kcal/mol at the products. Analysis of the orbital coefficients for the two singly occupied molecular orbitals confirmed that these orbitals reside on separate molecules, consistent with a single electron transfer from FMN to nitrofuran.

This suggests that the actual reaction studied is the transfer of a single electron, and a proton from FMN to nitrofuran. It is noticeable that as the optimised product still prefers the triplet state, the second electron will not be transferred—completing net hydride transfer—until some other event occurs to restabilise the singlet state.

3.6 Infinite Separation Hydride Transfer Calculations for CB1954

Infinite separation calculations were performed for CB1954 in a manner similar to those performed for nitrofuran. Because CB1954 has two nitro groups that are reduced equally by wild-type NTR, it is of interest to compare the 2-nitro and 4-nitro reduction products independent of intermolecular interactions. Because there are two nitro groups, and two potential hydride acceptors per nitro group, there are a total of four possible hydride transfer products per CB1954 molecule.

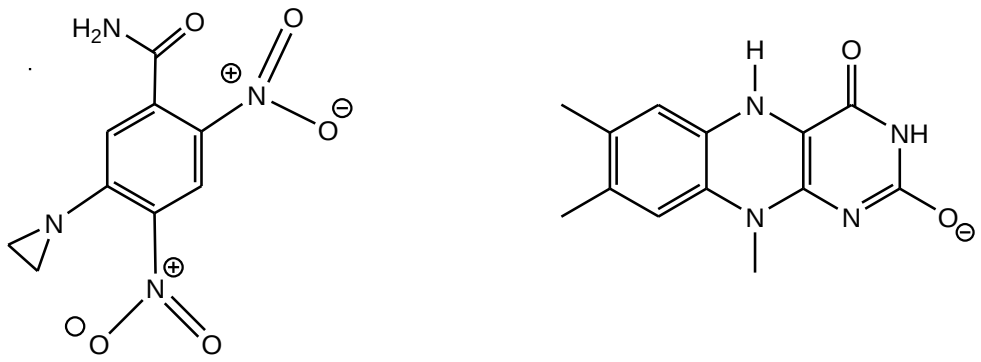

Figure 3.11: Infinite separation hydride transfer reactants for CB1954.

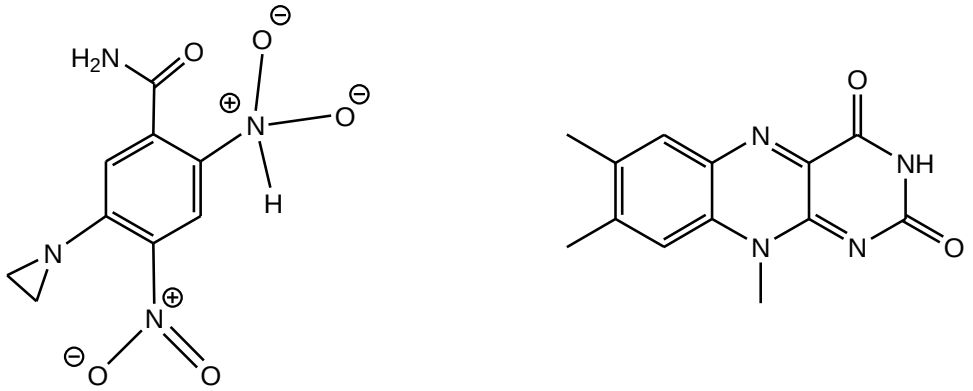

Figure 3.12: Infinite separation hydride transfer to 2-nitro nitrogen of CB1954 products.

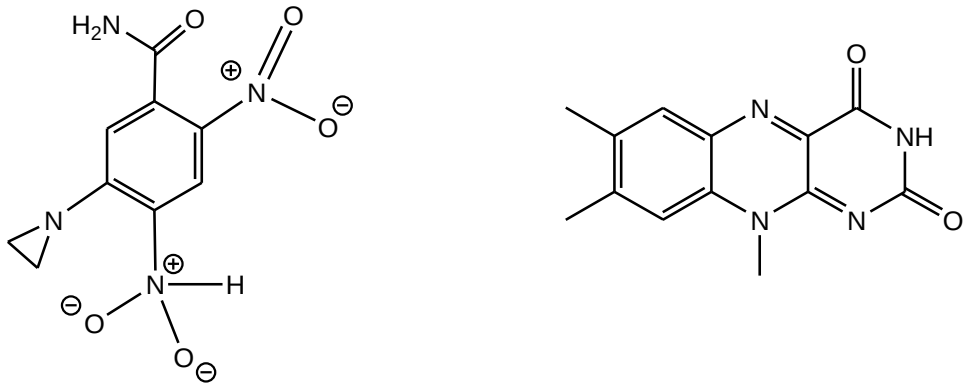

Figure 3.13: Infinite separation hydride transfer to 4-nitro nitrogen of CB1954 products.

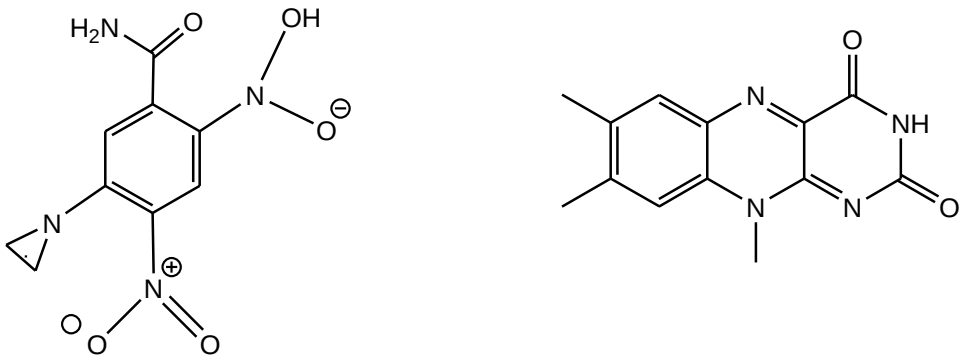

Figure 3.14: Infinite separation hydride transfer to 2-nitro oxygen of CB1954 products.

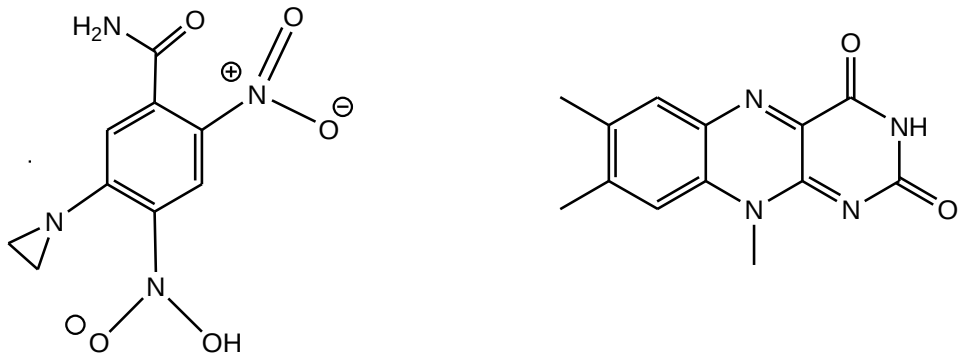

Figure 3.15: Infinite separation hydride transfer to 4-nitro oxygen of CB1954 products.

3.6.1 Results of CB1954 Hydride Transfer Infinite Separation Calculations

MPW1PW91/6-31G**	Energy (Hartree)	Energy relative to Reactants (kcal/mol)
Reactants	−1815.05690	0
Hydride transfer to 2-nitro nitrogen products	−1815.00968	29.61
Hydride transfer to 4-nitro nitrogen products	−1814.99150	41.02
Hydride transfer to 2-nitro oxygen products	−1815.03792	11.91
Hydride transfer to 4-nitro oxygen products	−1815.02955	17.15

Table 3.4: Reactants and products of hydride transfer to CB1954 at infinite separation.

Reaction enthalpies for infinite separation hydride transfer to both oxygen and nitrogen are ~ 25-35 kcal/mol less for CB1954 than for similar transfers to nitrofuran, but still endothermic in each case. This difference between CB1954 and nitrofuran is likely due to the fact that CB1954 is a larger molecule, with a greater potential to distribute the electron density throughout.

Surprisingly, the reaction enthalpy for 2-nitro reduction is ~ 5 kcal/mol less than the 4-nitro for the hydride transfer to oxygen, and ~ 10 kcal/mol less for transfer to nitrogen. This is contrary to experimental evidence, which has the 4-nitro as the group with the highest electron-affinity in the entire molecule[31]. However, the method of determining this electron affinity was radiolytic reduction using sodium formate, rather than hydride transfer. This difference may be due to the stretching of the N-O bond in the 2-nitro group, allowing formation of a hydrogen bond between one of the oxygens and a hydrogen of the adjacent amide group—something not possible for the 4-nitro product.

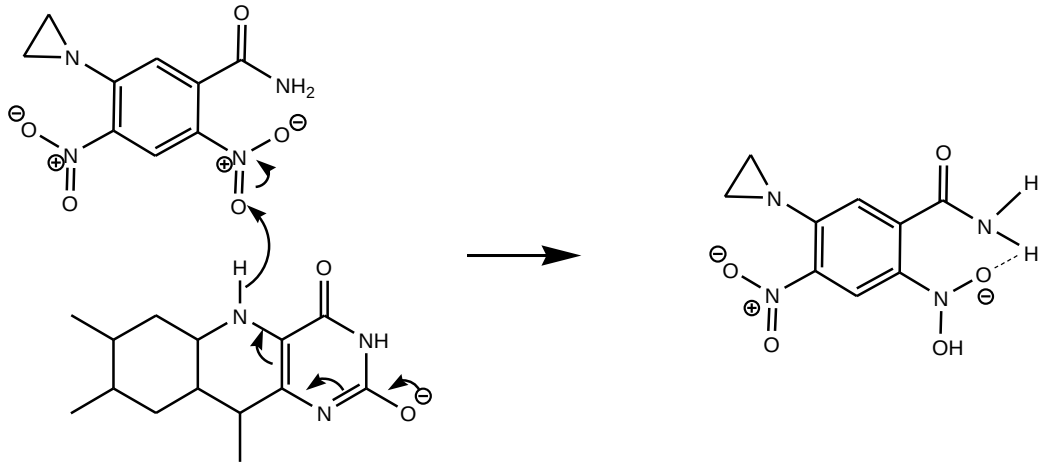

Figure 3.16: Close proximity of the 2-nitro group to the amide of CB1954 allows for interaction between one of the 2-nitro oxygens and the amide group during hydride transfer.

3.7 Ab Initio *Transition State Calculations for CB1954*

All of the semi-empirical transition state configurations, as well as the single *ab initio* transition state configuration (orientation C) were used as starting geometries for *ab initio* transition state calculations with CB1954. This was done in InsightII, with a simple overlay of the CB1954 nitro group and the nitrofuran nitro group. For each nitrofuran transition state, four possible CB1954 transition state geometries are generated; two because each CB1954 has two nitro groups, and two because of the asymmetry of the CB1954 molecule—a 180^{o} rotation around the C-N bond of the nitro group.

Like the transition state calculations for nitrofuran, transition state calculations for CB1954 were performed in the singlet state, with RHF.

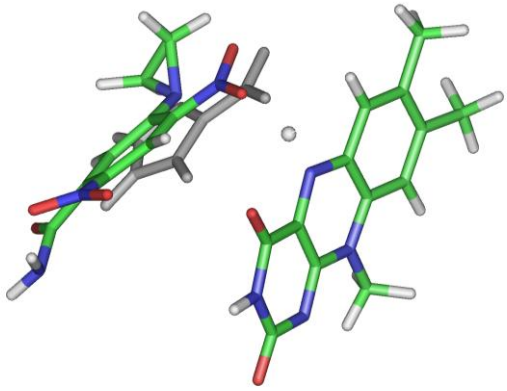

Figure 3.17: Nitro group overlay of CB1954 and nitrofuran in the *ab intio* transition state of nitrofuran and FMN. Nitrofuran is shown in grey, and CB1954 is offset slightly so the nitrofuran may be seen.

Of all the possible hydride transfer to CB1954 orientations, only one—to the 4-nitro oxygen, from the *ab initio* transition state of nitrofuran orientation C—converged to a transition state. Moreover, it took almost a full year for this single calculation to complete. All others either terminated in convergence failures, or optimised to reactants or products.

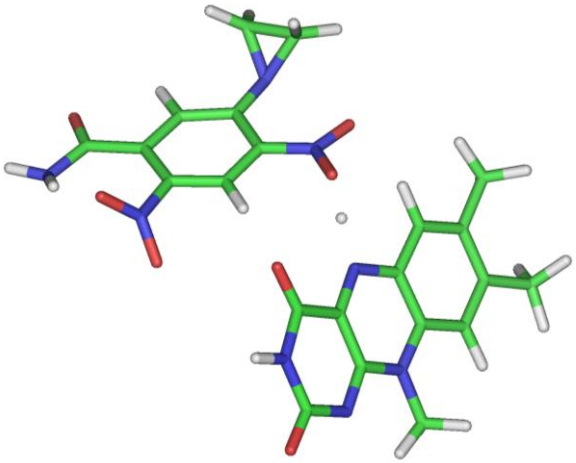

Figure 3.18: Hydride transfer from FMN to a nitro group oxygen at the MPW1PW91/6-31G** level.

As was the case for the nitrofuran transition state, IRC calculations were used to find reactants and products, and Mulliken charges were used to find the molecular charge of FMN and CB1954 for the reactants, transition state, and products.

Step	N_{FMN} – H distance (Å)	H – O_{CB} distance (Å)	Charge on FMN[a]	Charge on CB1954[a]	Energy[b] (kcal/mol)	Activation Energy (kcal/mol)	Reaction Energy (kcal/mol)
react.	1.02	1.96	−0.70	−0.30	0	13.11	7.41
t.s.	1.37	1.14	−0.68	−0.79	13.11		
prod.	2.27	0.98	−0.46	−0.54	7.41		

Table 3.5: Reactants, products and transition state for the hydride transfer from FMN to CB1954 at the MPW1PW91/6-31G** level. [a] The partial charge for the hydrogen being transferred is included in the charge on FMN for the reactants and on CB1954 for the products, but not included on either for the transition state. [b] Energy values are converted from Hartree to kcal/mol, with the value for reactants set to zero.

The activation energy for the hydride transfer to an oxygen of the CB1954 4-nitro group is ~ 8 kcal/mol less than for the equivalent reaction involving nitrofuran, and the energy of reaction is ~ 10 kcal/mol less. Additionally, there is significantly more charge transfer with CB1954. While a greater portion of the charge remains on FMN for the nitrofuran hydride transfer, and the charge on both molecules is similar for both reactants and products, the

CB1954 products show the CB1954 with a more negative charge than FMN. Even for the reactants there is significantly more of a negative charge on the CB1954 than there is for the nitrofuran. Again, this is likely due to the greater ability of CB1954 to delocalise electron density throughout the molecule.

It could be argued that this fits more closely with true hydride transfer than did the equivalent reaction involving nitrofuran, though even here we see transfer of only 0.24 of an electron charge. There is still significant charge on the FMN even for the products; this is likely due to the extensive orbital overlap between the two molecules.

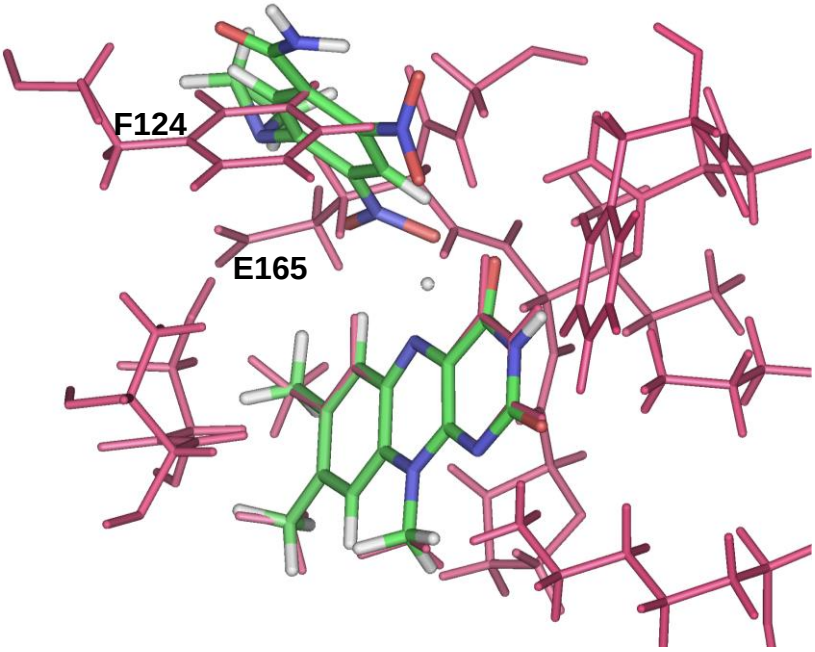

Figure 3.19: CB1954 gas-phase transition state geometry superimposed in the active site of the 1YKI crystal structure[16] of NTR.

Once again, the optimised gas-phase transition state was superimposed on the enzyme structure so that the flavin portions were overlayed. Figure 3.19 shows that like the nitrofuran transition state, the CB1954 gas-phase transition state does not fit well in the active site of NTR. Specifically, the position of CB1954 conflicts with the E165 side-chain and backbone, and the F124 side-chain.

3.8 Reaction Profiles for Hydride Transfer to CB1954

Hydride transfer reaction profiles were determined for CB1954 in a manner similar to the reaction profile determined for nitrofuran. Because no transition state geometry was found for hydride transfer to nitrogen, a full reaction profile was determined for comparison.

Reaction profiles were determined for the 4-nitro group only. Although infinite separation calculations showed the 2-nitro products to be lower in energy, the amide group adjacent to the 2-nitro consistently interfered with the stepwise hydride transfer to the 2-nitro, for example the amide group would donate a proton to one of the 2-nitro oxygens. Attempts to correct for this yielded convergence failures or meaningless results.

3.8.1 Reaction Profile for the Hydride Transfer to Nitrogen of CB1954

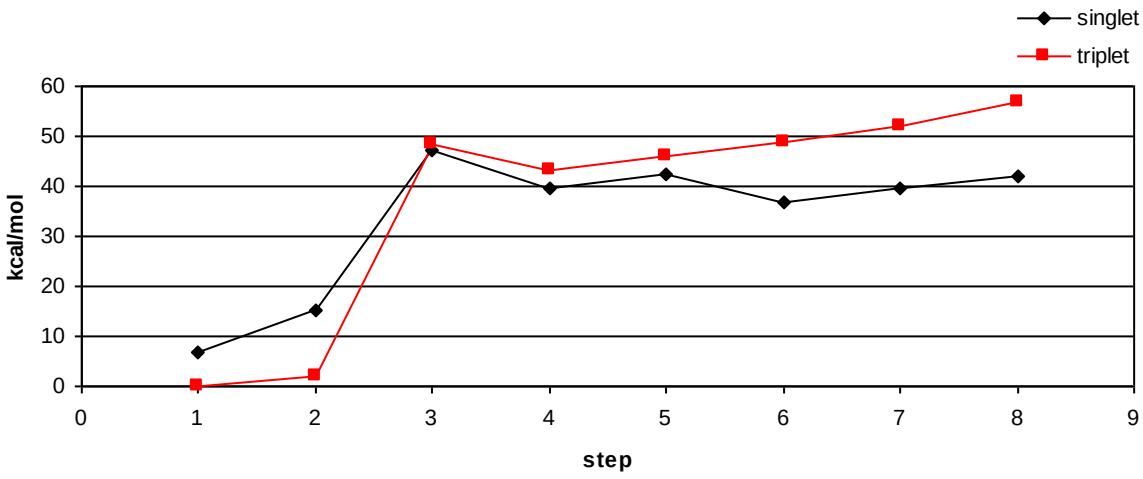

Figure 3.20: Reaction profile for the hydride transfer from FMN to the 4-nitro nitrogen of CB1954.

	Charge on FMN	Charge on CB1954	Energy (Hartree)	Energy relative to Reactants (kcal/mol)
Reactants triplet	−0.16	−0.84	−1815.064261	0
Reactants singlet	−0.66	−0.34	−1815.053132	6.98
Products triplet	−0.82	−0.18	−1814.973801	56.73
Products singlet	−0.18	−0.82	−1814.997453	41.90

Table 3.6: Molecular charges and energy of reactants and products in singlet and triplet states for the hydride transfer from FMN to nitrogen of the 4-nitro group on CB1954 at the MPW1PW91/6-31G** level.

With an activation energy of ~ 50 kcal/mol and an energy of reaction of ~ 40 kcal/mol, hydride transfer to nitrogen requires a substantial amount of energy. In fact, there is little difference in reaction energy between the infinite separation hydride transfer and the hydride transfer with FMN and CB1954 in close contact. Moreover, while there does appear to be a net transfer of a hydride, the fact that the triplet is lower in energy for the reactants and shows a predominantly negative charge on CB1954 indicates that the first electron transfer happens immediately, followed by the second electron as the proton moves from FMN to CB1954. The fact that the singlet is lower in energy for the products and the negative charge is predominantly on CB1954 shows that a total of two electrons and one proton have indeed been transferred.

Transition state optimisations in Gaussian03 for the hydride transfer to nitrogen at the MPW1PW91/6-31G** level failed to complete, resulted in convergence failure, or minimised to reactant geometry. Because a transition state was never found for the hydride transfer to nitrogen of CB1954, the 50 kcal/mol should be considered an upper limit, rather than the true reaction barrier. However, it could not be much less than that, as the energy of reaction is close to 40 kcal/mol.

3.8.2 Reaction Profile for the Hydride Transfer to Oxygen of CB1954

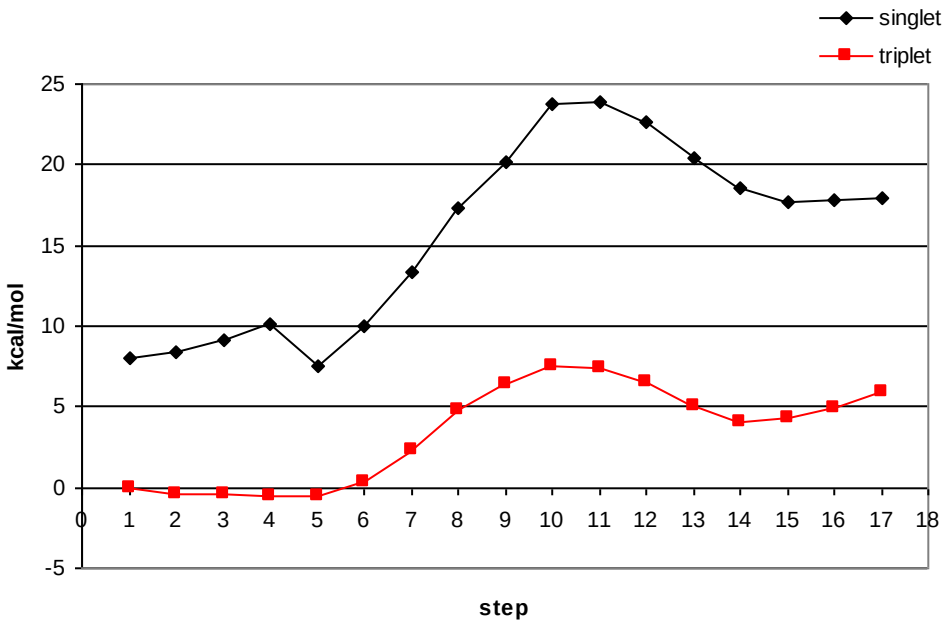

Figure 3.21: Reaction profile for the hydride transfer to a 4-nitro oxygen of CB1954. The sharp decrease between steps 4 and 5 for the singlet represents internal reorientation.

	Charge on FMN	Charge on CB1954	Energy (Hartree)	Energy relative to Reactants (kcal/mol)
Reactants triplet	−0.12	−0.88	−1815.08519897	0
Reactants singlet	−0.67	−0.33	−1815.07249632	7.97
Products singlet	−0.46	−0.54	−1815.05650742	17.99
Products triplet	−0.89	−0.11	−1815.07578849	5.90

Table 3.7: Molecular charges and energy of reactants and products in singlet and triplet states for the hydride transfer from FMN to oxygen of the 4-nitro group on CB1954 at the MPW1PW91/6-31G** level.

While the singlet line in Figure 3.21 truly represents hydride transfer (as reflected by the negative charge on FMN at singlet reactants being transferred to CB1954 at products), the triplet is lower in energy at every single point on the reaction profile. The actual reaction, therefore, involves an immediate transfer of an electron as the two molecules come into contact, followed by the transfer of a proton from FMN to CB1954. The molecular charges of both reactant and product complexes in the triplet state support this.

Obviously this reaction profile does not give a complete picture, as a total of two electrons must be transferred from FMN to CB1954. One possibility is that the amino acids in the active site affect the redox potentials of both FMN and CB1954 that the second electron is indeed transferred with the proton when CB1954 is bound to NTR. Another possibility is that the transfer of a proton from solution to the oxygen of CB1954—either before or after the proton from N5 of FMN—drives the transfer of the second electron.

3.9 Summary of Hydride Transfer Results

Infinite separation calculations for the hydride transfer from FMN to nitrofuran show that hydride transfer to oxygen is substantially more favourable than hydride transfer to nitrogen, and semi-empirical calculations confirm this. Only one *ab initio* transition state was found for hydride transfer to nitrofuran—to an oxygen of the nitro group—and the full reaction profile showed that the more favourable pathway was the transfer of a single electron, followed by the proton from FMN to nitrofuran.

Similar trends were found for CB1954 as for nitrofuran. Surprisingly however, the enthalpy for the hydride transfer to the 2-nitro group was lower compared to the 4-nitro, but this may be due to the interaction of the 2-nitro hydride product with the adjacent amide.

Hydride transfer reaction profiles show that while hydride transfer to the nitrogen of a nitro group on CB1954 is theoretically possible, it is thermodynamically prohibitive compared to a similar transfer to oxygen. Additionally, the lowest-energy pathway is actually the transfer of an electron, followed by a proton from FMN, rather than a hydride.

Essentially, hydride transfer to nitrogen can be ruled out as a possible mechanism, due to the high reaction enthalpy and consistent failure to find a transition state, while full hydride transfer to oxygen, while not ruled out, requires the presence of further functionality in addition to CB1954 and FMN in the gas phase. This latter observation is highlighted by a consideration of structures with unpaired electrons. For both nitrofuran and CB1954 reductions, a stepwise process involving the transfer of an electron followed by a proton is observed, but in both cases, the triplet state remains the most favourable "product" structure.

Chapter 4
Electron Transfer and Reaction Profiles

This chapter describes the gas-phase quantum mechanics calculations utilised to study the electron transfer mechanism, as well as full reaction profiles for all of the thermodynamically feasible mechanisms for the reaction between CB1954 and the FMN cofactor of NTR.

4.1 Electron Transfer

The idea behind the electron transfer mechanism is that the CB1954 obtains two electrons from FMN, and two protons from solution. Unlike the hydride transfer (or 'net' hydride transfer) mechanism, this does not require either nitro group to be bound in the active site; rather the nitro groups must simply be exposed to solution while some portion of the molecule is sufficiently close to FMN to obtain the electrons.

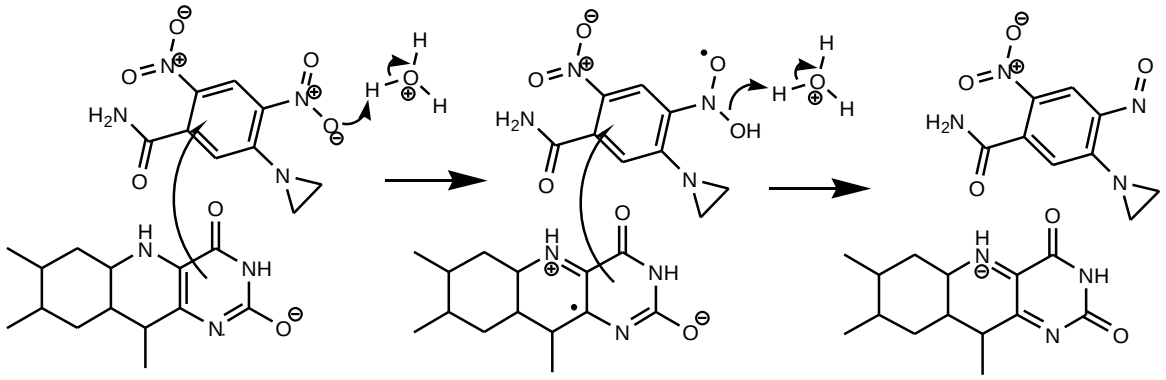

Figure 4.1: Electron transfer mechanism for the reduction of CB1954 by FMN. Individual electron transfers cannot be localised to particular atoms as both HOMO and LUMO [and SOMOs (singly occupied molecular orbitals) for the second step] are delocalised across their respective molecules. Hydroxonium ions represent solution.

4.2 Determination of Orbitals Relevant to Electron Transfer

Gaussian03 output files from simple geometry optimisations of reduced, truncated FMN and CB1954 at the MPW1PW91/6-31G** level were used in the visualisation program Molden[(141)] in order to obtain a graphical representation of the HOMO on FMN and the LUMO on CB1954.

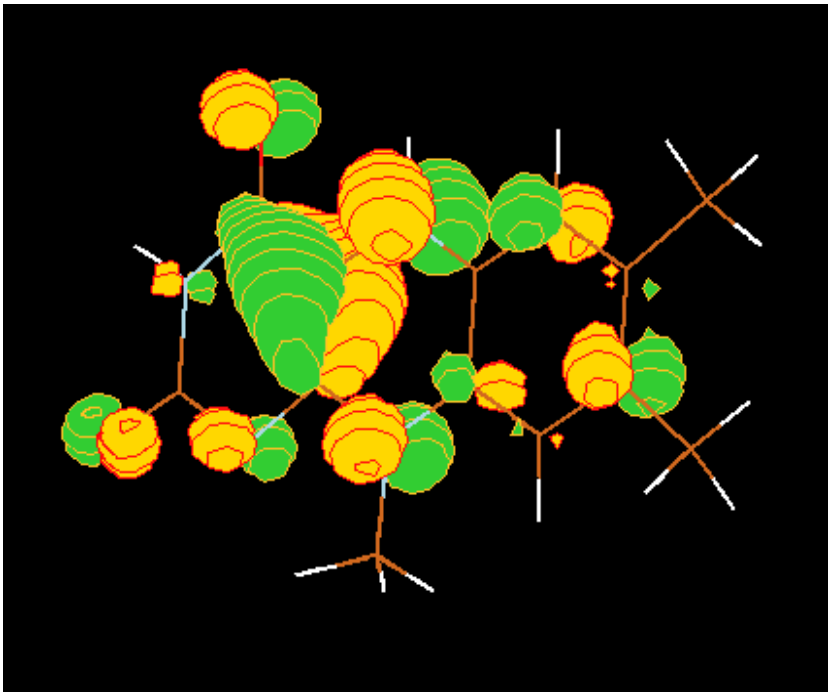

Figure 4.2: The HOMO on reduced, truncated FMN at the MPW1PW91/6-31G** level in Gaussian03.

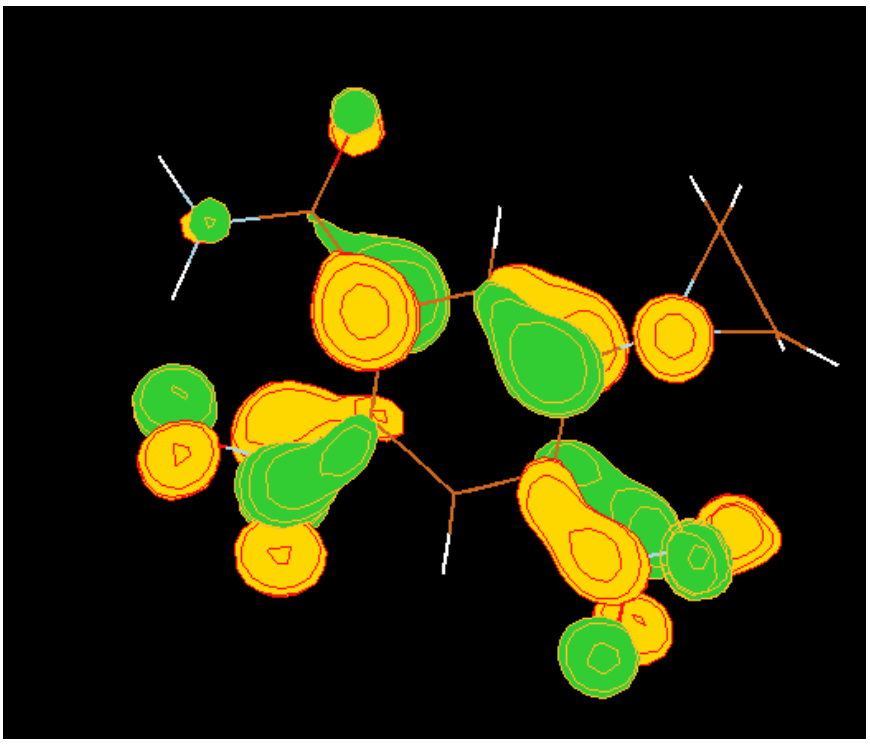

Figure 4.3: The LUMO on CB1954 at the MPW1PW91/6-31G** level in Gaussian03.

Both frontier orbitals show extensive delocalisation across their respective molecules. The electron density of the HOMO on FMN seems to be primarily concentrated around what is known to be the reactive area of the molecule—also closest to the opening of the active site of NTR. The LUMO on CB1954 appears to have a high degree of symmetry, with the orbital dispersed more or less equally across both nitro groups.

4.3 Electron Transfer Geometries

The extensive delocalisation of both the FMN HOMO and CB1954 LUMO causes some difficulty in identifying an appropriate orientation of the two molecules for electron transfer—so long as some part of each orbital is involved in effective overlap, electron transfer should be feasible. An initial orientation of the two molecules providing the maximum orbital overlap was determined.

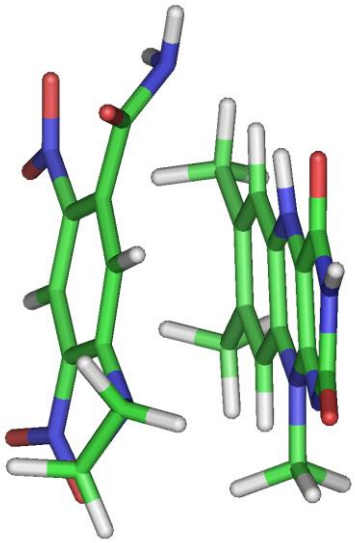

Figure 4.4: Molecular orientation of CB1954 and FMN to maximise overlap of HOMO on FMN and LUMO on CB1954.

While maximum orbital overlap is not strictly required for electron transfer, it is useful as a starting orientation, as an orientation with greater orbital overlap with have a lower barrier to electron transfer.

A series of geometry optimisations without constraints at the MPW1PW91/6-31G** level was performed on this structure for both the singlet and triplet state, in order to find the geometry with the lowest energy for the singlet state—the reactants for the first electron transfer—and the geometry with the lowest energy for the triplet state—the products for the first electron transfer.

While neither structure fits particularly well in the active site of NTR, the differences in charge on the two molecules and energy of the singlet and triplet state as the molecular orientation is changed does give useful information about the dependence of charge transfer on geometrical configuration.

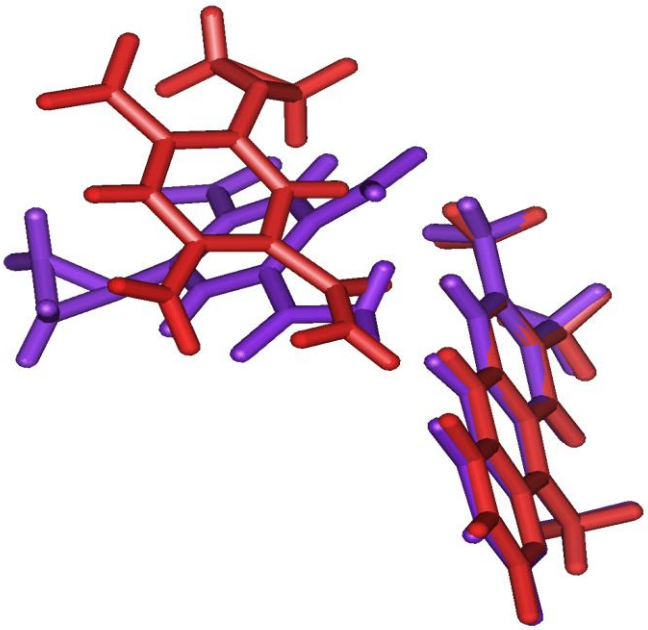

Figure 4.5: Optimal orientations for the singlet (red) and triplet (purple) states of FMN and CB1954.

	Charge on FMN	Charge on CB1954	Energy (Hartree)	Energy relative to singlet (kcal)
Optimised singlet (red) - reactant	−0.70	−0.30	−1815.079836	0
Triplet in reactant conformation	−0.04	−0.96	−1815.063832	10.04
Optimised triplet (purple) - product	−0.09	−0.91	−1815.076653	2.00
Singlet in product conformation	−0.48	−0.52	−1815.059104	13.00

Table 4.1: Molecular charges and energies for the optimal orientations for the singlet (red) and triplet (purple) states of FMN and CB1954.

Interestingly, while the position of CB1954 with respect to FMN is similar in both the singlet and triplet, there is a nearly 180^{o} difference in rotation across the amide – 4-nitro axis.

4.4 Electron Transfer Reaction Profiles

A full reaction profile for the transfer of the first electron from FMN to CB1954 is far more difficult to generate than a reaction profile for hydride transfer. For hydride transfer, only two variables were frozen: the distance from the hydride to the N5 of FMN, and to an oxygen or nitrogen of the nitro group of nitrofuran or CB1954. Because one hydrogen of the amide group of CB1954 remains nearly in the same position relative to the FMN for both the singlet and triplet geometries (see Figure 4.5), the distance from this hydrogen to the H_{N5} hydrogen of FMN, as well as the angles and dihedrals that define the amide group relative to FMN are frozen, and varied incrementally from step to step.

As for the study of hydride transfer (Chapter 3), reaction profiles were generated by fixing the specified variables at 10% intervals between each point transforming from reactant to product geometries.

4.4.1 Single-Point Electron Transfer Reaction Profile

Because of the difficulty in generating a full reaction profile with so many coordinates frozen (due to convergence failures, and optimisations to unreal geometries) for the first electron transfer reaction profile, only a single-point calculation, rather than a full geometry optimisation, was done for each point along the reaction pathway. In other words, starting from the reactants configuration, key interatomic distances, angles and dihedrals were incrementally changed stepwise, and the energy was calculated for the singlet and triplet at each step, in order to generate the following reaction profile (Figure 4.6).

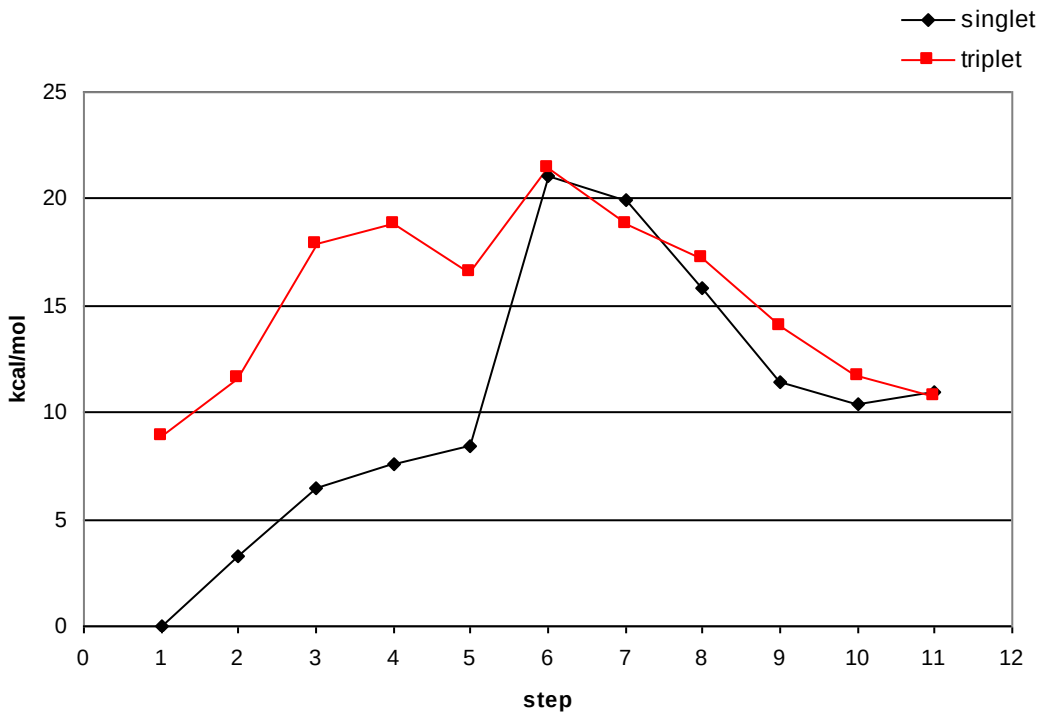

Figure 4.6: Reaction profile for the single-point electron transfer from FMN to CB1954.

As expected, the energy for the singlet state is substantially less than the energy for the triplet at reactants, and while there is definitely a barrier to the change in configuration from reactants to products, the energy of the singlet and products is almost exactly the same as the energy of the triplet. This is almost certainly because the entire reaction profile was generated from the initial singlet reactant geometry and as a result, the product configuration does not exactly match up with the optimised triplet in Figure 4.5.

4.4.2 Optimised-Geometry Electron Transfer Reaction Profile

The process of generating a reaction profile with the geometry optimised for both the singlet and triplet states at each step was difficult and time-consuming. Several attempts had to be made, and the number of variables frozen and incrementally stepped had to be changed multiple times. Finally, a full reaction profile, Figure 4.7, was generated.

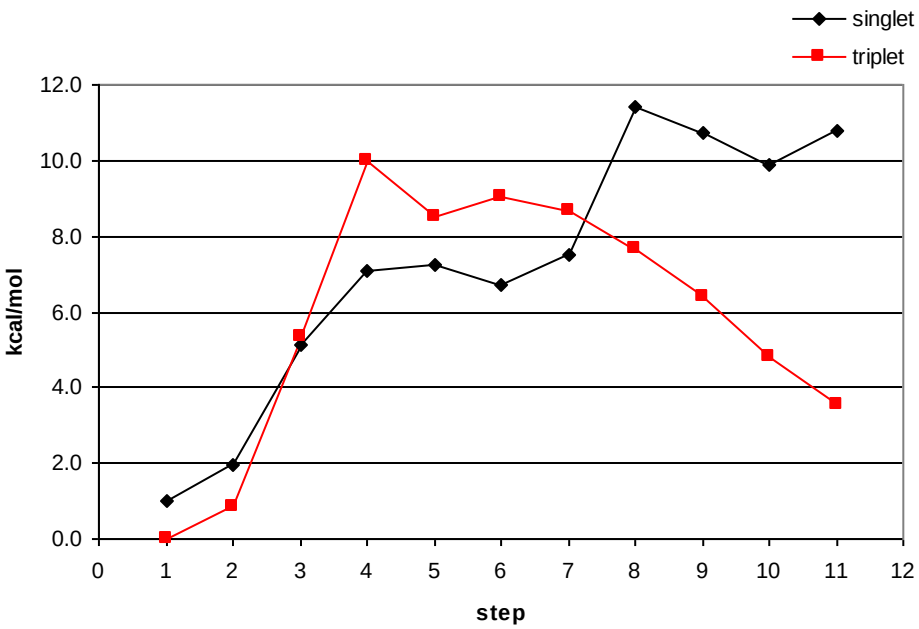

Figure 4.7: Reaction profile for the optimised-geometry electron transfer from FMN to CB1954.

Now the triplet is substantially lower in energy than the singlet at the products. However, it is also lower in energy at the reactants. This was confounding, as the reactant geometry was expected to be the global minimum for the singlet for all possible molecular orientations, and the geometry for the triplet was expected to be the global minimum for all possible molecular orientations. Figure 4.7 indicates that this is not, in fact the case. It would appear therefore that there are orientations of the FMN-CB1954 complex that favour spontaneous electron transfer. In these cases, there is not any specific change in the orientation of CB1954 with respect to FMN that facilitates the electron transfer, but instead the first electron transfer simply occurs spontaneously as soon as there is orbital overlap between CB1954 is and the FMN cofactor, i.e. the two come close to van der Waals contact.

4.4.3 Infinite Separation Calculations for Electron Transfer

Step	Charge on FMN	Charge on CB1954	Energy (kcal/mol)
Reactants	−1	0	0
$1e^-$	0	−1	−1
$2e^-$	1	−2	209

Table 4.2: Infinite separation calculations for electron transfer from reduced FMN to CB1954.

Table 4.2 supports the supposition that the first electron transfer from FMN to CB1954 occurs spontaneously, provided the molecules are in an appropriate orientation. However, the second electron transfer is not possible without the addition of a proton—either from solution, or from FMN.

4.4.4 Discussion of Electron Transfer Calculations

The fact that the triplet state appears to be more stable in the gas phase could be the result of the choice of basis set or DFT functional. However, other studies with FMN have shown that the choice of basis set and DFT functional make little difference, although there are significant differences between DFT and MP2 results[142].

The one-electron redox potential for CB1954 is −385 mV[143]. The two-electron redox potential cannot be measured, as the second two-electron reduction (from nitroso to hydroxylamine) is 10^4 faster[39]. The one-electron redox potential for FMN for the reduction of the protonated semiquinone radical to the protonated, fully reduced state is −150mV[34]. These values are for an aqueous environment and support the observation that free FMN does not reduce CB1954 *in vivo*[2]. This illustrates how important the charge environment in the NTR active site is to substrate reduction.

Interestingly, the FMN butterfly angle was found to be close to 0 degrees for both the optimised singlet and the optimised triplet. It has been observed experimentally that an increase in the FMN butterfly angle destabilises both the fully oxidised and semiquinone radical states of FMN, while stabilising the reduced state[17,142]. Therefore the key factors in the enzyme are charge environment and FMN butterfly angle.

Electron transfer calculations show that in the gas phase, a one-electron transfer from fully reduced FMN to CB1954 is feasible in the absence of any proton transfer. These calculations also show that the relative stability of the singlet and triplet states is dependent on the orientation of the two molecules. The next step is to examine all possible electron and proton transfer combinations, as well as an examination of the singlet and triplet states in the enzyme active site (Section 5.3).

4.5 Infinite Separation Calculations for the Full Reduction

As described previously, it is known that CB1954 is reduced by NTR via the addition of two protons and two electrons to a nitro group. One of the protons must come from solution, and both electrons must come from FMN, which only leaves the question of where the second proton comes from—FMN or solution. If it comes from FMN, the reaction mechanism is effectively *net* hydride transfer (because hydride transfer calculations have already shown that the proton and both electrons are not transferred simultaneously). If both protons come from solution, the reaction mechanism is effectively electron transfer.

In order to determine which combinations of electrons and protons are thermodynamically feasible, infinite separation calculations were performed for all possible permutations of said electrons and protons.

4.5.1 Infinite Separation Calculations with Hydroxonium

One of the inherent difficulties with this type of calculation is accurately modelling the proton(s) that come from solution. *In vivo*, at pH 7, the concentration of hydroxonium ions is 10^{-7}M. Theoretically, the CB1954 does not actually have to obtain a proton directly from a hydroxonium ion, but rather a water molecule which is part of a hydrogen bond chain that eventually reaches a hydroxonium ion.

In the first round of infinite separation calculations, two hydroxonium ions are used to represent the solution as the proton donors. Combined reactant and product energies along with all possible combinations of intermediates have been compiled into Table 4.3 to investigate the feasibility of various sequences of proton and electron transfer. Distinction has

been made between protons transferred from FMN (Hf in Table 4.3) and from solvent ions (Hs).

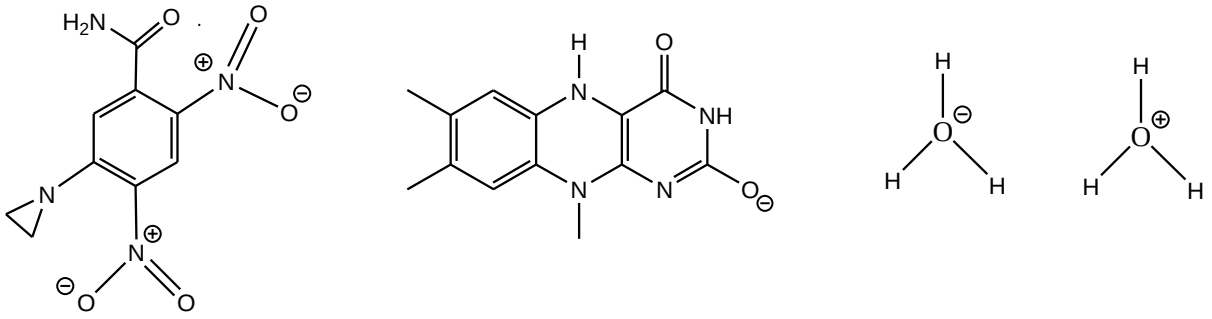

Figure 4.8: Reactants at infinite separation.

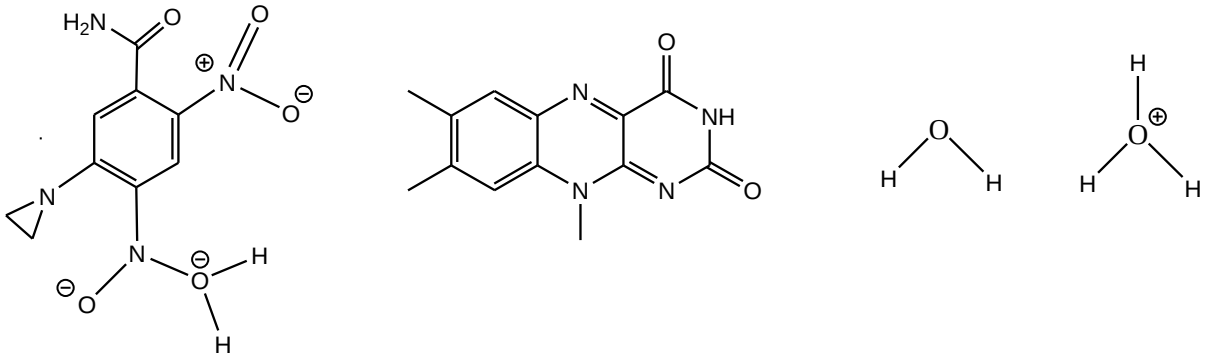

Figure 4.9: 4-nitro reduction products at infinite separation: hydride transfer from FMN and proton transfer from hydroxonium.

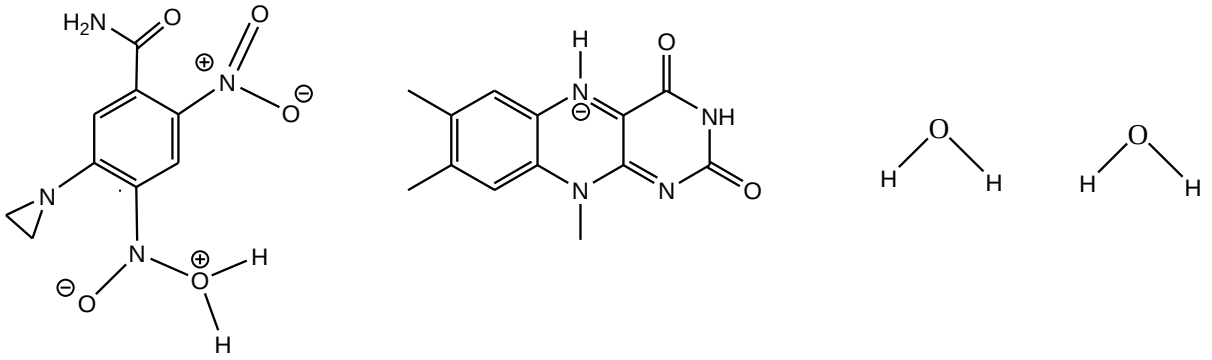

Figure 4.10: 4-nitro reduction products at infinite separation: two electrons from FMN, protons from separate hydroxonium ions.

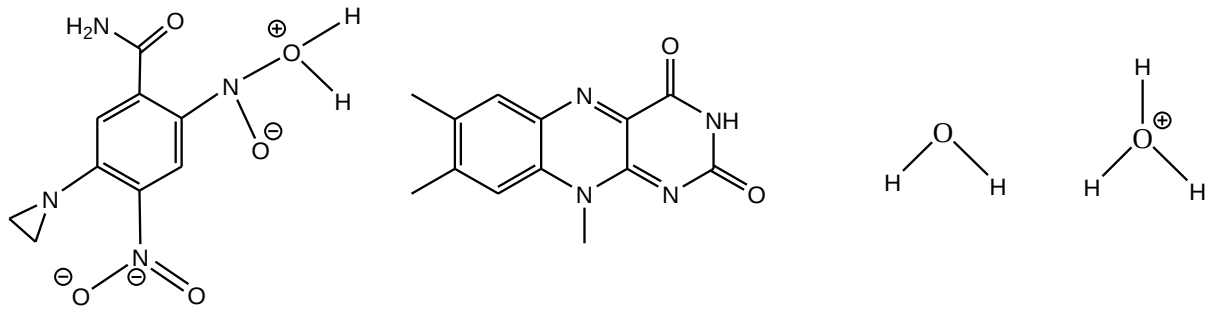

Figure 4.11: 2-nitro reduction products at infinite separation: hydride transfer from FMN, proton transfer from hydroxonium.

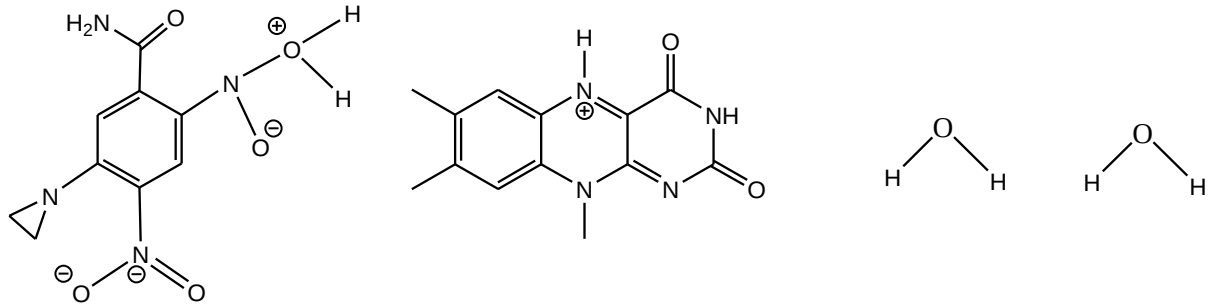

Figure 4.12: 2-nitro reduction products at infinite separation: two electrons transferred from FMN, two protons from separate hydroxonium ions.

Step[a]	Charge on FMN	Charge on CB1954	Energy (kcal/mol) 4-nitro	Energy (kcal/mol) 2-nitro
Reactants	−1	0	0	0
1Hs	−1	1	−28	−33
1Hs $1e^-$	0	0	−148	−148
1Hs $2e^-$	1	−1	−32	−38
2Hs	−1	2	60	49
2Hs $1e^-$	0	1	−194	−198
2Hs $2e^-$	1	0	−216	−217
1Hs 1Hf	−2	2	330	319
1Hs 1Hf $1e^-$	−1	1	−32	−35
1Hs 1Hf $2e^-$	0	0	−167	−167
1Hf	−2	1	242	237
1Hf $1e^-$	−1	0	15	15
1Hf $2e^-$	0	−1	17	12
$1e^-$	0	−1	−1	−1
$2e^-$	1	−2	209	209

Table 4.3: Infinite separation calculations of all possible steps for the reduction of the 2-nitro and 4-nitro groups of CB1954. [a] Hs represents proton transfer from hydroxonium, Hf proton transfer from FMN.

Table 4.3 yields some key information about the possible ways in which a nitro group of CB1954 may be reduced. While it is thermodynamically unfavourable for more than one proton to be added to an oxygen of the nitro group without electrons, the addition of a single proton from hydroxonium is exothermic, while a single proton from FMN is strongly endothermic. The latter results in a −2 charge remaining on FMN so it is perhaps reasonable to expect any proton transfer from FMN to either follow electron transfer or occur simultaneously. Additionally, while a single electron transfer from FMN to CB1954 is thermodynamically favoured, the transfer of the second electron without the addition of any protons is energetically prohibitive, as this would now place a −2 charge on CB1954.

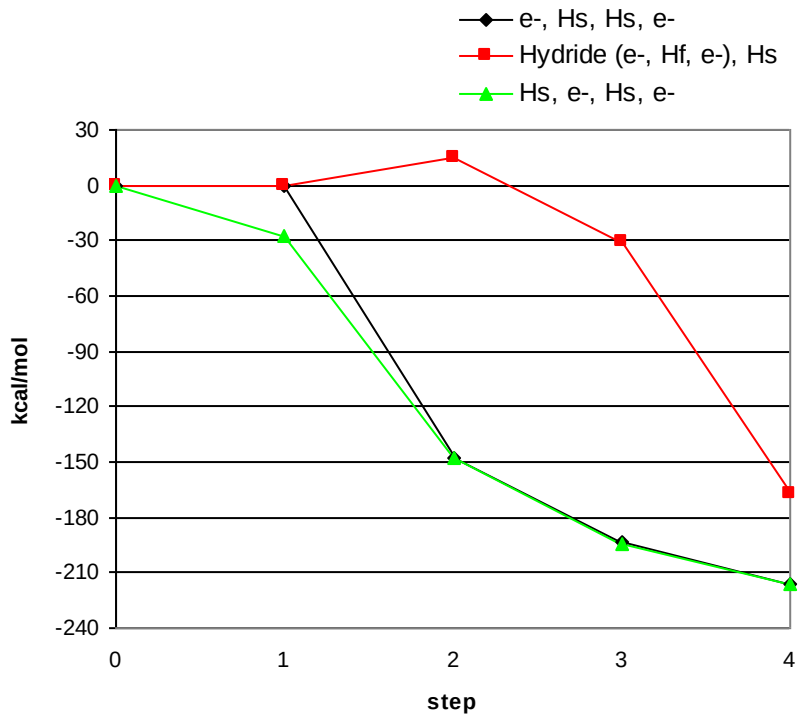

Figure 4.13: Infinite separation electron transfer (black and green) and hydride transfer (red) reactions with hydroxonium representing solvent (Hs). Hf represents a proton from N5 of FMN.

Figure 4.13 shows the difference between the hydride and electron transfer reactions at infinite separation with hydroxonium representing solution. As expected, the electron transfer reaction is strongly favoured with each individual step being exothermic, This is partially due to the fact that transferring a proton from a single gas-phase hydroxonium molecule is itself strongly exothermic. Processes Hs-e-e-Hs and Hs-e-e-Hf have a strongly endothermic step (second electron transfer, which will inevitably have a large barrier) so can be discounted.

Another important result from the infinite separation calculations is that regardless of the electrons, if two protons are added to the same oxygen of the nitro group, the N-O bond is broken to form a nitroso group and a water molecule (Figure 4.14). While some steps have lower energy for the 2-nitro (due to orbital overlap with the adjacent amide group), these differences are small compared with the enthalpy changes for each step and products for both 2-nitro and 4-nitro reductions have almost exactly the same energy (within 1 kcal/mol).

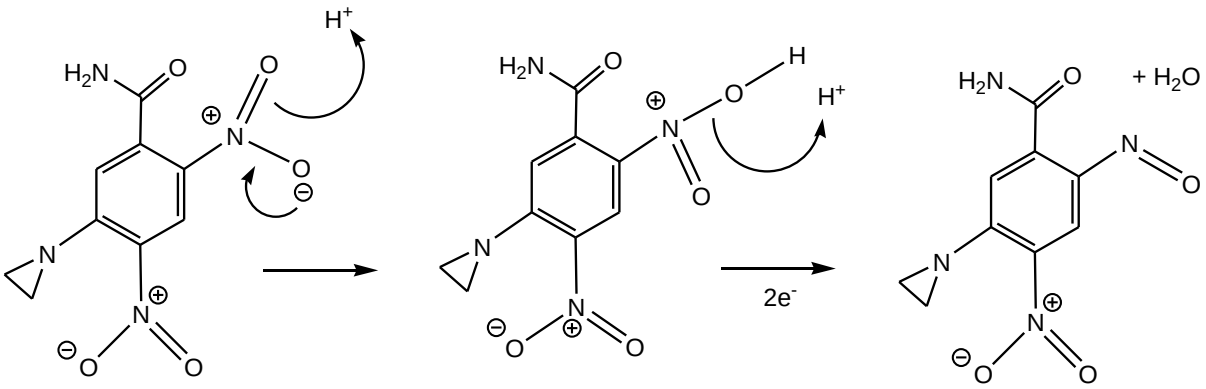

Figure 4.14: General reduction of a CB1954 nitro group to a nitroso.

4.5.2 Infinite Separation Calculations with Hydroxonium and Dielectric

An isolated hydroxonium ion is not a good model for solution. One way to improve upon this is to use a dielectric to model the system as if each component were still at infinite separation, but in solution rather than gas-phase. A solvated hydroxonium ion is a much more appropriate model for solution than a hydroxonium is the gas phase.

Step	Charge on FMN	Charge on CB1954	PCM Energy (kcal/mol) 4-nitro	PCM Energy (kcal/mol) 2-nitro
Reactants	−1	0	0	0
1Hs	−1	1	3	−3
1Hs $1e^-$	0	0	−32	−33
1Hs $2e^-$	1	−1	3	−2
2Hs	−1	2	46	43
2Hs $1e^-$	0	1	−38	−45
2Hs $2e^-$	1	0	−62	−63
1Hs 1Hf	−2	2	120	117
1Hs 1Hf $1e^-$	−1	1	5	−1
1Hs 1Hf $2e^-$	0	0	−49	−50
1Hf	−2	1	77	71
1Hf $1e^-$	−1	0	11	11
1Hf $2e^-$	0	−1	16	11
$1e^-$	0	−1	0	0
$2e^-$	1	−2	50	50

Table 4.4: Infinite separation calculations with the PCM solvent model of all possible steps for the reduction of the 2-nitro and 4-nitro groups of CB1954. As with Table 4.2, Hs represents a proton transferred from hydroxonium.

There are several important differences between the gas-phase infinite separation calculations with hydroxonium and the solvated infinite separation calculations. It is no longer strongly favourable for CB1954 to obtain a proton from hydroxonium before reacting with FMN. Furthermore, while the electron transfer mechanism is still favoured, there is only

a 13 kcal/mol difference between the possible products when solvated, as opposed to a 49 kcal/mol difference in the gas phase. The possibility of FMN transferring two electrons is also much less prohibitive, at 50 kcal/mol, as opposed to 209 kcal/mol in the gas phase.

Finally, while in the gas phase, the hydride transfer was a consecutive electron-proton-electron, for the solvated electron calculations the order is electron, proton from FMN, proton from solution, electron.

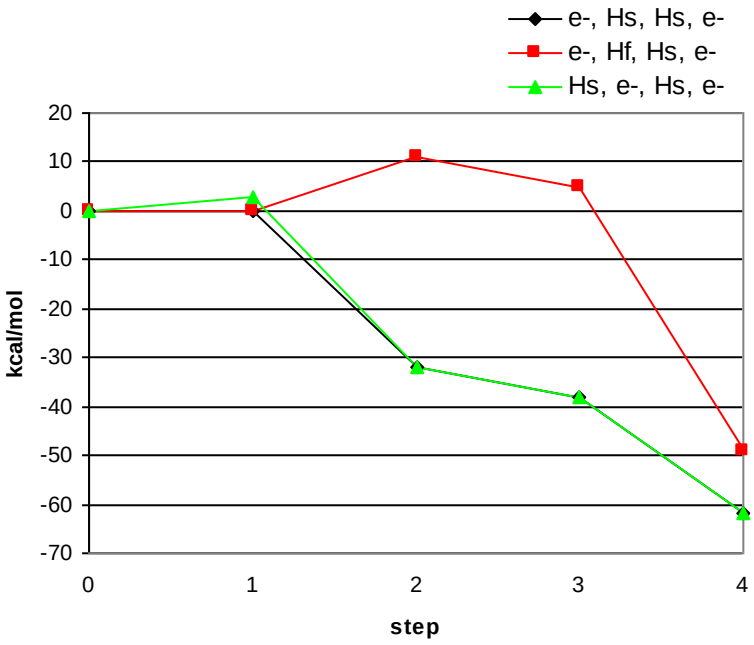

Figure 4.15: Infinite separation electron transfer (black and green) and net hydride transfer (red) reactions with hydroxonium (Hs) and solvation. Hf represents a proton from N5 of FMN.

The overall shape of the graph for the solvated infinite separation profile is similar to that for the gas phase, with the major distinction being that the difference in energy between products and reactants is less when the constituents are in solution.

4.5.3 Infinite Separation Calculations with Water Molecules

Even using a dielectric continuum to represent solvation, it may be argued that a hydroxonium ion is not a good representative of a proton donor likely to be involved in the reduction of CB1954 by NTR. Instead, it is far more likely that the proton donor will be a water molecule in a hydrogen-bonding chain that terminates with a hydroxonium ion.

Step	Charge on FMN	Charge on CB1954	Energy (kcal/mol) 4-nitro	Energy (kcal/mol) 2-nitro
Reactants	−1	0	0	0
1Hs	−1	1	227	222
1Hs $1e^-$	0	0	108	107
1Hs $2e^-$	1	−1	223	217
2Hs	−1	2	570	560
2Hs $1e^-$	0	1	316	313
2Hs $2e^-$	1	0	294	293
1Hs 1Hf	−2	2	585	575
1Hs 1Hf $1e^-$	−1	1	224	220
1Hs 1Hf $2e^-$	0	0	88	88
1Hf	−2	1	242	237
1Hf $1e^-$	−1	0	15	15
1Hf $2e^-$	0	−1	17	12
$1e^-$	0	−1	−1	−1
$2e^-$	1	−2	209	209

Table 4.5: Infinite separation calculations of all possible steps for the reduction of the 2-nitro and 4-nitro groups of CB1954 with water molecules representing solution. Hs represents proton transfer from water.

While a gas-phase water molecule is not an ideal model for solution either, it is worth looking at simply as a basis for comparison. In these calculations, the products and reactants are the same as those for the infinite separation calculations with hydroxonium, except that

hydroxonium ions are replaced with water molecules, and water molecules in the products are replaced with hydroxide ions.

As expected, the removal of a proton from a gas-phase water molecule is thermodynamically prohibitive. In this scenario, even the hydride transfer mechanism is not plausible.

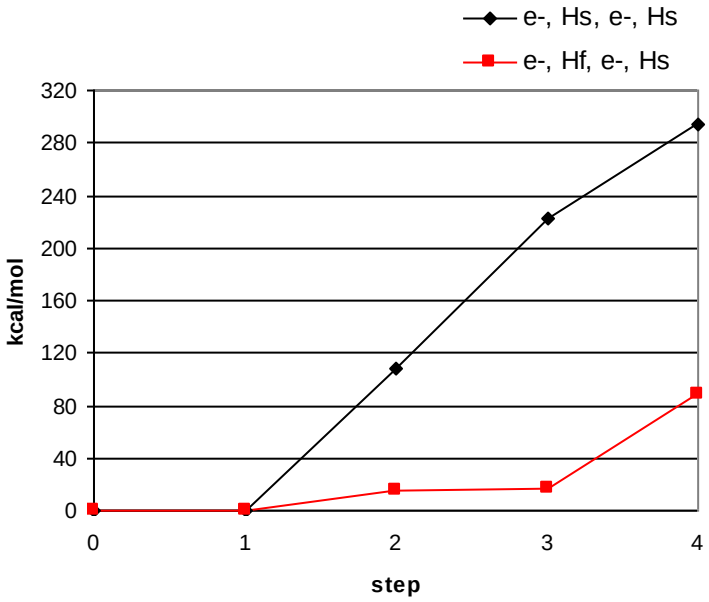

Figure 4.16: Infinite separation electron transfer (black) and hydride transfer (red) reactions with water molecules representing solution (Hs). Hf represents a proton from N5 of FMN.

4.5.3.1 Infinite Separation Calculations with The N-O Bond Broken

It has already been determined that the N-O bond of the nitro group breaks if two protons are added to the same oxygen. However, it is also possible that the N-O bond breaks *before* the addition of the second proton.

Step	Charge on FMN	Charge on CB1954	Energy (kcal/mol) N-O broken[a]	Energy (kcal/mol) 4-nitro[b]
Reactants	−1	0	0	0
1Hs	−1	1	582	227
1Hs $1e^-$	0	0	328	108
1Hs $2e^-$	1	−1	301	223
2Hs	−1	2	582	570
2Hs $1e^-$	0	1	328	316
2Hs $2e^-$	1	0	301	294
1Hs 1Hf	−2	2	597	585
1Hs 1Hf $1e^-$	−1	1	235	224
1Hs 1Hf $2e^-$	0	0	96	88
1Hf	−2	1	597	242
1Hf $1e^-$	−1	0	235	15
1Hf $2e^-$	0	−1	96	17
$1e^-$	0	−1	−1	−1
$2e^-$	1	−2	209	209

Table 4.6: Infinite separation calculations of all possible steps for the reduction of the and 4-nitro groups of CB1954 with water molecules representing solution. Hs represents proton transfer from water. [a] Represents the reaction if the N-O bond of the nitro group is broken after the first proton is added to the oxygen. [b] Represents transfer to the same nitro group with the N-O bond remaining intact.

Table 4.6 shows that it is not favourable for the N-O bond to break before the addition of the second proton.

4.5.4 Infinite Separation Calculations with Water Molecules and Dielectric

As for Section 4.5.2, representation of solvent by a dielectric continuum may help to stabilise charged species and result in more favourable proton transfer from a water molecule, see Table 4.7.

Step	Charge on FMN	Charge on CB1954	PCM Energy (kcal/mol) 4-nitro	PCM Energy (kcal/mol) 2-nitro
Reactants	−1	0	0	0
1Hs	−1	1	96	90
1Hs $1e^-$	0	0	61	60
1Hs $2e^-$	1	−1	97	91
2Hs	−1	2	232	229
2Hs $1e^-$	0	1	148	141
2Hs $2e^-$	1	0	124	123
1Hs 1Hf	−2	2	213	210
1Hs 1Hf $1e^-$	−1	1	98	92
1Hs 1Hf $2e^-$	0	0	44	43
1Hf	−2	1	77	71
1Hf $1e^-$	−1	0	11	11
1Hf $2e^-$	0	−1	16	11
$1e^-$	0	−1	0	0
$2e^-$	1	−2	50	50

Table 4.7: Infinite separation calculations of all possible steps with the PCM solvent model for the reduction of the 2-nitro and 4-nitro groups of CB1954 with water molecules representing solution. Hs represents water.

With all constituents solvated, net hydride transfer becomes feasible, though still endothermic, but the electron transfer mechanism is still prohibited.

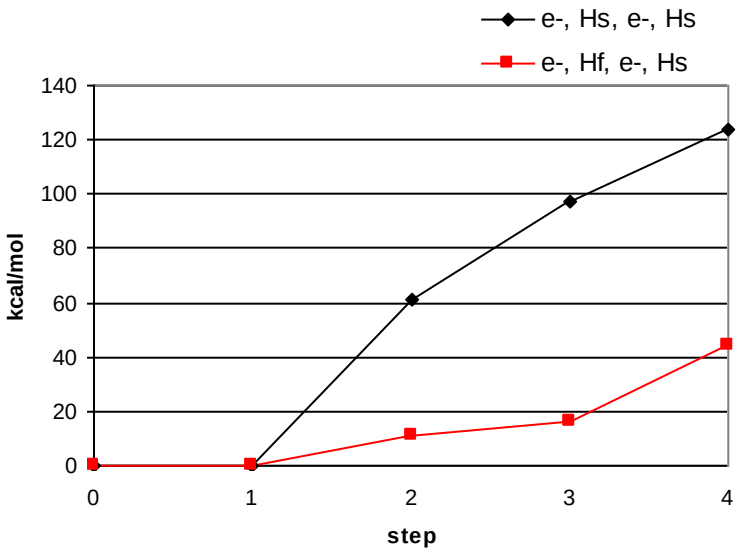

Figure 4.17: Infinite separation electron transfer (black) and hydride transfer (red) reactions with water molecules (Hs) and solvation. Hf represents a proton from N5 of FMN.

4.5.5 Infinite Separation Calculations with Eigen Cation

The hydroxonium ion and an isolated water molecule represent the opposite extremes regarding their ability to model solvent-derived proton donors; hydroxonium donates a proton too easily, while a single gas-phase molecule does not give up a proton easily enough. One possible intermediate between the two is the Eigen cation, $H_9O_4^+$. A hydroxonium ion surrounded by, and hydrogen bonded to, three water molecules, the Eigen cation gives a more accurate representation of the proton-donating ability of solution *in vivo*.

Step	Charge on FMN	Charge on CB1954	Energy (kcal/mol) 4-nitro	Energy (kcal/mol) 2-nitro
Reactants	−1	0	0	0
1Hs	−1	1	24	20
1Hs $1e^-$	0	0	−95	−95
1Hs $2e^-$	1	−1	20	15
2Hs	−1	2	165	155
2Hs $1e^-$	0	1	−88	−92
2Hs $2e^-$	1	0	−111	−111
1Hs 1Hf	−2	2	383	372
1Hs 1Hf $1e^-$	−1	1	21	18
1Hs 1Hf $2e^-$	0	0	−114	−115
1Hf	−2	1	242	237
1Hf $1e^-$	−1	0	15	15
1Hf $2e^-$	0	−1	17	12
$1e^-$	0	−1	−1	−1
$2e^-$	1	−2	209	209

Table 4.8: Infinite separation calculations of all possible steps for the reduction of the 2-nitro and 4-nitro groups of CB1954 with Eigen cations representing solution. Hs represents proton transfer from an Eigen cation.

With the Eigen cation representing the proton donor from solution, the net hydride transfer mechanism is more thermodynamically favoured than the electron transfer mechanism.

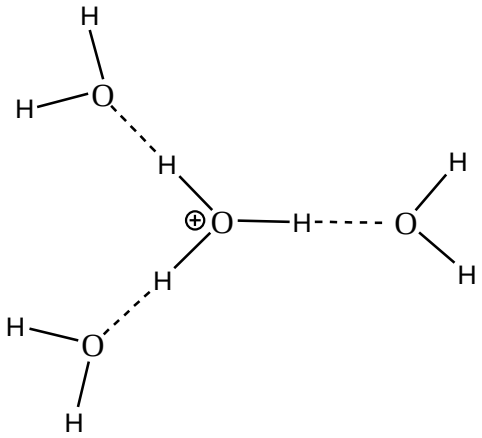

Figure 4.18: The Eigen cation.

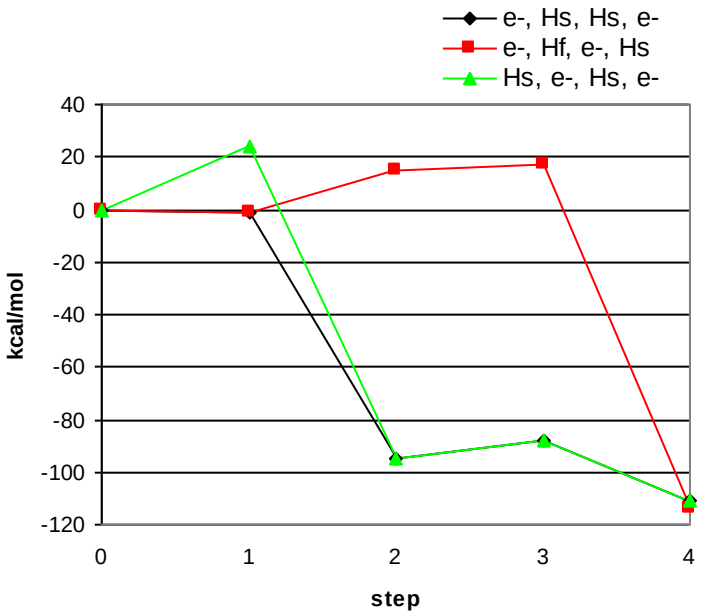

Figure 4.19: Infinite separation electron transfer (black and green) and hydride transfer (red) reactions with Eigen cations (Hs) to represent solution. Hf represents a proton from N5 of FMN.

4.5.6 Infinite Separation Calculations with Eigen Cation and Solvation

The final infinite separation calculation involves the Eigen cation as the model for solution, with all constituents solvated. This is probably the most reasonable approximation for the actual solution *in vivo*.

Step	Charge on FMN	Charge on CB1954	PCM Energy (kcal/mol) 4-nitro	PCM Energy (kcal/mol) 2-nitro
Reactants	−1	0	0	0
1Hs	−1	1	26	20
1Hs $1e^-$	0	0	−9	−10
1Hs $2e^-$	1	−1	26	21
2Hs	−1	2	92	89
2Hs $1e^-$	0	1	8	1
2Hs $2e^-$	1	0	−16	−17
1Hs 1Hf	−2	2	143	140
1Hs 1Hf $1e^-$	−1	1	28	22
1Hs 1Hf $2e^-$	0	0	−26	−27
1Hf	−2	1	77	71
1Hf $1e^-$	−1	0	11	11
1Hf $2e^-$	0	−1	16	11
$1e^-$	0	−1	0	0
$2e^-$	1	−2	50	50

Table 4.9: Infinite separation calculations of all possible steps with the PCM solvent model for the reduction of the 2-nitro and 4-nitro groups of CB1954 with Eigen cations representing solution. Hs represents proton transfer from an Eigen cation.

In this case, the energy of the products for net hydride transfer is a full 10 kcal/mol lower than the energy for the products for electron transfer, but with higher energy intermediates, hydride transfer may show a higher reaction barrier.

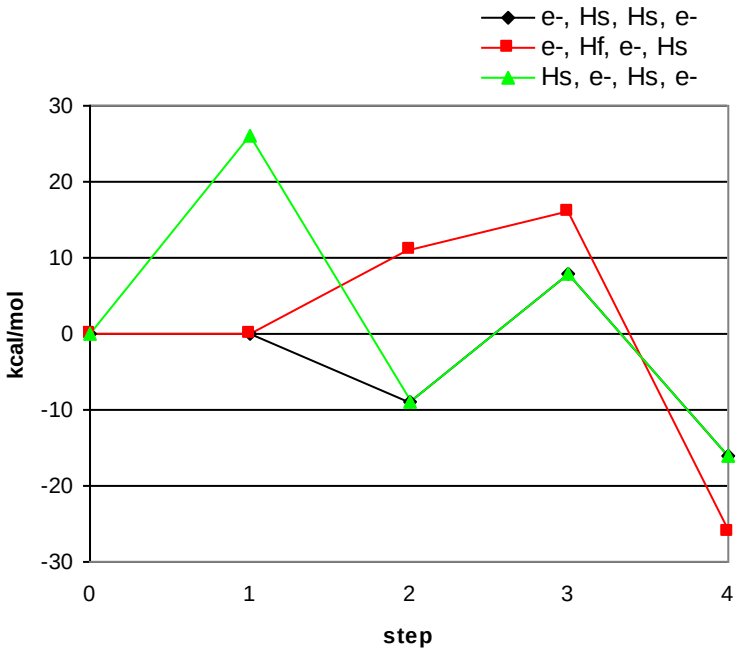

Figure 4.20: Infinite separation electron transfer (black and green) and hydride transfer (red) reactions with Eigen cations (Hs) to represent solution and solvation. Hf represents a proton from N5 of FMN.

4.5.7 Summary of Infinite Separation Calculations

The viability of various reaction mechanisms appears to depend on the choice of the model for solution used. When hydroxonium ions are used, both net hydride transfer and electron transfer mechanisms are possible, but electron transfer is strongly favoured. Additionally, the transfer of a proton to CB1954 from solution is favoured to occur *before* the transfer of an electron from FMN. When a hydroxonium ions are used with a dielectric, the electron transfer mechanism is still favoured, but the transfer of an electron from FMN to CB1954 is favoured to occur before the transfer of the first proton from solution.

When isolated water molecules are used, neither reaction mechanism is possible. When water molecules are used with a dielectric, only the net hydride transfer mechanism is possible, although strongly endothermic.

With the Eigen cation, the net hydride transfer is slightly favoured, although it has a greater barrier compared to the electron transfer. When Eigen cations are used with a dielectric, the net hydride is even more favoured, with a similar overall barrier to the electron transfer mechanism. Overall, these calculations suggest that the ready availability of protons may have an impact on the overall thermodynamics of CB1954 reduction by NTR.

4.6 Single Proton Transfer Reaction Profiles

A reaction profile has effectively already been determined for the transfer of a proton from N5 of FMN to an oxygen atom of a nitro group on CB1954 (Section 3.8.2) in that rather than transferring a true hydride ion, the system preferred to transfer an electron and proton separately. The infinite separation calculations above do not conclusively rule out either net hydride transfer or electron transfer as possible mechanisms, so the next step is to look at all possible single-proton transfers from different sources.

At pH 7, hydroxonium ions are present at a proportion of 1 in 500 million. Therefore, with pure water, a hydrogen bonding chain of 14 water molecules would be needed to have a better than 50% chance of including a hydroxonium ion in the chain. This is slightly improved *in vivo*, because of the presence of other ions, and a pH of less than 7. While hydroxonium is not an ideal representation of true solution, it is a convenient model because of its simplicity.

As with the reaction profiles in Chapter 3, protons are moved incrementally, and energies and relative molecular charges are determined for the singlet and triplet at each step.

4.6.1 Proton transfer from Hydroxonium, After Proton Transfer from FMN

In Section 3.8.2 it was determined if a proton is moved incrementally from N5 of FMN to an oxygen of a nitro group on CB1954 in the gas phase, there is no hydride transfer. Rather, one electron is transferred immediately from FMN to CB1954, followed by the proton. Therefore, the next logical thing to do is to examine the final step of the reaction—the transfer of a proton from solution to the same oxygen on CB1954.

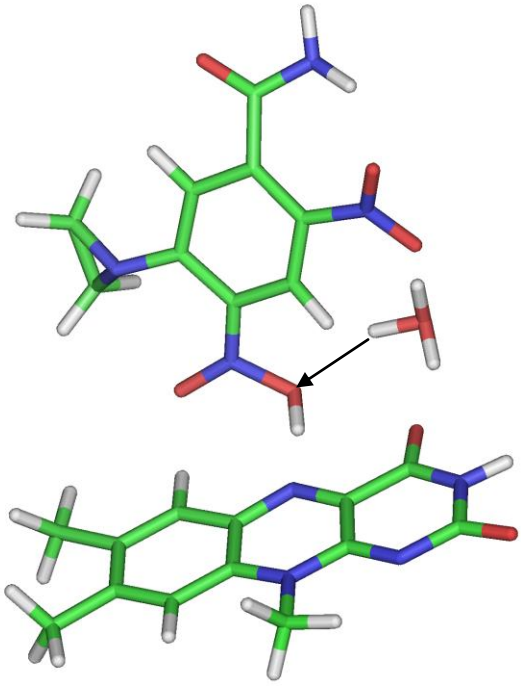

Figure 4.21: Transfer of proton from hydroxonium to an oxygen of the 4-nitro group, with the proton from N5 of FMN already transferred to that same oxygen.

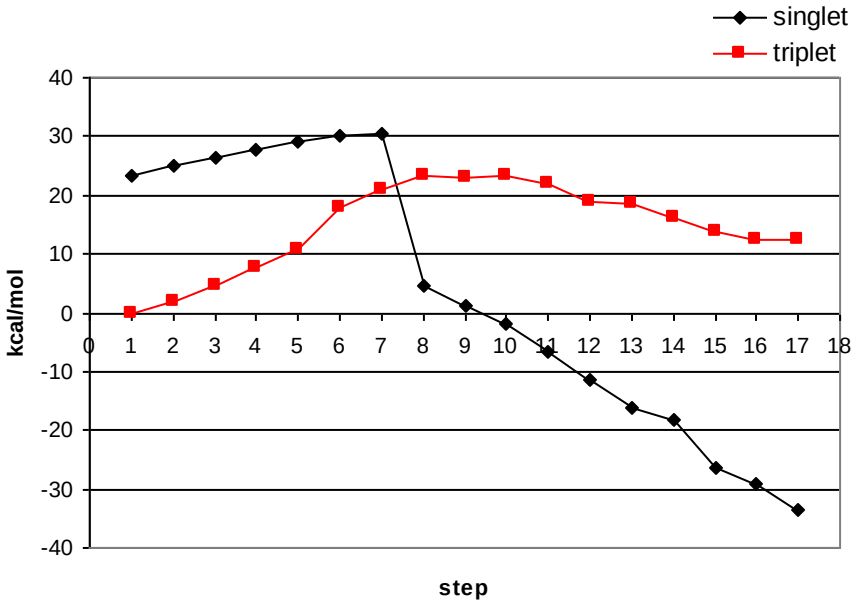

Figure 4.22: Reaction profile for the proton transfer from hydroxonium to a 4-nitro oxygen of CB1954, with the proton from N5 of FMN already on that oxygen. Step 1 represents reactants (Figure 4.21), step 17 represents products, with the H from hydroxonium completely transferred to the oxygen of the nitro group. The large decrease in energy between steps 7 and 8 for the singlet represents the nitro N-O bond breaking.

	Charge on FMN	Charge on CB1954	Energy (Hartree)	Energy relative to Reactants (kcal)
Reactants triplet	−0.69	0.03	−1891.9895973	0
Reactants singlet	−0.17	−0.54	−1891.9523621	23
Products triplet	−0.68	0.61	−1891.9699574	12
Products singlet	−0.01	0.00	−1892.0432664	−34

Table 4.10: Molecular charges and energy of reactants and products in singlet and triplet states for the proton transfer from hydroxonium to a 4-nitro oxygen of CB1954, with the proton from N5 of FMN already on that oxygen.

The sharp decrease in energy between steps 7 and 8 for the singlet curve in Figure 4.22 corresponds to the breaking of the N-O bond of the nitro group to form a nitroso, plus a water molecule. The fact that this event corresponds to the crossing of the singlet and triplet

curves shows that the transfer of the second electron from FMN to CB1954 is concerted with the N-O bond breaking.

The point where the singlet and triplet lines cross can be considered the upper limit of the energy barrier for the reaction, as the true reaction will follow an avoided crossing. With an energy barrier of ~ 7 kcal/mol for the transfer of the proton from N5 of FMN (Figure 3.19), the transfer of the proton from solution, coupled with the second electron transfer and breaking of the N-O bond would appear to be the rate-limiting step for the net hydride transfer mechanism.

4.6.2 Proton transfer from Hydroxonium as the First Step

Infinite separation calculations with hydroxonium show that it is thermodynamically favourable for CB1954 to obtain a proton from hydroxonium even before any electrons are transferred from FMN. Therefore it is possible for the proton from solution to be transferred to CB1954 before the net hydride transfer. Also, this would be the first step for the electron transfer mechanism.

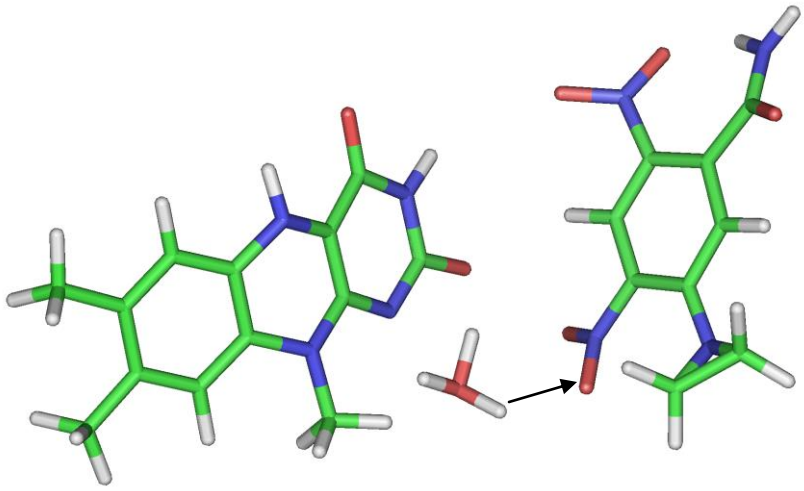

Figure 4.23: Transfer of proton from hydroxonium to an oxygen of the 4-nitro group.

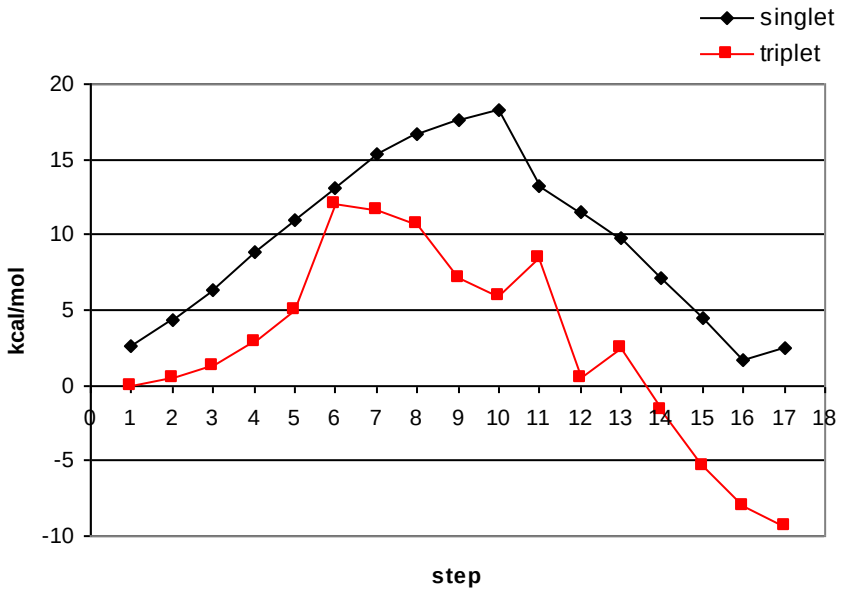

Figure 4.24: Reaction profile for the proton transfer from hydroxonium to a 4-nitro oxygen of CB1954. Step 1 represents reactants (Figure 4.23), step 17 represents products, with the H from hydroxonium completely transferred to the oxygen of the nitro group.

	Charge on FMN	Charge on CB1954	Energy (Hartree)	Energy relative to Reactants (kcal)
Reactants triplet	0.05	−0.71	−1892.0086944	0
Reactants singlet	−0.69	0.02	−1892.0044562	3
Products singlet	−0.15	0.10	−1892.0048361	2
Products triplet	0.05	−0.09	−1892.0236068	−9

Table 4.11: Molecular charges and energy of reactants and products in singlet and triplet states for the proton transfer from hydroxonium to a 4-nitro oxygen of CB1954.

Like the proton transfer from N5 of FMN, with the first proton transfer from hydroxonium one electron from FMN is transferred first, followed by the proton. The energy barrier from the proton transfer from hydroxonium is ≈12 kcal/mol, compared to ≈7 kcal/mol for the proton transfer from N5 of FMN.

The shape of the curve is uneven due to various local rearrangements of the molecules during the proton transfer.

4.6.3 Proton Transfer from FMN, After the Proton Transfer from Solution

This reaction profile represents the second half of the second possible net hydride transfer mechanism, where a proton from solution is already on CB1954, and the proton from N5 of FMN is then transferred.

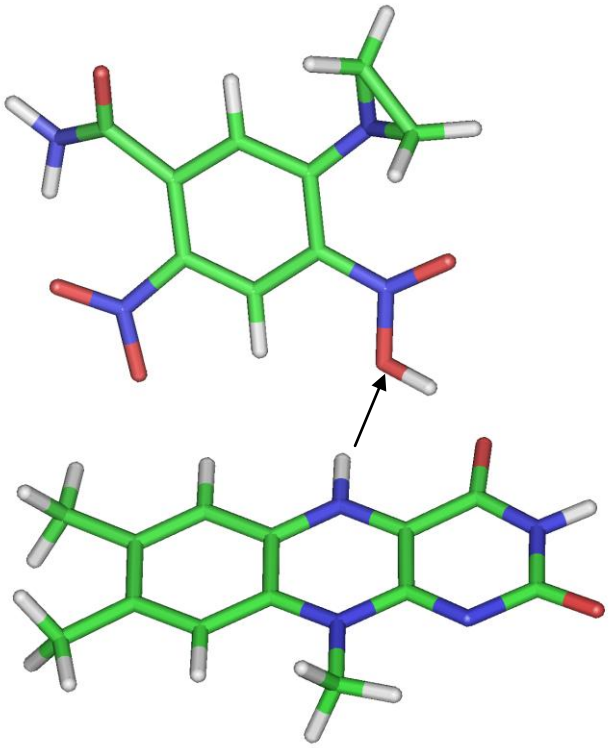

Figure 4.25: Transfer of proton from FMN to an oxygen of the 4-nitro group, after a proton from solution has already been transferred to that oxygen.

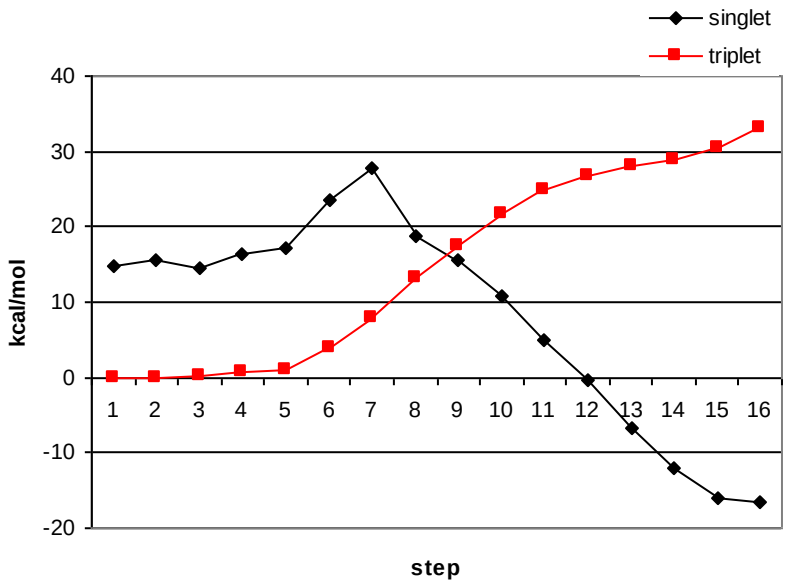

Figure 4.26: Reaction profile for the proton transfer from FMN to an oxygen of the 4-nitro group, after a proton from solution has already been transferred to that oxygen. Step 1 represents reactants (Figure 4.25), step 16 represents products, with the H from FMN completely transferred to the oxygen of the nitro group. The large decrease in energy between steps 7 and 8 for the singlet represents the nitro N-O bond breaking.

	Charge on FMN	Charge on CB1954	Energy (Hartree)	Energy relative to Reactants (kcal)
Reactants triplet	0.06	−0.06	−1815.5954188	0
Reactants singlet	−0.09	0.09	−1815.5717260	15
Products triplet	−0.64	0.64	−1815.5428958	33
Products singlet	0.01	−0.01	−1815.6219316	−17

Table 4.12: Molecular charges and energy of reactants and products in singlet and triplet states for the proton transfer from FMN to an oxygen of the 4-nitro group, after a proton from solution has already been transferred to that oxygen.

Interestingly, in this scenario charges indicate that both the singlet and triplet states have one electron already transferred from FMN to CB1954 at reactants, but the triplet is still 15 kcal/mol lower in energy. Additionally, in this reaction the N-O bond breaks for the

singlet between steps 7 and 8, before crossing the triplet curve, indicating that the second electron transfer occurs as the N-O bond is broken.

4.6.4 Proton Transfer from Hydroxonium, After Proton Transfer from Solution

This represents the final step in the electron transfer mechanism; one proton from solution is already on the oxygen of the nitro group, and the next is transferred from hydroxonium.

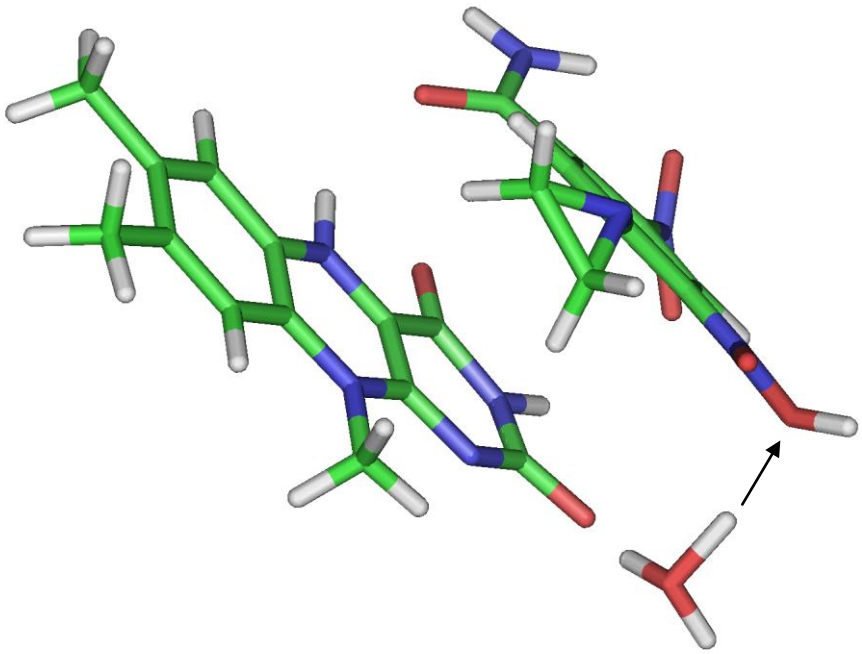

Figure 4.27: Transfer of proton from hydroxonium to an oxygen of the 4-nitro group, after a proton from solution has already been transferred to that oxygen.

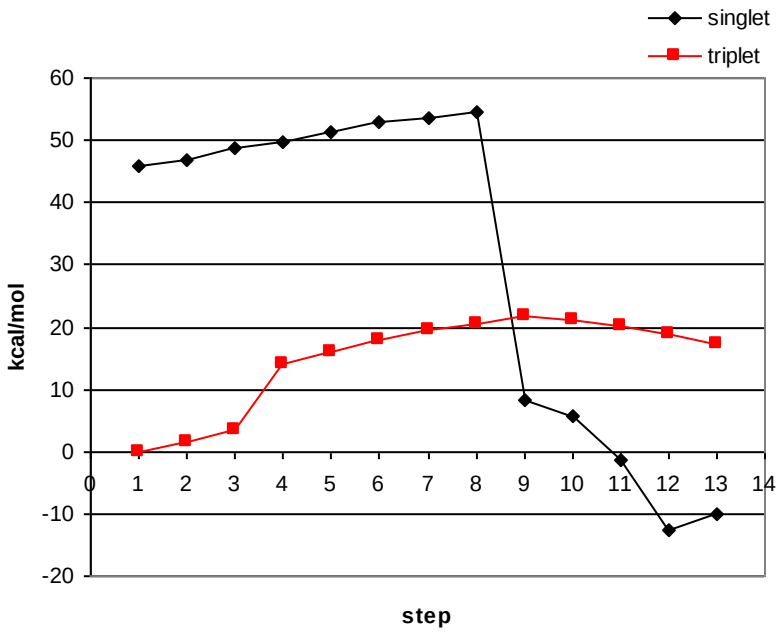

Figure 4.28: Reaction profile for the proton transfer from hydroxonium to an oxygen of the 4-nitro group, after a proton from solution has already been transferred to that oxygen. Step 1 represents reactants (Figure 4.27), step 13 represents products, with the H from hydroxonium completely transferred to the oxygen of the nitro group. The large decrease in energy between steps 8 and 9 for the singlet represents the nitro N-O bond breaking.

	Charge on FMN	Charge on CB1954	Energy (Hartree)	Energy relative to Reactants (kcal)
Reactants triplet	0.19	0.13	−1892.4217435	0
Reactants singlet	0.22	0.02	−1892.3488264	46
Products triplet	0.10	0.80	−1892.3944368	17
Products singlet	0.80	0.11	−1892.4377879	−10

Table 4.13: Molecular charges and energy of reactants and products in singlet and triplet states for the proton transfer from hydroxonium to an oxygen of the 4-nitro group, after a proton from solution has already been transferred to that oxygen.

Like the final step in the hydride transfer mechanism, the N-O bond breaking is concerted with the transfer of the second electron from FMN to CB1954.

4.6.5 Single Proton Transfers from Water

Infinite separation calculations show that hydroxonium is not a good model for solution because it gives up a proton too readily. While a single water molecule is not a good model for solution either because it is too difficult to remove a proton, the calculations were performed substituting hydroxonium for water as a basis for comparison.

4.6.5.1 Proton transfer from Water, After Proton Transfer from FMN

This is the same reaction profile as determined in Section 4.6.1, with the hydroxonium ion replaced with a water molecule. The overall shape of the singlet and triplet curves is similar to the analogous reaction with hydroxonium—including the breaking of the N-O bond concerted with the second electron transfer. As expected, the energy required for this reaction is higher—although not prohibitively so.

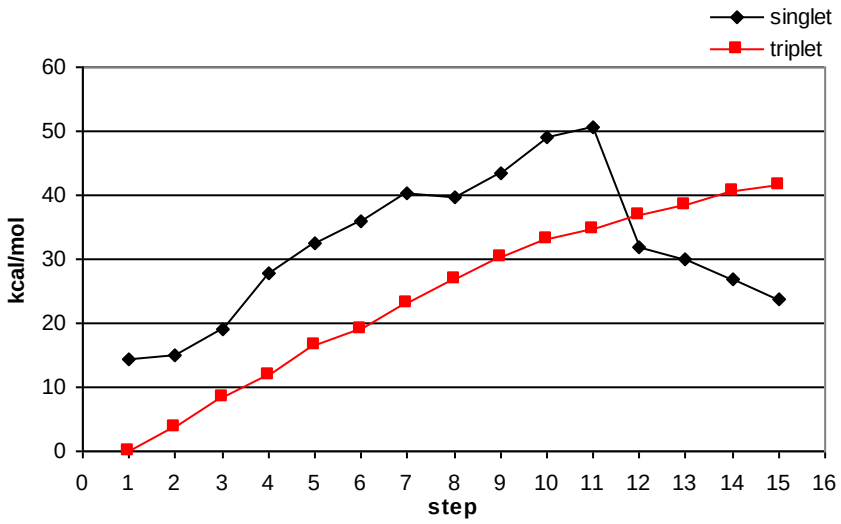

Figure 4.29: Reaction profile for the proton transfer from a water molecule to a 4-nitro oxygen of CB1954, with the proton from N5 of FMN already on that oxygen. Step 1 represents reactants, step 15 represents products, with the H from water completely transferred to the oxygen of the nitro group. The large decrease in energy between steps 11 and 12 for the singlet represents the nitro N-O bond breaking.

4.6.5.2 Proton Transfer from Water as the First Step

This is the same reaction profile as determined in Section 4.6.2, with the hydroxonium ion replaced with a water molecule.

Interestingly, unlike the analogous reaction with hydroxonium, the first electron transfer does not occur before the transfer of the proton. Instead, it only occurs after the proton has been almost completely transferred from water to CB1954. This shows how important the charge environment of the reaction complex is to electron transfer.

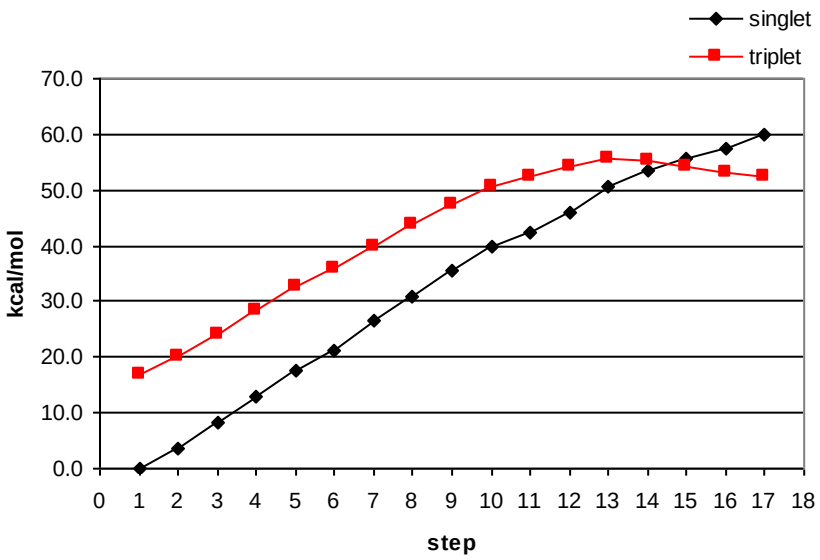

Figure 4.30: Reaction profile for the proton transfer from water to a 4-nitro oxygen of CB1954. Step 1 represents reactants, step 17 represents products, with the H from water completely transferred to the oxygen of the nitro group.

4.6.5.3 Proton Transfer from Water, after Proton Transfer from Solution

This is the same reaction profile as determined in Section 4.6.4, with the hydroxonium ion replaced with a water molecule.

Like the analogous reaction with hydroxonium, this reaction has the first electron already transferred with the first proton. But unlike the hydroxonium reaction, neither the second electron transfer nor the break of the N-O bond occur. This is possibly due to the proximity of the negatively-charged hydroxyl, which again illustrates the importance of the charge distribution around the reacting system.

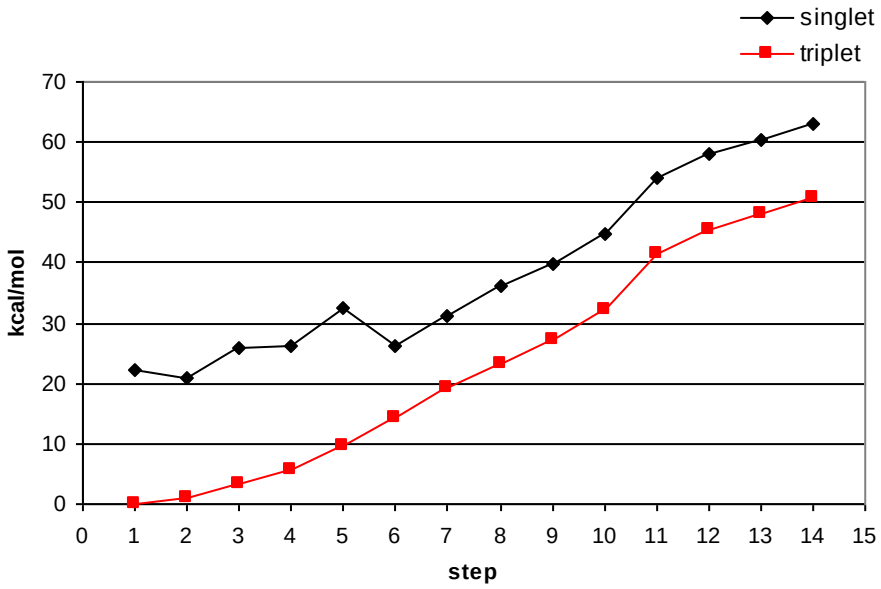

Figure 4.31: Reaction profile for the proton transfer from water to an oxygen of the 4-nitro group, after a proton from solution has already been transferred to that oxygen. Step 1 represents reactants, step 14 represents products, with the H from water completely transferred to the oxygen of the nitro group.

4.7 Full Reaction Profiles

Based on the infinite separation calculations and the single proton transfer reaction profiles, there are three possible mechanisms for the full reduction of CB1954 by NTR: the transfer of a proton from FMN followed by the transfer of a proton from solution, the transfer of a proton from solution followed by the transfer of a proton from FMN, and the transfer of two protons from solution. The first two mechanisms both represent net hydride transfer, while the third represents the electron transfer mechanism.

4.7.1 First Proton from FMN, Second from Hydroxonium

If the reaction were true hydride transfer, both electrons would be transferred from FMN to CB1954 as the proton is transferred from N5 of FMN to an oxygen atom on one of the nitro groups.

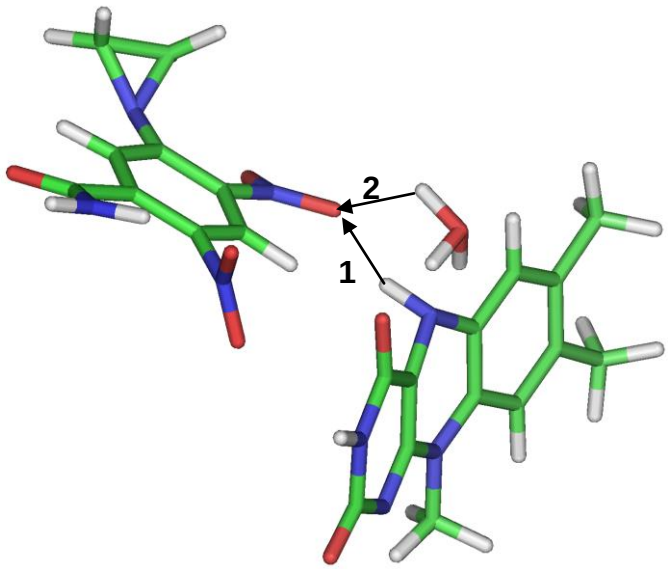

Figure 4.32: Transfer of proton from N5 of FMN to an oxygen of the 4-nitro group, followed by the transfer of a proton from hydroxonium to the same oxygen.

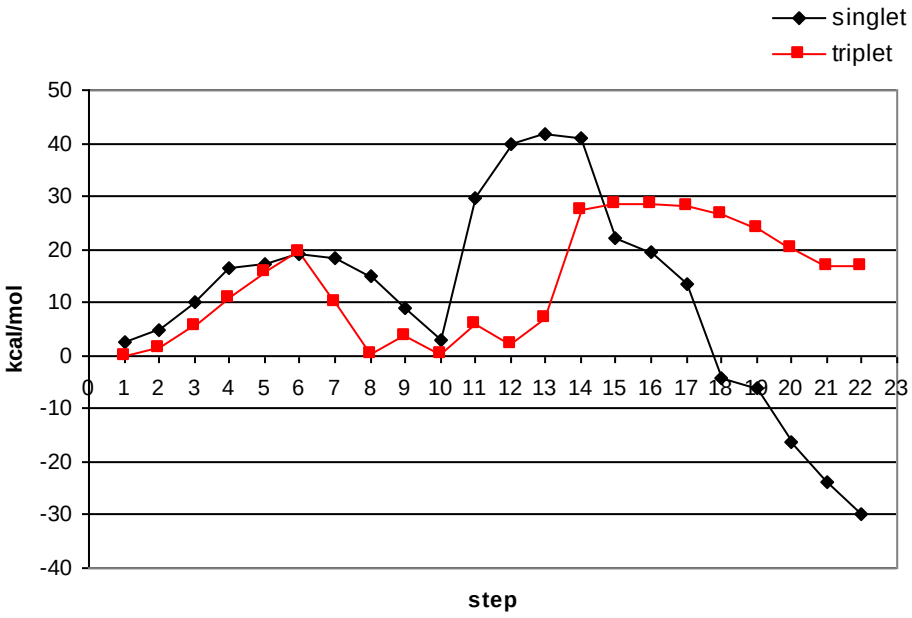

Figure 4.33: Reaction profile for the transfer of a proton from N5 of FMN to an oxygen of the 4-nitro group, followed by the transfer of a proton from hydroxonium to the same oxygen. Step 1 represents reactants (Figure 4.32), steps 1 through 10 represent the transfer of a proton from N5 to an oxygen of the 4-nitro group. Steps 11 through 22 represent the transfer of a proton from hydroxylamine to the same oxygen. The large decrease in energy between steps 14 and 15 for the singlet represents the nitro N-O bond breaking.

	Charge on FMN	Charge on CB1954	Energy (Hartree)	Energy relative to Reactants (kcal)
Reactants triplet	−0.01	−0.69	−1891.987122	0
Reactants singlet	−0.65	−0.02	−1891.983123	3
Products triplet	−0.70	0.63	−1891.960416	17
Products singlet	0.03	−0.09	−1892.034421	−30

Table 4.14: Molecular charges and energy of reactants and products in singlet and triplet states for the proton transfer from N5 of FMN to an oxygen of the 4-nitro group, followed by the transfer of a proton from hydroxonium to the same oxygen.

The overall reaction occurs as follows: one electron is transferred from FMN to CB1954, followed by the proton from N5 of FMN, and midway through the transfer of the proton from the hydroxonium ion, the N-O bond is broken, concerted with the transfer of the

second electron from FMN to CB1954. While there is a net transfer of a proton and two electrons from FMN to CB1954, there is no concerted hydride transfer. The barrier height for the first proton transfer is around 20 kcal/mol, while the upper limit (due to an avoided crossing) for the barrier for the concerted transfer of both the second proton and second electron is 28 kcal/mol.

4.7.2 First Proton from Hydroxonium, Second from FMN

This is the second possible net hydride transfer mechanism. The reactant geometry is the same as that for the previous reaction, but in this case the proton from hydroxonium is transferred first, followed by the proton from FMN.

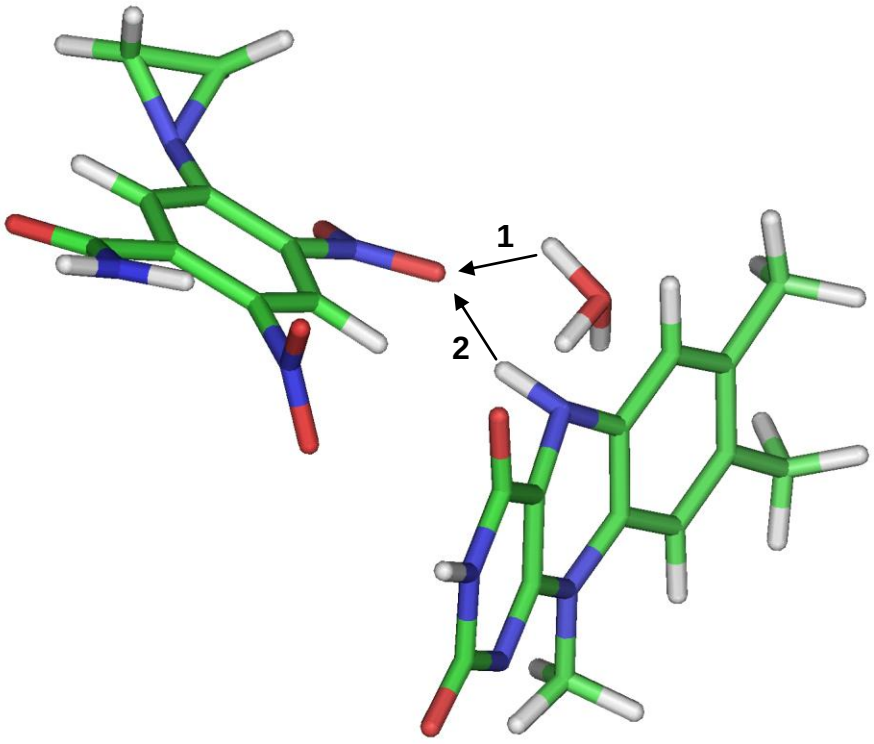

Figure 4.34: Transfer of proton from hydroxonium to an oxygen of the 4-nitro group, followed by the transfer of a proton from N5 of FMN to the same oxygen.

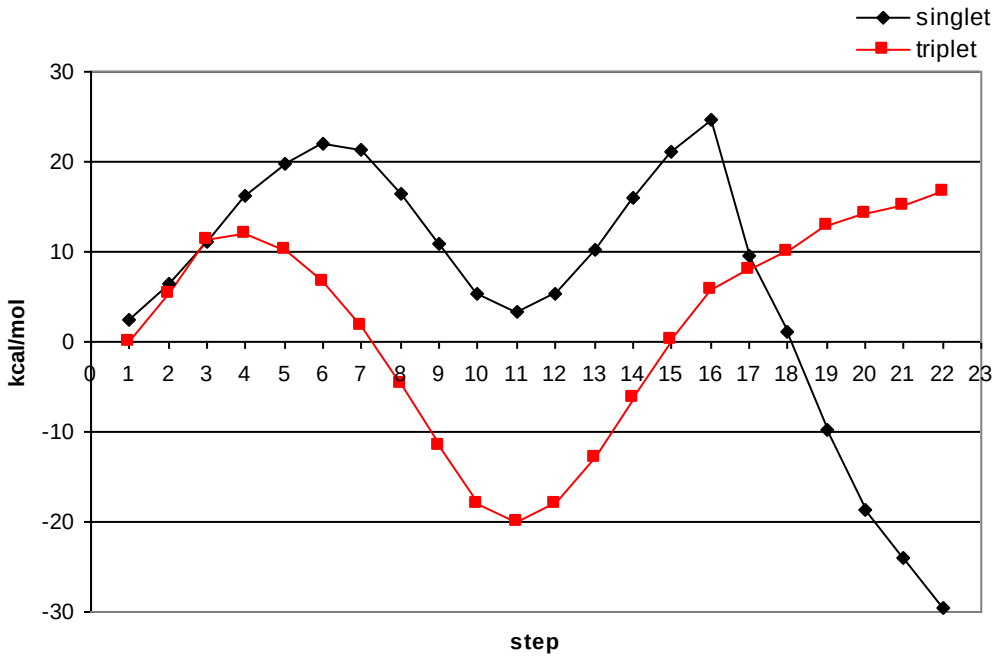

Figure 4.35: Reaction profile for the transfer of a proton from hydroxonium to an oxygen of the 4-nitro group, followed by the transfer of a proton from N5 of FMN to the same oxygen. Step 1 represents reactants (Figure 4.34), steps 1 through 11 represent the transfer of a proton from hydroxonium to an oxygen of the 4-nitro group. Steps 12 through 22 represent the transfer of a proton from N5 of FMN to the same oxygen. The large decrease in energy between steps 16 and 17 for the singlet represents the nitro N-O bond breaking.

	Charge on FMN	Charge on CB1954	Energy (Hartree)	Energy relative to Reactants (kcal)
Reactants triplet	−0.01	−0.69	−1891.987122	0
Reactants singlet	−0.65	−0.02	−1891.983123	3
Products triplet	−0.70	0.63	−1891.960416	17
Products singlet	0.03	−0.09	−1892.034421	−30

Table 4.15: Molecular charges and energy of reactants and products in singlet and triplet states for the proton transfer from hydroxonium to an oxygen of the 4-nitro group, followed by the transfer of a proton from N5 of FMN to the same oxygen.

Although the protons are transferred in the opposite order, the reaction is essentially the same: one electron is transferred from FMN to CB1954, followed by the proton from hydroxonium, and midway through the transfer of the proton from N5 of FMN, the N-O bond is broken, concerted with the transfer of the second electron from FMN to CB1954. Again, while there is a net transfer of a proton and two electrons from FMN to CB1954, there is no concerted hydride transfer. From the graph, the barrier for transfer of the first proton is around 8 kcal/mol but, as with the previous mechanism, the upper limit (again due to an avoided crossing) on the barrier for the concerted transfer of the second proton and second electron is 28 kcal/mol.

4.7.3 First Proton from Hydroxonium, Second from Another Hydroxonium

This represents the electron transfer mechanism, where both electrons come from FMN and both protons come from solution—represented in this case by two hydroxonium ions.

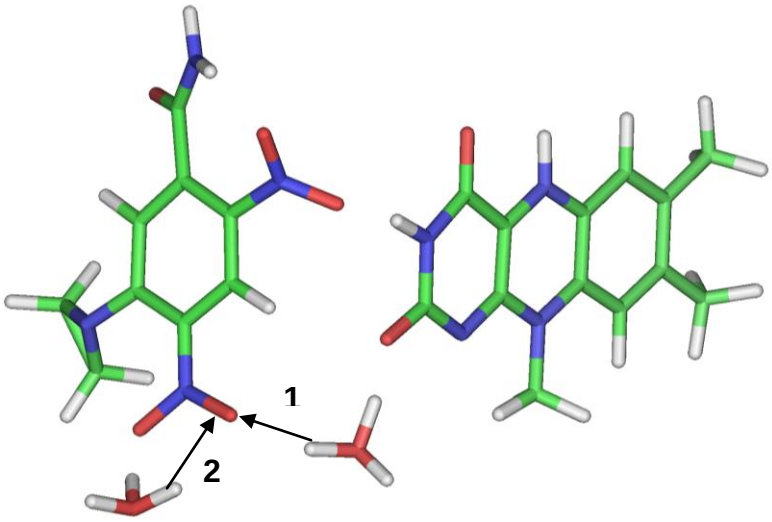

Figure 4.36: Transfer of proton from hydroxonium to an oxygen of the 4-nitro group, followed by the transfer of a proton from an additional hydroxonium to the same oxygen.

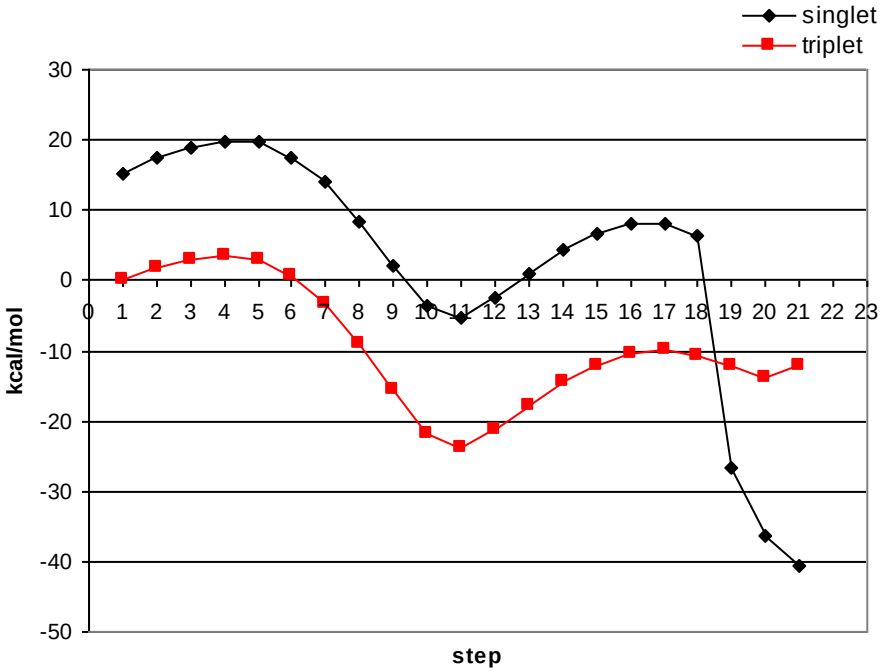

Figure 4.37: Reaction profile for the transfer of a proton from hydroxonium to an oxygen of the 4-nitro group, followed by the transfer of a proton from an additional hydroxonium to the same oxygen. Step 1 represents reactants (Figure 4.36), steps 1 through 11 represent the transfer of a proton from hydroxylamine to an oxygen of the 4-nitro group. Steps 12 through 22 represent the transfer of a proton from a second hydroxylamine to the same oxygen. The large decrease in energy between steps 18 and 19 for the singlet represents the nitro N-O bond breaking.

	Charge on FMN	Charge on CB1954	Energy (Hartree)	Energy relative to Reactants (kcal)
Reactants triplet	0.18	−0.61	−1968.790762	0
Reactants singlet	−0.02	−0.43	−1968.766322	15
Products triplet	0.08	0.76	−1968.809969	−12
Products singlet	0.81	0.11	−1968.855566	−41

Table 4.16: Molecular charges and energy of reactants and products in singlet and triplet states for the proton transfer from hydroxonium to an oxygen of the 4-nitro group, followed by the transfer of a proton from an additional hydroxonium to the same oxygen.

In common with both hydride transfer mechanisms, the electron transfer mechanism occurs as the transfer of an electron from FMN to CB1954, followed by a proton from solution, with the transfer of the second electron concerted with the breaking of the N-O bond as the second proton is transferred. There is a greater stabilisation of the triplet reactant compared with the two net hydride transfer mechanisms due to the presence of an additional positive charge close to CB1954, thus highlighting once again, the importance of the charge environment in influencing this first electron transfer. In this case, the barrier for the first proton transfer is reduced to around 4 kcal/mol, while the barrier for the concerted transfers of the second proton and second electron has an upper limit of 14 kcal/mol (again on account of the avoided crossing).

4.7.4 Full Reaction Profiles with a Dielectric

As mentioned previously, gas-phase hydroxonium ions are not a good model for solution. One way to ameliorate this is to use a dielectric to model the behaviour of the system as if it were solvated.

Because the PCM solvent model calculation is a single-point calculation, the geometries from Sections 4.7.1, 4.7.2, and 4.7.3 were used as input for the calculations.

Missing points on the graphs represent convergence failures.

4.7.4.1 First Proton from FMN, Second from Hydroxonium, with Solvation

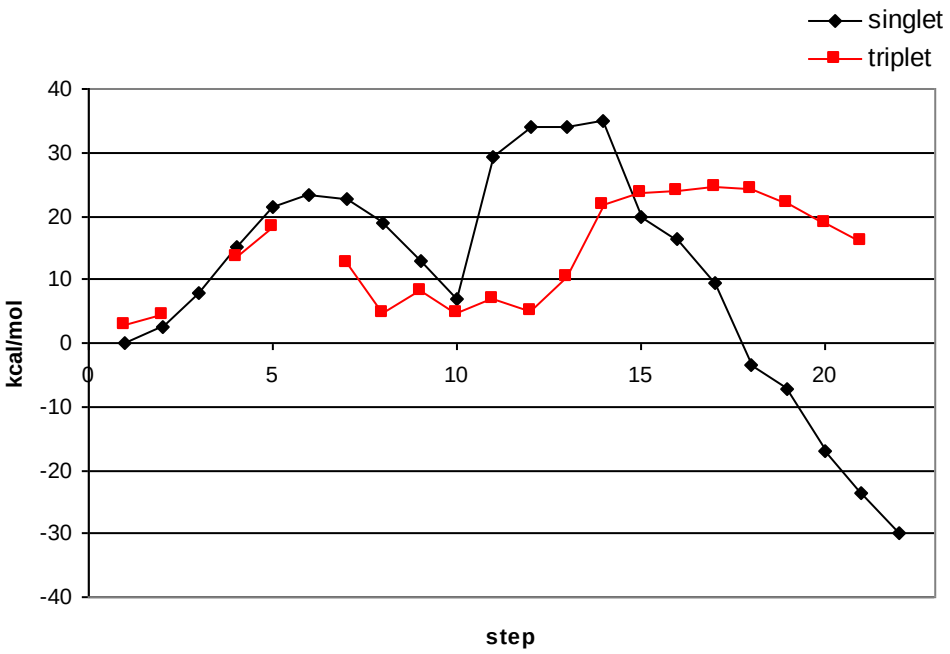

Figure 4.38: Reaction profile for the transfer of a proton from N5 of FMN to an oxygen of the 4-nitro group, followed by the transfer of a proton from hydroxonium to the same oxygen, with the PCM solvent model. Step 1 represents reactants (Figure 4.32), steps 1 through 10 represent the transfer of a proton from N5 to an oxygen of the 4-nitro group. Steps 11 through 22 represent the transfer of a proton from hydroxylamine to the same oxygen. The large decrease in energy between steps 14 and 15 for the singlet represents the nitro N-O bond breaking.

The primary differences between the gas phase and solvated reaction profiles for the first net hydride transfer mechanism (proton from FMN first, followed by proton from hydroxonium) are that at reactants, the singlet is now slightly lower in energy compared to the triplet, the barriers for proton transfer are slightly lower (upper limit on the second step now around 24 kcal/mol), and the energy of the intermediate is slightly higher. Otherwise, the overall shapes of the curves are largely the same.

4.7.4.2 First Proton from Hydroxonium, Second from FMN, with Solvation

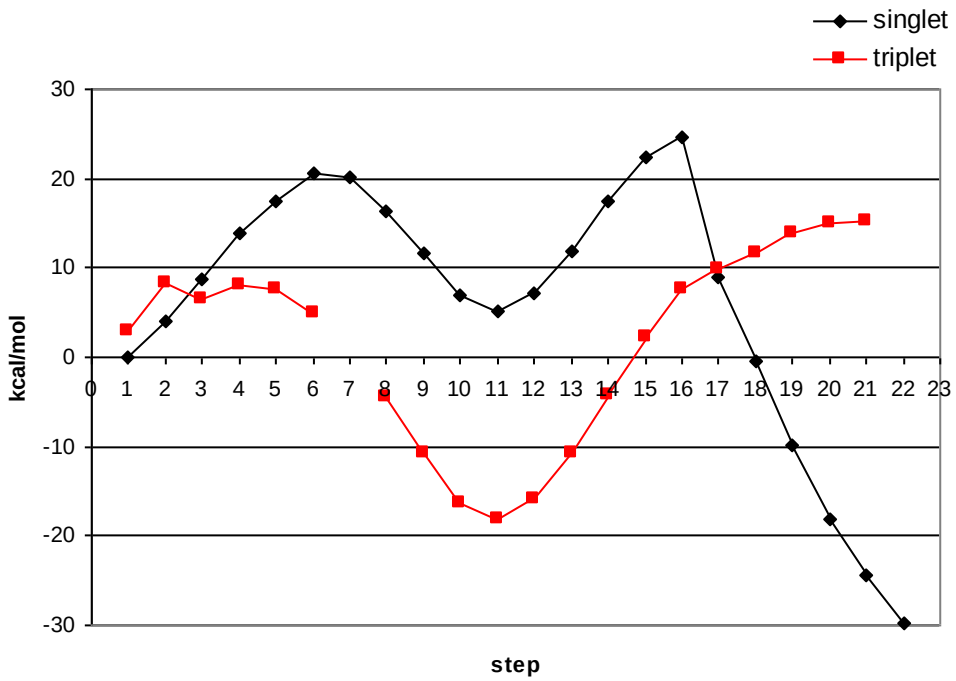

Figure 4.39: Reaction profile for the transfer of a proton from hydroxonium to an oxygen of the 4-nitro group, followed by the transfer of a proton from N5 of FMN to the same oxygen, with the PCM solvent model. Step 1 represents reactants (Figure 4.34), steps 1 through 11 represent the transfer of a proton from hydroxonium to an oxygen of the 4-nitro group. Steps 12 through 22 represent the transfer of a proton from N5 of FMN to the same oxygen. The large decrease in energy between steps 16 and 17 for the singlet represents the nitro N-O bond breaking.

Like the first net hydride transfer mechanism, the differences between the gas-phase and solvated reaction profiles for the second net hydride transfer mechanism are that at reactants, the singlet is now slightly lower in energy compared to the triplet, the barriers for proton transfer are slightly lower, and the energy of the intermediate is slightly higher.

4.7.4.3 First Proton from Hydroxonium, Second from Hydroxonium, with Solvation

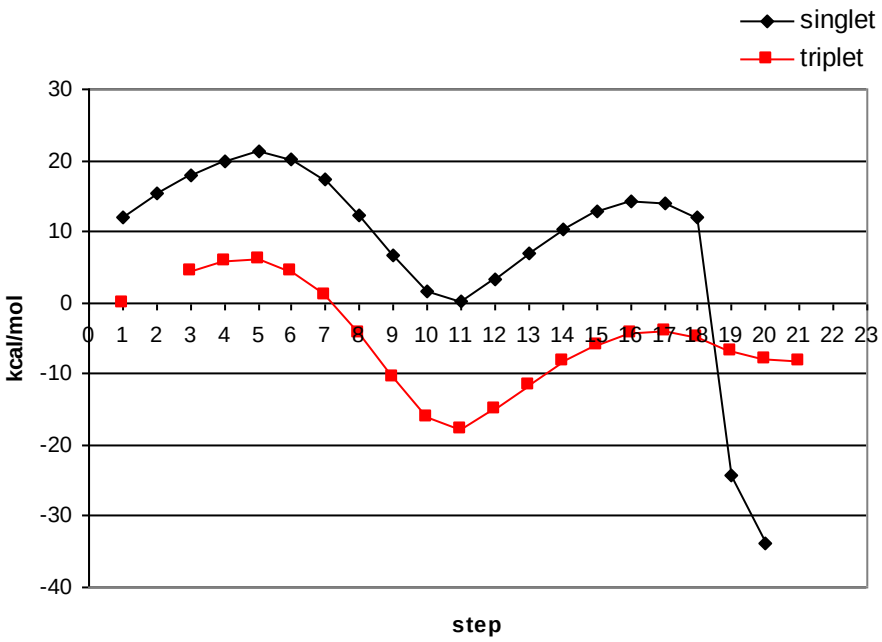

Figure 4.40: Reaction profile for the transfer of a proton from hydroxonium to an oxygen of the 4-nitro group, followed by the transfer of a proton from hydroxonium to the same oxygen, with the PCM solvent model. Step 1 represents reactants (Figure 4.36), steps 1 through 11 represent the transfer of a proton from hydroxylamine to an oxygen of the 4-nitro group. Steps 12 through 22 represent the transfer of a proton from a second hydroxylamine to the same oxygen. The large decrease in energy between steps 18 and 19 for the singlet represents the nitro N-O bond breaking.

Interestingly, for the electron transfer mechanism both transition states and the intermediate are relative to the reactant triplet state when compared to the gas-phase. As a result, the barrier for the concerted transfer of the second proton and second electron is essentially unchanged.

4.7.5 Full Reaction Profiles with Water

Attempts were made to determine full reaction profiles with water as the model for solution, but no useful results were obtained. After a proton was removed from the water molecule, the resulting hydroxyl group bonded either with the FMN or CB1954 in unrealistic ways. Similarly, use of the Eigen cation involves a large number of distinct fragments in the calculation leading to difficulties obtaining interpretable reaction profiles.

4.8 CASSCF Calculations

The point where the singlet and triplet lines cross can be considered the upper limit of the energy barrier for the second electron transfer in all three of the potential mechanisms, as the true pathway will follow an avoided crossing, as discussed in Chapter 2.

For a CASSCF calculation with an active space of two orbitals (The HOMO on FMN and LUMO on CB1954) and two electrons, the result will be two states. If the states have the same energy, the two potential energy surface meet in a conical intersection; if the energies of the two states are different, then we have an avoided crossing, the lower energy state being the "transition state" for the avoided crossing.

For the electron transfer reaction mechanism, attempts were made to perform CASSCF optimisations on a range of structures including the reactant complex, the approximate transition state for the first proton transfer, the intermediate complex, and all points surrounding the second electron transfer/N-O bond breaking event. Unfortunately, all calculations failed after the first step due to lack of memory, but the results effectively yielded a single-point CASSCF calculation for the steps of interest.

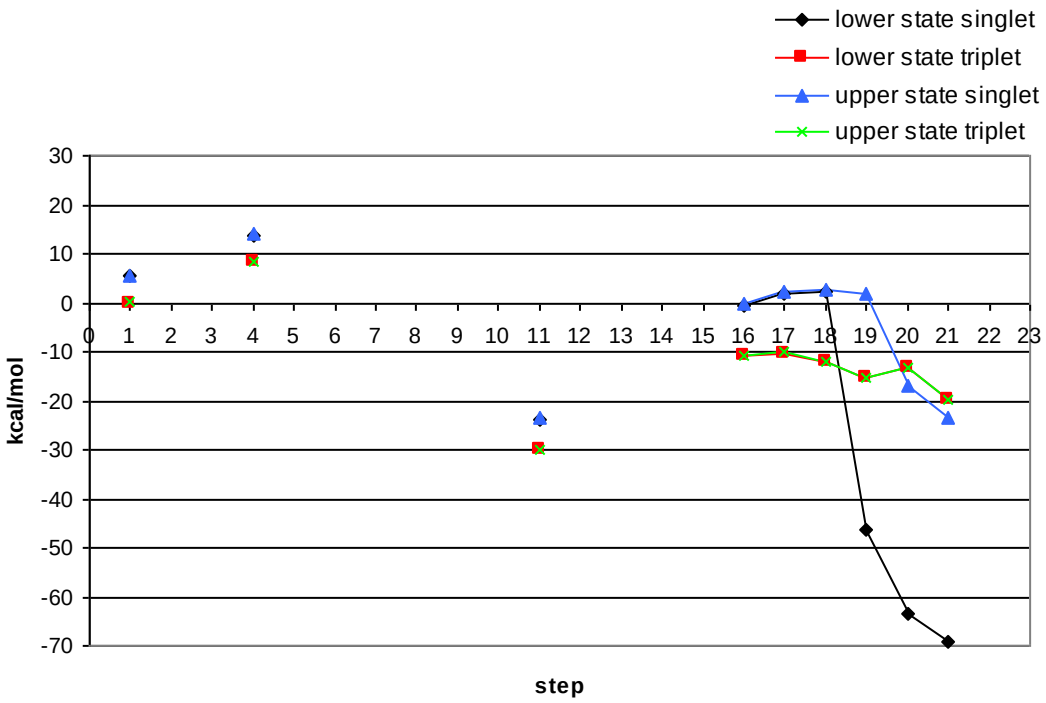

Figure 4.41: Single-point CASSCF calculations for the electron transfer reaction mechanism. Step 1 represents reactants (Figure 4.36), step 4 represents the maximum barrier for the transfer of a proton from hydroxylamine to an oxygen of the 4-nitro group. Step 11 represents the products of the first proton transfer. Step 18 represents the maximum barrier for the transfer of a proton from a second hydroxylamine to the same oxygen. The large decrease in energy between steps 18 and 19 for the singlet represents the nitro N-O bond breaking.

For the triplet, the energy of the upper and lower states was the same for every point. For the singlet, however, the energies of the two states diverge after the N-O bond breaking event. This suggests that the second electron transfer happens after the N-O bond is broken.

4.9 Summary of Chapter 4 Results

Infinite separation and reaction profiles show that either mechanism—net hydride transfer or electron transfer—is thermodynamically viable. In both cases however, the reaction proceeds via single electron transfer, then transfer of the first proton and finishing with a single concerted step in which the N-O bond is broken, alongside transfer of both the second electron and the second proton.

It is difficult to distinguish the three processes on the basis of barrier heights as these calculations use very small model systems, including only the reacting species and a simple model for salvation. Though the electron transfer mechanism has the lowest overall barrier in these simple models (14 kcal/mol compared with 24 kcal/mol for net hydride transfer), neither mechanism can be ruled out and we need to investigate the behaviour of the reactant complex in the enzyme active site to determine which actually occurs in wild-type NTR.

Chapter 5

Molecular Mechanics and Hybrid QM/MM Methods

This chapter describes the docking, molecular mechanics minimisations, and molecular dynamics runs utilised to determine the binding orientation for CB1954 in the active site of NTR. Additionally, the results of hybrid QM/MM calculations for CB1954 with FMN and key NTR active site amino acids are also discussed.

5.1 Docking

As discussed in Chapter 2, docking calculations were performed in order to examine possible binding orientations for CB1954 in the NTR active site. Additionally, calculations were performed for NADH, dicoumarol, and nitrofurazone, for comparison.

All docking runs were carried out using Autodock 3.1 and the 1YKI crystal structure. This structure is of NTR in the oxidised form, with nitrofurazone bound. In all docking runs the reduced form of FMN was used. This was done by adding a hydride to the N5 of FMN, and while this does not change the geometry of FMN, it does give it the correct charge.

Run	CB1954 K_i (M)	NADH K_i (M)	Dicoumarol K_i (M)	Nitrofurazone K_i (M)
1	1.66E-04	2.28E-06	1.57E-06	7.44E-05
2	1.18E-04	2.47E-06	1.49E-06	7.26E-05
3	2.08E-05	7.63E-07	7.99E-07	8.75E-05
4	9.31E-05	2.42E-06	3.57E-07	2.57E-05
5	5.85E-06	2.88E-06	1.07E-06	1.27E-04
6	9.10E-05	6.30E-07	2.03E-07	2.61E-05
7	1.39E-04	7.36E-07	4.72E-06	2.86E-05
8	5.55E-06	9.44E-07	1.82E-06	9.11E-05
9	1.50E-04	7.26E-07	2.98E-07	7.45E-05
10	9.94E-06	6.80E-07	1.76E-06	7.38E-05

Table 5.1: Docking results for CB1954, NADH, Dicoumarol and Nitrofurazone with reduced NTR.

5.1.1 Docking Results for CB1954

Of the ten docking runs for CB1954 with NTR, all were found within the active site, but only three had K_i values of 10^{-5} M or smaller. The best two were in the same position in space, but were mirror images of each other. This is reasonable, considering the symmetry in the LUMO of CB1954.

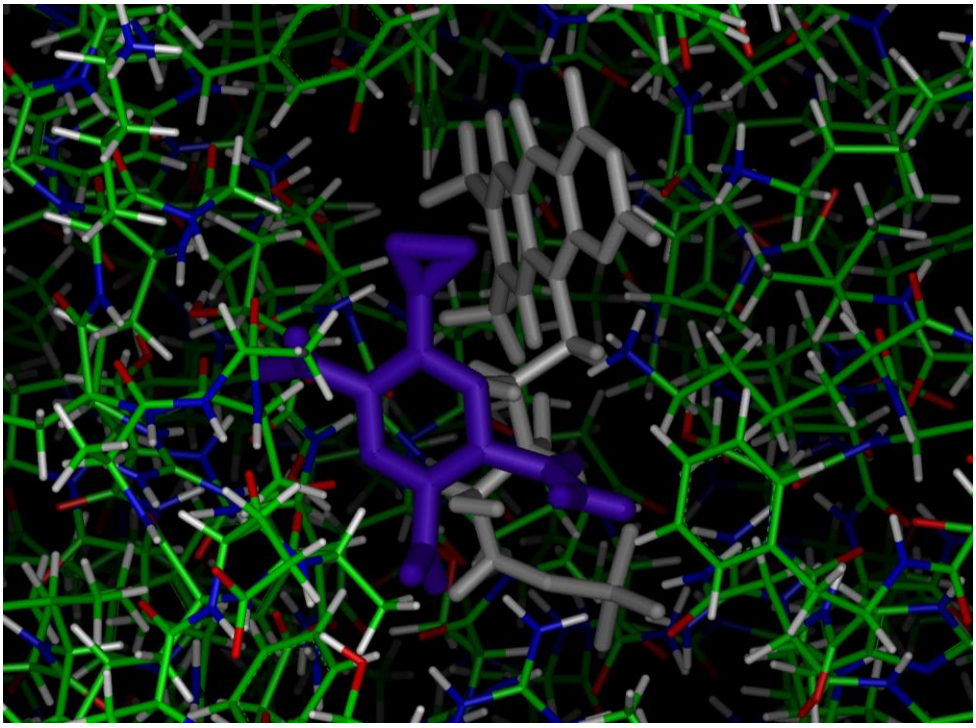

Figure 5.1: Docking run 5 for CB1954 with NTR. CB1954 is blue, while the FMN cofactor is grey. The Autodock K_i value for this run was 5.85×10^{-6} M.

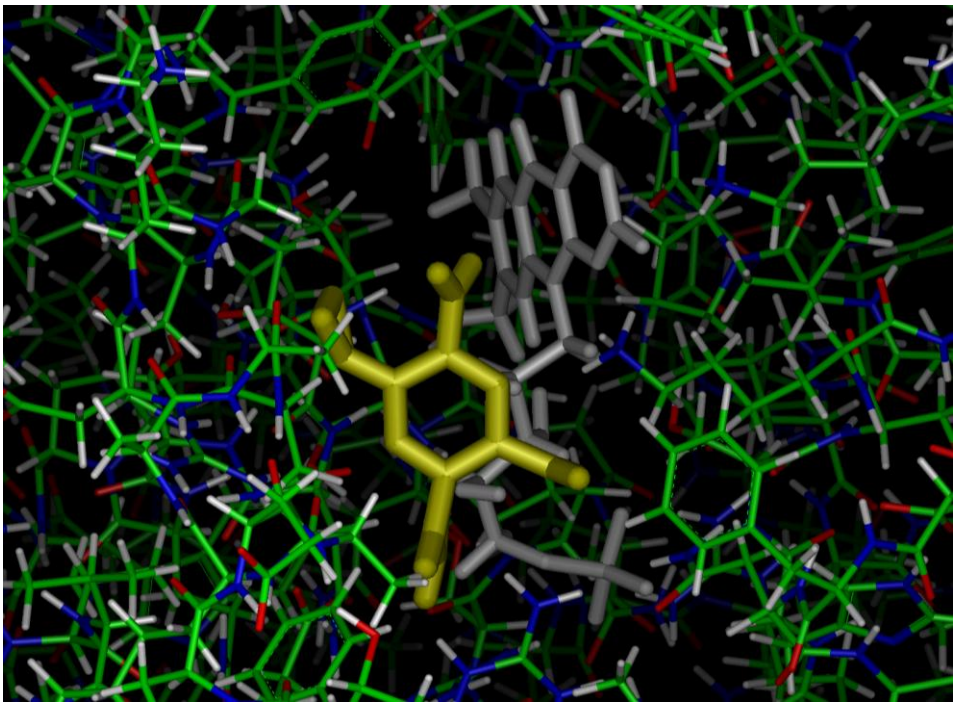

Figure 5.2: Docking run 10 for CB1954 with NTR. CB1954 is yellow, while the FMN cofactor is grey. The Autodock K_i value for this run was 9.94×10^{-6} M.

In both cases, CB1954 is found approximately five angstroms from FMN, and is not in a particularly good position for hydride transfer. It is, however, found in a reasonably good position for electron transfer.

K_i values for all ten docking runs were between 10^{-4} and 10^{-6} M (Autodock cuts off all values greater than 10^{-4} M). These K_i values indicate that CB1954 is very poorly bound, even by Autodock standards (we have found that Autodock substantially overestimates binding interactions giving K_i values rather lower than might be expected experimentally[111]. This is in agreement with experimental data that shows CB1954 binding poorly to NTR[40].

It is, however, important to note that the 1YKI crystal structure that was used for docking was of the enzyme in its oxidised form, and therefore may not give an accurate indication of how the ligand would bind to the reduced enzyme, despite the fact that the reduced FMN cofactor was used for all docking runs.

5.1.2 Docking Results for NADH

As the reduction of NTR by NAD(P)H is the first step in the overall reaction, it is important to know how NAD(P)H binds, so that any changes made to NTR to improve CB1954 binding do not disrupt the NAD(P)H binding.

Unfortunately, NADH is a relatively large ligand, with many rotatable bonds. This makes it difficult for a docking program to find the optimal binding orientation. It is possible to freeze rotatable bonds, but this too may decrease accuracy, if the wrong bonds are frozen.

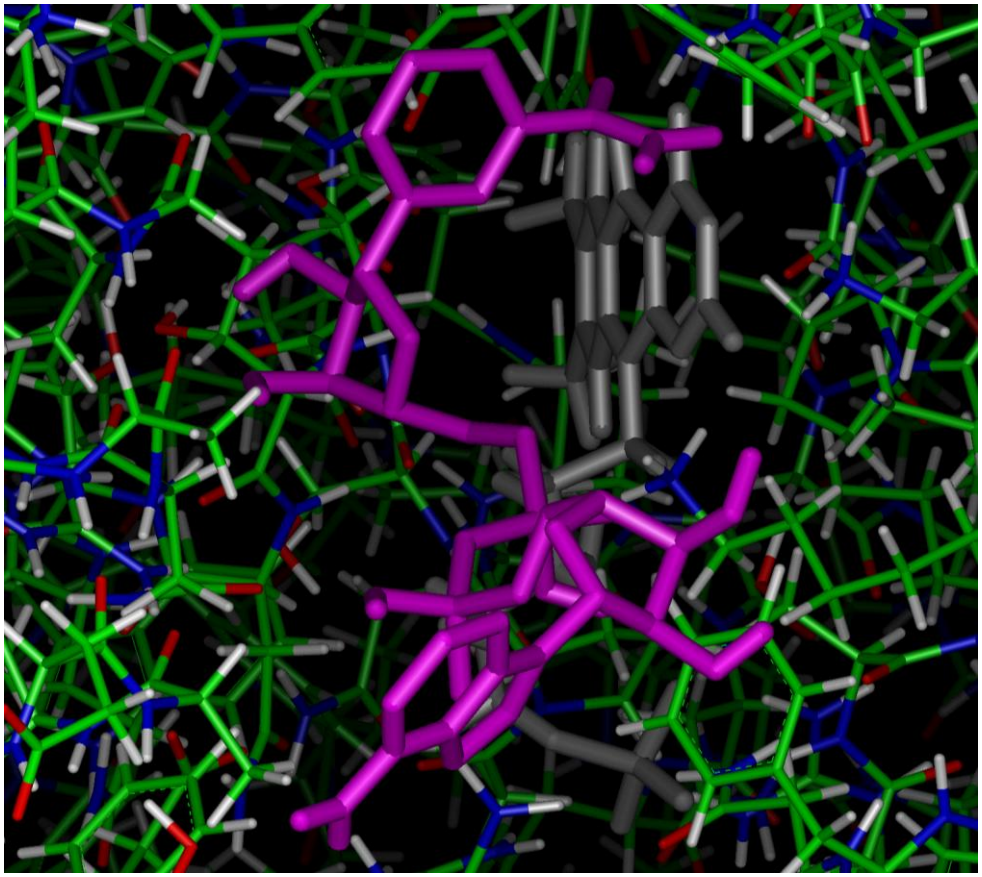

Figure 5.3: Docking run 8 for NADH with NTR. NADH is magenta, while the FMN cofactor is grey. The Autodock K_i value for this run was 9.4×10^{-7} M.

Three attempts at docking NADH with NTR were made, with various rotatable bonds frozen, but none yielded NADH with the C4 carbon (the hydride donor) within an adequate distance of N5 of FMN. The closest run is shown in Figure 5.3.

5.1.3 Docking Results for Dicoumarol

Dicoumarol is a known inhibitor of NTR. Unlike CB1954 and NADH, there is a crystal structure with dicoumarol bound to reduced NTR, which can be used as a basis for comparison.

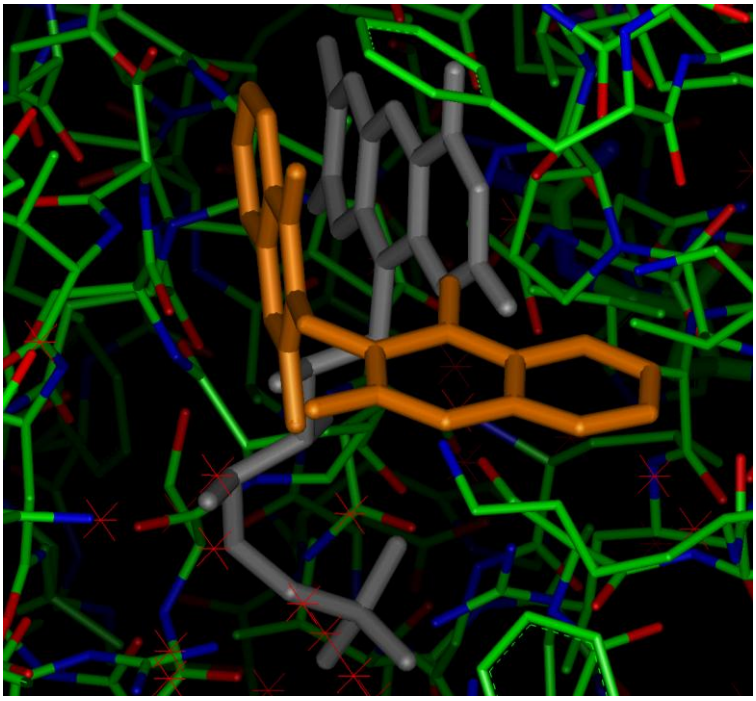

Figure 5.4: Crystal structure of dicoumarol with NTR. Dicoumarol is orange, while the FMN cofactor is grey.

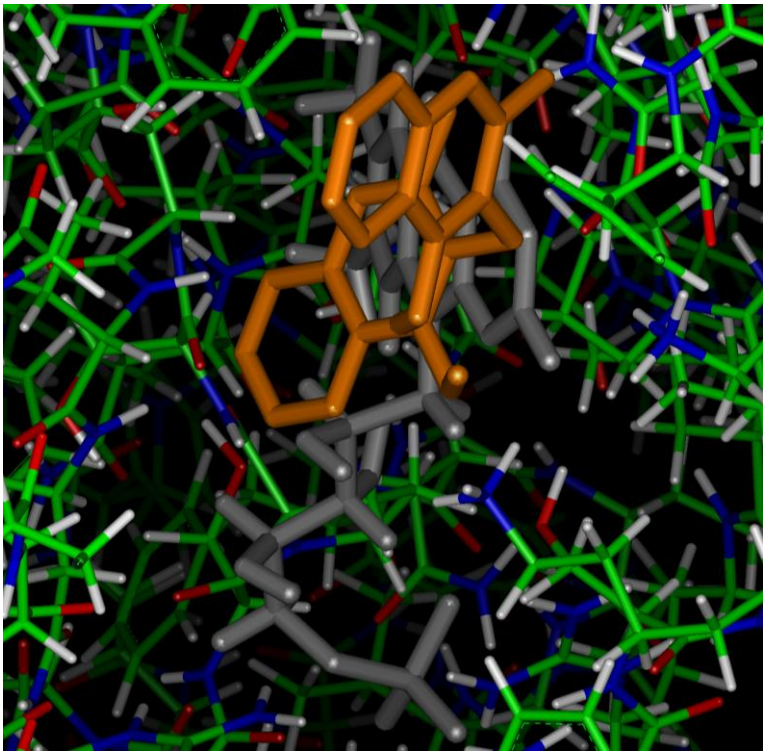

Figure 5.5: Docking run 3 for dicoumarol with NTR. Dicoumarol is orange, while the FMN cofactor is grey. The Autodock K_i value for this run was 3.0×10^{-7} M.

Although the docking run does have dicoumarol in the active site of NTR, it does not give the correct molecular orientation, which is of utmost importance.

5.1.4 Docking Results for Nitrofurazone

Nitrofurazone was the ligand originally bound in the 1YKI crystal structure used for the docking runs. Therefore it is another useful ligand for a basis for comparison.

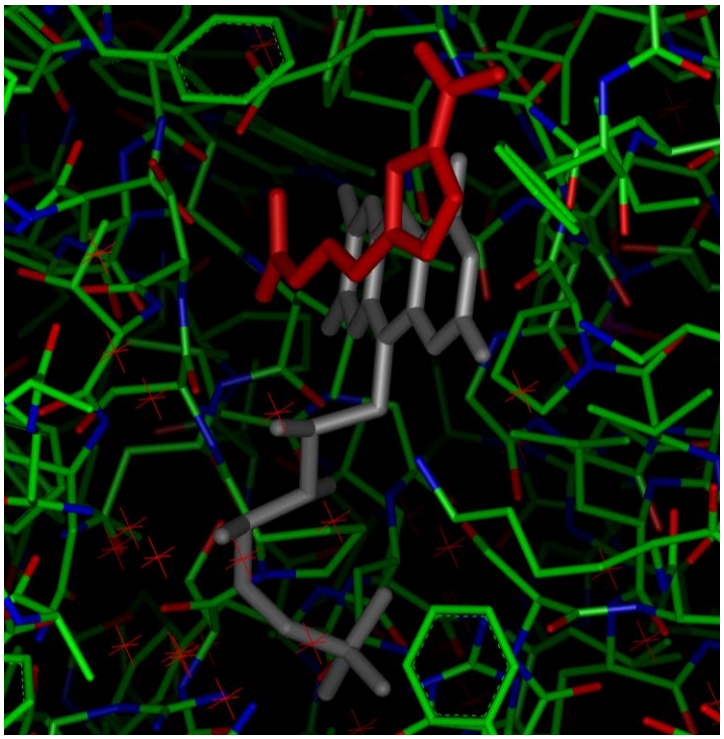

Figure 5.6: Crystal structure of nitrofurazone with NTR. Nitrofurazone is red, while the FMN cofactor is grey.

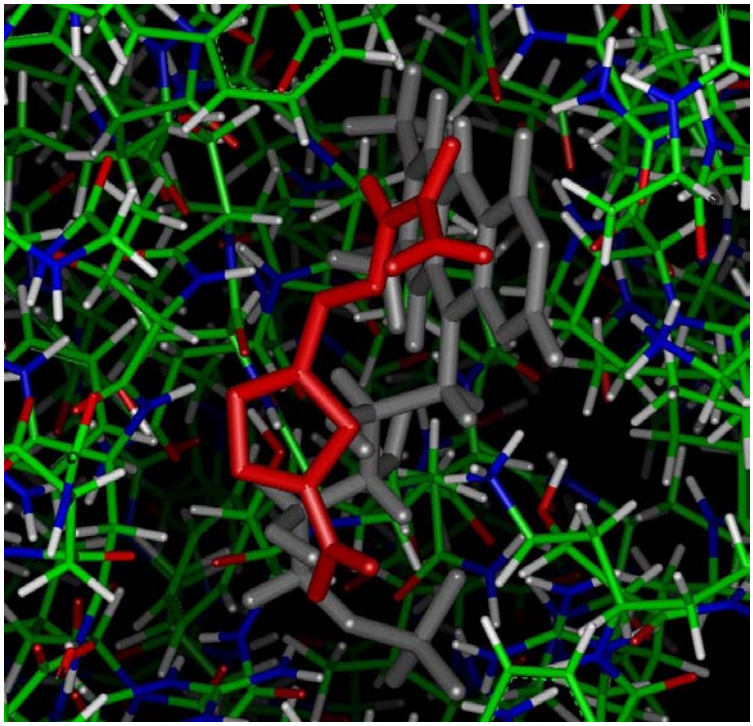

Figure 5.7: Docking run 6 for nitrofurazone with NTR. Nitrofurazone is red, while the FMN cofactor is grey. The Autodock K_i value for this run was 2.6×10^{-5} M.

The fact that even the ligand originally bound in the crystal structure does not dock very well indicates that docking results for NTR with ligands of interest cannot necessarily be trusted.

5.1.5 A Comparison of Docking K_i Values to Experimental Values

Although none of the docking results gave useful conformations, it is still interesting to compare docking K_i values to those obtained from experiment.

Ligand	Experimental K_i or K_m (M)	Autodock K_i (M)
CB1954	1.72×10^{-2}	5.8×10^{-6}
NADH	3.6×10^{-4}	9.4×10^{-7}
Dicoumarol	1.0×10^{-5}	3.0×10^{-7}
Nitrofurazone	1.9×10^{-3}	2.6×10^{-5}

Table 5.2: Comparison of experimental values of K_i or K_m[16,40] and Autodock K_i values.

Autodock K_i values are smaller than experimental values by at least a factor of 100. This is in agreement with previous work which has shown Autodock to overestimate binding affinity[111]. Interestingly, a graph of the logarithm of the values is a straight line for NADH, dicoumarol and CB1954, with nitrofurazone as an outlier. The straight line fit for this graph has a slope of 0.4976 and a y-intercept of −3.9837, with an R^2 value of 0.6282. Previous work by Richard Ward with Inositol Monophosphatase produced a calibration line with a slope of 1.378 and y-intercept of −3.5756, with an R^2 value of 0.931[111].

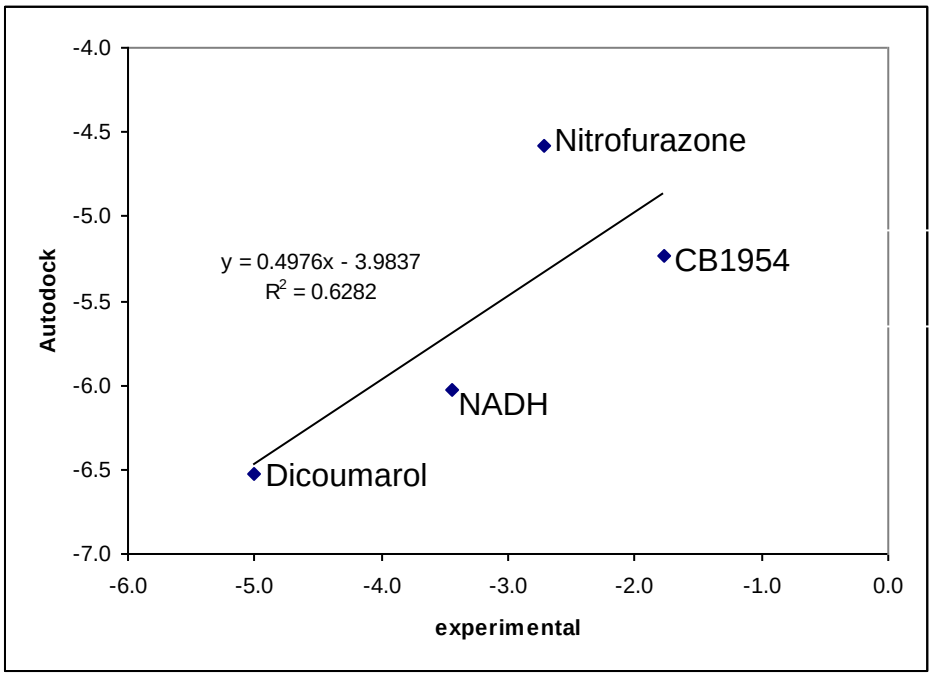

Figure 5.8: Graph of the logarithm of Autodock vs experimental K_i values for NTR.

5.2 Molecular Mechanics and Dynamics Calculations

NTR may be found in both oxidised and reduced forms, and there are a wide variety of mutants that have been studied experimentally. Therefore there are a vast amount of possible combinations of oxidation states, mutants, and ligands which can be examined computationally and compared to experimental and crystallographic data.

However, because NTR has two active sites per molecule, this allows for the possibility of looking at two different binding orientations in a single dynamics run.

Although interactions between the ligand, protein, and solution are of great importance, much of the information gained from molecular dynamics calculations is qualitative; does the ligand stay in the active site, in a particular orientation, or not?

Additionally, it is not only important *if* the ligand comes out, but also *when*. If the ligand comes out during the molecular mechanics minimisation, this indicates a poor binding orientation, or an incorrectly solved crystal structure. If the ligand comes out during the equilibrium run of the molecular dynamics this does not necessarily mean anything except perhaps faulty setup, but if it comes out during the data gathering portion of the molecular dynamics, this indicates either poor binding, or an insufficient equilibrium run.

Other possible sources of error include poor charges or parameters for the cofactors and ligands, inadequate treatment of non-bonded cutoffs, and wrong choice of protonation states of amino acids.

Prep files for the cofactors and ligands were generated using Antechamber, and can be found in Appendix B. Charges and parameters are generally in good agreement with the FF03 force field used for the amino acids, e.g. ligand amide groups have similar charges to the analogous amino acid groups.

Acetate	Partial Charges		
Atom	**AM1-BCC**	**AM1**	**Aspartate (FF03)**
CH3	−0.34	−0.26	−0.05 (CB)
C	0.29	0.30	0.75 (CG)
O	0.11	−0.60	−0.73 (OD1)
OXT	−0.63	−0.60	−0.73 (OD2)
CB1954 amide	**Partial Charges**		
Atom	**AM1-BCC**	**MPW1PW91/6-31G****	**Glutamine (FF03)**
C3	0.65	0.58	0.67 (CD)
O	−0.57	−0.51	−0.63 (OE1)
N1	−0.61	−0.66	−0.88 (NE2)
H11	0.31	0.31	0.41 (HE21)
H12	0.31	0.34	0.41 (HE22)
CB1954 2-nitro	**Partial Charges**		
Atom	**AM1-BCC**	**MPW1PW91/6-31G****	
N	0.32	0.37	
O1	−0.18	−0.42	
O2	−0.22	−0.36	

Table 5.3: Comparison of ligand partial charges at various levels of theory with partial charges for analogous atoms in the FF03 force field[118]. Full ligand partial charges may be found in Appendix B.

As Table 5.3 shows, the AM1-BCC charges for acetate are an exception. The O and OXT oxygens of acetate should be equivalent, yet at the AM1-BCC level they are clearly not. At the AM1 level, the carboxylate oxygens are equivalent, but the group is less polar than the analogous aspartate carboxylate group.

For the CB1954 amide group, charges are similar at the AM1-BCC and MPW1PW91/6-31G** levels, yet in both cases slightly less polar than the analogous glutamine amide group. The nitro group is less polar at the AM1-BBC level compared to MPW1PW91/6-31G**, but in both cases, the nitro group is less polar than the amide group.

When using a Particle Mesh Ewald, the default non-bonded cutoff of 8 angstroms should be adequate. Moreover, if there were any essential long-range interactions, their effects would be observed in kinetic experiments and X-ray crystal data.

For amino acid protonation states, initially all carboxyl groups are deprotonated and all amine groups are protonated. This is followed by an analysis of potential hydrogen bonding patterns, and amino acids are protonated or deprotonated accordingly.

For all molecular dynamics simulations, ligands are designated as "coming out" or "remaining bound" based on key interactions with active site amino acids, or the FMN cofactor. More detail on the molecular dynamics runs can be found in Appendix C.

5.2.1 Acetate in Oxidised NTR

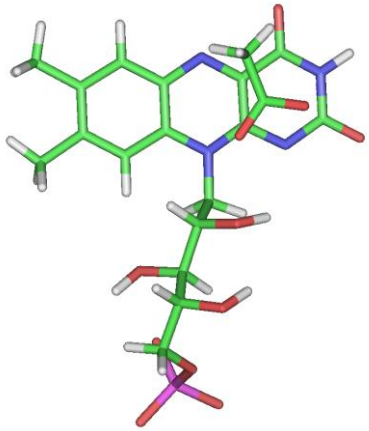

Figure 5.9: Acetate and oxidised FMN from the 1YLR crystal structure[16].

Acetate is commonly found in crystal structures, as it is present in the buffer solution in which the enzyme is crystallised. The primary reasons for running molecular mechanics and dynamics calculations on acetate are the fact that there is a well-resolved crystal structure for NTR with bound acetate[16], in which the carboxylate group forms a hydrogen bond with the T41 backbone. It is also believed that the electron density attributed to CB1954 in x-ray structure 1IDT is more consistent with acetate[36]. It is interesting to see if the acetate stays bound in the active site for both the oxidised and reduced states of NTR.

For the molecular mechanics minimisation, the crystal structure was taken directly, without any modifications. Acetate is bound in the same orientation in both active sites.

Dynamics Run	Protein RMSd			Active Site	Outcome
	mean	min	max		
1	1.45	1.21	1.69	A	Acetate comes out, but remains close
				B	Acetate comes out, but remains close
2	1.30	0.94	1.56	A	Acetate remains bound
				B	Acetate comes completely out
3	1.42	1.09	1.76	A	Acetate comes completely out
				B	Acetate comes completely out

Table 5.4: Molecular dynamics runs with acetate and oxidised NTR.

Three molecular dynamics runs and two active sites per molecule give a total of six simulations of acetate bound within the active site of NTR. Of the six, two remained bound in the site with the methyl group in the active site, two lost the hydrogen bond to the T41 backbone but remained close to the active site during data gathering, and two were removed completely from the active site during equilibration.

The molecular dynamics runs were repeated with AM1 charges for acetate (Table 5.3) with no improvement in binding.

5.2.2 Acetate in Reduced NTR

For the molecular mechanics and dynamics simulations of acetate with reduced NTR, the same 1YLR crystal structure was used, with a hydride added to the N5 of FMN. No other changes to the crystal structure were made prior to minimisation.

Of the six possible simulations for acetate bound in the active site of NTR in the reduced form, all six acetate molecules came out of the active site completely during data gathering. This contrasts with the simulations of the oxidised enzyme, in which two acetate molecules remained bound in the active site. As there is a change in the charge on FMN on reduction becoming negative, it is perhaps not surprising that we may see different acetate binding affinities for oxidised and reduced states of NTR. The molecular dynamics runs were repeated with AM1 charges for acetate (Table 5.3) with no improvement in binding.

Dynamics Run	Protein RMSd			Active Site	Outcome
	mean	min	max		
1	1.64	0.98	2.10	A	Acetate comes out
				B	Acetate comes out
2	1.61	1.19	1.96	A	Acetate comes out
				B	Acetate comes out
3	1.55	1.18	1.91	A	Acetate comes out
				B	Acetate comes out

Table 5.5: Molecular dynamics runs with acetate and reduced NTR.

5.2.3 Menadione and Reduced NTR

Menadione is a relatively good substrate for NTR, with a K_m of 20 μM[144]. As menadione is a quinone, it is able to be reduced via net hydride transfer, with one carboxyl group obtaining a hydride from N5 of FMN, and the opposite carboxyl group obtaining a proton from solution.

There is no crystal structure for menadione bound to NTR. Therefore the orientation of menadione with respect to the flavin ring system of the FAD cofactor of NQO2 from the 2QR2[45] crystal structure was superimposed onto FMN in the 1YKI crystal structure of NTR.

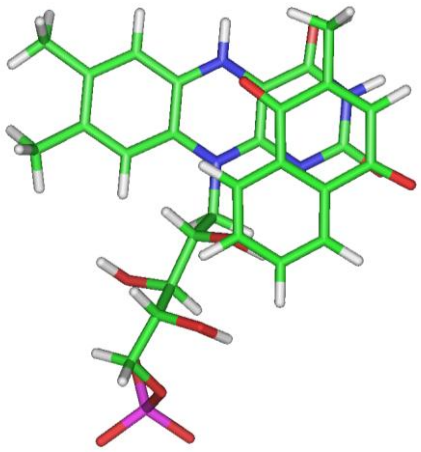

Figure 5.10: Menadione and reduced FMN from bound complex prior to minimisation.

Of the six simulations of menadione, not one stayed in the active site. This may be because menadione has no binding interactions in the active site aside from ring stacking, or because the crystal structure contains oxidised FMN and was determined with nitrofurazone as a substrate, and as such may not accommodate menadione properly.

Dynamics Run	Protein RMSd			Active Site	Outcome
	mean	min	max		
1	1.71	1.10	2.02	A	Menadione comes out
				B	Menadione comes out
2	1.69	1.08	1.01	A	Menadione comes out
				B	Menadione comes out
3	1.58	1.01	1.90	A	Menadione comes out
				B	Menadione comes out

Table 5.6: Molecular dynamics runs with menadione and reduced NTR.

5.2.4 Nitrofurazone and Oxidised NTR

The 1YKI crystal structure has nitrofurazone bound to the oxidised enzyme with the amide group in the active site, with hydrogen bonds to the T41 backbone and E165 side chain. However, in order to be reduced via hydride transfer, there must be a binding orientation with the nitro group of nitrofurazone in the active site within about four angstroms of N5 of FMN.

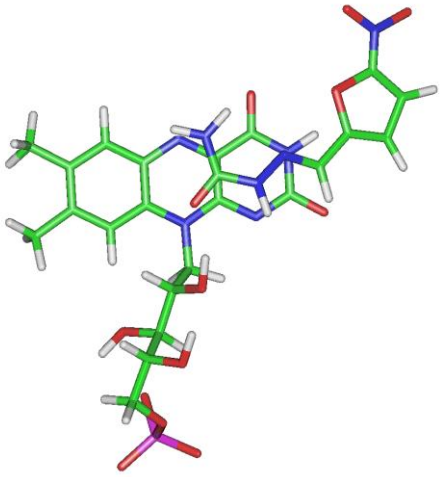

Figure 5.11: Nitrofurazone and FMN from the 1YKI crystal structure, with the amide group in the active site.

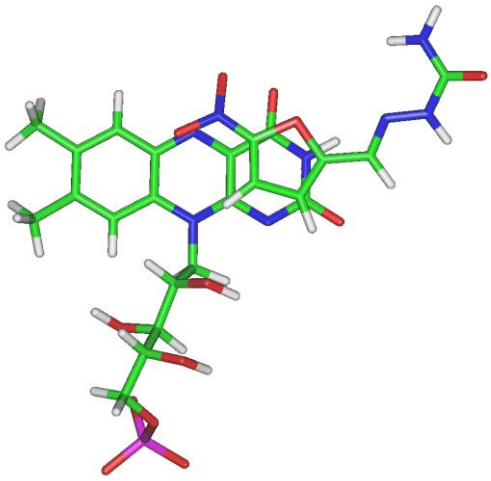

Figure 5.12: Nitrofurazone and FMN from the 1YKI crystal structure, with nitrofurazone reoriented to present its nitro group in the active site.

As NTR has two active sites, for the molecular mechanics and dynamics calculations one nitrofurazone molecule was reoriented in its site so that the nitro group was in the active site, close to N5 of FMN.

Dynamics Run	Protein RMSd			Active Site	Outcome
	mean	min	max		
1	1.50	1.08	1.80	amide	Nitrofurazone remains bound
				nitro	Nitrofurazone comes out
2	1.52	1.09	1.88	amide	Nitrofurazone comes out
				nitro	Nitrofurazone comes out
3	1.46	1.14	1.73	amide	Nitrofurazone remains bound
				nitro	Nitrofurazone comes out

Table 5.6: Molecular dynamics runs with nitrofurazone and oxidised NTR.

In runs 1 and 3, the nitrofurazone with the amide group bound in the active site remains bound. In run 2, the nitrofurazone with the amide group in the active site comes out during the equilibration run. In every run, the nitrofurazone with the nitro group in the active site comes out in the molecular mechanics minimisation.

5.2.5 Nitrofurazone and Reduced NTR

For the molecular mechanics and dynamics simulations of nitrofurazone with reduced NTR, the same initial configuration as the oxidised enzyme was used, with a hydride added to the N5 of FMN and the resulting complex optimised. No other changes were made.

Dynamics Run	Protein RMSd			Active Site	Outcome
	mean	min	max		
1	1.55	1.19	1.86	amide	Nitrofurazone remains bound
				nitro	Nitrofurazone comes out
2	1.60	0.98	2.13	amide	Nitrofurazone remains bound
				nitro	Nitrofurazone comes out
3	1.60	1.04	2.10	amide	Nitrofurazone remains bound
				nitro	Nitrofurazone comes out

Table 5.7: Molecular dynamics runs with nitrofurazone and reduced NTR.

With nitrofurazone, the results for the enzyme in the reduced state are almost exactly the same as the results for the oxidised state; the nitrofurazone with the amide group in the active site remains bound, while the nitrofurazone with the nitro group in the active site comes out during the molecular mechanics minimisation. This may indicate that despite the charge change on FMN, amide groups bind preferentially over nitro groups in both the oxidised and reduced forms of the enzyme. In both oxidised and reduced FMN, the binding mode of nitrofurazone corresponds to that observed in the crystal structure 1YKI, which goes against the argument presented by Race *et al.*[15] that the binding mode of nitrofurazone changes with FMN oxidation state. However, the arguments presented by Race *et al.*[15] were predicated on a belief that FMN in NTR is acting as a hydride donor rather than an electron donor.

5.2.6 CB1954 with Reduced NfsA

NfsA is known to favour the 2-nitro reduction over the 4-nitro. Unfortunately, there is no crystal structure for CB1954 bound to nfsA, so there is some difficulty in finding a good starting orientation for the prodrug in the active site.

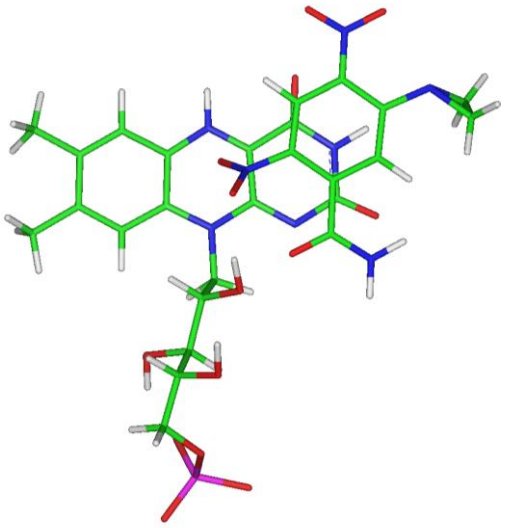

Figure 5.13: CB1954 and FMN orientation 1, with the 2-nitro group in the active site of nfsA.

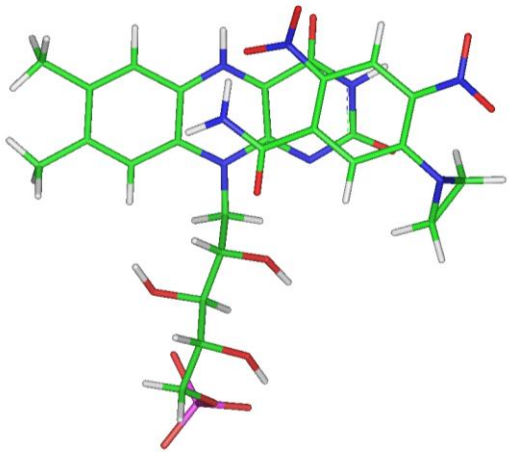

Figure 5.14: CB1954 and FMN orientation 2, with the 2-nitro group in the active site of nfsA.

In both cases, the oxygen of the 2-nitro group is within 4 angstroms of N5 of FMN. Not only is the binding of CB1954 to nfsA of interest for its own sake, but a stable binding orientation from nfsA can be used as a starting point to find a binding orientation for NTR.

Unfortunately, CB1954 did not stay in the active site for a single molecular dynamics run. In all cases, the CB1954 came partially out of the site during the molecular mechanics minimisation and equilibrium runs, and came completely out during data gathering.

Alternative orientations of CB1954 with the 2-nitro group in the active site were attempted, but all of these failed to yield useful results as well. This may be because the initial orientations were not close enough to the actual binding orientation, and initial forces expelled the prodrug from the active site.

Dynamics Run	Protein RMSd			Active Site	Outcome
	mean	min	max		
1	1.63	0.96	2.08	A	CB1954 comes out
				B	CB1954 comes out
2	1.48	1.16	1.80	A	CB1954 comes out
				B	CB1954 comes out
3	1.50	1.03	2.01	A	CB1954 comes out
				B	CB1954 comes out

Table 5.8: Molecular dynamics runs with CB1954 and reduced nfsA.

5.2.7 CB1954 with Reduced NQO2

NQO2 is known to favour the 4-nitro reduction over the 2-nitro. Unlike nfsA, there is a crystal structure with CB1954 bound in the active site, with the 4-nitro group at 2.92 angstroms from N5 of FMN.

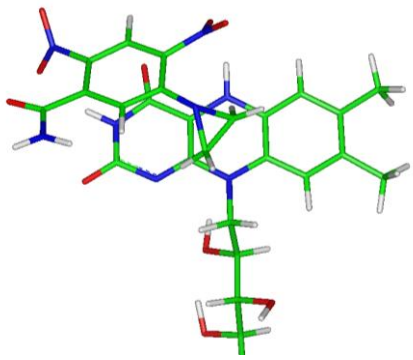

Figure 5.15: CB1954 and FAD from the 1ZX1 crystal structure, with the 4-nitro group in the active site of NQO2. The full FAD chain is not shown.

In all of the molecular dynamics runs, both CB1954 molecules moved in such a way that the oxygens of the nitro group were no longer within a reasonable distance of N5 of FMN for hydride transfer. However, in one of the dynamics runs, the 4-nitro oxygens did stay within approximately four angstroms for about 5 nanoseconds.

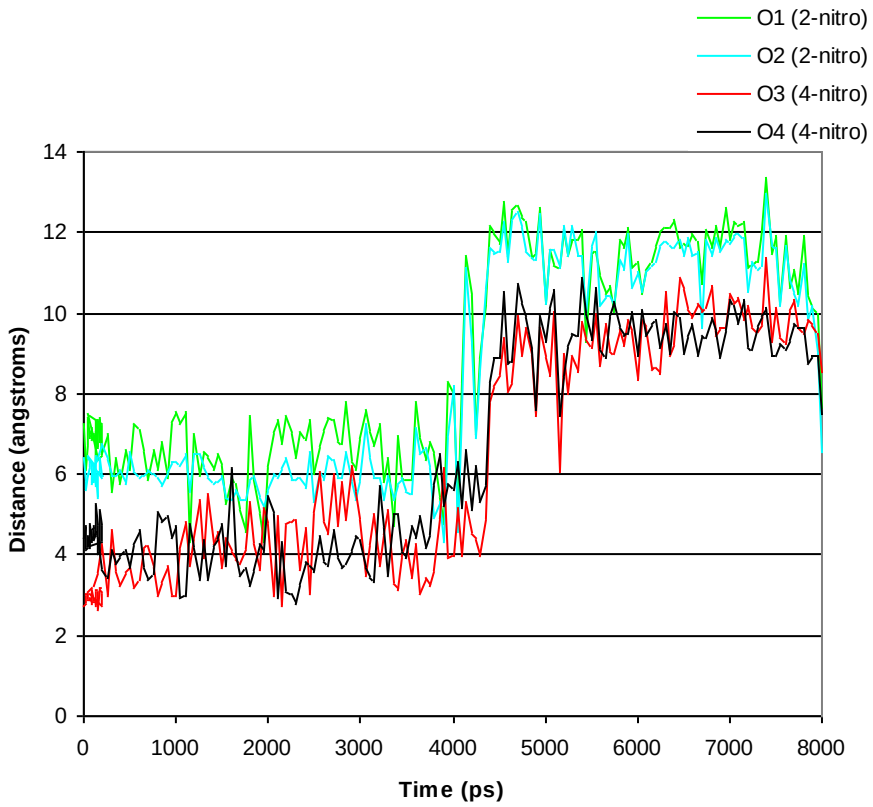

Figure 5.16: Distance from N5 of the FAD cofactor of NQO2 to oxygens of the nitro groups of CB1954.

Interestingly, for all of the dynamics runs, CB1954 was never completely expelled from the site, and the molecule remained within van der Waals contact with FAD, with the 4-nitro group exposed to solution—appropriate for an electron transfer mechanism.

Dynamics Run	Protein RMSd			Active Site	Outcome
	mean	min	max		
1	1.55	1.16	1.83	A	CB1954 comes out
				B	CB1954 comes out
2	1.38	0.98	1.62	A	CB1954 comes out
				B	CB1954 comes out
3	1.28	1.08	1.41	A	CB1954 comes out
				B	CB1954 comes out

Table 5.9: Molecular dynamics runs with CB1954 and reduced NQO2.

5.2.8 CB1954 with Nitro Groups in the Active Site of Reduced NTR

The results discussed in Chapter 4 indicate that both net hydride transfer and electron transfer are thermodynamically feasible reaction mechanisms for the reduction of CB1954 by NTR.

In order for CB1954 to be reduced by NTR via net hydride transfer, there must be a stable binding orientation for the prodrug in the active site of the enzyme with one of the oxygens within ~ 4 angstroms of N5 of FMN. Additionally, as experimental data shows that the wild-type enzyme reduces the 2-nitro and 4-nitro groups in equal proportions, there must be binding orientations for both nitro groups in the active site, of approximately equal energy, differing by less than 1kcal/mol in the experimental system.

The 1IDT crystal structure provides a good starting point for molecular mechanics and dynamics calculations, as it has CB1954 bound with the 2-nitro group in one active site, and the 4-nitro group in the other.

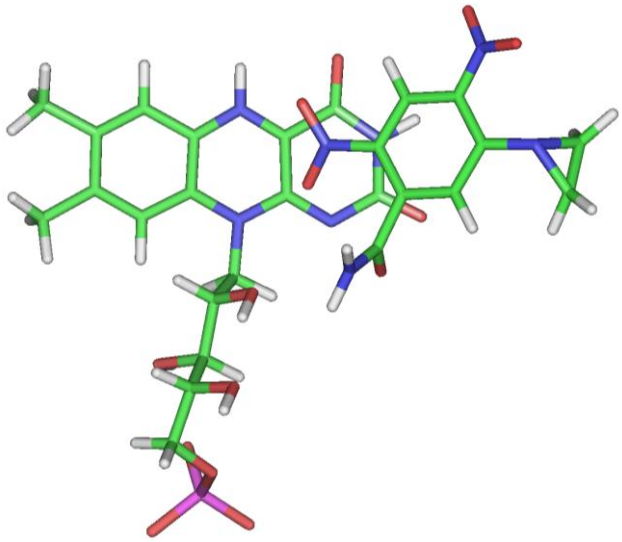

Figure 5.17: CB1954 and FMN from one active site of the 1IDT crystal structure, with the 2-nitro group in the active site of NTR. The oxygen of the 2-nitro group is 3.94 angstroms from N5 of FMN.

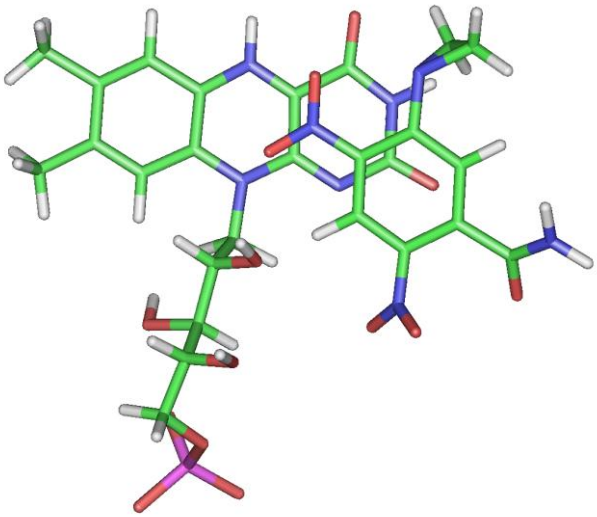

Figure 5.18: CB1954 and FMN from the other active site of the 1IDT crystal structure, with the 4-nitro group in the active site of NTR. The oxygen of the 4-nitro group is 3.77 angstroms from N5 of FMN.

In all but one case, the CB1954 was completely expelled from the active site during the molecular dynamics run. Interestingly, in the one instance where this did not happen, the CB1954 molecule with the 4-nitro group in the active site actually reoriented in such a way

that the amide group was found in the active site in a similar position to the amide group of nitrofurazone in the 1YKI crystal structure.

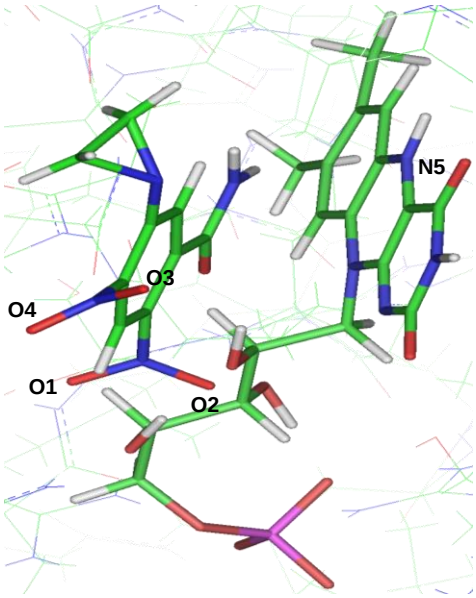

Figure 5.19: CB1954 in the active site of NTR after spontaneous reorientation.

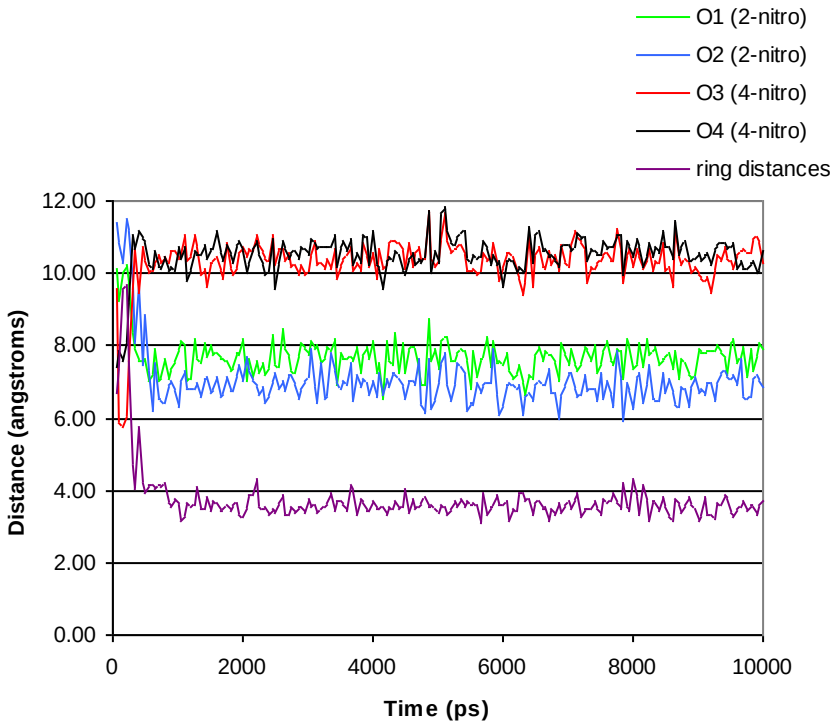

Figure 5.20: Distance from N5 of FMN to oxygens of the nitro groups of CB1954. "Ring distances" indicates the average intermolecular distance between the rings of CB1954 and FMN.

As Figure 5.20 shows, the CB1954 is relatively stable throughout the simulation with the amide group in the active site. Although none of the oxygens of either of the nitro groups are sufficiently close to N5 of FMN for hydride transfer, the prodrug and cofactor are within van der Waals contact throughout the dynamics run, which is sufficient for electron transfer.

In this orientation, the amide group makes two hydrogen bonds with NTR; to the backbone of T41, and to one of the hydroxyl groups of the ribityl tail of FMN.

The orientations of CB1954 from the 1ZX1 crystal structure (NQO2), as well as several others, were also used as starting orientations for CB1954 with NTR, but none yielded a stable binding of either nitro group in the active site of NTR.

Dynamics Run	Protein RMSd			Active Site	Outcome
	mean	min	max		
1	1.53	0.88	1.86	A	CB1954 comes out
				B	CB1954 comes out
2	1.41	0.88	1.69	A	CB1954 comes out
				B	CB1954 comes out, reorients*
3	1.61	0.82	2.01	A	CB1954 comes out
				B	CB1954 comes out

Table 5.10: Molecular dynamics runs with CB1954 and reduced NTR, with the 2-nitro group of CB1954 in active site A and the 4-nitro group of NTR in active site B. *In this dynamics run, the CB1954 comes out of the active site, and reorients to the "aziridine up" orientation (discussed in Section 5.2.10).

5.2.9 CB1954 with Nitro Groups in the Active Site of Reduced NTR Mutants

Molecular mechanics and dynamics simulations were also performed for the best single, double, and triple mutants of NTR, using the 1IDT crystal structure as a starting point. Additionally, the T41L mutant was studied, as it favours the 4-nitro in a 3:1 ratio.

Of all the simulations on NTR mutants, all but one resulted in CB1954 coming out of the active site. The one dynamics run that retained CB1954 within the active site showed the same substrate reorientation as observed with the wild-type enzyme (shown previously in Figure 5.20). The fact that not one single orientation of CB1954 with a nitro group in the active site of NTR yielded a stable binding configuration—while two of the simulations resulted in a spontaneous reorientation—indicates that it is unlikely CB1954 binds with a nitro group in the active site.

Mutant	Dynamics Run	Protein RMSd			Active Site	Outcome
		mean	min	max		
T41L	1	1.50	1.16	1.86	A	CB1954 comes out
					B	CB1954 comes out
	2	1.52	1.22	1.82	A	CB1954 comes out
					B	CB1954 comes out
	3	1.77	1.28	2.10	A	CB1954 comes out
					B	CB1954 comes out
F124N	1	1.62	1.12	2.13	A	CB1954 comes out
					B	CB1954 comes out
	2	1.79	1.21	2.19	A	CB1954 comes out
					B	CB1954 comes out
	3	1.76	1.46	1.97	A	CB1954 comes out
					B	CB1954 comes out
T41L/ N71S	1	1.55	1.35	1.78	A	CB1954 comes out
					B	CB1954 comes out
	2	1.70	1.31	2.02	A	CB1954 comes out
					B	CB1954 comes out
	3	1.78	1.37	2.16	A	CB1954 comes out
					B	CB1954 comes out
T41Q/ N71S/ F124T	1	9.65	1.31	47.16	A	CB1954 comes out
					B	CB1954 comes out
	2	1.70	1.19	2.07	A	CB1954 comes out
					B	CB1954 comes out
	3	1.81	1.45	2.15	A	CB1954 comes out
					B	CB1954 comes out*

Table 5.11: Molecular dynamics runs with CB1954 and reduced NTR mutants, with the 2-nitro group of CB1954 in active site A and the 4-nitro group of NTR in active site B. *In this dynamics run, the CB1954 comes out of the active site, and reorients to the "aziridine up" orientation (discussed in Section 5.2.10).

5.2.10 CB1954 with Amide Group in the Active Site of Reduced NTR

The stability of nitrofurazone with the amide group bound in the active site of both oxidised and reduced NTR, as well as the fact that two of the nitro group simulations of CB1954 spontaneously reoriented to put the amide in the active site, indicate a strong likelihood that CB1954 binds with amide group in the active site. This orientation leaves both nitro groups exposed to solution—ideal for electron transfer, but prohibitive of hydride transfer.

As CB1954 may be rotated across the amide-4-nitro axis with little change in gross shape, there are two molecular orientations for CB1954 with the amide group bound in the active site, arbitrarily labelled “aziridine up” and “aziridine down” because of the orientation of the aziridine ring of CB1954 with respect to FMN, shown in Figures 5.21 and 5.22. These orientations were set up by an overlay of the amide group of CB1954 molecule with the amide group of nitrofurazone in the 1YKI crystal structure.

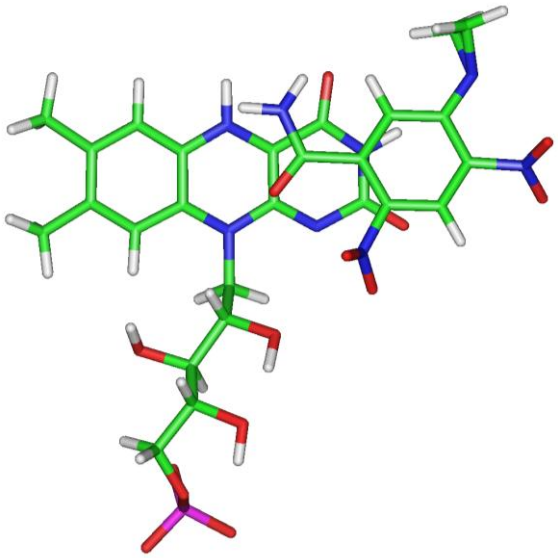

Figure 5.21: CB1954 and FMN from the amide overlay of nitrofurazone in the 1YKI crystal structure, “aziridine up.”

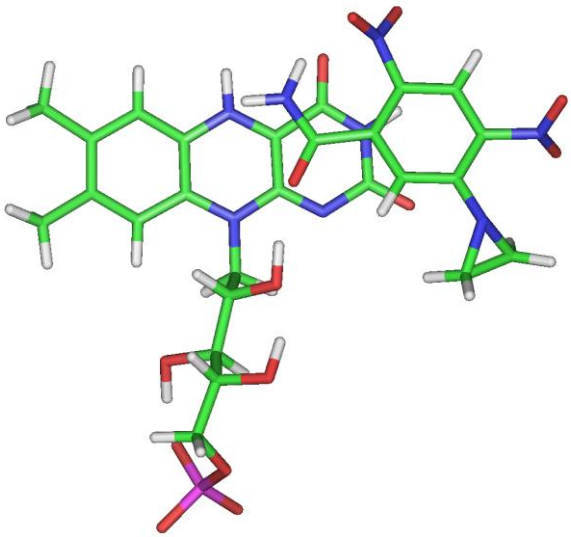

Figure 5.22: CB1954 and FMN from the amide overlay of nitrofurazone in the 1YKI crystal structure, "aziridine down."

Dynamics Run	Protein RMSd			Aziridine Orientation	Outcome
	mean	min	max		
1	1.46	1.04	1.71	down	CB1954 comes out
				up	CB1954 stays bound
2	1.53	1.06	2.05	down	CB1954 comes out
				up	CB1954 comes out
3	1.53	1.12	1.87	down	CB1954 stays bound
				up	CB1954 stays bound

Table 5.12: Molecular dynamics runs with CB1954 amide orientations and reduced NTR.

Although not every CB1954 molecule stays in the active site for every dynamics run, Table 5.12 shows that both the "aziridine up" and "aziridine down" orientations of CB1954 are viable. In every case where the CB1954 does come out of the active site, it occurs during data collection. This may be because the active site is compact, and the crystal structure was optimised for nitrofurazone rather than CB1954. Because the initial forces in the dynamics

runs are random, it is possible that these initial forces are responsible for causing the CB1954 to come out of the active site in the cases where this occurs.

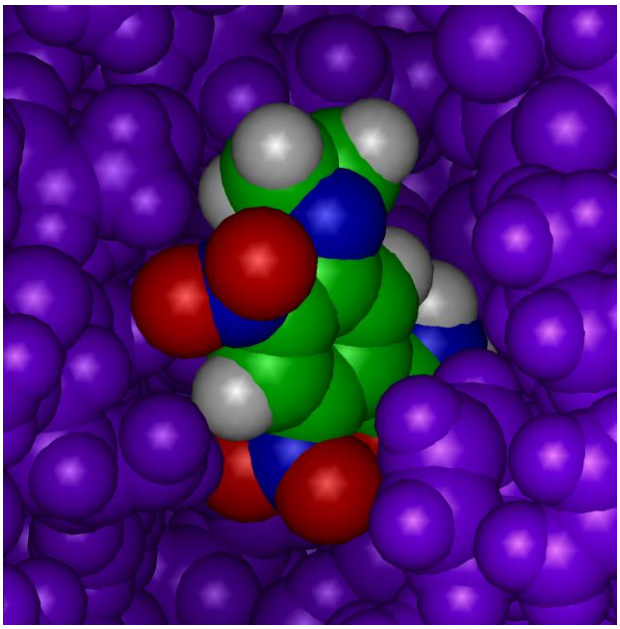

Figure 5.23: Space-filling model of CB1954 in the active site of NTR, "aziridine up" orientation. NTR, has been coloured purple, CB1954 in atomic colours to show groups accessible to solvent.

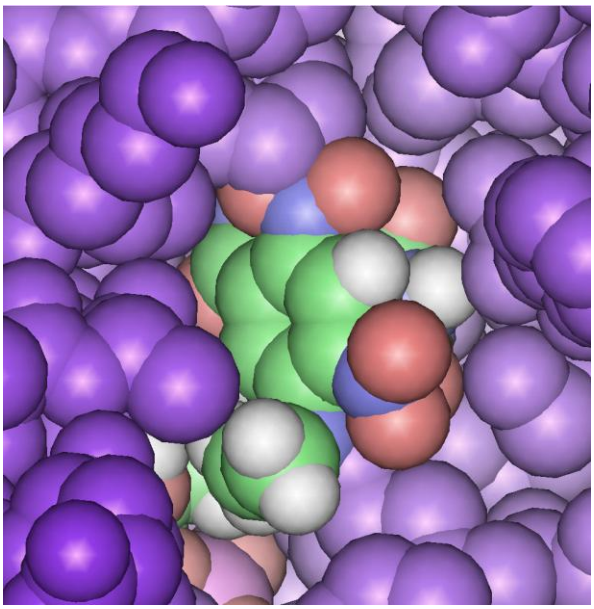

Figure 5.24: Space-filling model of CB1954 in the active site of NTR, "aziridine down" orientation, coloured as for Figure 5.23.

In order for these orientations to be viable for the electron transfer mechanism, both nitro groups must be sufficiently exposed to solution to be able to obtain protons from water molecules. Figures 5.23 and 5.24 show that this is indeed the case for both the "aziridine up" and "aziridine down" orientations.

name	atom	Occupancy (out of 40)	Total Occupancy
aziridine down 2-nitro	O1	0	20
aziridine down 2-nitro	O2	20	
aziridine down 4-nitro	O3	26	55
aziridine down 4-nitro	O4	29	
aziridine up 2-nitro	O1	6	38
aziridine up 2-nitro	O2	32	
aziridine up 4-nitro	O3	15	43
aziridine up 4nitro	O4	28	

Table 5.13: Solvent hydrogen bonding to the oxygens of the nitro groups of CB1954 bound to NTR. Occupancy refers to the number of steps in which the atom in question is found with a hydrogen bond to a water molecule. A 10 ns run with steps taken every 250 ps will give a total of 40 steps. Hydrogen bonds were defined as the oxygens of the CB1954 nitro groups as 'donors' and all water molecule hydrogens as potential 'acceptors,' with a distance cutoff of 3.0 angstroms and an angle cutoff of 120 degrees..

Table 5.13 shows that for both orientations, access to the 4-nitro group is slightly favoured over the 2-nitro group, but not substantially so.

5.2.11 CB1954 with Amide Orientations for Reduced NTR Mutants

As with the nitro group orientations, molecular mechanics and dynamics calculations were performed with CB1954 in the amide group orientations for the best single, double, and triple mutants, as well as the T41L mutant.

Mutant	Dynamics Run	Protein RMSd			Aziridine Orientation	Outcome
		mean	min	max		
T41L	1	1.23	0.90	1.70	down	CB1954 comes out
					up	CB1954 comes out
	2	1.63	0.93	2.02	down	CB1954 stays bound
					up	CB1954 comes out
	3	1.71	1.10	2.01	down	CB1954 comes out
					up	CB1954 comes out
F124N	1	1.53	1.07	1.95	down	CB1954 stays bound
					up	CB1954 comes out
	2	1.85	1.10	2.38	down	CB1954 stays bound
					up	CB1954 comes out
	3	1.43	1.07	1.79	down	CB1954 stays bound
					up	CB1954 stays bound
T41L/ N71S	1	1.74	1.06	2.07	down	CB1954 stays bound
					up	CB1954 comes out
	2	1.53	1.06	1.86	down	CB1954 comes out
					up	CB1954 comes out
	3	1.70	1.12	2.12	down	CB1954 comes out
					up	CB1954 stays bound
T41Q/ N71S/ F124T	1	2.00	1.27	2.54	down	CB1954 stays bound
					up	CB1954 comes out
	2	1.83	1.57	2.13	down	CB1954 stays bound
					up	CB1954 comes out
	3	1.79	1.24	2.12	down	CB1954 comes out
					up	CB1954 stays bound

Table 5.14: Molecular dynamics runs with CB1954 amide orientations and reduced NTR mutants.

Table 5.14 shows that while CB1954 stays in for some dynamics runs and comes out for others, there is no immediately discernable pattern or correlation between amino acid mutations and the strength of the binding. However, the fact that the amide binding orientation results from the wild-type are repeatable across a variety of mutants indicates that they are indeed viable binding orientations. Like the wild-type, in all cases the CB1954 came out of the site during data collection.

name	atom	Occupancy (out of 40)	Total Occupancy
aziridine down 2-nitro	O1	0	26
aziridine down 2-nitro	O2	26	
aziridine down 4-nitro	O3	39	67
aziridine down 4-nitro	O4	28	
aziridine up 2-nitro	O1	40	71
aziridine up 2-nitro	O2	31	
aziridine up 4-nitro	O3	38	67
aziridine up 4nitro	O4	29	

Table 5.15: Hydrogen bonding to the oxygens of the nitro groups of CB1954 bound to the T41L/N71S double mutant of NTR. Occupancy refers to the number of steps in which the atom in question is found with a hydrogen bond to a water molecule. A 10 ns run with steps taken every 250 ps will give a total of 40 steps. Hydrogen bonds were defined as the oxygens of the CB1954 nitro groups as 'donors' and all water molecule hydrogens as potential 'acceptors,' with a distance cutoff of 3.0 angstroms and an angle cutoff of 120 degrees.

The T41L/N71S double mutant is known to favour the 4-nitro reduction over the 2-nitro reduction[40]. One possible explanation is that the 2-nitro group is somehow blocked from access to solution in the mutant, but Table 5.15 shows that this is not the case, at least for the "aziridine up" orientation. However, for the "aziridine down" orientation, there is significantly more hydrogen bonding to solvent for the 4-nitro group. Unfortunately, these simulations give no information about the relative energies of the two orientations.

5.2.12 Summary and Discussion of Molecular Dynamics Simulations

Many of the ligands studied were known to bind poorly to the enzyme and this resulted in a good number of the simulations failing to bind their respective ligands. Small inaccuracies in initial positioning of the ligands could lead to the molecule being expelled from the active site early in the simulation process. However, once a stable binding mode had been identified, simulations were largely reproducible.

Molecular dynamics simulations with acetate in both the oxidised and reduced forms of NTR show that there may in fact be different binding properties for the different redox states of the enzyme.

Simulations with nitrofurazone show that there is a stable binding orientation for an amide group in both the oxidised and reduced states of the enzyme, with the oxygen of the nitrofurazone amide group forming hydrogen bonds with the T41 backbone and the hydroxyl group of the ribityl tail of FMN. No stable binding orientation with the nitrofurazone nitro group in the active site was found for either redox state of NTR. This latter orientation would be required if reduction of nitrofurazone were to proceed by net hydride transfer so this may be evidence in support of the electron transfer mechanism described in Chapter 4.

While it is known that nfsA favours the 2-nitro reduction of CB1954 and NQO2 favours the 4-nitro reduction, no stable binding orientation was found for either of these enzymes with a nitro group in the active site.

Similarly, for CB1954 with NTR, no binding orientation was found with a nitro group in the active site of wild-type NTR or any of the mutants. As a result, mechanisms involving hydride transfer from FMN to the nitro-groups of CB1954 can be considered less likely as the catalytic mechanism for the enzyme. This would include either true or net hydride transfer as described in Chapter 4. Though the results for enzyme-free model systems described in Chapter 4 showed that the net hydride transfer mechanism had a similar overall barrier height to the electron transfer mechanism, net hydride transfer requires the accepting nitro-group be in close proximity with N5 of FMN. Perhaps the most conclusive evidence comes from the two simulations in which CB1954 spontaneously reoriented in the active site in such a way that the amide group was bound in a similar orientation to the amide group of nitrofurazone in x-ray structure 1YKI. Once identified, this amide binding orientation was consistently stable

in both the wild-type NTR and the three mutants examined. Binding CB1954 with the amide group in the binding site in this fashion results in both nitro-groups being exposed to solvent and ready to pick up two solvent-derived protons as would be expected for the electron transfer mechanism described in Chapter 4. Thus these molecular dynamics simulations give considerable support to the electron transfer mechanism being the catalytic mechanism of the enzyme. This does not, however, conclusively prove that hydride transfer does not occur, as no binding orientation was found for menadione and menadione is known to be a good substrate for NTR.

With the amide group of CB1954 in the active site, there is both an "aziridine up" and "aziridine down" orientation—both of which were observed repeatedly in wild-type NTR and the mutants. Both orientations have the two nitro groups sufficiently exposed to solution, and both show approximately equal hydrogen bonding with solution for the two nitro groups, as might be expected from the observation that wild-type NTR is able to reduce either nitro-group at comparable rates.

Simple analysis of the molecular dynamics simulation and the frequency with which nitro groups form hydrogen bonds with water does not entirely explain fact that the T41L/N71S is observed experimentally to favour the 4-nitro reduction of CB1954. To examine this property of the mutant, we need to look in more detail at aspects of the mechanism.

5.3 ONIOM Calculations

Gas phase reaction profiles are useful for comparing various reaction mechanisms, but as the term implies, their utility is limited to the gas phase, and cannot show how amino acids in the active site of the enzyme affect the reaction. And while molecular mechanics and dynamics calculations can give an idea about how a ligand binds in the active site of an enzyme, they cannot compare various reaction mechanisms.

ONIOM calculations were meant to bridge the gap by combining quantum mechanics and molecular mechanics calculations. By studying the CB1954 and FMN cofactor of NTR in the QM section, and selected relevant amino acids of the NTR active site in the MM section, the effect of the amino acids on the potential reaction mechanisms can be examined. However, the sheer number of possible combinations of configurations of amino acids, CB1954 orientations, electronic states, and coordinate movement is daunting.

For all ONIOM calculations, selected amino acids are in the MM section, and CB1954 and a reduced, truncated FMN are in the QM section.

Amino acids		
	Chain A	**Chain B**
1	Ser14, Phe70, Asn71, Lys74, Glu165, Gly166	Ser40, Thr41, Phe124
2,3[a]	Ser14, Phe70, Asn71, Lys74, Pro163, Ile164, Glu165, Gly166	Ser40, Thr41, Phe124
4	Lys14, Tyr68, Phe70, Asn71, Lys74, Pro163, Glu165, Gly166	Ser40, Thr41, Phe124
5	Ser12, Lys14, Phe70, Asn71, Lys74, Ile164, Glu165, Gly166	Pro38, Ser39, Ser40, Gly120, Arg121, Phe124, Leu145

Table 5.16: Amino acid combinations from NTR used in ONIOM calculations. Chain A amino acids are primarily involved in FMN binding, while Chain B amino acids are primarily involved in ligand binding. [a] The third amino acid configuration is the same as the second, with protons added to the backbone carbon and nitrogen of the amino acids that do not have another amino acid adjacent.

Electronic State	
singlet	
triplet	
Amino Acid Charges	
on	
off	
Coordinates Frozen	
1	all amino acids and FMN
2	all amino acids and the first carbon of the ribityl tail of FMN
3	all backbone amino acid atoms and the first carbon of the ribityl tail of FMN
CB1954 Orientation	
1	Nitrofurazone amide overlay from 1YKI crystal structure, “aziridine up”
2	Nitrofurazone amide overlay from 1YKI crystal structure, “aziridine down”
3	from 1IDT crystal structure, 2-nitro group in active site
4	from 1IDT crystal structure, 4-nitro group in active site
5	benzoate ring overlay from 1KQB crystal structure, “aziridine up”
6	benzoate ring overlay from 1KQB crystal structure, “aziridine down”
7	benzoate ring overlay from 1KQB crystal structure, 2-nitro group in active site
8	benzoate ring overlay from 1KQB crystal structure, 4-nitro group in active site
9	from 1ZX1 crystal structure, 2-nitro group in active site
10	from 1ZX1 crystal structure, 4-nitro group in active site

Table 5.17: List of ONIOM calculation variables used for each amino acid combination.

Amino Acid Configuration	CB1954 Orientation	Coordinates Frozen	Electronic State	Amino Acid Charges
1	2	1	singlet	on
1	2	2	singlet	on
1	5	1	singlet	on
1	5	2	singlet	on
1	5	2	singlet	off
1	5	2	triplet	on
1	5	2	triplet	off
1	10	1	singlet	on
1	10	1	triplet	on
2	4	1	singlet	on
2	4	1	triplet	on
2	4	1	triplet	off
2	4	3	singlet	on
3	4	1	singlet	on
3	4	2	singlet	on
5	5	1	singlet	on

Table 5.18: List of ONIOM calculations that reached SCF convergence.

Unfortunately, things did not go as planned. Of the hundreds of ONIOM calculations set up, only a few completed successfully. Some ran for as long as six months before resulting in convergence failure. The average time for completion was two months. Still, from these few, some useful information can be obtained.

5.3.1 Comparison of CB1954 Orientations

Molecular mechanics and dynamics simulations are not sensitive enough to distinguish energetically between different binding orientations of CB1954 in the active site of NTR. ONIOM calculations, on the other hand, employ quantum mechanics for CB1954 and FMN, and as such are able to determine the energetic difference between various orientations of CB1954 in the active site of NTR.

In order for the comparison to be valid, the amino acid configuration, electronic state, use of amino acid charges, and coordinates frozen must all be the same. Fortunately, for amino acid configuration 1, there is a CB1954 orientation for the 2-nitro, 4-nitro, and amide group in the active site that fit the criteria.

CB1954 Orientation	Energy (Hartree)	Energy relative to amide orientation (kcal/mol)
2 ("aziridine down" amide in site)	−1818.05008752	0
5 (2-nitro in site)	−1818.01586877	21
10 (4-nitro in site)	−1818.04573594	3

Table 5.19: Energies of the QM section for binding orientations for CB1954 in the NTR active site. In each case, the system is in the singlet state.

Table 5.19 shows that while the amide and 4-nitro orientations are similar in energy, the energy for the 2-nitro orientation is substantially higher in energy. This reinforces the conclusion that electron transfer is the mechanism for wild-type NTR, as even a small difference in energy between the 2-nitro and 4-nitro orientations would cause a large difference in the ratio of 2-nitro and 4-nitro reductions. But while 3 kcal/mol is probably within the margin of error, particularly as this is an energy measurement only with no consideration of entropy, a difference of 18 kcal/mol between the two hydride transfer orientations is sufficiently large that we should expect to observe only reduction of the 4-nitro group, if the mechanism were hydride transfer.

5.3.2 Single-Point ONIOM Calculations on MD Binding Orientations

ONIOM calculations have so far proven to be of limited utility for this project, due to the amount of time required to complete, and tendency to result in convergence failures. Still, with ONIOM calculations it is possible to examine properties that cannot be determined by molecular mechanics, such as molecular charges, orbital configurations, and relative energies of different electronic states, both with and without the amino acid charges included.

For the single-point ONIOM calculations, the “aziridine up” and “aziridine down” binding orientations were used from the wild-type and T41L/N71S double mutant molecular dynamics runs, with amino acid configuration 4 from Table 5.16.

Parameters	Charge on FMN	Charge on CB1954	Energy (Hartree)	Relative Energy (kcal/mol)
wild-type, "aziridine down" singlet, charges on	−0.661	−0.339	−1818.42475	0
wild-type, "aziridine down" triplet, charges on	−0.030	−0.970	−1818.41838	4
wild-type, "aziridine up" singlet, charges on	−0.977	−0.023	−1818.37356	32
wild-type, "aziridine up" triplet, charges on	−0.121	−0.879	−1818.32507	63
T41L/N71S, "aziridine down" singlet, charges on	−0.883	−0.117	−1818.19864	142
T41L/N71S, "aziridine down" triplet, charges on	−0.039	−0.961	−1818.15931	166
T41L/N71S, "aziridine up" singlet, charges on	−0.707	−0.293	−1818.36609	37
T41L/N71S, "aziridine up" triplet, charges on	−0.032	−0.968	−1818.34755	48

Table 5.20: Molecular charges and overall QM energy for CB1954 bound in the active site of NTR, with selected amino acids and amino acid charges included in the ONIOM calculation.

Parameters	Charge on FMN	Charge on CB1954	Energy (Hartree)	Relative Energy (kcal/mol)
wild-type, "aziridine down" singlet, charges off	−0.795	−0.205	−1814.99276	0
wild-type, "aziridine down" triplet, charges off	−0.032	−0.968	−1814.97129	13
wild-type, "aziridine up" singlet, charges off	−0.967	−0.033	−1814.98460	5
wild-type, "aziridine up" triplet, charges off	−0.039	−0.961	−1814.95135	26
T41L/N71S, "aziridine down" singlet, charges off	−0.814	−0.186	−1814.99829	-3
T41L/N71S, "aziridine down" triplet, charges off	−0.026	−0.974	−1814.97031	14
T41L/N71S, "aziridine up" singlet, charges off	−0.788	−0.212	−1815.00283	-6
T41L/N71S, "aziridine up" triplet, charges off	−0.031	−0.969	−1814.97258	13

Table 5.21: Molecular charges and overall QM energy for CB1954 bound in the active site of NTR, with amino acid charges not included in the ONIOM calculation.

Table 5.20 and Table 5.21 show that in all cases, the singlet is lower in energy than the triplet. However, as these were single point calculations, the geometries were derived by molecular mechanics calculations, and are not necessarily ideal for either electronic state. Comparing the changes from Table 5.21 (no charges) to Table 5.20 (protein charges on) shows the effects of the electrostatic environment from the protein on electron transfer. With the favoured "aziridine down" configuration for the wild-type enzyme, adding protein charges stabilises the triplet by 9 kcal/mol relative to the singlet. In the double mutant, the "aziridine up" orientation is favoured, and adding protein charges stabilises the triplet relative to the singlet by 8 kcal/mol. Whether this will have any impact on the outcome of reduction is not yet clear.

As expected, the differences in energy between different CB1954 orientations are less when the amino acid charges are not included in the calculation. Unfortunately, it is not useful to compare the energies of the wild-type and mutant with the amino acid charges on, as the differences in amino acids causes substantial differences in energy.

In the future, full reaction profiles similar to those discussed in Section 4.7 should be determined with the amino acids present, in order to determine the true reaction barrier, and the effect of various amino acids on the reaction mechanism.

5.3.2.1 Orbital Analysis of Single-Point ONIOM Calculations

Molecular mechanics and dynamics calculations cannot entirely explain why the wild-type NTR reduces both nitro groups of CB1954 in equal proportions, while the T41L/N71S mutant reduces predominantly the 4-nitro group.

One possible explanation is that while the LUMO is equally distributed across the nitro groups of CB1954, the amino acids of the T41L/N71S mutant of NTR perturb the orbital in such a way that the 4-nitro group has a greater electron density after the first electron is transferred from FMN. If this were indeed the case, it would make the 4-nitro group more likely to accept a proton from solution and thus be reduced.

Parameters	**Charge on 4-nitro group**	**Charge on 2-nitro group**
wild-type, "aziridine down" triplet, charges on	−0.7359	−0.5580
T41L/N71S, “aziridine down” triplet, charges on	−0.6057	−0.5687
wild-type, “aziridine up” triplet, charges on	−0.5612	−0.4771
T41L/N71S, “aziridine up” triplet, charges on	−0.7262	−0.5296

Table 5.22: Charge on the 4-nitro and 2-nitro groups of CB1954 in the active site of NTR with one electron transferred from FMN to CB1954, from the single-point ONIOM calculations.

Unfortunately, Table 5.22 shows that there is no clear relationship between the electron density (represented by the charge) on the nitro group and the likelihood that it is the group that is reduced. However, this is merely a single-point calculation from a geometry optimised by molecular mechanics, and an optimised ONIOM calculation may yield a more clear result. Perhaps the most disappointing observation is that the CB1954 orientations showing the lowest energy for wild-type and double mutant (aziridine “down” and “up” respectively) show almost exactly the same charge distribution between the two nitro-groups.

5.4 Summary of Chapter 5 Results

Docking results proved to be inconclusive, given that Autodock was unable to correctly dock ligands with NTR in a similar position to known, well-resolved crystal structures. While CB1954 was found near the active site, no useful binding information could be gained from the docking runs. This is not unexpected, however, as CB1954 has been shown experimentally to have poor binding with NTR.

Molecular mechanics and dynamics simulations have shown consistently that the binding of CB1954 in NTR is with the amide group in the active site—an orientation suitable only for the electron transfer mechanism. The amide binding is similar to that observed with nitrofurazone in the 1YKI crystal structure, with the oxygen of the amide group forming hydrogen bonds with the T41 backbone and hydroxyl group of the ribityl tail of FMN.

Hydrogen bonding analysis of the nitro group oxygens shows that in the wild-type enzyme, for both "aziridine up" and "aziridine down" orientations, the 2-nitro and 4-nitro groups have similar hydrogen bonding occupancies with water, while with the T41L/N71S mutant, the 4-nitro group has greater occupancy in the "aziridine down" orientation.

ONIOM calculations showed that the CB1954 orientations with the 2-nitro group versus the 4-nitro group in the active site have quite different energies—further evidence against a possible hydride transfer mechanism, as that would require 2-nitro and 4-nitro orientations with similar energies.

Interestingly, the "aziridine down" orientation of CB1954 seems to be favoured by the wild-type enzyme, while the "aziridine up" orientation appears to be favoured by the T41L/N71S mutant. Unfortunately, there is still no complete explanation for why the T41L/N71S mutant favours the 4-nitro reduction of CB1954.

Chapter 6
Conclusions and Future Work

This chapter discusses the overall conclusions reached from this work, and describes what work should be done in the future.

6.1 Conclusions

A combination of quantum mechanics, molecular dynamics, and hybrid QM/MM results strongly supports the mechanism for the reduction of CB1954 by wild-type NTR involving electron transfer from FMN with both protons being picked up from solution. The reactive complex of the enzyme has the CB1954 amide group bound in the active site and both nitro groups exposed to solution[(145)].

Quantum mechanics calculations show that true hydride transfer (a concerted proton and two electrons) from FMN to CB1954 is possible in gas-phase, but not favoured. Additionally, transfer of the hydride directly to an oxygen of a nitro group is substantially favoured over initial transfer to the nitrogen. Interestingly, the mechanism for the reaction between isolated FMN and CB1954 (i.e. in the absence of the rest of the enzyme) was shown to be electron from FMN, proton, then second proton and electron concerted with the breaking of the N-O bond of the nitro group to form a nitroso, regardless of the source (FMN or solution) or order of the protons.

While quantum mechanics calculations could not definitively determine which mechanism was favoured by the enzyme, and docking results were of little use, molecular mechanics and dynamics simulations showed consistently that CB1954 binds with the amide group in the active site, with hydrogen bonds from the oxygen of the amide group to the T41 backbone and hydroxyl group of the ribityl tail of FMN. Additionally, there are two possible orientations of CB1954 with the amide bound (defined as “aziridine up” and “aziridine down” in this work).

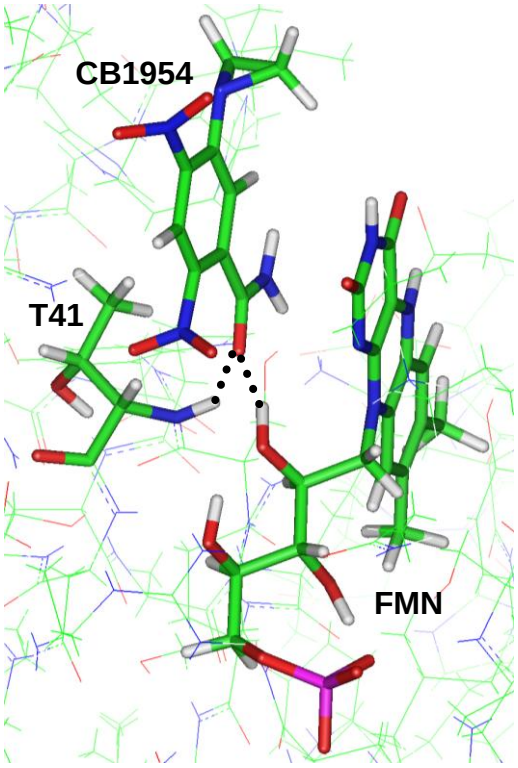

Figure 6.1: CB1954 bound with amide group in active site of NTR, "aziridine up" orientation.

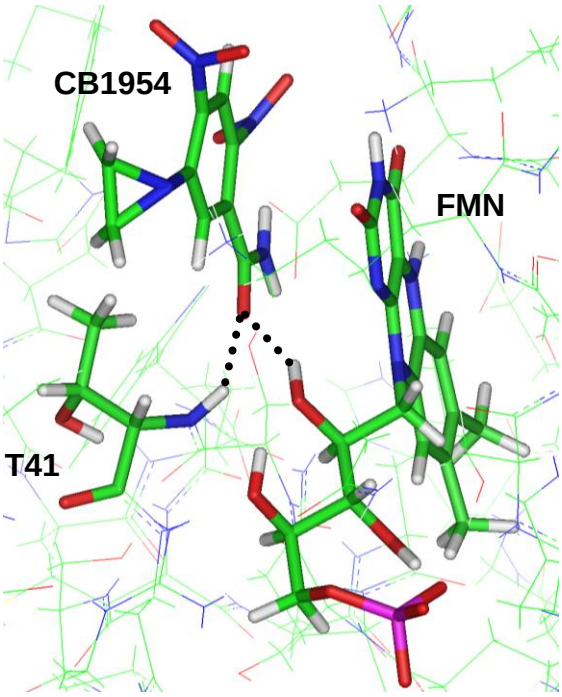

Figure 6.2: CB1954 bound with amide group in active site of NTR, "aziridine down" orientation.

Space filling models show that for both orientations, both nitro groups are sufficiently exposed to solution to gain protons, while hydrogen-bonding analysis of the molecular dynamics trajectories shows that both nitro groups have similar hydrogen-bonding with solvent molecules in both amide orientations for the wild-type enzyme, while in the T41L/N71S mutant the "aziridine down" orientation has greater hydrogen bonding to solvent for the 4-nitro group—which may explain why the 4-nitro reduction is favoured in the double mutant.

Finally, ONIOM calculations show that the CB1954 orientations with the 2-nitro group versus the 4-nitro group in the active site have quite different energies—further evidence against a possible hydride transfer mechanism, as that would require 2-nitro and 4-nitro orientations with similar energies.

6.2 Future Work

While this work has demonstrated a potential binding orientation and reaction mechanism for the reduction of CB1954 by wild-type NTR, there are a number of questions that remain to be answered.

6.2.1 Gas-Phase Barriers for Concerted Electron-Proton Transfer

Single-point CASSCF calculations indicate that the second electron transfer occurs during the transfer of the second proton, after the N-O bond of the nitro group is broken. While the energies of the single-point CASSCF calculations may be considered the upper limit of the reaction barrier, in order to obtain the true barrier to the reaction, a CASSCF

optimisation—where the geometry of the system is optimised for a mixing of electronic states—must be performed. This optimization is complicated by the fact that the reaction profiles described in this thesis point to there being at least some element of N-O bond breaking while the electron/proton transfer is taking place and so these calculations would not simply be a case of taking our best estimate of the cross-over point between singlet and triplet states and optimizing it within a CASSCF framework; rather a number of possible points need to be considered involving different degrees of proton transfer and N-O bond breaking.

6.2.2 Reaction Profiles in the Active Site of NTR and Known Mutants

Gas-phase reaction profiles are useful for comparing various possible reaction mechanisms, but to get an idea of the reaction profile for the actual reaction within the enzyme, key amino acids must be present in the calculation. ONIOM calculations for the stepwise transfer of protons from either FMN or solution in the QM section, and active site amino acids in the MM section, will show conclusively how the active site amino acids affect the energies of the various reaction mechanisms. A comparison of full reaction profiles with wild-type active site amino acids versus mutant amino acids may yield insight into the exact function of each amino acid, as well as explain why the wild-type enzyme reduces both nitro groups in equal proportions while the T41L/N71S mutant reduces primarily the 4-nitro group.

As this work has shown, the CB1954 binding is similar in both wild-type NTR and in the T41L/N71S mutant. Additionally, in the T41L/N71S mutant, both nitro groups are equally exposed to solution, and have similar hydrogen-bonding with water. Therefore, there must be another explanation for why the T41L/N71S mutant favours the 4-nitro reduction. To explain this preference, it may require a CASSCF optimisation within an ONIOM (or other

QM/MM) framework, looking in more detail at the proton transfers in the electron transfer mechanism, with a number of water molecules present in the system. Unfortunately, the hardware necessary to do this is not available at this time.

6.3 Applications of This Work

Knowledge of the reaction mechanism for the reduction of CB1954 by NTR has the potential to aid in the development of new and better NTR mutants, and thereby increase the efficacy of the CB1954/NTR combination in cancer chemotherapy. However, in order to have a more efficient therapy, it is necessary to improve K_m, and it may be useful to be able to modulate the proportions of 4-nitro (which is more cytotoxic) and 2-nitro (which has a better bystander effect) reductions.

As a result of the work describe in this thesis, it is now known that the CB1954 binds with the amide group in the active site and the nitro groups exposed to solution, it my be possible to create mutants with a greater affinity for amide groups, favour the "aziridine up" or "aziridine down" orientation, or to shield one or the other of the nitro groups from solution, as desired. However, care must be taken not to detrimentally affect the first step of the reaction—the reduction of NTR by NAD(P)H.

It may not be possible to create any better mutants for CB1954 as visual inspection of the binding site of NTR in the vicinity of our bound CB1954 highlights many of the residues that have already been subject to mutation. For example, mutating Thr41 to a larger hydrophobic side-chain may help stabilise the "aziridine down" conformation (see Figure 6.2), but we have already seen that the T41L mutant improves binding[32]. In this case the

experimental data is in good agreement with the computational results, but the computational results are not able to provide any new insight.

Alternatively, it may be more useful to consider modifications to CB1954 to aid binding, possibly in conjunction with mutations to the enzyme. For example, the binding orientation shown in Figure 6.2 reveals a significant cavity close to the aziridine ring, thus modification to this group may allow further interactions with amino acids lining this pocket, for example Gly120, Ala116, or Lys14.

References

References

1. World Health Organization (2005) *Global Action Against Cancer*, WHO Press, Geneva
2. Palmer, D. H., Mautner, V., Mirza, D., Oliff, S., Gerritsen, W., van der Sijp, J. R., Hubscher, S., Reynolds, G., Bonney, S., Rajaratnam, R., Hull, D., Horne, M., Ellis, J., Mountain, A., Hill, S., Harris, P. A., Searle, P. F., Young, L. S., James, N. D., and Kerr, D. J. (2004) *Journal of Clinical Oncology* **22,** 1546-1552.
3. Weedon, S. J., Green, N. K., McNeish, I. A., Gilligan, M. G., Mautner, V., Wrighton, C. J., Mountain, A., Young, L. S., Kerr, D. J., and Searle, P. F. (2000) *International Journal of Cancer* **86,** 848-854.
4. Knox, R. J., Friedlos, F., Marchbank, T., and Roberts, J. J. (1991) *Biochemical Pharmacology* **42,** 1691-1697.
5. Grove, J. I., Searle, P. F., Weedon, S. J., Green, N. K., McNeish, I. A., and Kerr, D. J. (1999) *Anti-Cancer Drug Design* **14,** 461-472.
6. Anlezark, G. M., Knox, R. J., Friedlos, F., Sherwood, R. F., and Melton, R. G. (1992) *Biochemical Pharmacology* **44,** 2297-2301.
7. White, C. L., Menghistu, T., Twigger, K. R., Searle, P. F., Bhide, S. A., Vile, R. G., Melcher, A. A., Pandha, H. S., and Harrington, K. J. (2008) *Gene Therapy* **15,** 424-433.
8. McNeish, I. A., Green, N. K., Gilligan, M. G., Ford, M. J., Mautner, V., Young, L. S., Kerr, D. J., and Searle, P. F. (1998) *Gene Therapy* **5,** 1061-1069.
9. Djeha, A. H., Hulme, A., Dexter, M. T., Mountain, A., Young, L. S., Searle, P. F., Kerr, D. J., and Wrighton, C. J. (2000) *Cancer Gene Therapy* **7,** 721-731.
10. Roberts, J. J., Friedlos, F., and Knox, R. J. (1986) *Biochemical and Biophysical Research Communications* **140,** 1073-1078.

11. Knox, R. J., Boland, M. P., Friedlos, F., Coles, B., Southan, C., and Roberts, J. J. (1988) *Biochemical Pharmacology* **37,** 4671-4677.

12. Boland, M. P., Knox, R. J., and Roberts, J. J. (1991) *Biochemical Pharmacology* **41,** 867-875.

13. Bridgewater, J. A., Knox, R. J., Pitts, J. D., Collins, M. K., and Springer, C. J. (1997) *Human Gene Therapy* **8,** 709-717.

14. Bridgewater, J. A., Springer, C. J., Knox, R. J., Minton, N. P., Michael, N. P., and Collins, M. K. (1995) *European Journal of Cancer* **31A,** 2362-2370.

15. Helsby, N. A., Ferry, D. M., Patterson, A. V., Pullen, S. M., and Wilson, W. R. (2004) *British Journal of Cancer* **90,** 1084-1092.

16. Race, P. R., Lovering, A.L., Green, R.M., Ossor, A., White, S.A., Searle, P.F., Wrighton, C.J., and Hyde E.I. (2005) *Journal of Biological Chemistry* **280,** 13256-13264.

17. Haynes, C. A., Koder, R. L., Miller, A.-F., and Rodgers, D. W. (2002) *Journal of Biological Chemistry* **277,** 11513-11520.

18. Bryant, C., and DeLuca, M. (1991) *Journal of Biological Chemistry* **266,** 4119-4125.

19. Koder, R. L., and Miller, A.-F. (1998) *Biochimica et Biophysica Acta* **1387,** 395-405.

20. Lovering, A. L., Hyde, E. I., Searle, P. F., and Scott, A. W. (2001) *Journal of Molecular Biology* **309,** 203-213.

21. Parkinson, G. N., Skelly, J. V., and Neidle, S. (2000) *Journal of Medicinal Chemistry* **43,** 3624-3631.

22. Massey, V. (1995) *Faseb Journal* **9,** 473-475.

23. Fraaije, M. W., and Mattevi, A. (2000) *Trends in Biochemical Sciences* **25,** 126-132.

24. Kurfurst, M., Macheroux, P., Ghisla, S., and Hastings, J. W. (1989) *European Journal of Biochemistry* **181,** 453-457.

25. Anlezark, G. M., Melton, R. G., Sherwood, R. F., Coles, B., Friedlos, F., and Knox, R. J. (1992) *Biochemical Pharmacology* **44,** 2289-2295.

26. Zenno, S., Koike, H., Tanokura, M., and Saigo, K. (1996) *Journal of Biochemistry* **120,** 736-744.

27. Berman, H. M., Westbrook, J., Feng, Z., Gilliland, G., Bhat, T. N., Weissig, H., Shindyalov, I. N., and Bourne, P. E. (2000) *Nucleic Acids Research* **28,** 235-242.

28. The RCSB Protein Data Bank: www.pdb.org

29. Wouters, J., Durant, F., Champagne, B., and André, J.-M. (1997) *International Journal of Quantum Chemistry* **64,** 721-733.

30. Barna, T. M., Khan, H., Bruce, N. C., Barsukov, I., Scrutton, N. S., and Moody, P. C. E. (2001) *Journal of Molecular Biology* **310,** 433-447.

31. Palmer, B. D., van Zijl, P., Denny, W. A., and Wilson, W. R. (1995) *Journal of Medicinal Chemistry* **38,** 1229-1241.

32. Grove, J. I., Lovering, A. L., Guise, C., Race, P. R., Wrighton, C. J., White, S. A., Hyde, E. I., and Searle, P. F. (2003) *Cancer Research* **63,** 5532-5537.

33. Wilkie, J. (2005), Unpublished observations.

34. Kyte, J. (1995) *Mechanism in Protein Chemistry*, Garland Publishing, Inc., New York.

35. Johansson, E., Parkinson, G. N., Denny, W. A., and Neidle, S. (2003) *Journal of Medicinal Chemistry* **46,** 4009-4020.

36. White, S. A. (2008), Unpublished observations.

37. Zenno, S., Kobori, T., Tanokura, M., and Saigo, K. (1998) *Journal of Bacteriology* **180,** 422-425.

38. Cleland, W. W. (1989) *Biochimica et Biophysica Acta* **1000,** 213-220.

39. Race, P. R., Lovering, A. L., White, S. A., Grove, J. I., Searle, P. F., Wrighton, C. W., and Hyde, E. I. (2007) *Journal of Molecular Biology* **368,** 481-492.

40. Jarrom, D., Jaberipour, M., Guise, C., Daff, S., Hicks, M. R., Burns, G., Searle, P. F., White, S. A., and Hyde, E. I. (2008) *Biochemistry* **48,** 7665-7672.

41. Guise, C. P., Grove, J. I., Hyde, E. I., and Searle, P. F. (2007) *Gene Therapy* **14,** 690-698.

42. Chung-Faye, G., Palmer, D., Anderson, D., Clark, J., Downes, M., Baddeley, J., Hussain, S., Murray, P. I., Searle, P., Seymour, L., Harris, P. A., Ferry, D., and Kerr, D. J. (2001) *Clinical Cancer Research* **7,** 2662-2668.

43. Searle, P., Vass, S., Guise, C., Jaberi-Pour, M., Jarrom, D., and Hyde, E. (2007) *Human Gene Therapy* **18,** 1000-1001.

44. Kobori, T., Sasaki, H., Lee, W. C., Zenno, S., Saigo, K., Murphy, M. E. P., and Tanokura, M. (2001) *Journal of Biological Chemistry* **276,** 2816-2823.

45. Foster, C. E., Bianchet, M. A., Talalay, P., Zhao, Q., and Amzel, L. M. (1999) *Biochemistry* **38,** 9881-6.

46. Jansson, A., Wu, X., Kavanagh, K., Kerr, D., Knox, R., Walton, R., Gunther, U., Ludwig, C., Edwards, A., Arrowsmith, C., Sundstrom, M., von Delft, F., and Oppermann, U. (2009) *Human quinone oxidoreductase 2 (NQO2) in complex with the cytostatic prodrug CB1954,* Unpublished manuscript.

47. Knox, R. J., Jenkins, T. C., Hobbs, S. M., Chen, S., Melton, R. G., and Burke, P. J. (2000) *Cancer Research* **60,** 4179-4186.

48. Seiler, F. J. (1990) *MOPAC 6.0,* U.S. Air Force Academy, Colorado Springs, CO.

49. Frisch, M. J., Trucks, G. W., Schlegel, H. B., Scuseria, G. E., Robb, M. A., Cheeseman, J. R., J. A. Montgomery, J., Vreven, T., Kudin, K. N., Burant, J. C., Millam, J. M., Iyengar, S. S., Tomasi, J., Barone, V., Mennucci, B., Cossi, M., Scalmani, G., Rega, N., Petersson, G. A., Nakatsuji, H., Hada, M., Ehara, M., Toyota, K., Fukuda, R., Hasegawa, J., Ishida, M., Nakajima, T., Honda, Y., Kitao, O., Nakai, H., Klene, M., Li, X., Knox, J. E., Hratchian, H. P., Cross, J. B., Bakken, V., Adamo, C., Jaramillo, J., Gomperts, R., Stratmann, R. E., Yazyev, O., Austin, A. J., Cammi, R., Pomelli, C., Ochterski, J. W., Ayala, P. Y., Morokuma, K., Voth, G. A., Salvador, P., Dannenberg, J. J., Zakrzewski, V. G., Dapprich, S., Daniels, A. D., Strain, M. C., Farkas, O., Malick, D. K., Rabuck, A. D., Raghavachari, K., Foresman, J. B., Ortiz, J. V., Cui, Q., Baboul, A. G., Clifford, S., Cioslowski, J., Stefanov, B. B., Liu, G., Liashenko, A., Piskorz, P., Komaromi, I., Martin, R. L., Fox, D. J., Keith, T., Al-Laham, M. A., Peng, C. Y., Nanayakkara, A., Challacombe, M., Gill, P. M. W., Johnson, B., Chen, W., Wong, M. W., Gonzalez, C., and Pople, J. A. (2004) *Gaussian 03, Revision C.02*, Gaussian, Inc., Wallingford CT.

50. Case, D. A., Darden, T. A., Cheatham, T. E., Simmerling, C. L., Wang, J., Duke, R. E., Luo, R., Merz, K. M., Wang, B., Pearlman, D. A., Crowley, M., Brozell, S., Tsui, V., Gohlke, H., Mongan, J., Hornak, V., Cui, G., Beroza, P., Schafmeister, C., Caldwell, J. W., Ross, W. S., and Kollman, P. A. (2004) *AMBER 8*, University of California, San Francisco

51. Case, D. A., T.E. Cheatham, I., Darden, T., Gohlke, H., Luo, R., K.M. Merz, J., Onufriev, A., Simmerling, C., Wang, B., and Woods, R. (2005) *Journal of Computational Chemistry* **26,** 1668-1688.

52. Morris, G. M., Goodsell, D. S., Halliday, R. S., Huey, R., Hart, W. E., Belew, R. K., and Olson, A. J. (1998) *Journal of Computational Chemistry* **19,** 1639-1662.

53. Leach, A. R. (2001) *Molecular Modelling: Principles and Applications*, Pearson Education, Harlow.

54. Cramer, C. J. (2004) *Essentials of Computational Chemsitry, 2nd Ed.*, John Wiley & Sons, Ltd., West Sussex, England.

55. Born, M., and Oppenheimer, R. (1927) *Annalen Der Physik* **84,** 0457-0484.

56. Frenking, G. (2000) *Theoretical Chemistry Accounts* **103,** 187.

57. Berson, J. A. (1996) *Angewandte Chemie International Edition* **35,** 2750.

58. Hückel, E. (1931) *Zeitschrift für Physik* **70,** 204.

59. MacDonald, J. K. L. (1933) *Physical Review* **43,** 830.

60. Roothaan, C. C. J. (1951) *Review of Modern Physics* **23,** 69.

61. Hall, G. G. (1951) *Proceedings of the Royal Society of London* **A205,** 541.

62. Ditchfield, R., Hehre, W. J., and Pople, J. A. (1971) *Journal of Chemical Physics* **54,** 724.

63. Hehre, W. J., Ditchfield, R., and Pople, J. A. (1972) *Journal of Chemical Physics* **56,** 2257.

64. Hariharan, P. C., and Pople, J. A. (1974) *Molecular Physics* **27,** 209.

65. Gordon, M. S. (1980) *Chemical Physics Letters* **73,** 163.

66. Hariharan, P. C., and Pople, J. A. (1973) *Theoretica Chimica Acta* **28,** 213.

67. Blaudeau, J.-P., McGrath, M. P., Curtiss, L. A., and Radom, L. (1997) *Journal of Chemical Physics* **107,** 5016.

68. Francl, M. M., Pietro, W. J., Hehre, W. J., Binkley, J. S., DeFrees, D. J., Pople, J. A., and Gordon, M. S. (1982) *Journal of Chemical Physics* **77,** 3654.

69. R. C. Binning, J., and Curtiss, L. A. (1990) *Journal of Computational Chemistry* **11,** 1206.

70. Rassolov, V. A., Pople, J. A., Ratner, M. A., and Windus, T. L. (1998) *Journal of Chemical Physics* **109,** 1223.

71. Rassolov, V. A., Ratner, M. A., Pople, J. A., Redfern, P. C., and Curtiss, L. A. (2001) *Journal of Computational Chemistry* **22,** 976.

72. Frisch, M. J., Pople, J. A., and Binkley, J. S. (1984) *Journal of Chemical Physics* **80,** 3265.

73. Hohenburg, P., and Kohn, W. (1964) *Physical Review B* **136,** 864-871.

74. Kohn, W., and Sham, L. J. (1965) *Physical Review A* **140,** 1133-1138.

75. Adamo, C., and Barone, V. (1998) *Journal of Chemical Physics* **108,** 664.

76. Burke, K., Perdew, J. P., and Wang, Y. (1998) *Electronic Density Functional Theory: Recent Progress and New Directions*, Ed. J. F. Dobson, G. Vignale, and M. P. Das, Plenum.

77. Perdew, J. P. (1991) *Electronic Structure of Solids ' 91*, Ed. P. Ziesche and H. Eschrig, Akademie Verlag, Berlin.

78. Perdew, J. P., Chevary, J. A., Vosko, S. H., Jackson, K. A., Pederson, M. R., Singh, D. J., and Fiolhais, C. (1992) *Physical Review B* **46**.

79. Perdew, J. P., Chevary, J. A., Vosko, S. H., Jackson, K. A., Pederson, M. R., Singh, D. J., and Fiolhais, C. (1993) *Physical Review B* **48**.

80. Perdew, J. P., Burke, K., and Wang, Y. (1996) *Physical Review B* **54,** 16533.

81. Kamerlin, S. C. L. (2005) *Ph.D. Thesis*, School of Chemistry, University of Birmingham, Birmingham, UK.

82. Dewar, M. J. S., Zoebisch, E. G., Healy, E. F., and Stewart, J. J. P. (1985) *Journal of the American Chemical Society* **107,** 3902-3909.

83. Reed, A. E., and Weinhold, F. (1983) *Journal of Chemical Physics* **78,** 4066.

84. Schlegel, H. B. (1982) *Journal of Computational Chemistry* **3,** 214.

85. Schlegel, H. B. (1989) *New Theoretical Concepts for Understanding Organic Reactions, Ed. J. Bertran*, Kluwer Academic, The Netherlands.

86. Peng, C., Ayala, P. Y., Schlegel, H. B., and Frisch, M. J. (1996) *Journal of Computational Chemistry* **17,** 49.

87. Schlegel, H. B. (1995) *Modern Electronic Structure Theory, Ed. D. R. Yarkony*, World Scientific Publishing, Singapore.

88. Mulliken, R. S. (1955) *Journal of Chemical Physics* **23,** 1833-1840.

89. Miertus, S., Scrocco, E., and Tomasi, J. (1981) *Chemical Physics* **55,** 117.

90. Miertus, S., and Tomasi, J. (1982) *Chemical Physics* **65,** 239.

91. Cossi, M., Barone, V., Cammi, R., and Tomasi, J. (1996) *Chemical Physics Letters* **255,** 327.

92. Mennucci, B., and Tomasi, J. (1997) *Journal of Chemical Physics* **106,** 5151.

93. Mennucci, B., Cancès, E., and Tomasi, J. (1997) *Journal of Physical Chemistry B* **101,** 10506.

94. Cammi, R., Mennucci, B., and Tomasi, J. (1999) *Journal of Physical Chemistry A* **103,** 9100.

95. Cossi, M., Barone, V., and Robb, M. A. (1999) *Journal of Chemical Physics* **111,** 5295.

96. Cammi, R., Mennucci, B., and Tomasi, J. (2000) *Journal of Physical Chemistry A* **104,** 5631.

97. Cossi, M., and Barone, V. (2000) *Journal of Chemical Physics* **112,** 2427.

98. Cossi, M., and Barone, V. (2001) *Journal of Chemical Physics* **115,** 4708.

99. Cossi, M., Rega, N., Scalmani, G., and Barone, V. (2001) *Journal of Chemical Physics* **114,** 5691.

100. Cossi, M., Scalmani, G., Rega, N., and Barone, V. (2002) *Journal of Chemical Physics* **117,** 43.

101. Cossi, M., Rega, N., Scalmani, G., and Barone, V. (2003) *Journal of Computational Chemistry* **24,** 669-681.

102. Gonzalez, C., and Schlegel, H. B. (1989) *Journal of Chemical Physics* **90,** 2154.

103. Gonzalez, C., and Schlegel, H. B. (1990) *Journal of Physical Chemistry* **94,** 5523.

104. Lewars, E. (2003) *Computational Chemistry: Introduction to the Theory and Applications of Molecular and Quantum Mechanics*, Kluwer Academic Publishers, Boston.

105. Roos, B. O., Taylor, P. R., and Siegbahm, E. M. (1980) *Chemical Physics* **48,** 157-173.

106. Ponder, J. W., and Case, D. A. (2003) *Advances in Protein Chemistry* **66,** 27-85.

107. Cornell, W. D., Cieplak, P., Bayly, C. I., Gould, I. R., Merz, K. M., Ferguson, D. M., Spellmeyer, D. C., Fox, T., Caldwell, J. W., and Kollman, P. A. (1995) *Journal of the American Chemical Society* **117,** 5179-5197.

108. Ewald, P. (1921) *Annalen der Physik* **64,** 253.

109. Blundell, T. L., Sibanda, B. L., Sternberg, M. J. E., and Thornton, J. M. (1987) *Nature* **326,** 347-352.

110. Johnson, D. J. R. (2008) *Ph.D. Thesis*, School of Chemistry, University of Birmingham, Birmingham, UK.

111. Ward, R. A. (2002) *Ph.D. Thesis*, School of Chemistry, University of Birmingham, Birmingham, UK.

112. Maple, J. R., Hwang, M.-J., Stockfisch, T. P., Dinur, U., Waldman, M., Ewig, C. S., and Hagler, A. T. (1994) *Journal of Computational Chemistry* **15,** 162.

113. Hwang, M.-J., Stockfisch, T. P., and Hagler, A. T. (1994) *Journal of the American Chemical Society* **116,** 2515.

114. *Insight II (2000),* Accelrys Inc., San Diego, CA, USA.

115. Snyman, J. A. (2005) *Practical mathematical optimization : an introduction to basic optimization theory and classical and new gradient-based algorithms,* Springer, New York.

116. Avriel, M. (2003) *Nonlinear programming : analysis and methods,* Dover Publications, Mineola, NY.

117. Hestenes, M. R., and Stiefel, E. (1952) *Journal of Research of the National Bureau of Standards* **49,** 409.

118. Duan, Y., Wu, C., Chowdhury, S., Lee, M. C., Xiong, G., Zhang, W., Yang, R., Cieplak, P., Luo, R., and Lee, T. (2003) *Journal of Computational Chemistry* **24,** 1999-2012.

119. Wang, J., Wolf, R. M., Caldwell, J. W., Kollamn, P. A., and Case, D. A. (2004) *Journal of Computational Chemistry* **25,** 1157-1174.

120. Jakalian, A., Bush, B. L., Jack, D. B., and Bayly, C. I. (2000) *Journal of Computational Chemistry* **21,** 132-146.

121. Collins, C. I. (2009) *Ph.D. Thesis,* School of Chemistry, University of Birmingham, Birmingham, UK.

122. Ljungberg, K. B., Marelius, J., Musil, D., Svensson, P., Norden, B., and Aqvist, J. (2001) *European Journal of Pharmaceutical Sciences* **12,** 441-446.

123. Chu, H. Y., Zheng, Q. C., Zhao, Y. S., and Zhang, H. X. (2009) *Journal of Molecular Modeling* **15,** 323-328.

124. Feenstra, K. A., Hess, B., and Berendsen, H. J. C. (1999) *Journal of Computational Chemistry* **20,** 786-798.

125. Dartigalongue, T., and Hache, F. (2005) *Chemical Physics Letters* **415,** 313-316.

126. Pande, V. S., Baker, I., Chapman, J., Elmer, S. P., Khaliq, S., Larson, S. M., Rhee, Y. M., Shirts, M. R., Snow, C. D., Sorin, E. J., and Zagrovic, B. (2003) *Biopolymers* **68,** 91-109.

127. Jackson, M. B. (1993) *Journal of Chemical Physics* **99,** 7253-7259.

128. Deng, H., Zhadin, N., and Callender, R. (2001) *Biochemistry* **40,** 3767-3773.

129. Jorgensen, W. L., Chandrasekhar, J., Madura, J. D., Impey, R. W., and Klein, M. L. (1983) *Journal of Chemical Physics* **79,** 926-935.

130. Berendsen, H. J. C., Postma, J. P. M., van Gunsteren, W. F., DiNola, A., and Haak, J. R. (1984) *Journal of Chemical Physics* **81,** 3684-3690.

131. Ryckaert, J.-P., Ciccotti, G., and Berendsen, H. J. C. (1977) *Journal of Computational Physics* **23,** 327-341.

132. Maseras, F., and Morokuma, K. (1995) *Journal of Computational Chemistry* **16,** 1170.

133. Humbel, S., Sieber, S., and Morokuma, K. (1996) *Journal of Chemical Physics* **105,** 1959.

134. Matsubara, T., Sieber, S., and Morokuma, K. (1996) *International Journal of Quantum Chemistry* **60,** 1101.

135. Svensson, M., Humbel, S., Froese, R. D. J., Matsubara, T., Sieber, S., and Morokuma, K. (1996) *Journal of Physical Chemistry* **100,** 19357.

136. Svensson, M., Humbel, S., and Morokuma, K. (1996) *Journal of Chemical Physics* **105,** 3654.

137. Dapprich, S., Komáromi, I., Byun, K. S., Morokuma, K., and Frisch, M. J. (1999) *Journal of Molecular Structure: Theochem* **462,** 1.

138. Vreven, T., and Morokuma, K. (2000) *Journal of Computational Chemistry* **21,** 1419.

139. Walters, P., and Stahl, M. (1996) *Babel version 1.6*, babel@mercury.aichem.arizona.edu

140. Rappe, A. K., Casewit, C. J., Colwell, K. S., Goddard, W. A., and Skiff, W. M. (1992) *Journal of the American Chemical Society* **114,** 10024-10035.

141. Schaftenaar, G. (1991) *Molden*, CAOS/CAMM Center Nijmegen, Toernooiveld, The Netherlands.

142. Walsh, J. D., and Miller, A. F. (2003) *Journal of Molecular Structure-Theochem* **623,** 185-195.

143. Wardman, P. (1989) *Journal of Physical Chemistry Reference Data* **18,** 1637-1755.

144. Jackson, J. C., Hammill, J. T., and Mehl, R. A. (2007) *Journal of the American Chemical Society* **129,** 1160-1166.

145. Christofferson, A., and Wilkie, J. (2009) *Biochemical Society Transactions* **37,** 413-418.

Appendix A
Mulliken Charges

This appendix contains the atomic Mulliken charges for the tabulated molecular partial charges in Chapters 3 and 4. The H transferred is shown in **bold**.

Nitrofuran TS Mulliken charges (Table 3.3):

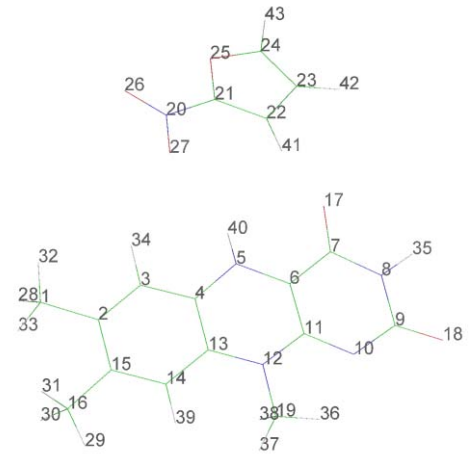

Figure A.1: Atom numbers for nitrofuran and FMN.

		Reactants	T.S.	Products
1	C	-0.450449	-0.448487	-0.446401
2	C	0.057267	0.051567	0.051492
3	C	-0.232628	-0.183631	-0.134474
4	C	0.314889	0.321052	0.245874
5	N	-0.756345	-0.805785	-0.638937
6	C	0.12341	0.199863	0.128096
7	C	0.595415	0.604857	0.634992
8	N	-0.657644	-0.658561	-0.65869
9	C	0.704039	0.71599	0.716927
10	N	-0.684714	-0.677619	-0.680137
11	C	0.575972	0.581468	0.620279
12	N	-0.68833	-0.674704	-0.682402
13	C	0.34811	0.349238	0.37158
14	C	-0.219518	-0.21438	-0.215307
15	C	0.045198	0.049969	0.054181
16	C	-0.446569	-0.448045	-0.448825
17	O	-0.654822	-0.58456	-0.605293
18	O	-0.602276	-0.574895	-0.573759
19	C	-0.241158	-0.250775	-0.25097
20	N	0.332918	0.135866	0.098664
21	C	0.480059	0.564048	0.568353
22	C	-0.074669	-0.158279	-0.1933
23	C	-0.209773	-0.196003	-0.182946
24	C	0.126691	0.099265	0.096063
25	O	-0.432654	-0.456185	-0.454579
26	O	-0.418121	-0.459334	-0.469174
27	O	-0.414613	-0.497945	-0.45762
28	H	0.124631	0.129171	0.131618
29	H	0.118524	0.11971	0.119324
30	H	0.123595	0.129094	0.128715
31	H	0.123612	0.133184	0.134952
32	H	0.135343	0.14754	0.139926
33	H	0.123659	0.120597	0.117403
34	H	0.122839	0.147363	0.136353
35	H	0.268789	0.278161	0.278691
36	H	0.189665	0.197433	0.196696
37	H	0.11293	0.12738	0.127955
38	H	0.113037	0.130435	0.13337
39	H	0.094495	0.097839	0.096017
40	**H**	**0.293259**	**0.434328**	**0.375552**
41	H	0.237269	0.182773	0.152116
42	H	0.15153	0.118909	0.119417
43	H	0.147138	0.122088	0.118209

CB1954 TS Mulliken charges (Table 3.5):

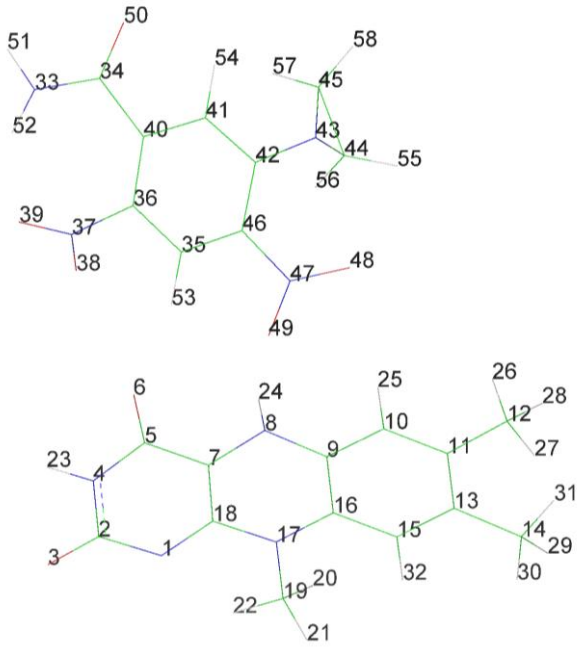

Figure A.2: Atom numbers for CB1954 and FMN (Table 3.5).

		Reactants	TS	Products
1	N	-0.68201	-0.67392	-0.66573
2	C	0.71227	0.72226	0.73014
3	O	-0.58535	-0.55604	-0.54723
4	N	-0.66077	-0.65903	-0.65357
5	C	0.61582	0.63162	0.66336
6	O	-0.62335	-0.55105	-0.57590
7	C	0.14664	0.18671	0.11543
8	N	-0.76621	-0.78670	-0.59126
9	C	0.31710	0.29765	0.21527
10	C	-0.21969	-0.19159	-0.12463
11	C	0.05166	0.04477	0.06654
12	C	-0.45233	-0.45560	-0.44905
13	C	0.04938	0.05458	0.06937
14	C	-0.44796	-0.44954	-0.45286
15	C	-0.21817	-0.21072	-0.20074
16	C	0.35793	0.36444	0.38266
17	N	-0.69236	-0.67364	-0.66812
18	C	0.58804	0.59659	0.62978
19	C	-0.24726	-0.25664	-0.27729
20	H	0.12110	0.13792	0.18599
21	H	0.11987	0.13574	0.12734
22	H	0.19577	0.20469	0.20059
23	H	0.28109	0.29412	0.29278
24	**H**	**0.32420**	**0.46948**	**0.37754**
25	H	0.13807	0.18059	0.14332
26	H	0.14378	0.16449	0.14152
27	H	0.12557	0.12764	0.12174
28	H	0.12704	0.13006	0.13677
29	H	0.12796	0.13775	0.13214
30	H	0.12134	0.12506	0.13032
31	H	0.12880	0.14006	0.14171
32	H	0.10012	0.10781	0.12022
33	N	-0.69196	-0.69619	-0.69234
34	C	0.59585	0.58228	0.59465
35	C	-0.04470	-0.12113	-0.20435
36	C	0.10589	0.13215	0.17951
37	N	0.35264	0.34034	0.36669

38	O	-0.32943	-0.35159	-0.37867
39	O	-0.43490	-0.44492	-0.45461
40	C	0.03368	0.01217	-0.01553
41	C	-0.20518	-0.20865	-0.20797
42	C	0.29105	0.24830	0.22798
43	N	-0.42830	-0.42194	-0.41190
44	C	-0.14715	-0.12196	-0.12016
45	C	-0.16794	-0.17395	-0.17195
46	C	0.20844	0.30576	0.31837
47	N	0.29233	0.12992	0.11440
48	O	-0.41337	-0.48463	-0.50256
49	O	-0.42696	-0.51283	-0.46222
50	O	-0.54053	-0.55787	-0.58058
51	H	0.28886	0.27690	0.27565
52	H	0.33029	0.31681	0.32067
53	H	0.25124	0.23871	0.19166
54	H	0.17037	0.15880	0.15211
55	H	0.16290	0.14666	0.14316
56	H	0.15392	0.14310	0.13855
57	H	0.14627	0.13908	0.13352
58	H	0.14861	0.13514	0.12778

CB1954 Hydride transfer to nitrogen Mulliken charges (Table 3.6):

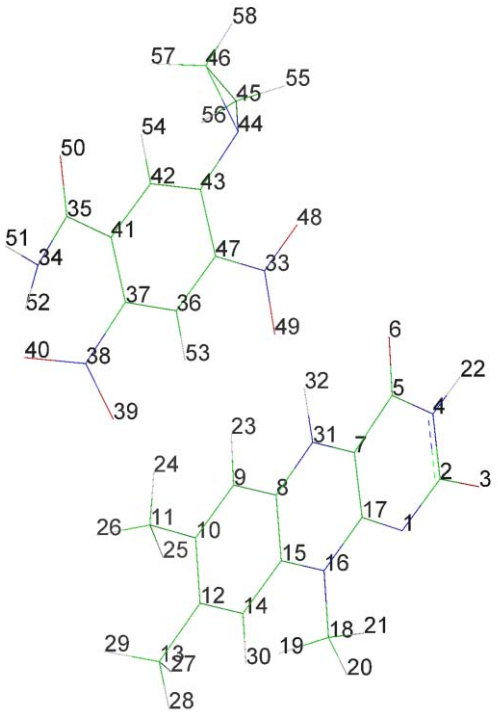

Figure A.3: Atom numbers for CB1954 and FMN (Table 3.6).

		R.T.	R.S.	P.T.	P.S.
1	N	-0.672026	-0.674751	-0.672989	-0.660457
2	C	0.723167	0.711264	0.715521	0.733043
3	O	-0.550933	-0.583161	-0.570821	-0.530668
4	N	-0.665402	-0.662984	-0.664417	-0.657356
5	C	0.628494	0.620214	0.654843	0.68541
6	O	-0.534143	-0.622609	-0.624206	-0.535022
7	C	0.208699	0.148656	0.120651	0.145404
8	C	0.323955	0.307745	0.252443	0.227894
9	C	-0.192592	-0.19925	-0.187585	-0.084903
10	C	0.05742	0.050966	0.060769	0.053916
11	C	-0.451921	-0.449776	-0.449242	-0.457446
12	C	0.058795	0.050452	0.049481	0.06649
13	C	-0.450701	-0.448126	-0.448293	-0.454723
14	C	-0.204799	-0.213055	-0.21155	-0.209289
15	C	0.362779	0.343723	0.350641	0.39097
16	N	-0.685048	-0.670993	-0.673856	-0.662781
17	C	0.607121	0.573998	0.604624	0.619302
18	C	-0.25895	-0.243535	-0.252317	-0.264383
19	H	0.142936	0.125319	0.131752	0.15897
20	H	0.136046	0.122531	0.129702	0.145692
21	H	0.205488	0.192452	0.196752	0.209465
22	H	0.292117	0.2744	0.28568	0.295281
23	H	0.173943	0.137146	0.150876	0.170444
24	H	0.148424	0.144916	0.141182	0.187154
25	H	0.131622	0.124303	0.125124	0.126059
26	H	0.14162	๐.130192	0.130765	0.129734
27	H	0.136972	0.129165	0.130082	0.144502
28	H	0.127471	0.121658	0.121454	0.12678
29	H	0.144802	0.132518	0.133735	0.155426
30	H	0.112809	0.101407	0.099219	0.112642
31	N	-0.777503	-0.763004	-0.645179	-0.552387
32	**H**	**0.422905**	**0.332108**	**0.429731**	**0.288889**
33	N	0.262808	0.325161	0.061041	0.030231
34	N	-0.683787	-0.641633	-0.618372	-0.641702
35	C	0.57437	0.558486	0.535101	0.551639
36	C	-0.144722	-0.145746	-0.115592	-0.096026
37	C	0.164707	0.176739	0.179024	0.162577
38	N	0.344291	0.359942	0.373843	0.361583
39	O	-0.391701	-0.406095	-0.403395	-0.405475
40	O	-0.459118	-0.45798	-0.460503	-0.464806
41	C	0.003921	0.028722	0.03889	0.027801
42	C	-0.203034	-0.184668	-0.185977	-0.178342
43	C	0.246243	0.31335	0.324408	0.281592
44	N	-0.421944	-0.41834	-0.431997	-0.498602
45	C	-0.116145	-0.12132	-0.108632	-0.176382
46	C	-0.174347	-0.169516	-0.182289	-0.163807
47	C	0.304879	0.268498	0.151709	0.228658
48	O	-0.467245	-0.47553	-0.445968	-0.606771
49	O	-0.603978	-0.435689	-0.387634	-0.567827
50	O	-0.558745	-0.528094	-0.515575	-0.5285
51	H	0.272812	0.284257	0.285481	0.278829
52	H	0.308381	0.301172	0.297582	0.295481
53	H	0.182707	0.212201	0.221825	0.196402
54	H	0.157595	0.170434	0.156921	0.160676
55	H	0.148422	0.190172	0.160636	0.171958
56	H	0.137767	0.138271	0.166143	0.193102
57	H	0.137801	0.138039	0.145444	0.139639
58	H	0.134494	0.17528	0.143309	0.14402

CB1954 hydride transfer to oxygen Mulliken charges (Table 3.7):

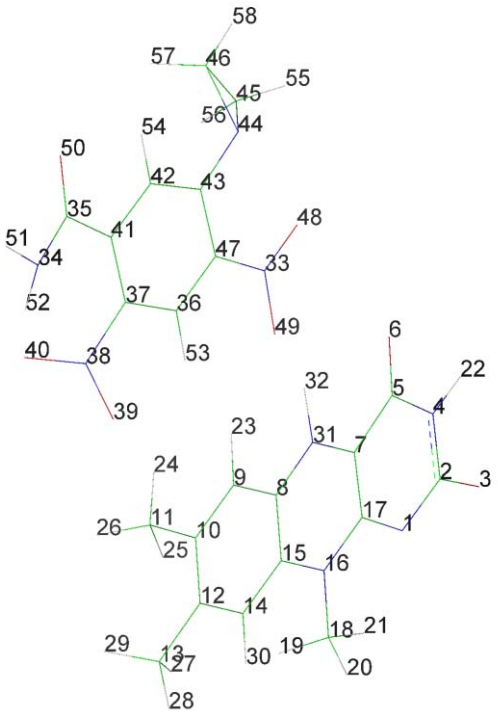

Figure A.4: Atom numbers for CB1954 and FMN (Table 3.7).

		React. Trip.	React. Sing.	Prod. Sing.	Prod. Trip.
1	N	-0.669346	-0.680395	-0.668215	-0.679124
2	C	0.726254	0.704616	0.725108	0.714534
3	O	-0.542888	-0.585825	-0.544954	-0.572798
4	N	-0.66686	-0.661407	-0.662309	-0.659309
5	C	0.637055	0.615319	0.632757	0.614849
6	O	-0.529827	-0.624143	-0.526035	-0.588894
7	C	0.191444	0.182639	0.169155	0.15513
8	N	-0.71634	-0.763787	-0.662298	-0.728617
9	C	0.29361	0.346479	0.305028	0.299362
10	C	-0.151423	-0.218602	-0.147751	-0.206569
11	C	0.032129	0.0598	0.048568	0.05566
12	C	-0.458681	-0.450116	-0.450527	-0.450973
13	C	0.06264	0.045953	0.057504	0.048204
14	C	-0.450356	-0.448359	-0.451379	-0.448423
15	C	-0.211116	-0.216588	-0.208186	-0.211882
16	C	0.365278	0.352824	0.369517	0.350216
17	N	-0.685437	-0.694721	-0.673202	-0.675399
18	C	0.612265	0.587937	0.609349	0.585518
19	C	-0.260989	-0.249524	-0.261346	-0.252293
20	H	0.296869	0.282446	0.293117	0.283994
21	H	0.197119	0.11894	0.147391	0.142856
22	H	0.115057	0.101213	0.111418	0.100173
23	H	0.142223	0.122919	0.146532	0.128546
24	H	0.142923	0.122356	0.14186	0.128061
25	H	0.207758	0.196514	0.207323	0.199596
26	H	0.171428	0.131645	0.14899	0.144788
27	H	0.134391	0.129179	0.13029	0.125676
28	H	0.133169	0.130323	0.139264	0.127546
29	H	0.144094	0.127857	0.14061	0.130586
30	H	0.127764	0.122192	0.128165	0.122196
31	H	0.143556	0.128557	0.144961	0.131547
32	**H**	**0.345593**	**0.313834**	**0.394073**	**0.40272**

33	O	-0.533677	-0.459455	-0.464786	-0.451982
34	N	-0.423223	-0.442899	-0.42593	-0.427778
35	C	-0.174275	-0.174924	-0.174694	-0.17389
36	C	-0.119442	-0.123781	-0.118841	-0.134073
37	C	0.244495	0.310803	0.234414	0.265453
38	C	0.268883	0.282159	0.339981	0.303892
39	N	0.268344	0.351947	0.093486	0.10493
40	O	-0.503909	-0.414682	-0.514842	-0.417207
41	C	-0.137448	-0.127642	-0.16016	-0.102563
42	C	0.162596	0.161048	0.158869	0.131065
43	N	0.342372	0.347161	0.351443	0.363236
44	O	-0.463861	-0.456054	-0.443647	-0.433928
45	O	-0.400662	-0.391285	-0.383138	-0.350686
46	C	-0.001061	0.017507	-0.007466	0.021242
47	C	0.569219	0.596337	0.568867	0.59047
48	O	-0.567223	-0.542345	-0.56678	-0.544944
49	N	-0.693154	-0.687658	-0.698408	-0.691337
50	C	-0.207702	-0.202044	-0.204763	-0.199155
51	H	0.140716	0.141796	0.138929	0.147894
52	H	0.131691	0.163353	0.131604	0.143865
53	H	0.141424	0.186869	0.148133	0.158533
54	H	0.135265	0.14991	0.134164	0.149771
55	H	0.205526	0.207238	0.194932	0.24818
56	H	0.269646	0.282359	0.271006	0.286004
57	H	0.313171	0.323086	0.310493	0.331373
58	H	0.152931	0.17112	0.152354	0.16416

Optimised CB1954 orientation singlet and triplet Mulliken charges (Table 4.1):

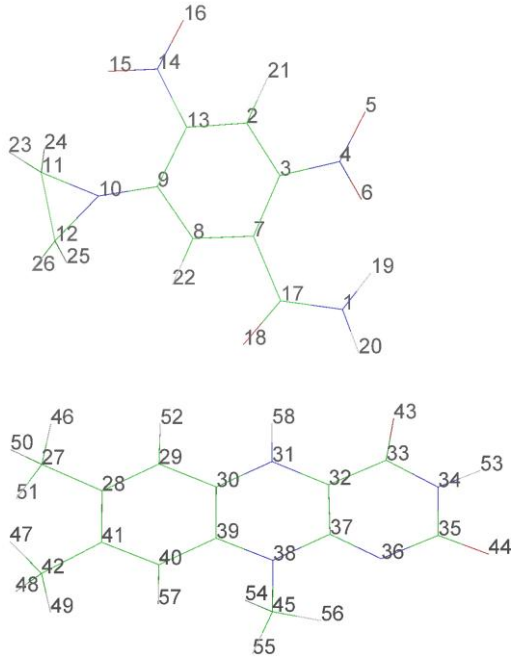

Figure A.5: Atom numbers for CB1954 and FMN (Table 4.1).

		React. Sing.	React. Trip.	Prod. Trip.	Prod. Sing.
1	N	-0.676112	-0.689834	-0.762108	-0.749119
2	C	-0.128163	-0.136397	-0.134595	-0.124161
3	C	0.167193	0.154617	0.161784	0.179642
4	N	0.342433	0.322575	0.284733	0.308459
5	O	-0.406342	-0.461292	-0.481553	-0.42553
6	O	-0.42187	-0.491814	-0.528211	-0.4802
7	C	0.033905	-0.002251	0.004888	0.031433
8	C	-0.19286	-0.201385	-0.199024	-0.190987
9	C	0.278965	0.238222	0.24084	0.264024
10	N	-0.429051	-0.431513	-0.438984	-0.430839
11	C	-0.136052	-0.12186	-0.119918	-0.122631
12	C	-0.172781	-0.168828	-0.169415	-0.171167
13	C	0.225962	0.212248	0.219305	0.231376
14	N	0.349576	0.334642	0.344879	0.348582
15	O	-0.421848	-0.473854	-0.434987	-0.420051
16	O	-0.429475	-0.485291	-0.446638	-0.42718
17	C	0.602538	0.57815	0.539315	0.554614
18	O	-0.572378	-0.622624	-0.540392	-0.520809
19	H	0.291842	0.293157	0.333233	0.332924
20	H	0.378492	0.350448	0.315669	0.326335
21	H	0.211988	0.191621	0.193742	0.205539
22	H	0.177478	0.129947	0.155143	0.170203
23	H	0.161341	0.140205	0.140595	0.151481
24	H	0.150455	0.133357	0.13701	0.143955
25	H	0.16179	0.128333	0.142519	0.149349
26	H	0.154868	0.123334	0.133931	0.147135
27	C	-0.44775	-0.45404	-0.474106	-0.472096
28	C	0.059409	0.053743	0.051944	0.056569
29	C	-0.221538	-0.18587	-0.168789	-0.192016
30	C	0.345187	0.328037	0.317242	0.329558
31	N	-0.79456	-0.723142	-0.741673	-0.790879
32	C	0.188545	0.217288	0.194464	0.166234
33	C	0.618214	0.655422	0.644933	0.621187
34	N	-0.658083	-0.660886	-0.663727	-0.662046
35	C	0.712524	0.73454	0.726755	0.714034
36	N	-0.679896	-0.664938	-0.667859	-0.677255
37	C	0.583473	0.605683	0.613076	0.596125
38	N	-0.693512	-0.680917	-0.685087	-0.697807
39	C	0.347556	0.363128	0.362616	0.354618
40	C	-0.21737	-0.208103	-0.203749	-0.210072
41	C	0.047409	0.065536	0.0603	0.047629
42	C	-0.448007	-0.452767	-0.451229	-0.449053
43	O	-0.657133	-0.587822	-0.560741	-0.597237
44	O	-0.58108	-0.539498	-0.542108	-0.56361
45	C	-0.249189	-0.265082	-0.261802	-0.254376
46	H	0.125836	0.159559	0.187153	0.166844
47	H	0.128009	0.150794	0.157239	0.144558
48	H	0.128213	0.149381	0.146004	0.13658
49	H	0.122767	0.134523	0.125269	0.1215
50	H	0.129001	0.1461	0.167308	0.154233
51	H	0.129929	0.142978	0.123308	0.123176
52	H	0.138804	0.196721	0.167039	0.12688
53	H	0.280719	0.306994	0.296455	0.284747
54	H	0.123018	0.148653	0.146836	0.133022
55	H	0.122307	0.146462	0.143409	0.13152
56	H	0.197485	0.213403	0.207373	0.20112
57	H	0.101458	0.123164	0.117063	0.108366
58	H	0.316362	0.33704	0.373322	0.36557

Proton transfer from hydroxonium to CB1954 Mulliken charges (Table 4.10):

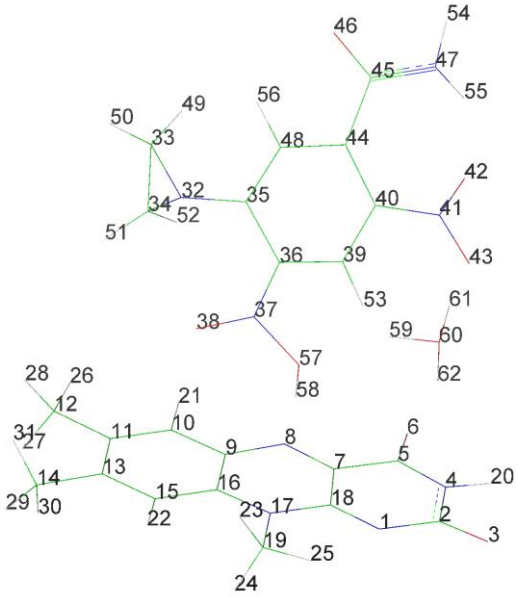

Figure A.6: Atom numbers for CB1954 and FMN (Table 4.10).

		React. Trip.	React. Sing.	Prod. Trip.	Prod. Sing.
1	N	-0.658091	-0.648621	-0.659665	-0.645255
2	C	0.734109	0.742166	0.731193	0.742035
3	O	-0.519709	-0.496653	-0.526218	-0.49156
4	N	-0.652504	-0.658371	-0.657757	-0.661949
5	C	0.642443	0.692508	0.640146	0.689464
6	O	-0.658024	-0.634389	-0.673872	-0.531476
7	C	0.168214	0.190151	0.198673	0.15386
8	N	-0.86087	-0.678037	-0.845128	-0.554094
9	C	0.306065	0.269737	0.340853	0.207866
10	C	-0.219906	-0.152644	-0.210064	-0.145591
11	C	0.064603	0.042098	0.061722	0.039616
12	C	-0.458362	-0.460205	-0.454651	-0.458666
13	C	0.05312	0.067257	0.052712	0.069815
14	C	-0.45345	-0.455555	-0.452907	-0.45569
15	C	-0.199201	-0.199613	-0.201144	-0.197871
16	C	0.367234	0.379699	0.35639	0.39447
17	N	-0.683898	-0.668997	-0.681003	-0.667564
18	C	0.627933	0.62824	0.61401	0.635769
19	C	-0.267377	-0.274525	-0.266167	-0.275331
20	H	0.309137	0.31278	0.3027	0.31599
21	H	0.123213	0.197143	0.12437	0.195331
22	H	0.131291	0.137724	0.127931	0.138942
23	H	0.153026	0.167253	0.150838	0.167713
24	H	0.152526	0.166521	0.150043	0.167663
25	H	0.215857	0.221765	0.214028	0.222712
26	H	0.149183	0.177735	0.14624	0.170342
27	H	0.149381	0.148782	0.146995	0.149669
28	H	0.149141	0.147521	0.147026	0.148672
29	H	0.151443	0.161669	0.149446	0.16281
30	H	0.141324	0.143602	0.139271	0.144814

31	H	0.151454	0.163343	0.14952	0.162388
32	N	-0.448829	-0.432407	-0.44698	-0.442104
33	C	-0.1727	-0.1761	-0.170724	-0.17409
34	C	-0.136284	-0.117054	-0.14473	-0.167603
35	C	0.283843	0.273193	0.290722	0.328778
36	C	0.340297	0.380985	0.292854	0.204759
37	N	0.116747	0.054003	0.062433	-0.085848
38	O	-0.486414	-0.532505	-0.328476	-0.292644
39	C	-0.135297	-0.306554	-0.091357	-0.104033
40	C	0.160659	0.201237	0.137201	0.159276
41	N	0.36889	0.355404	0.358998	0.373192
42	O	-0.417599	-0.405698	-0.412661	-0.411823
43	O	-0.352656	-0.491925	-0.345391	-0.386211
44	C	0.02327	0.002346	0.036876	0.03794
45	C	0.608434	0.597912	0.597479	0.580193
46	O	-0.522094	-0.531771	-0.520328	-0.512471
47	N	-0.683115	-0.688967	-0.676182	-0.662555
48	C	-0.189756	-0.198519	-0.190847	-0.18218
49	H	0.168971	0.157057	0.167951	0.170307
50	H	0.169641	0.156591	0.169794	0.163839
51	H	0.173734	0.161041	0.174415	0.165783
52	H	0.163161	0.158144	0.160749	0.208998
53	H	0.216348	0.155805	0.21255	0.192159
54	H	0.305346	0.294805	0.305708	0.304558
55	H	0.338435	0.31362	0.337808	0.331398
56	H	0.187521	0.176113	0.185892	0.185929
57	O	-0.466535	-0.513198	-0.430297	-0.703153
58	H	0.414126	0.412227	0.451904	0.3073
59	**H**	**0.436425**	**0.413507**	**0.426521**	**0.408368**
60	O	-0.57702	-0.546257	-0.654755	-0.704646
61	H	0.440085	0.437982	0.380755	0.339258
62	H	0.363062	0.408897	0.346584	0.372432

Proton transfer from hydroxonium to CB1954 Mulliken charges (Table 4.11):

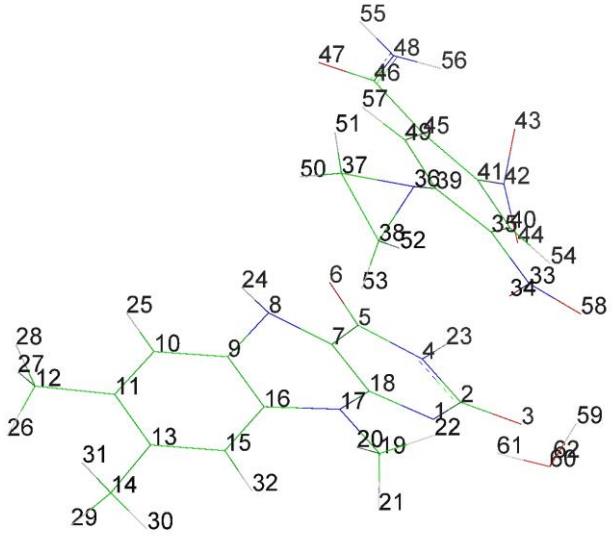

Figure A.7: Atom numbers for CB1954 and FMN (Table 4.11).

		React. Trip.	React. Sing.	Prod. Sing.	Prod. Trip.
1	N	-0.799209	-0.830264	-0.728304	-0.738721
2	C	0.784451	0.806911	0.764141	0.781236
3	O	-0.542659	-0.65921	-0.580497	-0.545932
4	N	-0.660478	-0.657086	-0.646048	-0.669057
5	C	0.667392	0.621617	0.640188	0.6629
6	O	-0.544851	-0.582907	-0.572468	-0.545277
7	C	0.198947	0.085838	0.198675	0.171287
8	N	-0.716595	-0.687847	-0.727627	-0.73012
9	C	0.318611	0.266868	0.325063	0.344897
10	C	-0.193525	-0.204931	-0.198182	-0.181974
11	C	0.056435	0.059562	0.045506	0.062111
12	C	-0.454676	-0.452923	-0.453506	-0.454582
13	C	0.061547	0.047445	0.062239	0.055014
14	C	-0.45447	-0.451438	-0.452894	-0.459595
15	C	-0.200168	-0.202665	-0.222849	-0.204955
16	C	0.355313	0.29194	0.359403	0.352281
17	N	-0.680922	-0.644056	-0.681811	-0.697565
18	C	0.663851	0.58344	0.617436	0.669515
19	C	-0.27201	-0.240471	-0.26974	-0.262909
20	H	0.165617	0.152642	0.154341	0.173153
21	H	0.197539	0.151628	0.192172	0.180338
22	H	0.17345	0.14383	0.17006	0.189431
23	H	0.327297	0.319511	0.318111	0.315386
24	H	0.356398	0.296682	0.330037	0.318062
25	H	0.179322	0.122385	0.172469	0.14158
26	H	0.156652	0.147711	0.155664	0.159019
27	H	0.154264	0.145303	0.147039	0.159337
28	H	0.153969	0.138575	0.15171	0.145455
29	H	0.15857	0.14695	0.156861	0.156105
30	H	0.144201	0.132941	0.142048	0.1634
31	H	0.157583	0.144402	0.150321	0.156019
32	H	0.138574	0.118381	0.133163	0.179475
33	N	0.208424	0.371816	0.197371	0.139538
34	O	-0.588396	-0.400405	-0.444861	-0.430716
35	C	0.276914	0.234533	0.306074	0.33013
36	N	-0.444289	-0.462262	-0.448742	-0.437918
37	C	-0.177256	-0.174976	-0.176553	-0.175868
38	C	-0.106955	-0.138786	-0.115816	-0.12807
39	C	0.262356	0.342333	0.290021	0.279066
40	C	-0.14773	-0.117789	-0.157202	-0.145608
41	C	0.188107	0.168865	0.193235	0.16225
42	N	0.391496	0.375197	0.420234	0.373669
43	O	-0.430435	-0.418901	-0.428218	-0.421619
44	O	-0.385931	-0.367665	-0.390915	-0.412498
45	C	-0.004952	0.04579	-0.006477	0.018427
46	C	0.584512	0.6319	0.559987	0.598953
47	O	-0.577617	-0.521058	-0.531323	-0.528369
48	N	-0.638567	-0.683189	-0.619161	-0.686709
49	C	-0.197032	-0.18929	-0.173147	-0.193852
50	H	0.146026	0.18617	0.163478	0.158689
51	H	0.152148	0.165866	0.161346	0.160316
52	H	0.159814	0.165438	0.169213	0.170166
53	H	0.141159	0.192551	0.15716	0.156809
54	H	0.210888	0.228607	0.225181	0.197929
55	H	0.301933	0.305878	0.304867	0.298437
56	H	0.334819	0.340108	0.323565	0.331098
57	H	0.14755	0.192788	0.158882	0.179008
58	O	-0.521012	-0.448764	-0.441	-0.495157
59	**H**	**0.429686**	**0.390396**	**0.405501**	**0.414904**
60	O	-0.566833	-0.529244	-0.662488	-0.681889
61	H	0.415714	0.414618	0.34913	0.373692
62	H	0.385041	0.388713	0.357939	0.349876

Proton transfer from FMN to CB1954 Mulliken charges (Table 4.12):

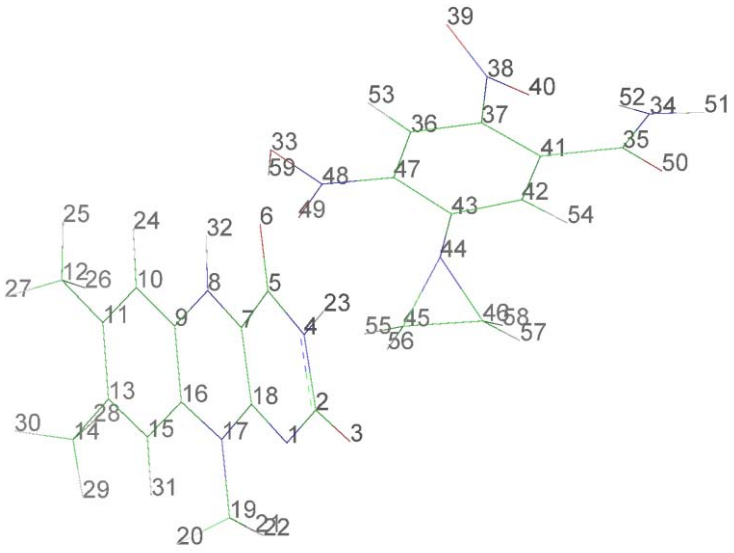

Figure A.8: Atom numbers for CB1954 and FMN (Table 4.12).

		React. Trip.	React. Sing.	Prod. Trip.	Prod. Sing.
1	N	-0.65326	-0.653178	-0.659927	-0.648268
2	C	0.741824	0.734737	0.734563	0.740752
3	O	-0.503186	-0.509709	-0.524873	-0.496558
4	N	-0.661743	-0.660372	-0.651453	-0.664242
5	C	0.690976	0.644486	0.633129	0.664346
6	O	-0.628562	-0.647632	-0.684101	-0.505377
7	C	0.208018	0.195864	0.198102	0.20131
8	N	-0.751798	-0.72576	-0.812319	-0.623686
9	C	0.336265	0.341438	0.333215	0.260171
10	C	-0.186796	-0.177347	-0.197689	-0.184612
11	C	0.060545	0.056319	0.066318	0.057041
12	C	-0.455099	-0.454033	-0.453063	-0.466431
13	C	0.062019	0.059517	0.052276	0.079175
14	C	-0.455157	-0.454525	-0.453459	-0.468123
15	C	-0.197056	-0.202667	-0.19901	-0.185905
16	C	0.371426	0.35936	0.361559	0.401021
17	N	-0.689953	-0.691866	-0.681754	-0.673244
18	C	0.633292	0.619433	0.624578	0.638238
19	C	-0.271987	-0.269776	-0.266392	-0.276034
20	H	0.161513	0.158696	0.153337	0.172857
21	H	0.159106	0.153594	0.150911	0.164676
22	H	0.220639	0.21727	0.214333	0.220739
23	H	0.315582	0.313809	0.306843	0.311997
24	H	0.157418	0.15038	0.107807	0.184278
25	H	0.150299	0.147895	0.139332	0.148821
26	H	0.156068	0.154566	0.149296	0.14465
27	H	0.157182	0.153713	0.149734	0.183032
28	H	0.157359	0.155037	0.150142	0.151384
29	H	0.144949	0.142603	0.140154	0.135636
30	H	0.158466	0.156071	0.150258	0.200539
31	H	0.14022	0.136234	0.129219	0.138443
32	**H**	**0.331723**	**0.310331**	**0.393086**	**0.377755**
33	O	-0.507015	-0.464645	-0.401008	-0.695688
34	N	-0.675033	-0.690039	-0.687564	-0.618203
35	C	0.609302	0.618965	0.622883	0.542827
36	C	-0.147485	-0.14486	-0.093248	-0.071181
37	C	0.162873	0.156799	0.141294	0.206647
38	N	0.359942	0.366669	0.364429	0.386714

39	O	-0.382379	-0.356854	-0.34806	-0.398355
40	O	-0.426209	-0.419732	-0.416383	-0.431605
41	C	0.022467	0.016016	0.025868	-0.015385
42	C	-0.193615	-0.19256	-0.19218	-0.163278
43	C	0.278005	0.288978	0.298368	0.317866
44	N	-0.43966	-0.436886	-0.445366	-0.432378
45	C	-0.131351	-0.144511	-0.154697	-0.137429
46	C	-0.173246	-0.169839	-0.165325	-0.172755
47	C	0.345283	0.327086	0.298009	0.147743
48	N	0.114361	0.138662	0.059011	-0.050408
49	O	-0.392379	-0.409574	-0.307073	-0.301498
50	O	-0.52274	-0.52467	-0.519741	-0.482519
51	H	0.299049	0.302703	0.306253	0.305903
52	H	0.319088	0.33515	0.339464	0.300785
53	H	0.166824	0.208278	0.198665	0.224861
54	H	0.186945	0.190468	0.196295	0.161701
55	H	0.172008	0.173273	0.180612	0.180583
56	H	0.157774	0.162391	0.164417	0.163639
57	H	0.160202	0.164928	0.16453	0.155182
58	H	0.163792	0.168947	0.174468	0.170021
59	H	0.412905	0.420368	0.441926	0.321831

Proton transfer from hydroxonium to CB1954 Mulliken charges (Table 4.13):

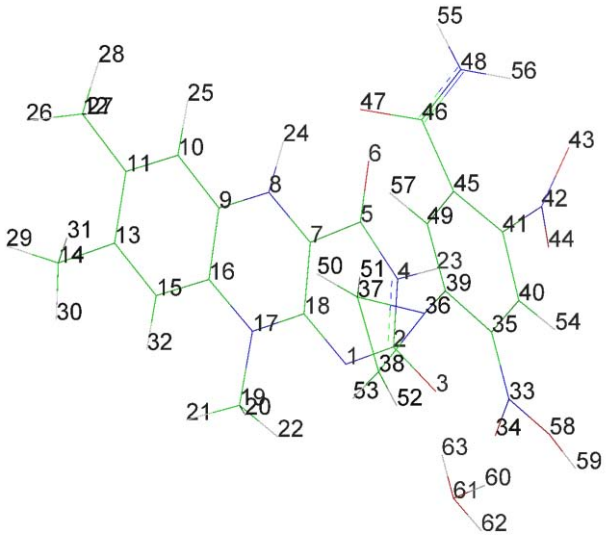

Figure A.9: Atom numbers for CB1954 and FMN (Table 4.13).

		React. Trip.	React. Sing.	Prod. Trip.	Prod. Sing.
1	N	-0.820057	-0.679639	-0.683155	-0.621654
2	C	0.833425	0.794257	0.795093	0.784017
3	O	-0.589563	-0.653598	-0.64549	-0.517368
4	N	-0.668021	-0.645358	-0.683792	-0.686704
5	C	0.675751	0.642733	0.659008	0.692467
6	O	-0.513127	-0.522329	-0.525234	-0.510027
7	C	0.168494	0.210577	0.188952	0.272203
8	N	-0.725345	-0.68644	-0.725912	-0.683648
9	C	0.34767	0.343751	0.345049	0.297101
10	C	-0.172789	-0.164099	-0.176169	-0.144688
11	C	0.064451	0.059554	0.06314	0.059265
12	C	-0.45817	-0.457125	-0.457237	-0.456045
13	C	0.065062	0.063616	0.063692	0.078617
14	C	-0.458255	-0.457968	-0.457287	-0.461978
15	C	-0.194785	-0.200949	-0.194963	-0.186738
16	C	0.354644	0.358542	0.361229	0.398518
17	N	-0.683032	-0.688881	-0.687248	-0.678157
18	C	0.707234	0.640855	0.646957	0.662881
19	C	-0.27284	-0.275474	-0.270559	-0.288585
20	H	0.184837	0.166263	0.172217	0.187798
21	H	0.184555	0.18424	0.174644	0.192165
22	H	0.18495	0.202539	0.196408	0.237299
23	H	0.331905	0.336316	0.335179	0.388351
24	H	0.33135	0.335632	0.326004	0.390088
25	H	0.161716	0.170539	0.155281	0.192012
26	H	0.171716	0.171178	0.167695	0.175749
27	H	0.171083	0.167274	0.167672	0.174917
28	H	0.158532	0.160503	0.154908	0.158066
29	H	0.172523	0.174671	0.168443	0.181736
30	H	0.153029	0.152313	0.150743	0.164618
31	H	0.172258	0.169364	0.1682	0.18111
32	H	0.153278	0.149901	0.148165	0.169348
33	N	0.160007	0.116869	0.110679	-0.085874
34	O	-0.512236	-0.452597	-0.284995	-0.277314
35	C	0.318174	0.350157	0.23953	0.18677
36	N	-0.659746	-0.435309	-0.67317	-0.441855
37	C	-0.147579	-0.174873	-0.139634	-0.174771
38	C	-0.144316	-0.135499	-0.146854	-0.142043
39	C	0.33504	0.285623	0.345101	0.342365
40	C	-0.108358	-0.152549	-0.05544	-0.083739
41	C	0.165365	0.166605	0.155266	0.215812
42	N	0.37519	0.38484	0.387928	0.348439
43	O	-0.394496	-0.391104	-0.380243	-0.403491
44	O	-0.339711	-0.375718	-0.359995	-0.396142
45	C	0.015308	0.008877	0.028419	-0.000804
46	C	0.625313	0.595456	0.618379	0.59422
47	O	-0.511814	-0.562853	-0.503675	-0.552788
48	N	-0.68129	-0.65427	-0.674974	-0.617623
49	C	-0.179829	-0.19086	-0.170988	-0.160141
50	H	0.196418	0.158399	0.198964	0.167381
51	H	0.192283	0.183878	0.197548	0.186278
52	H	0.192397	0.189344	0.199569	0.197212
53	H	0.190641	0.146099	0.196936	0.177211
54	H	0.219406	0.204984	0.223386	0.225768
55	H	0.319362	0.314929	0.323498	0.321559
56	H	0.339553	0.342032	0.339699	0.327288
57	H	0.199593	0.181029	0.202102	0.16625
58	O	-0.456802	-0.462101	-0.453915	-0.7604
59	H	0.421332	0.37411	0.429109	0.337293
60	**H**	**0.453499**	**0.408462**	**0.449645**	**0.413207**
61	O	-0.575457	-0.497702	-0.664758	-0.6422
62	H	0.415258	0.417376	0.357516	0.349349
63	H	0.38502	0.433609	0.40374	0.38005

Proton transfer from FMN, then hydroxonium to CB1954 Mulliken charges (Table 4.14):

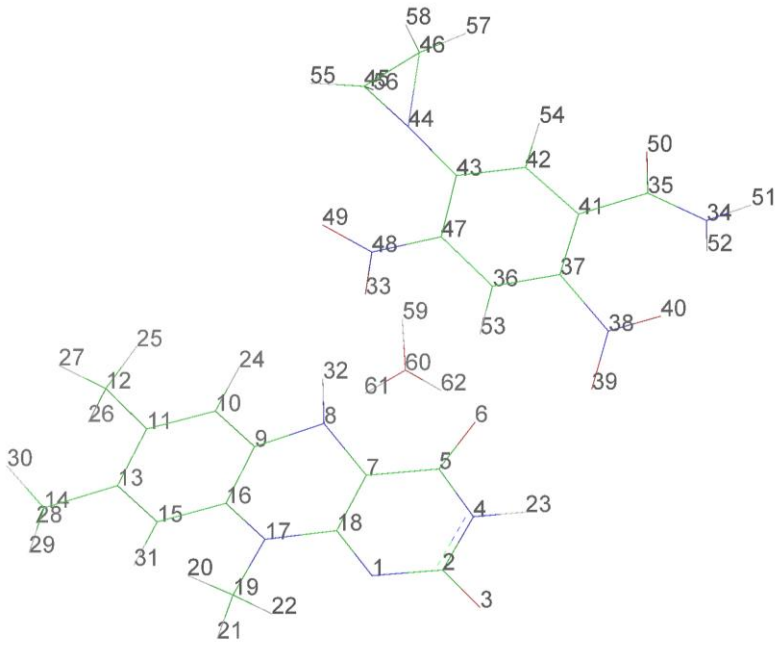

Figure A.10: Atom numbers for CB1954 and FMN (Table 4.14).

		React. Trip.	React. Sing.	Prod. Trip.	Prod. Sing.
1	N	-0.654682	-0.660456	-0.660185	-0.646681
2	C	0.739441	0.728361	0.730902	0.743308
3	O	-0.507724	-0.54097	-0.533185	-0.491617
4	N	-0.658382	-0.656785	-0.662216	-0.661474
5	C	0.680868	0.633067	0.662109	0.697425
6	O	-0.669795	-0.722574	-0.700911	-0.547443
7	C	0.202017	0.067613	0.187816	0.187506
8	N	-0.741003	-0.85888	-0.781234	-0.607849
9	C	0.305552	0.254964	0.321903	0.253016
10	C	-0.175916	-0.197408	-0.199645	-0.157259
11	C	0.050081	0.056866	0.063238	0.054772
12	C	-0.467753	-0.451737	-0.453211	-0.452567
13	C	0.0628	0.058417	0.051537	0.069432
14	C	-0.45401	-0.453461	-0.452574	-0.458682
15	C	-0.199602	-0.202059	-0.202963	-0.194172
16	C	0.37106	0.37618	0.35356	0.390953
17	N	-0.684495	-0.692838	-0.680542	-0.669398
18	C	0.626857	0.617515	0.617217	0.629668
19	C	-0.27095	-0.254961	-0.264501	-0.275897
20	H	0.160069	0.138455	0.149107	0.170182
21	H	0.15984	0.142942	0.147712	0.167652
22	H	0.219361	0.206888	0.211502	0.223183
23	H	0.312822	0.308642	0.295606	0.315104
24	H	0.180011	0.107535	0.111199	0.203743
25	H	0.178719	0.133813	0.14107	0.159089
26	H	0.148688	0.149127	0.145319	0.133952
27	H	0.149886	0.147016	0.14595	0.182709
28	H	0.157084	0.149836	0.14693	0.163314
29	H	0.142116	0.140776	0.137703	0.143068
30	H	0.158854	0.147997	0.147449	0.170432
31	H	0.137195	0.129698	0.124976	0.139474
32	**H**	**0.333278**	**0.343649**	**0.417235**	**0.344959**
33	O	-0.655886	-0.491277	-0.430148	-0.748215
34	N	-0.691095	-0.68081	-0.685363	-0.676286

35	C	0.609484	0.60818	0.614848	0.588235
36	C	-0.143296	-0.056929	-0.0689	-0.056865
37	C	0.160181	0.12422	0.130376	0.125318
38	N	0.363518	0.362333	0.355315	0.367656
39	O	-0.367385	-0.332131	-0.333548	-0.368398
40	O	-0.425089	-0.41238	-0.416579	-0.413842
41	C	0.012361	0.044164	0.033901	0.040955
42	C	-0.196372	-0.19464	-0.19404	-0.196396
43	C	0.267584	0.320058	0.299793	0.31823
44	N	-0.444967	-0.435248	-0.445803	-0.433325
45	C	-0.126834	-0.152881	-0.155907	-0.13881
46	C	-0.174106	-0.166418	-0.164199	-0.169679
47	C	0.313736	0.198887	0.272862	0.147388
48	N	0.170012	0.357199	0.04992	-0.075564
49	O	-0.462075	-0.355115	-0.286554	-0.31614
50	O	-0.531633	-0.511657	-0.517492	-0.51676
51	H	0.29847	0.309928	0.306896	0.303303
52	H	0.333095	0.33741	0.337733	0.336148
53	H	0.18893	0.22919	0.21249	0.231761
54	H	0.179585	0.195472	0.193948	0.182967
55	H	0.164881	0.184647	0.178635	0.171031
56	H	0.151888	0.157266	0.160449	0.16125
57	H	0.16041	0.163733	0.163089	0.158941
58	H	0.158194	0.178631	0.174397	0.16677
59	**H**	**0.386581**	**0.380566**	**0.428478**	**0.37657**
60	O	-0.510421	-0.536679	-0.65662	-0.648353
61	H	0.404047	0.430693	0.347202	0.330519
62	H	0.413913	0.396361	0.375949	0.371686

Proton transfer from hydroxonium, then FMN to CB1954 Mulliken charges (Table 4.15):

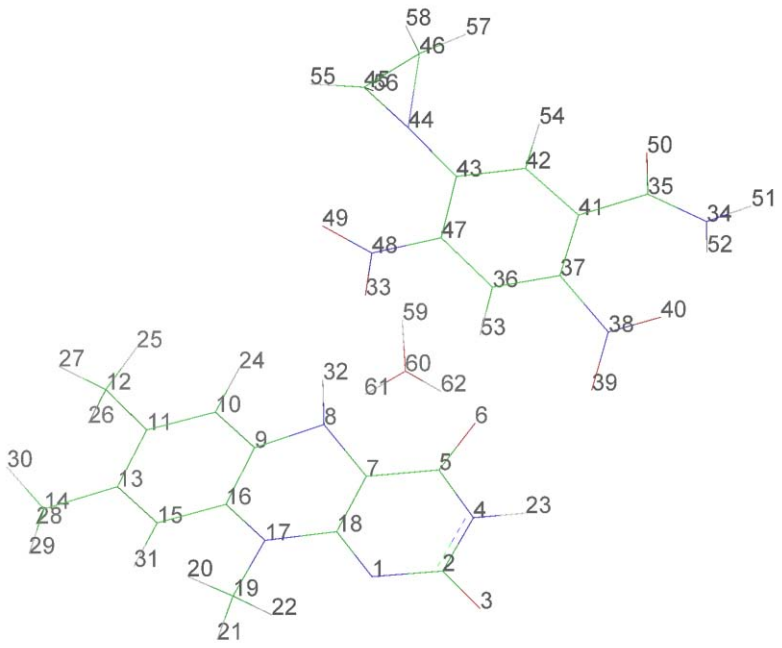

Figure A.11: Atom numbers for CB1954 and FMN (Table 4.15).

		React. Trip.	React. Sing.	Prod. Trip.	Prod. Sing.
1	N	-0.654682	-0.660456	-0.660185	-0.646681
2	C	0.739441	0.728361	0.730902	0.743308
3	O	-0.507724	-0.54097	-0.533185	-0.491617
4	N	-0.658382	-0.656785	-0.662216	-0.661474
5	C	0.680868	0.633067	0.662109	0.697425
6	O	-0.669795	-0.722574	-0.700911	-0.547443
7	C	0.202017	0.067613	0.187816	0.187506
8	N	-0.741003	-0.85888	-0.781234	-0.607849
9	C	0.305552	0.254964	0.321903	0.253016
10	C	-0.175916	-0.197408	-0.199645	-0.157259
11	C	0.050081	0.056866	0.063238	0.054772
12	C	-0.467753	-0.451737	-0.453211	-0.452567
13	C	0.0628	0.058417	0.051537	0.069432
14	C	-0.45401	-0.453461	-0.452574	-0.458682
15	C	-0.199602	-0.202059	-0.202963	-0.194172
16	C	0.37106	0.37618	0.35356	0.390953
17	N	-0.684495	-0.692838	-0.680542	-0.669398
18	C	0.626857	0.617515	0.617217	0.629668
19	C	-0.27095	-0.254961	-0.264501	-0.275897
20	H	0.160069	0.138455	0.149107	0.170182
21	H	0.15984	0.142942	0.147712	0.167652
22	H	0.219361	0.206888	0.211502	0.223183
23	H	0.312822	0.308642	0.295606	0.315104
24	H	0.180011	0.107535	0.111199	0.203743
25	H	0.178719	0.133813	0.14107	0.159089
26	H	0.148688	0.149127	0.145319	0.133952
27	H	0.149886	0.147016	0.14595	0.182709
28	H	0.157084	0.149836	0.14693	0.163314
29	H	0.142116	0.140776	0.137703	0.143068
30	H	0.158854	0.147997	0.147449	0.170432
31	H	0.137195	0.129698	0.124976	0.139474
32	**H**	**0.333278**	**0.343649**	**0.417235**	**0.344959**
33	O	-0.655886	-0.491277	-0.430148	-0.748215
34	N	-0.691095	-0.68081	-0.685363	-0.676286
35	C	0.609484	0.60818	0.614848	0.588235
36	C	-0.143296	-0.056929	-0.0689	-0.056865
37	C	0.160181	0.12422	0.130376	0.125318
38	N	0.363518	0.362333	0.355315	0.367656
39	O	-0.367385	-0.332131	-0.333548	-0.368398
40	O	-0.425089	-0.41238	-0.416579	-0.413842
41	C	0.012361	0.044164	0.033901	0.040955
42	C	-0.196372	-0.19464	-0.19404	-0.196396
43	C	0.267584	0.320058	0.299793	0.31823
44	N	-0.444967	-0.435248	-0.445803	-0.433325
45	C	-0.126834	-0.152881	-0.155907	-0.13881
46	C	-0.174106	-0.166418	-0.164199	-0.169679
47	C	0.313736	0.198887	0.272862	0.147388
48	N	0.170012	0.357199	0.04992	-0.075564
49	O	-0.462075	-0.355115	-0.286554	-0.31614
50	O	-0.531633	-0.511657	-0.517492	-0.51676
51	H	0.29847	0.309928	0.306896	0.303303
52	H	0.333095	0.33741	0.337733	0.336148
53	H	0.18893	0.22919	0.21249	0.231761
54	H	0.179585	0.195472	0.193948	0.182967
55	H	0.164881	0.184647	0.178635	0.171031
56	H	0.151888	0.157266	0.160449	0.16125
57	H	0.16041	0.163733	0.163089	0.158941
58	H	0.158194	0.178631	0.174397	0.16677
59	**H**	**0.386581**	**0.380566**	**0.428478**	**0.37657**
60	O	-0.510421	-0.536679	-0.65662	-0.648353
61	H	0.404047	0.430693	0.347202	0.330519
62	H	0.413913	0.396361	0.375949	0.371686

Proton transfer from hydroxonium, then FMN to CB1954 Mulliken charges (Table 4.16):

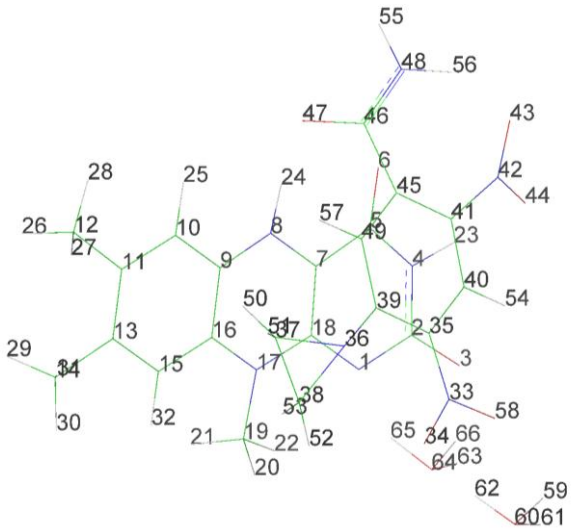

Figure A.12: Atom numbers for CB1954 and FMN (Table 4.16).

		React. Trip.	React. Sing.	Prod. Trip.	Prod. Sing.
1	N	-0.825018	-0.828342	-0.714079	-0.613255
2	C	0.829777	0.821109	0.765845	0.736484
3	O	-0.59998	-0.613828	-0.575757	-0.520408
4	N	-0.643711	-0.640996	-0.648466	-0.603769
5	C	0.653817	0.644476	0.650132	0.668726
6	O	-0.520455	-0.543699	-0.55419	-0.491011
7	C	0.199083	0.209684	0.194957	0.345028
8	N	-0.713998	-0.736266	-0.71689	-0.713625
9	C	0.32323	0.33142	0.316877	0.29003
10	C	-0.190137	-0.209214	-0.192004	-0.161555
11	C	0.059336	0.055276	0.057665	0.06096
12	C	-0.456954	-0.455976	-0.45626	-0.457135
13	C	0.063055	0.062969	0.06073	0.074933
14	C	-0.457156	-0.455717	-0.456717	-0.461101
15	C	-0.197444	-0.209935	-0.200162	-0.187856
16	C	0.353364	0.342093	0.349098	0.389951
17	N	-0.680799	-0.682563	-0.679579	-0.678538
18	C	0.665112	0.647436	0.612431	0.648838
19	C	-0.27913	-0.275264	-0.277966	-0.286125
20	H	0.172355	0.160451	0.1594	0.185063
21	H	0.189692	0.185925	0.183358	0.192604
22	H	0.1961	0.192092	0.209075	0.228271
23	H	0.341548	0.336815	0.331493	0.332933
24	H	0.366467	0.346611	0.35353	0.431349
25	H	0.186247	0.183906	0.177423	0.1941
26	H	0.173041	0.171223	0.172104	0.177115
27	H	0.163286	0.15723	0.160079	0.1726
28	H	0.162029	0.159903	0.157813	0.161446
29	H	0.175166	0.172612	0.173642	0.182402
30	H	0.152123	0.148284	0.151643	0.162695
31	H	0.166652	0.160569	0.162482	0.179065
32	H	0.14948	0.143298	0.148378	0.166216
33	N	0.170883	0.206758	0.063931	-0.035503
34	O	-0.56389	-0.550094	-0.288548	-0.31515
35	C	0.307921	0.319851	0.25323	0.135169
36	N	-0.433011	-0.437172	-0.455467	-0.461744
37	C	-0.176597	-0.173707	-0.169384	-0.17195
38	C	-0.125175	-0.12594	-0.161543	-0.141271
39	C	0.275201	0.288836	0.314737	0.374649

40	C	-0.152756	-0.161151	-0.103183	-0.09513
41	C	0.169919	0.182684	0.170467	0.24534
42	N	0.400223	0.422832	0.418623	0.414424
43	O	-0.401945	-0.403244	-0.39776	-0.421462
44	O	-0.390641	-0.389452	-0.381051	-0.385015
45	C	0.008666	0.002849	0.027191	-0.039431
46	C	0.595842	0.588872	0.608229	0.595594
47	O	-0.566735	-0.542474	-0.549134	-0.56545
48	N	-0.619465	-0.62087	-0.623076	-0.593008
49	C	-0.188083	-0.174108	-0.174655	-0.153292
50	H	0.154703	0.166376	0.175532	0.170464
51	H	0.175584	0.179836	0.19106	0.172593
52	H	0.17253	0.171361	0.192073	0.183435
53	H	0.136604	0.151007	0.160617	0.175138
54	H	0.209669	0.217025	0.221933	0.213765
55	H	0.320108	0.320262	0.324015	0.326063
56	H	0.336365	0.333428	0.338495	0.325678
57	H	0.169784	0.174776	0.187601	0.163583
58	O	-0.599576	-0.576913	-0.455992	-0.791591
59	**H**	**0.408971**	**0.415526**	**0.448767**	**0.395569**
60	O	-0.484068	-0.483537	-0.644097	-0.667239
61	H	0.417271	0.423387	0.37435	0.354831
62	H	0.418025	0.420599	0.37385	0.359823
63	**H**	**0.387325**	**0.382821**	**0.427072**	**0.386817**
64	O	-0.523355	-0.522094	-0.666991	-0.664076
65	H	0.416988	0.416341	0.348367	0.342551
66	H	0.396537	0.393746	0.374649	0.359394

Appendix B

AMBER Prep Files

This appendix contains all the preparatory files for cofactors and ligands used in molecular mechanics and molecular dynamics simulations.

Reduced, protonated FMN prep file (fmn.prep):

```
    0    0    2

This is a remark line
molecule.res
FMN     INT  0
CORRECT     OMIT DU   BEG
  0.0000
   1  DUMM  DU    M    0  -1  -2     0.000      .0        .0      .00000
   2  DUMM  DU    M    1   0  -1     1.449      .0        .0      .00000
   3  DUMM  DU    M    2   1   0     1.522   111.1        .0      .00000
   4  O4    o     M    3   2   1     1.540   111.208   180.000  -0.79034
   5  C4    c     M    4   3   2     1.237   104.992    -4.031   0.71720
   6  N3    n     M    5   4   3     1.340   120.686   175.483  -0.61262
   7  H3    hn    E    6   5   4     1.030   117.508     0.472   0.29708
   8  C2    c     M    6   5   4     1.421   125.010  -179.562   0.76250
   9  O2    o     E    8   6   5     1.206   116.738   179.585  -0.75071
  10  N1    n2    M    8   6   5     1.368   119.395    -0.134  -0.42098
  11  C10   cd    M   10   8   6     1.309   120.102     0.519   0.35074
  12  C4A   cc    M   11  10   8     1.485   122.259    -0.447  -0.32717
  13  N5    nh    M   12  11  10     1.314   122.772   179.002  -0.50788
  14  H5    hn    E   13  12  11     1.030   120.938   179.053   0.36650
  15  C5A   ca    M   13  12  11     1.356   118.087    -1.012   0.08406
  16  C6    ca    M   15  13  12     1.446   120.283  -177.546  -0.18561
  17  H6    ha    E   16  15  13     1.090   118.265    -1.777   0.10508
  18  C7    ca    M   16  15  13     1.349   123.419   178.262  -0.12429
  19  C7M   c3    3   18  16  15     1.531   123.995  -179.324  -0.02345
  20  H7M1  hc    E   19  18  16     1.089   109.525    55.326   0.01912
  21  H7M2  hc    E   19  18  16     1.090   109.507   175.395   0.02183
  22  H7M3  hc    E   19  18  16     1.090   109.468   -64.662   0.01121
  23  C8    ca    M   18  16  15     1.438   119.350     0.514  -0.08672
  24  C8M   c3    3   23  18  16     1.497   120.502  -179.807  -0.04395
  25  H8M1  hc    E   24  23  18     1.090   109.471    47.608   0.01366
  26  H8M2  hc    E   24  23  18     1.090   109.521   167.577   0.07704
  27  H8M3  hc    E   24  23  18     1.090   109.512   -72.309   0.01605
  28  C9    ca    M   23  18  16     1.362   118.015    -0.163  -0.16144
  29  H9    ha    E   28  23  18     1.091   118.152   179.860   0.19399
  30  C9A   ca    M   28  23  18     1.388   123.673    -0.182   0.15821
  31  N10   nh    M   30  28  23     1.386   123.026  -178.806  -0.53790
  32  C1*   c3    M   31  30  28     1.480   114.250    -0.276   0.19440
  33  H1*1  h1    E   32  31  30     1.090   108.293   164.385   0.08992
  34  H1*2  h1    E   32  31  30     1.090   108.276    44.354   0.05586
  35  C2*   c3    M   32  31  30     1.542   114.336   -75.599   0.11685
  36  O2*   oh    S   35  32  31     1.430   112.613   -69.306  -0.61737
  37  HO2*  ho    E   36  35  32     1.030   109.461   131.229   0.41601
  38  H2*   h1    E   35  32  31     1.090   112.651    50.695   0.06893
  39  C3*   c3    M   35  32  31     1.536   108.048   171.574   0.12350
  40  O3*   oh    S   39  35  32     1.448   106.357   -68.708  -0.68454
  41  HO3*  ho    E   40  39  35     1.030   109.532    47.881   0.51115
  42  H3*   h1    E   39  35  32     1.090   106.350    51.276   0.04378
  43  C4*   c3    M   39  35  32     1.516   117.420   170.655   0.08411
  44  O4*   oh    S   43  39  35     1.443   113.350   -60.849  -0.66463
  45  HO4*  ho    E   44  43  39     1.030   109.453   134.642   0.44004
  46  H4*   h1    E   43  39  35     1.090   113.334    59.135   0.02736
  47  C5*   c3    M   43  39  35     1.519   113.065   172.262   0.20288
  48  H5*1  h1    E   47  43  39     1.090   107.470   -60.678   0.04309
  49  H5*2  h1    E   47  43  39     1.090   107.492   179.334  -0.04027
  50  O5*   os    M   47  43  39     1.416   107.449    59.288  -0.57673
  51  P     p5    M   50  47  43     1.577   121.084  -119.967   1.55402
  52  O2P   o     E   51  50  47     1.503   108.440    57.754  -1.02564
  53  O3P   o     E   51  50  47     1.571   104.490   -60.499  -1.01830
  54  O1P   o     M   51  50  47     1.502   106.813  -178.974  -0.96565


LOOP
  C4A   C4
  N10  C10
  C9A  C5A
```

```
IMPROPER
  C4A   N3   C4   O4
   C4   C2   N3   H3
   N1   N3   C2   O2
  C4A   N1  C10  N10
   C4  C10  C4A   N5
  C5A  C4A   N5   H5
   C6  C9A  C5A   N5
  C5A   C7   C6   H6
  C7M   C6   C7   C8
  C8M   C7   C8   C9
   C8  C9A   C9   H9
  C5A   C9  C9A  N10
  C1*  C9A  N10  C10

DONE
STOP
```

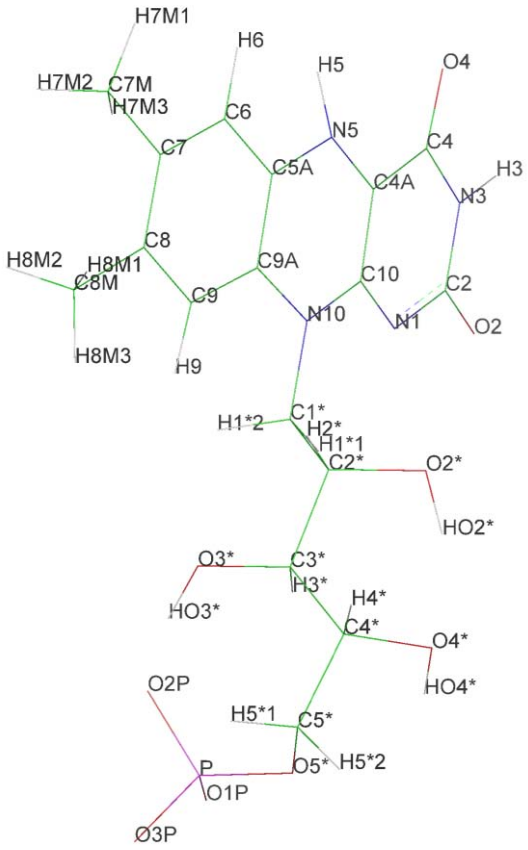

Figure B.1: Atom names for reduced, protonated FMN.

Reduced, protonated FMN frcmod file (frcmod.fmn):

```
remark goes here
MASS

BOND

ANGLE
c -cc-nh    66.700      122.760    same as c -ce-nh
n -c -n2    72.720      111.005    Calculated with empirical approach
c -n2-cd    66.200      120.970    same as c -n2-c2
n2-cd-cc    71.300      126.010    same as c2-c2-n2
n2-cd-nh    72.600      124.270    same as n2-c2-nh
cd-nh-ca    65.500      123.660    same as c2-nh-ca
cc-nh-ca    65.500      123.660    same as c2-nh-ca

DIHE
c -n2-cd-cc    1    4.150       180.000          2.000      same as X -c2-n2-X
c -n2-cd-nh    1    4.150       180.000          2.000      same as X -c2-n2-X

IMPROPER

NONBON
```

Oxidised FMN prep file (fmnox.prep):

```
    0    0    2

This is a remark line
molecule.res
FMN     INT  0
CORRECT     OMIT DU   BEG
  0.0000
   1  DUMM  DU    M    0  -1  -2     0.000      .0        .0      .00000
   2  DUMM  DU    M    1   0  -1     1.449      .0        .0      .00000
   3  DUMM  DU    M    2   1   0     1.522   111.1        .0      .00000
   4  O4    o     M    3   2   1     1.540   111.208   180.000  -0.63288
   5  C4    c     M    4   3   2     1.237   104.992    -4.031   0.63492
   6  N3    n     M    5   4   3     1.340   120.686   175.483  -0.62347
   7  H3    hn    E    6   5   4     1.030   117.508     0.472   0.32493
   8  C2    c     M    6   5   4     1.421   125.010  -179.562   0.85283
   9  O2    o     E    8   6   5     1.206   116.738   179.585  -0.64054
  10  N1    nc    M    8   6   5     1.368   119.395    -0.134  -0.71494
  11  C10   cd    M   10   8   6     1.309   120.102     0.519   0.62186
  12  C4A   cd    M   11  10   8     1.485   122.259    -0.447   0.20385
  13  N5    ne    M   12  11  10     1.314   122.772   179.002  -0.43371
  14  C5A   ca    M   13  12  11     1.356   118.087    -1.012   0.01170
  15  C6    ca    M   14  13  12     1.446   120.283  -177.546  -0.07500
  16  H6    ha    E   15  14  13     1.090   118.265    -1.777   0.13501
  17  C7    ca    M   15  14  13     1.349   123.419   178.262  -0.12018
  18  C7M   c3    3   17  15  14     1.531   123.995  -179.324  -0.04069
  19  H7M1  hc    E   18  17  15     1.089   109.525    55.326   0.03858
  20  H7M2  hc    E   18  17  15     1.090   109.507   175.395   0.04097
  21  H7M3  hc    E   18  17  15     1.090   109.468   -64.662   0.02515
  22  C8    ca    M   17  15  14     1.438   119.350     0.514  -0.02252
  23  C8M   c3    3   22  17  15     1.497   120.502  -179.807  -0.06790
  24  H8M1  hc    E   23  22  17     1.090   109.471    47.608   0.03164
  25  H8M2  hc    E   23  22  17     1.090   109.521   167.577   0.10808
  26  H8M3  hc    E   23  22  17     1.090   109.512   -72.309   0.03450
  27  C9    ca    M   22  17  15     1.362   118.015    -0.163  -0.16897
  28  H9    ha    E   27  22  17     1.091   118.152   179.860   0.27496
  29  C9A   ca    M   27  22  17     1.388   123.673    -0.182   0.17010
  30  N10   nh    M   29  27  22     1.386   123.026  -178.806  -0.50388
  31  C1*   c3    M   30  29  27     1.480   114.250    -0.276   0.16550
  32  H1*1  h1    E   31  30  29     1.090   108.293   164.385   0.09840
  33  H1*2  h1    E   31  30  29     1.090   108.276    44.354   0.11198
  34  C2*   c3    M   31  30  29     1.542   114.336   -75.599   0.04882
  35  O2*   oh    S   34  31  30     1.430   112.613   -69.306  -0.64185
  36  HO2*  ho    E   35  34  31     1.030   109.461   131.229   0.42620
  37  H2*   h1    E   34  31  30     1.090   112.651    50.695   0.02896
  38  C3*   c3    M   34  31  30     1.536   108.048   171.574   0.25899
  39  O3*   oh    S   38  34  31     1.448   106.357   -68.708  -1.00036
  40  HO3*  ho    E   39  38  34     1.030   109.532    47.881   0.47086
  41  H3*   h1    E   38  34  31     1.090   106.350    51.276  -0.04659
  42  C4*   c3    M   38  34  31     1.516   117.420   170.655   0.06444
  43  O4*   oh    S   42  38  34     1.443   113.350   -60.849  -0.65547
  44  HO4*  ho    E   43  42  38     1.030   109.453   134.642   0.42331
  45  H4*   h1    E   42  38  34     1.090   113.334    59.135   0.02492
  46  C5*   c3    M   42  38  34     1.519   113.065   172.262   0.17178
  47  H5*1  h1    E   46  42  38     1.090   107.470   -60.678   0.06980
  48  H5*2  h1    E   46  42  38     1.090   107.492   179.334  -0.01252
  49  O5*   os    M   46  42  38     1.416   107.449    59.288  -0.59654
  50  P     p5    M   49  46  42     1.577   121.084  -119.967   1.35613
  51  O2P   o     E   50  49  46     1.503   108.440    57.754  -0.52281
  52  O3P   o     E   50  49  46     1.571   104.490   -60.499  -0.86915
  53  O1P   o     M   50  49  46     1.502   106.813  -178.974  -0.83919


LOOP
  C4A   C4
  N10   C10
  C9A   C5A
```

```
IMPROPER
  C4A    N3    C4    O4
   C4    C2    N3    H3
   N3    N1    C2    O2
  C4A    N1   C10   N10
   C4   C10   C4A    N5
   C6   C9A   C5A    N5
  C5A    C7    C6    H6
  C7M    C6    C7    C8
  C8M    C7    C8    C9
   C8   C9A    C9    H9
  C5A    C9   C9A   N10
  C1*   C9A   N10   C10

DONE
STOP
```

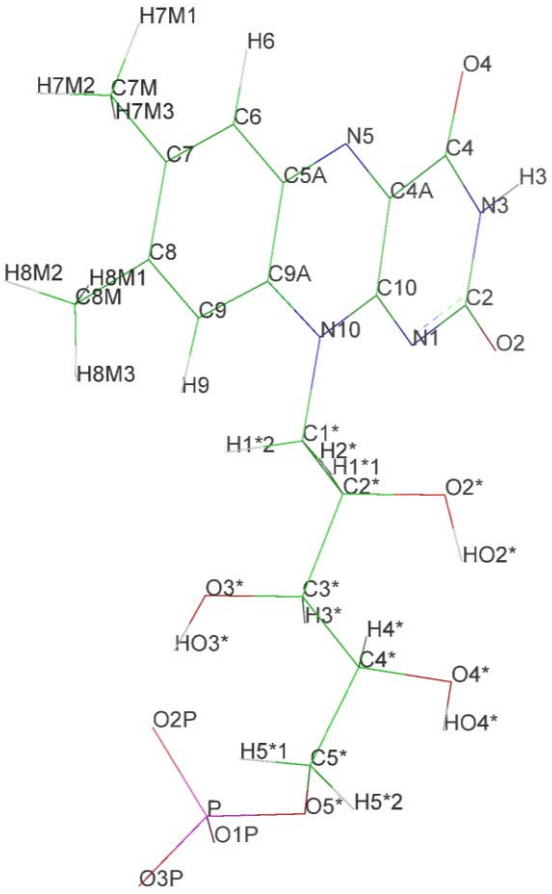

Figure B.2: Atom names for oxidised FMN.

Oxidised FMN frcmod file (frcmod.fmnox):

```
remark goes here
MASS

BOND
cd-ne  381.80   1.414       same as ce-ne

ANGLE
c -cd-ne    65.257     121.360   Calculated with empirical approach
c -cd-ne    68.400     120.890   same as c -cd-n2
cd-cd-ne    69.300     121.150   same as cd-cd-n2
cd-nh-ca    65.500     123.660   same as c2-nh-ca
cd-ne-ca    66.700     118.670   same as c2-ne-ca

DIHE
c -cd-ne-ca    1    0.800       180.000          2.000      same as X -ce-ne-X
cd-cd-ne-ca    1    0.800       180.000          2.000      same as X -ce-ne-X

IMPROPER

NONBON
```

Acetate prep file (ace.prep):

```
    0    0    2

This is a remark line
molecule.res
ACT    INT  0
CORRECT     OMIT DU   BEG
  0.0000
   1  DUMM  DU    M    0  -1  -2     0.000      .0        .0      .00000
   2  DUMM  DU    M    1   0  -1     1.449      .0        .0      .00000
   3  DUMM  DU    M    2   1   0     1.522   111.1        .0      .00000
   4  O     o     M    3   2   1     1.540   111.208   180.000   0.10563
   5  C     c     M    4   3   2     1.255    98.480   170.819   0.29276
   6  CH3   c3    3    5   4   3     1.504   123.278     2.114  -0.33507
   7  HH31  hc    E    6   5   4     1.089   109.483    73.763   0.32242
   8  HH32  hc    E    6   5   4     1.090   109.501  -166.166  -0.39668
   9  HH33  hc    E    6   5   4     1.091   109.420   -46.232  -0.19245
  10  OXT   o     M    5   4   3     1.256   115.797  -178.082  -0.63034


LOOP

IMPROPER
  CH3    O    C  OXT

DONE
STOP
```

Acetate frcmod file (frcmod.ace):

```
remark goes here
MASS

BOND

ANGLE

DIHE

IMPROPER

NONBON
```

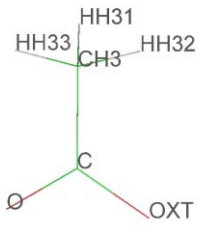

Figure B.3: Atom names for acetate.

Reduced, protonated FAD prep file (fad.prep):

```
    0    0    2

This is a remark line
molecule.res
FAD    INT  0
CORRECT     OMIT DU   BEG
  0.0000
   1  DUMM  DU    M    0  -1  -2     0.000      .0        .0      .00000
   2  DUMM  DU    M    1   0  -1     1.449      .0        .0      .00000
   3  DUMM  DU    M    2   1   0     1.522   111.1        .0      .00000
   4  O4    o     M    3   2   1     1.540   111.208   180.000  -0.78600
   5  C4    c     M    4   3   2     1.231    83.283   -38.792   0.72759
   6  N3    n     M    5   4   3     1.358   117.109     1.066  -0.59980
   7  H3    hn    E    6   5   4     1.030   119.538    -0.551   0.30862
   8  C2    c     M    6   5   4     1.375   120.957   179.523   0.75838
   9  O2    o     E    8   6   5     1.228   118.976  -179.579  -0.73968
  10  N1    n2    M    8   6   5     1.368   122.013     1.717  -0.45300
  11  C10   cd    M   10   8   6     1.374   117.887     0.194   0.33240
  12  C4X   cc    M   11  10   8     1.407   121.066    -1.005  -0.27736
  13  N5    nh    M   12  11  10     1.388   119.964   178.813  -0.62064
  14  H5    hn    E   13  12  11     1.030   120.519  -176.991   0.44830
  15  C5X   ca    M   13  12  11     1.386   118.969     3.088   0.19761
  16  C6    ca    M   15  13  12     1.396   117.973   178.374  -0.25121
  17  H6    ha    E   16  15  13     1.091   119.610     0.447   0.10994
  18  C7    ca    M   16  15  13     1.385   120.728  -179.591  -0.07694
  19  C7M   c3    3   18  16  15     1.504   117.719   179.132  -0.03031
  20  H7M1  hc    E   19  18  16     1.090   109.471  -108.511   0.02969
  21  H7M2  hc    E   19  18  16     1.090   109.467    11.520   0.01999
  22  H7M3  hc    E   19  18  16     1.090   109.472   131.547   0.02228
  23  C8    ca    M   18  16  15     1.408   118.801    -0.805  -0.13997
  24  C8M   c3    3   23  18  16     1.499   122.686  -178.650  -0.02983
  25  H8M1  hc    E   24  23  18     1.090   109.500   -34.355   0.01936
  26  H8M2  hc    E   24  23  18     1.090   109.470    85.665   0.01957
  27  H8M3  hc    E   24  23  18     1.090   109.514  -154.349   0.04741
  28  C9    ca    M   23  18  16     1.420   120.572     0.073  -0.15274
  29  H9    ha    E   28  23  18     1.090   119.770  -178.781   0.14028
  30  C9A   ca    M   28  23  18     1.387   120.463     1.247   0.14493
  31  N10   nh    M   30  28  23     1.408   121.776   179.874  -0.55426
  32  C1'   c3    M   31  30  28     1.527   125.300    -4.191   0.22747
  33  H1'1  h1    E   32  31  30     1.090   110.878   166.550   0.09908
  34  H1'2  h1    E   32  31  30     1.090   110.913    46.536   0.04992
  35  C2'   c3    M   32  31  30     1.544   110.937   -73.438   0.10181
  36  O2'   oh    S   35  32  31     1.423   111.138   -60.814  -0.57776
  37  HO2'  ho    E   36  35  32     1.031   109.509   -90.002   0.41781
  38  H2'   h1    E   35  32  31     1.090   111.218    59.157   0.05921
  39  C3'   c3    M   35  32  31     1.529   109.646   171.494   0.08164
  40  O3'   oh    S   39  35  32     1.414   108.022   -63.213  -0.61690
  41  HO3'  ho    E   40  39  35     1.030   109.556   -78.176   0.43414
  42  H3'   h1    E   39  35  32     1.090   108.073    56.822   0.05648
  43  C4'   c3    M   39  35  32     1.532   113.844   174.923   0.08873
  44  O4'   oh    S   43  39  35     1.398   110.570   -59.324  -0.60324
  45  HO4'  ho    E   44  43  39     1.030   109.482   -95.410   0.40564
  46  H4'   h1    E   43  39  35     1.090   110.567    60.732   0.10213
  47  C5'   c3    M   43  39  35     1.521   112.295  -177.128   0.18248
  48  H5'1  h1    E   47  43  39     1.090   107.712    62.918   0.00770
  49  H5'2  h1    E   47  43  39     1.090   107.738   -57.114   0.06000
  50  O5'   os    M   47  43  39     1.428   107.677  -177.131  -0.57721
  51  P     p5    M   50  47  43     1.615   120.799   115.376   1.62141
  52  O1P   o     E   51  50  47     1.518   105.171   -51.828  -0.94347
  53  O2P   o     E   51  50  47     1.505   112.191  -173.012  -0.92080
  54  O3P   os    M   51  50  47     1.614   104.292    69.085  -0.72946
  55  PA    p5    M   54  51  50     1.637   130.587  -162.574   1.53316
  56  O1A   o     E   55  54  51     1.535   107.215   103.696  -0.91348
  57  O2A   o     E   55  54  51     1.513   120.648   -23.610  -0.87093
  58  O5B   os    M   55  54  51     1.601   101.563  -143.428  -0.58462
  59  C5B   c3    M   58  55  54     1.407   120.814   -74.159   0.19836
  60  H5B1  h1    E   59  58  55     1.090   111.082    99.883   0.03469
  61  H5B2  h1    E   59  58  55     1.090   111.039   -20.094   0.06861
```

```
  62  C4B   c3    M   59  58  55     1.514   103.230  -140.062   0.14104
  63  C3B   c3    3   62  59  58     1.533   110.999    49.022   0.10419
  64  O3B   oh    S   63  62  59     1.420   108.290   122.998  -0.61218
  65  HO3B  ho    E   64  63  62     1.030   109.524   174.161   0.40882
  66  C2B   c3    B   63  62  59     1.534   105.094  -114.669   0.07947
  67  O2B   oh    S   66  63  62     1.418   114.616  -141.475  -0.61869
  68  HO2B  ho    E   67  66  63     1.030   109.542  -110.675   0.41554
  69  H2B   h1    E   66  63  62     1.090   108.220    98.533   0.09062
  70  H3B   h1    E   63  62  59     1.090   108.272     3.015   0.12168
  71  H4B   h1    E   62  59  58     1.091   109.166   171.150   0.04842
  72  O4B   os    M   62  59  58     1.418   109.133   -68.843  -0.39387
  73  C1B   c3    M   72  62  59     1.419   109.285   136.613   0.26007
  74  H1B   h2    E   73  72  62     1.090   106.283    89.166   0.07825
  75  N9A   na    M   73  72  62     1.481   110.468  -157.659  -0.14208
  76  C8A   cc    M   75  73  72     1.377   129.645    96.385   0.19857
  77  H8A   h5    E   76  75  73     1.090   125.976     0.291   0.10058
  78  N7A   nd    M   76  75  73     1.356   108.059  -179.760  -0.41513
  79  C5A   c2    M   78  76  75     1.366   109.346     0.184   0.00983
  80  C6A   c2    M   79  78  76     1.410   134.023  -179.724   0.24333
  81  N6A   n3    B   80  79  78     1.331   120.422    14.485  -0.78344
  82  H6A1  hn    E   81  80  79     1.030   119.998  -179.966   0.43449
  83  H6A2  hn    E   81  80  79     1.030   119.996    -0.006   0.46149
  84  N1A   n2    M   80  79  78     1.388   119.976   179.831  -0.33581
  85  C2A   c2    M   84  80  79     1.386   120.092    -0.483   0.02242
  86  H2A   ha    E   85  84  80     1.090   119.963  -179.684   0.18976
  87  N3A   n2    M   85  84  80     1.385   119.967     0.378  -0.24335
  88  C4A   c2    M   87  85  84     1.369   120.493    -0.080   0.02875
```

```
LOOP
  C4X   C4
  N10   C10
  C9A   C5X
  C1B   C2B
  C4A   N9A
  C4A   C5A

IMPROPER
  C4X    N3    C4    O4
   C4    C2    N3    H3
   N1    N3    C2    O2
  C4X    N1   C10   N10
   C4   C10   C4X    N5
  C5X   C4X    N5    H5
   C6   C9A   C5X    N5
  C5X    C7    C6    H6
  C7M    C6    C7    C8
  C8M    C7    C8    C9
   C8   C9A    C9    H9
  C5X    C9   C9A   N10
  C1'   C9A   N10   C10
  C4A   C1B   N9A   C8A
  H8A   N9A   C8A   N7A
  C6A   C4A   C5A   N7A
  C5A   N1A   C6A   N6A
  H2A   N1A   C2A   N3A
  C5A   N3A   C4A   N9A

DONE
STOP
```

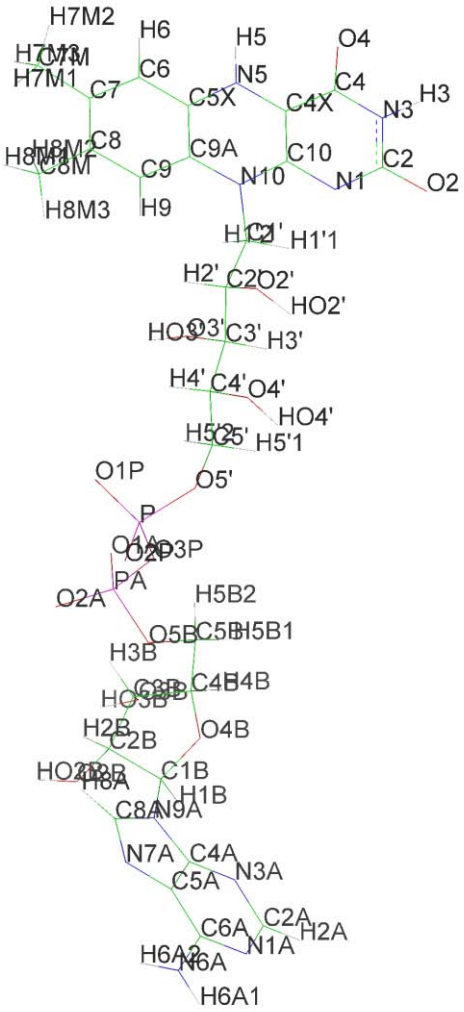

Figure B.4: Atom names for reduced, protonated FAD.

Reduced, protonated FAD frcmod file (frcmod.fad):

```
remark goes here
MASS

BOND

ANGLE
c -cc-nh   66.700     122.760   same as c -ce-nh
n -c -n2   72.720     111.005   Calculated with empirical approach
c -n2-cd   66.200     120.970   same as c -n2-c2
n2-cd-cc   71.300     126.010   same as c2-c2-n2
n2-cd-nh   72.600     124.270   same as n2-c2-nh
cd-nh-ca   65.500     123.660   same as c2-nh-ca
cc-nh-ca   65.500     123.660   same as c2-nh-ca
cc-nd-c2   70.800     118.180   same as c2-n2-c2
nd-c2-c2   71.300     126.010   same as c2-c2-n2
n3-c2-n2   75.237     116.145   Calculated with empirical approach

DIHE
c -n2-cd-cc   1    4.150       180.000           2.000      same as X -c2-n2-X
c -n2-cd-nh   1    4.150       180.000           2.000      same as X -c2-n2-X

IMPROPER

NONBON
```

Menadione prep file (men.prep):

```
    0    0    2

This is a remark line
molecule.res
VK3    INT  0
CORRECT     OMIT DU   BEG
  0.0000
   1  DUMM  DU    M    0  -1  -2     0.000      .0        .0      .00000
   2  DUMM  DU    M    1   0  -1     1.449      .0        .0      .00000
   3  DUMM  DU    M    2   1   0     1.522   111.1        .0      .00000
   4  O1K   o     M    3   2   1     1.540   111.208   180.000   0.13183
   5  C1K   c     M    4   3   2     1.238    73.669   119.176  -0.00894
   6  C2K   cc    M    5   4   3     1.468   116.447    99.485  -0.38424
   7  H2K   ha    E    6   5   4     1.090   119.986    -1.349  -0.19310
   8  C3K   cd    M    6   5   4     1.376   120.054   178.756  -0.42637
   9  C11   c3    3    8   6   5     1.546   119.123  -177.086   0.10688
  10  H111  hc    E    9   8   6     1.090   109.433    57.662  -0.11060
  11  H112  hc    E    9   8   6     1.090   109.505   177.683  -0.10158
  12  H113  hc    E    9   8   6     1.090   109.465   -62.273  -0.40835
  13  C4K   c     M    8   6   5     1.477   121.301     3.047   0.64062
  14  O4K   o     E   13   8   6     1.240   114.769   179.571  -0.59648
  15  C5K   ca    M   13   8   6     1.445   117.619     1.977  -0.17375
  16  C6K   ca    M   15  13   8     1.366   118.565   174.730  -0.00661
  17  H6K   ha    E   16  15  13     1.090   120.563     1.739  -0.16897
  18  C7K   ca    M   16  15  13     1.368   118.951  -178.285  -0.12770
  19  H7K   ha    E   18  16  15     1.090   119.180  -178.998   0.08850
  20  C8K   ca    M   18  16  15     1.364   121.649     1.069  -0.07500
  21  H8K   ha    E   20  18  16     1.091   119.898   179.723  -0.11188
  22  C9K   ca    M   20  18  16     1.363   120.276    -0.411  -0.11288
  23  H9K   ha    E   22  20  18     1.089   120.332  -179.885   0.18196
  24  C10   ca    M   22  20  18     1.374   119.418     0.174  -0.18649


LOOP
  C10  C1K
  C10  C5K
```

```
IMPROPER
  C10  C2K  C1K  O1K
  C1K  C3K  C2K  H2K
  C4K  C11  C3K  C2K
  C5K  C3K  C4K  O4K
  C4K  C6K  C5K  C10
  C5K  C7K  C6K  H6K
  C6K  C8K  C7K  H7K
  C7K  C9K  C8K  H8K
  C8K  C10  C9K  H9K
  C1K  C5K  C10  C9K

DONE
STOP
```

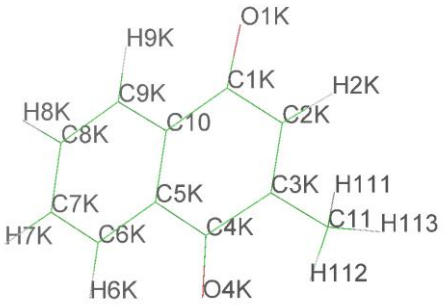

Figure B.5: Atom names for menadione.

Menadione frcmod file (frcmod.men):

```
remark goes here
MASS

BOND

ANGLE

DIHE

IMPROPER

NONBON
```

Nitrofurazone prep file (nfz.prep):

```
    0    0    2

This is a remark line
molecule.res
NFZ     INT  0
CORRECT     OMIT DU   BEG
  0.0000
   1  DUMM  DU    M    0  -1  -2     0.000      .0        .0      .00000
   2  DUMM  DU    M    1   0  -1     1.449      .0        .0      .00000
   3  DUMM  DU    M    2   1   0     1.522   111.1        .0      .00000
   4  O     o     M    3   2   1     1.540   111.208   180.000  -0.62293
   5  C     c     M    4   3   2     1.205   180.000    90.000   0.79792
   6  N     n     B    5   4   3     1.336   122.501   -90.000  -0.64861
   7  H     hn    E    6   5   4     1.030   120.052   180.000   0.33916
   8  H1    hn    E    6   5   4     1.030   119.964     0.000   0.33772
   9  N1    n     M    5   4   3     1.320   117.534    89.265  -0.32976
  10  H2    hn    E    9   5   4     1.030   119.389   -18.997   0.32933
  11  N2    n2    M    9   5   4     1.309   121.089   161.036  -0.39695
  12  C1    ce    M   11   9   5     1.256   118.519  -165.191   0.22239
  13  H3    ha    E   12  11   9     1.091   121.611    -0.296   0.01783
  14  C2    cc    M   12  11   9     1.458   116.760   179.771   0.29706
  15  O1    os    E   14  12  11     1.448   120.281     2.078  -0.29549
  16  C3    cd    M   14  12  11     1.338   126.981  -176.899  -0.27563
  17  H4    ha    E   16  14  12     1.090   126.654    -0.719   0.17746
  18  C4    cd    M   16  14  12     1.450   106.622   179.317  -0.12905
  19  H5    ha    E   18  16  14     1.091   126.381  -179.797   0.19040
  20  C5    cc    M   18  16  14     1.343   107.204     0.142   0.11791
  21  N3    no    M   20  18  16     1.319   125.719  -179.281   0.24734
  22  O3    o     E   21  20  18     1.223   118.598  -170.941  -0.17671
  23  O2    o     M   21  20  18     1.387   120.397    11.152  -0.19938
```

```
LOOP
   C5   O1

IMPROPER
    N   N1    C    O
   C2   H3   C1   N2
   C3   C1   C2   O1
   C2   C4   C3   H4
   C5   C3   C4   H5
   C4   N3   C5   O1
   C5   O3   N3   O2

DONE
STOP
```

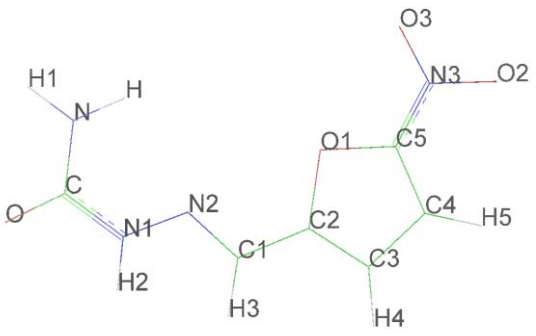

Figure B.6: Atom names for nitrofurazone.

Nitrofurazone frcmod file (frcmod.nfz):

```
remark goes here
MASS

BOND
ce-cc  390.50   1.451       same as ce-ce
cc-no  327.60   1.463       same as c2-no

ANGLE
n -n2-ce   70.400     117.240   same as c2-n2-n
n2-ce-cc   68.500     123.000   same as ce-ce-n2
ce-cc-os   70.500     119.310   same as c2-cc-os
ce-cc-cd   69.100     117.020   same as c2-cc-cd
ha-ce-cc   47.500     115.900   same as ce-ce-ha
os-cc-no   69.716     114.850   Calculated with empirical approach
cd-cc-no   70.300     124.550   same as c2-c2-n3
cc-no-o    69.300     116.870   same as c2-no-o

DIHE
n -n2-ce-ha   1    4.150       180.000          2.000      same as X -c2-n2-X
n -n2-ce-cc   1    4.150       180.000          2.000      same as X -c2-n2-X
n2-ce-cc-os   1    1.000       180.000          2.000      same as X -ce-ce-X
n2-ce-cc-cd   1    1.000       180.000          2.000      same as X -ce-ce-X
ce-cc-os-cc   1    1.050       180.000          2.000      same as X -c2-os-X
ha-ce-cc-os   1    1.000       180.000          2.000      same as X -ce-ce-X
ha-ce-cc-cd   1    1.000       180.000          2.000      same as X -ce-ce-X
cc-os-cc-cd   1    1.050       180.000          2.000      same as X -c2-os-X
cc-os-cc-no   1    1.050       180.000          2.000      same as X -c2-os-X
os-cc-no-o    1    0.750       180.000          2.000      same as X -c2-no-X
cd-cc-no-o    1    0.750       180.000          2.000      same as X -c2-no-X

IMPROPER

NONBON
```

CB1954 prep file (cb.prep):

```
    0    0    2

This is a remark line
molecule.res
CB1     INT  0
CORRECT     OMIT DU   BEG
  0.0000
   1  DUMM  DU    M    0  -1  -2     0.000      .0        .0      .00000
   2  DUMM  DU    M    1   0  -1     1.449      .0        .0      .00000
   3  DUMM  DU    M    2   1   0     1.522    111.1       .0      .00000
   4  O3    o     M    3   2   1     1.540   111.208   180.000  -0.19935
   5  N3    no    M    4   3   2     1.217    75.535    59.845   0.31729
   6  O4    o     E    5   4   3     1.219   123.263    15.461  -0.19370
   7  C8    ca    M    5   4   3     1.380   118.130  -166.290  -0.21924
   8  C     ca    M    7   5   4     1.416   119.999   -23.284   0.00848
   9  HC    ha    E    8   7   5     1.090   118.646     4.637   0.20693
  10  C1    ca    M    8   7   5     1.413   122.592  -175.424  -0.20231
  11  N     no    B   10   8   7     1.386   118.493   176.327   0.32355
  12  O1    o     E   11  10   8     1.218   117.644   -25.791  -0.18115
  13  O2    o     E   11  10   8     1.214   119.242   156.633  -0.21819
  14  C2    ca    M   10   8   7     1.428   118.320    -2.621  -0.01470
  15  C3    c     B   14  10   8     1.522   122.633  -176.962   0.65414
  16  N1    n     B   15  14  10     1.358   120.445   -95.998  -0.61292
  17  H11   hn    E   16  15  14     1.030   119.969     0.063   0.31042
  18  H12   hn    E   16  15  14     1.030   119.992  -179.885   0.31362
  19  O     o     E   15  14  10     1.224   118.212    84.087  -0.57306
  20  C4    ca    M   14  10   8     1.411   119.131     2.479  -0.15593
  21  H4    ha    E   20  14  10     1.090   119.068   176.716   0.17533
  22  C5    ca    M   20  14  10     1.407   121.838    -3.364   0.22604
  23  N6    nh    M   22  20  14     1.429   119.575  -175.103  -0.57755
  24  C7    cx    M   23  22  20     1.490   119.854    28.233   0.08894
  25  H71   h1    E   24  23  22     1.090   122.050   -10.902   0.08562
  26  H72   h1    E   24  23  22     1.090   121.992  -130.932   0.10569
  27  C9    cx    M   24  23  22     1.513    59.501   109.108   0.12710
  28  H91   h1    E   27  24  23     1.090   129.384   108.159   0.11869
  29  H92   h1    E   27  24  23     1.090   129.367  -108.218   0.08630

LOOP
   C5   C8
   C9   N6

IMPROPER
   C8   O3   N3   O4
   C5    C   C8   N3
   C8   C1    C   HC
   C2    C   C1    N
   C1   O1    N   O2
   C3   C4   C2   C1
   C2   N1   C3    O
   C2   C5   C4   H4
   C4   C8   C5   N6
   C5   C7   N6   C9

DONE
STOP
```

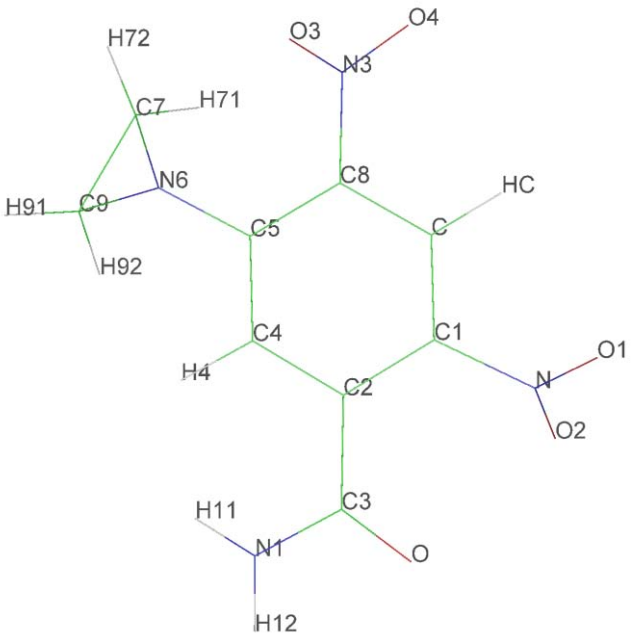

Figure B.7: Atom names for CB1954.

CB1954 frcmod file (frcmod.cb):

```
remark goes here
MASS

BOND
nh-cx  318.70   1.472       same as cx-n3

ANGLE
ca-nh-cx   64.600     117.770   same as c3-nh-ca
nh-cx-h1   49.700     109.960   same as h1-c3-nh
nh-cx-cx   65.300     116.300   same as cx-cx-n3
cx-nh-cx   64.000     110.900   same as c3-n3-c3

DIHE
ca-nh-cx-h1   1    0.000         0.000          2.000      same as X -c3-nh-X
ca-nh-cx-cx   1    0.000         0.000          2.000      same as X -c3-nh-X
cx-nh-cx-cx   1    0.000         0.000          2.000      same as X -c3-nh-X
cx-nh-cx-h1   1    0.000         0.000          2.000      same as X -c3-nh-X

IMPROPER

NONBON
```

Appendix C

MD Runs

This appendix contains graphs of key interatomic distances for all molecular dynamics simulations.

Acetate in oxidised NTR (Section 5.2.1):

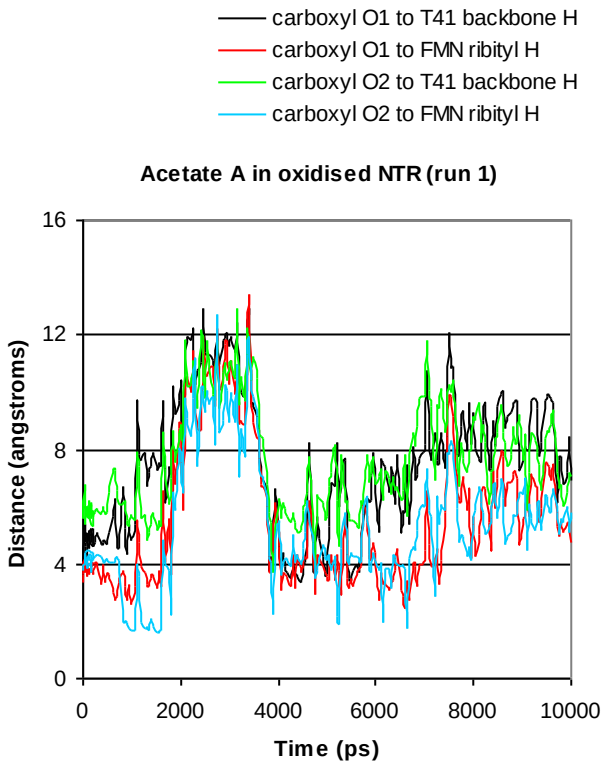

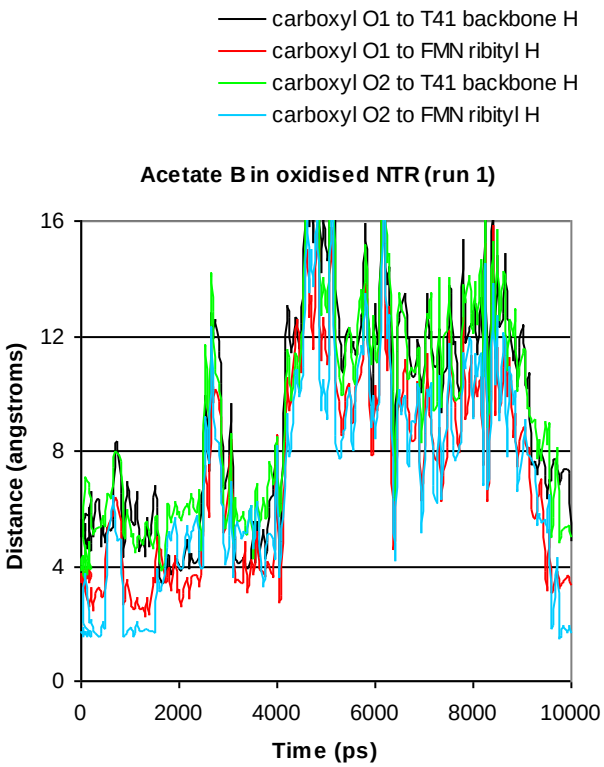

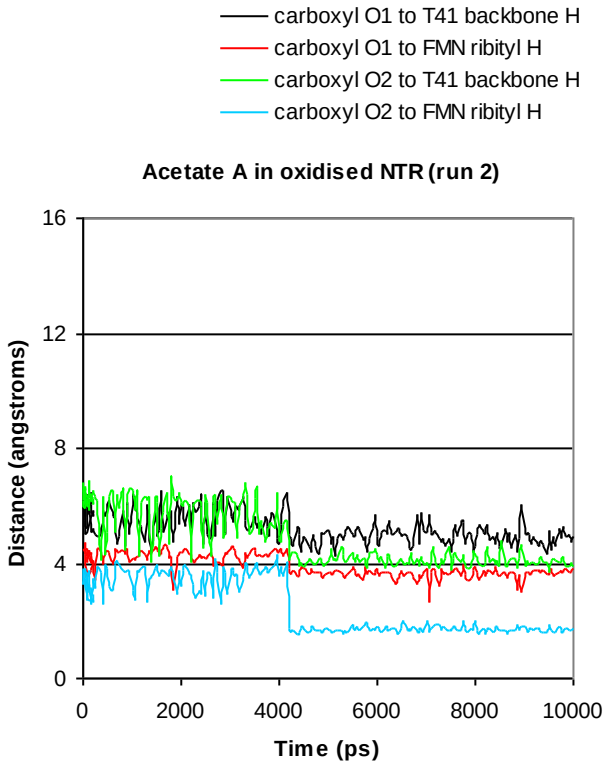

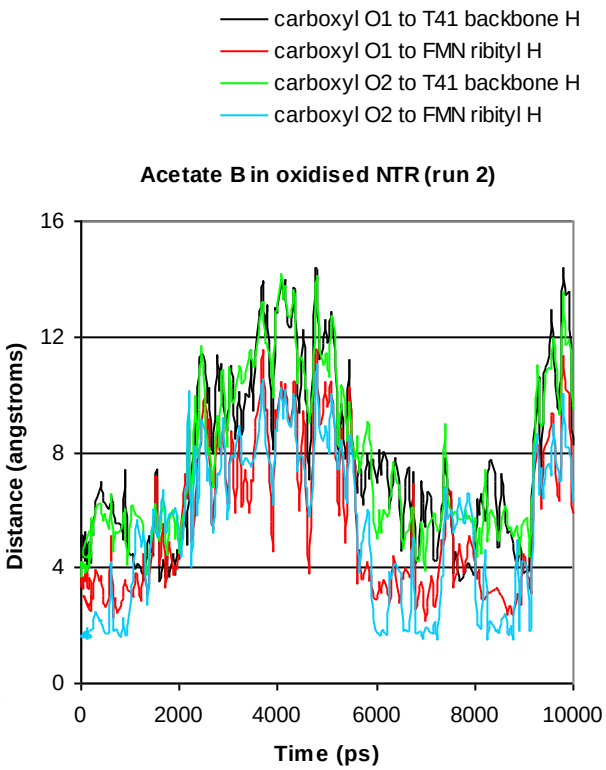

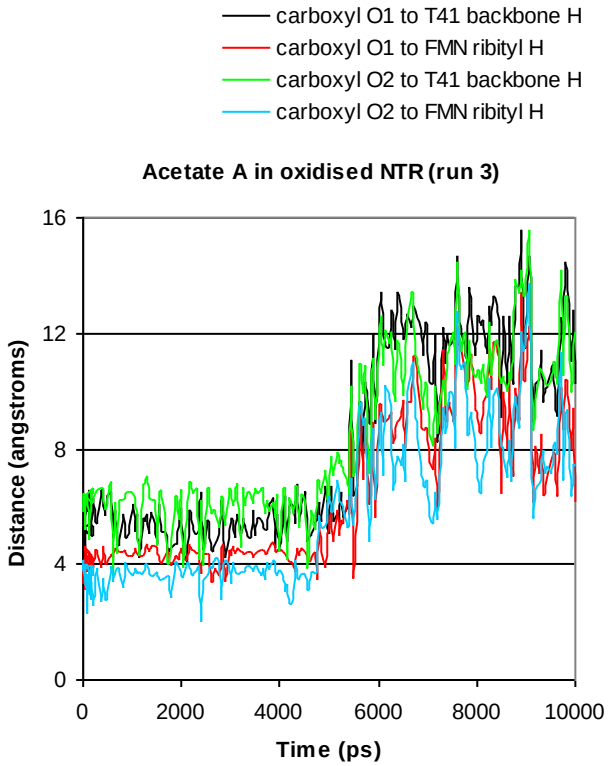

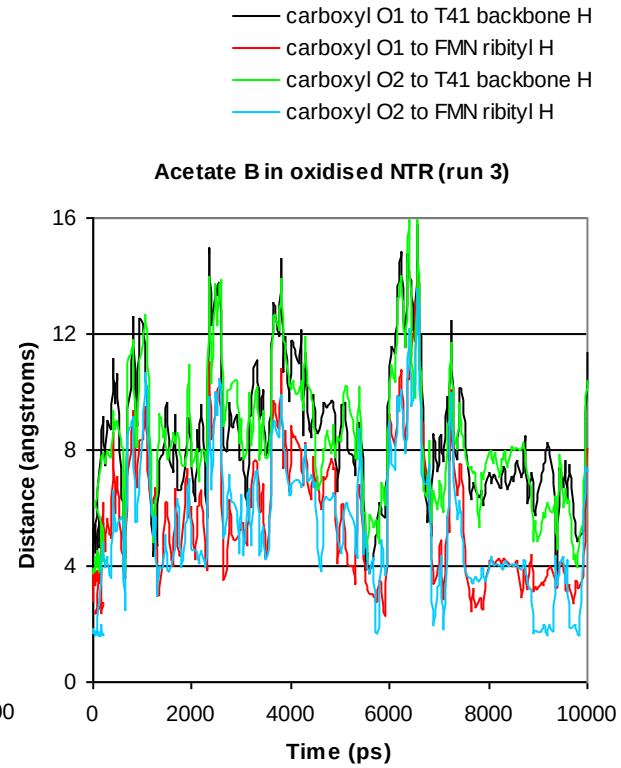

Acetate in reduced NTR (Section 5.2.2):

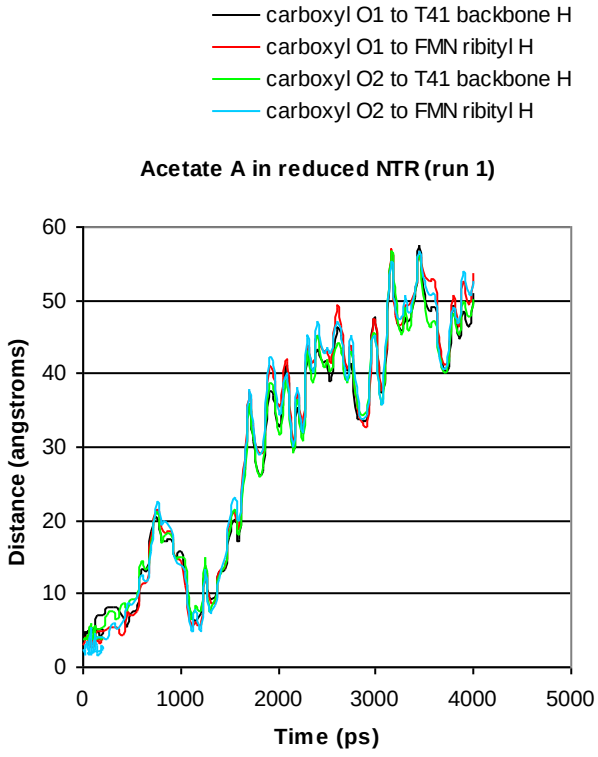

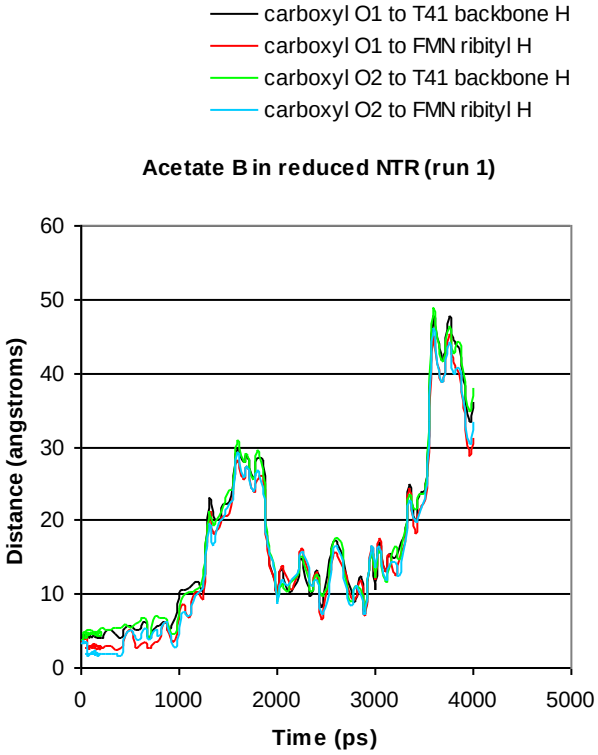

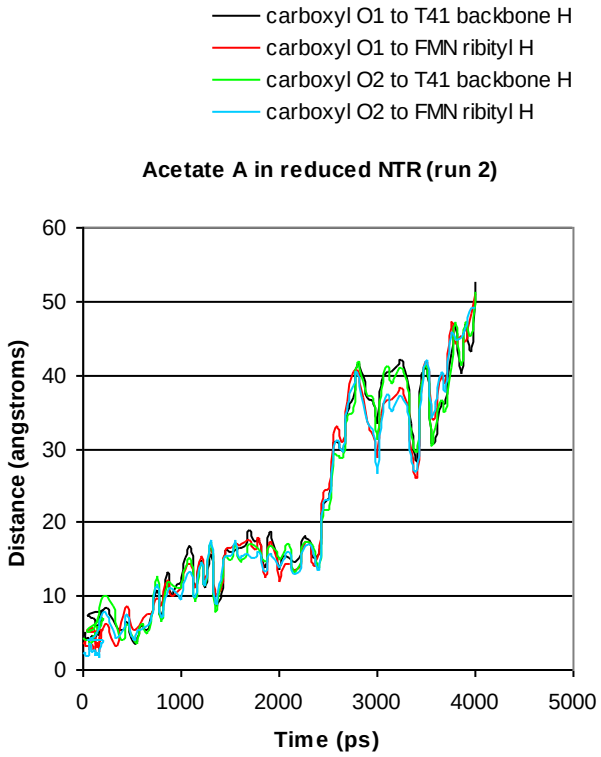
carboxyl O1 to T41 backbone H
carboxyl O1 to FMN ribityl H
carboxyl O2 to T41 backbone H
carboxyl O2 to FMN ribityl H
Acetate A in reduced NTR (run 2)
Distance (angstroms)
Time (ps)
0
10
20
30
40
50
60
0
1000
2000
3000
4000
5000

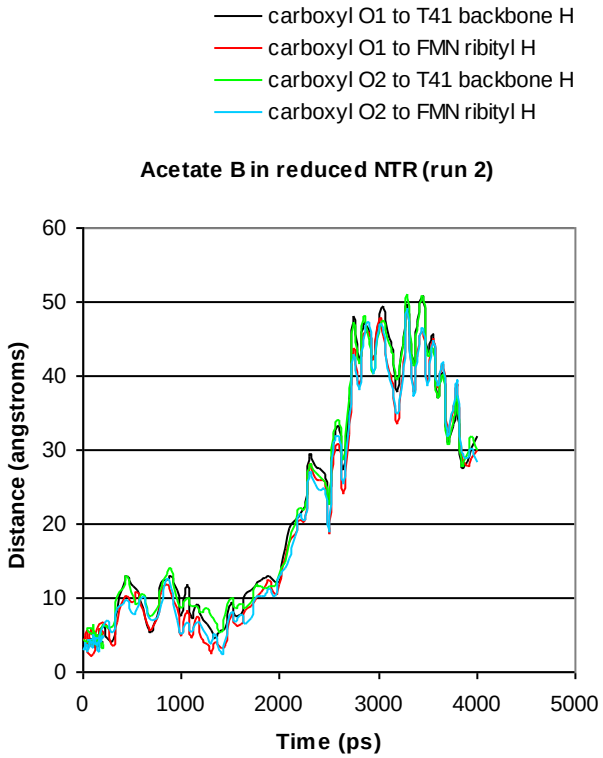
carboxyl O1 to T41 backbone H
carboxyl O1 to FMN ribityl H
carboxyl O2 to T41 backbone H
carboxyl O2 to FMN ribityl H
Acetate B in reduced NTR (run 2)
Distance (angstroms)
Time (ps)
0
10
20
30
40
50
60
0
1000
2000
3000
4000
5000

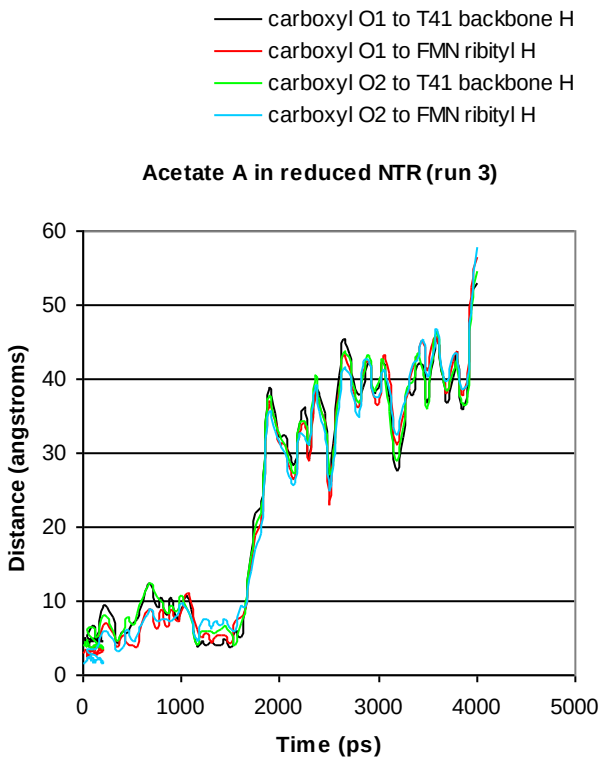
carboxyl O1 to T41 backbone H
carboxyl O1 to FMN ribityl H
carboxyl O2 to T41 backbone H
carboxyl O2 to FMN ribityl H
Acetate A in reduced NTR (run 3)
Distance (angstroms)
Time (ps)
0
10
20
30
40
50
60
0
1000
2000
3000
4000
5000

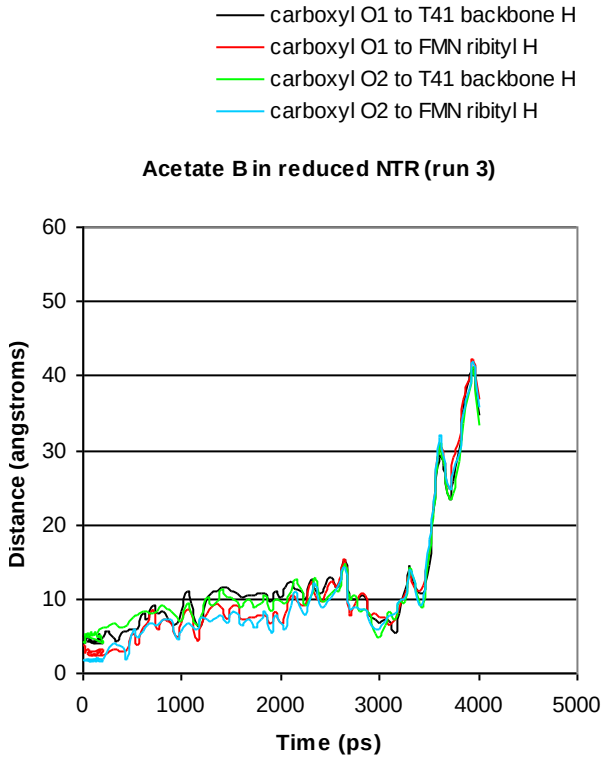
carboxyl O1 to T41 backbone H
carboxyl O1 to FMN ribityl H
carboxyl O2 to T41 backbone H
carboxyl O2 to FMN ribityl H
Acetate B in reduced NTR (run 3)
Distance (angstroms)
Time (ps)
0
10
20
30
40
50
60
0
1000
2000
3000
4000
5000

Menadione in reduced NTR (Section 5.2.3):

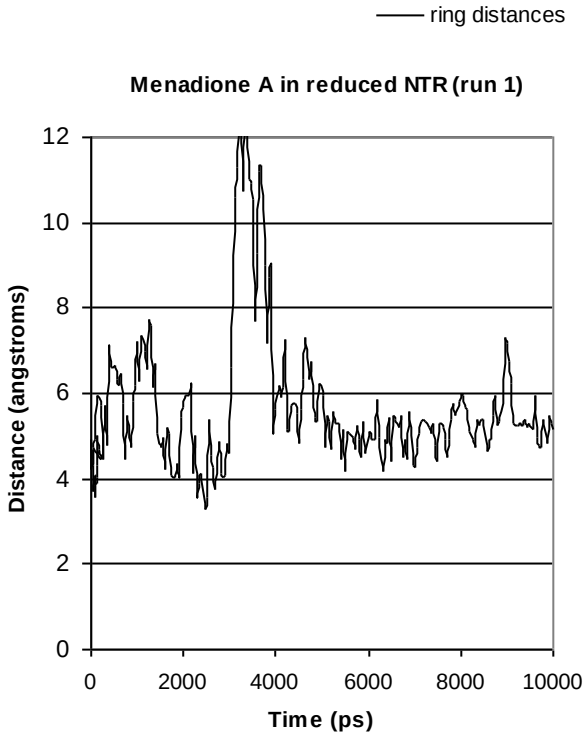

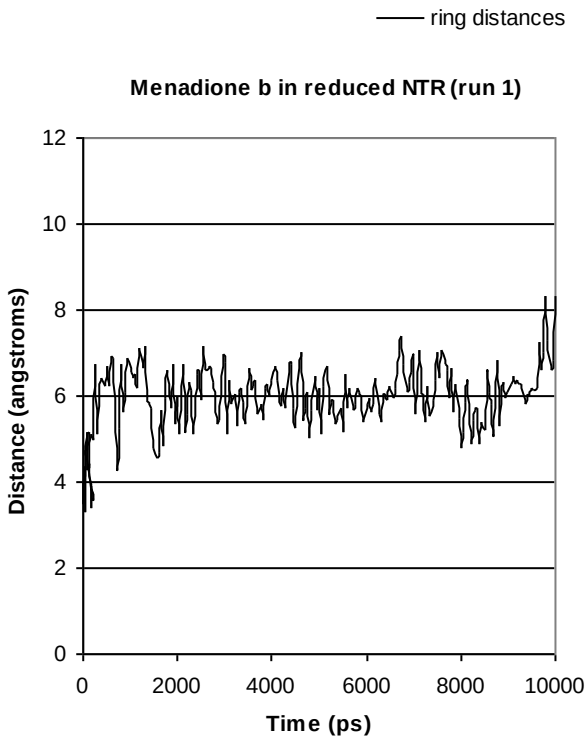

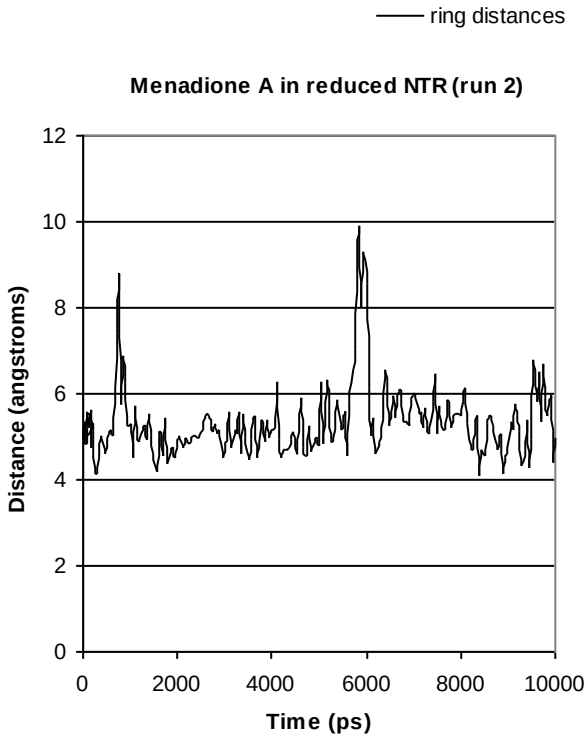

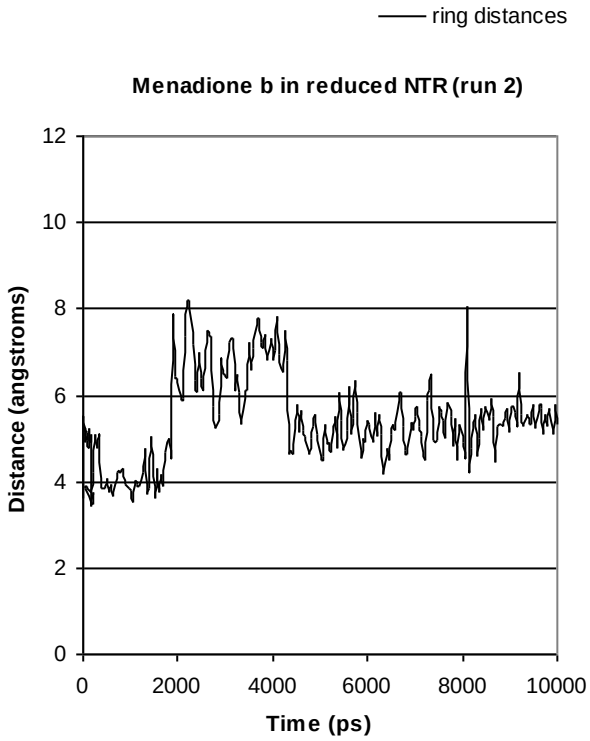

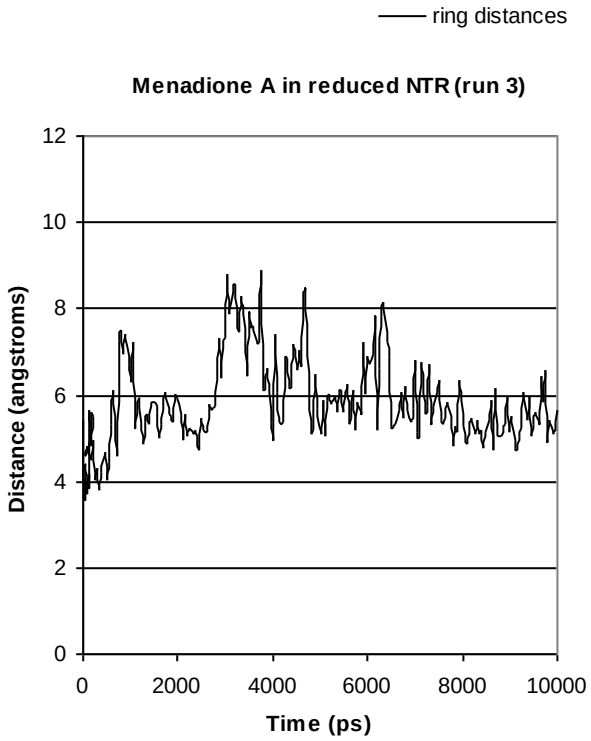

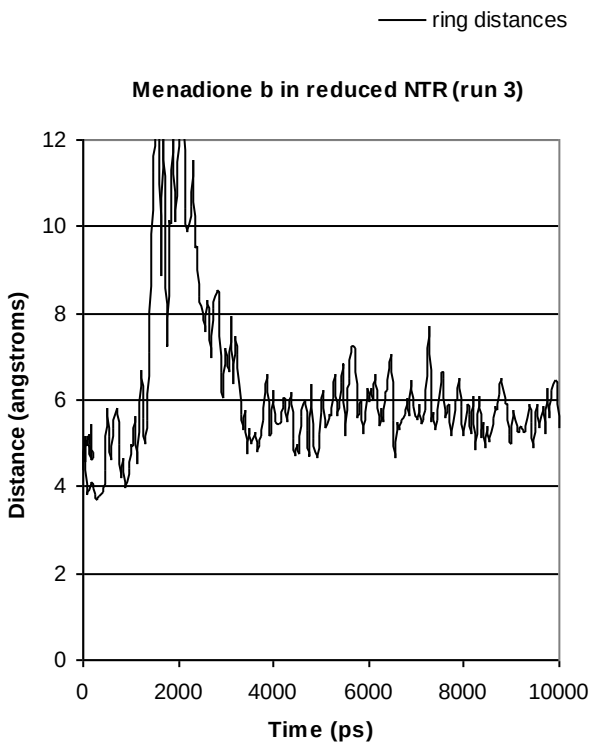

Nitrofurazone in oxidised NTR (Section 5.2.4):

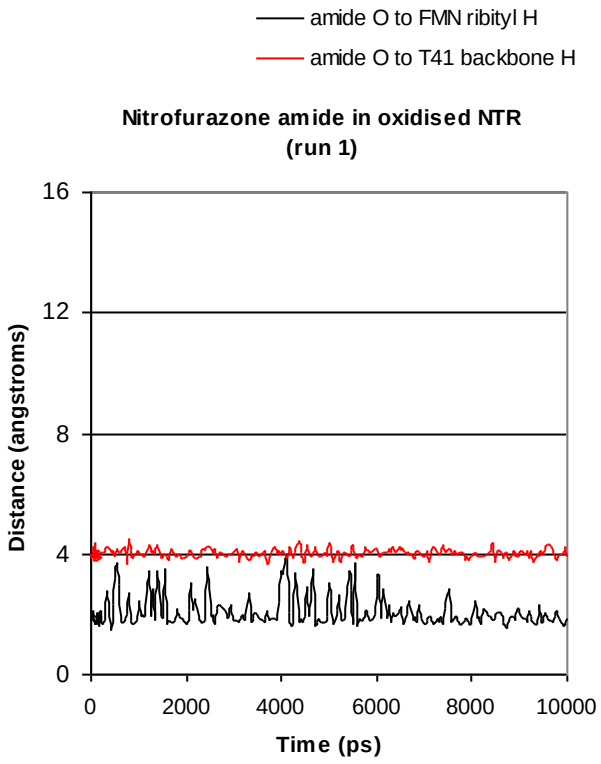

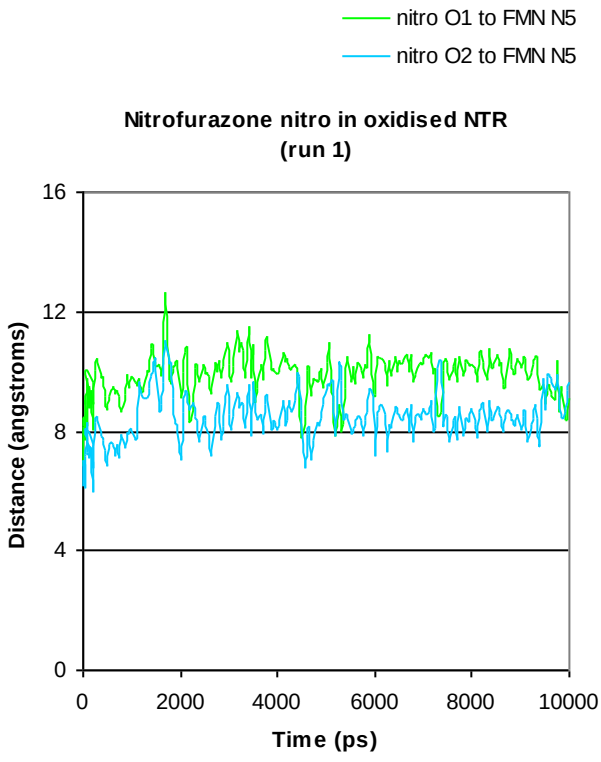

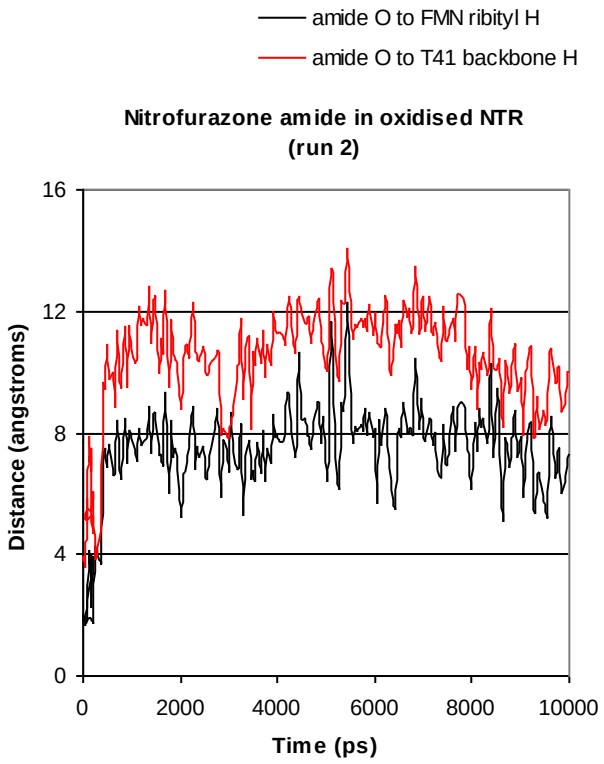
amide O to FMN ribityl H
amide O to T41 backbone H
Nitrofurazone amide in oxidised NTR
(run 2)
Distance (angstroms)
Time (ps)
0
4
8
12
16
0
2000
4000
6000
8000
10000

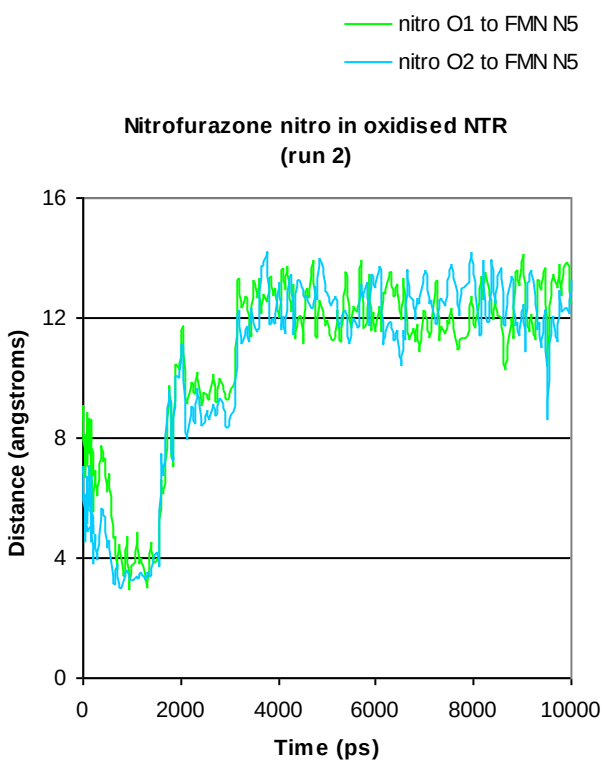
nitro O1 to FMN N5
nitro O2 to FMN N5
Nitrofurazone nitro in oxidised NTR
(run 2)
Distance (angstroms)
Time (ps)
0
4
8
12
16
0
2000
4000
6000
8000
10000

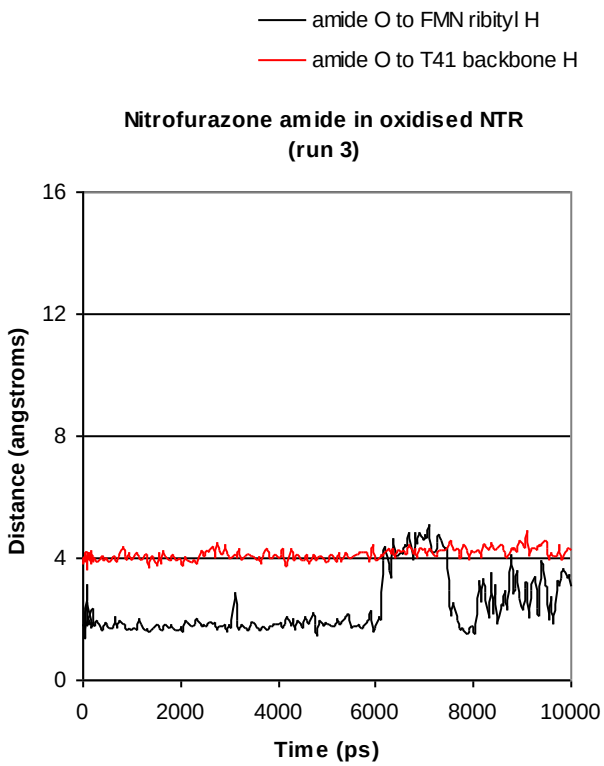
amide O to FMN ribityl H
amide O to T41 backbone H
Nitrofurazone amide in oxidised NTR
(run 3)
Distance (angstroms)
Time (ps)
0
4
8
12
16
0
2000
4000
6000
8000
10000

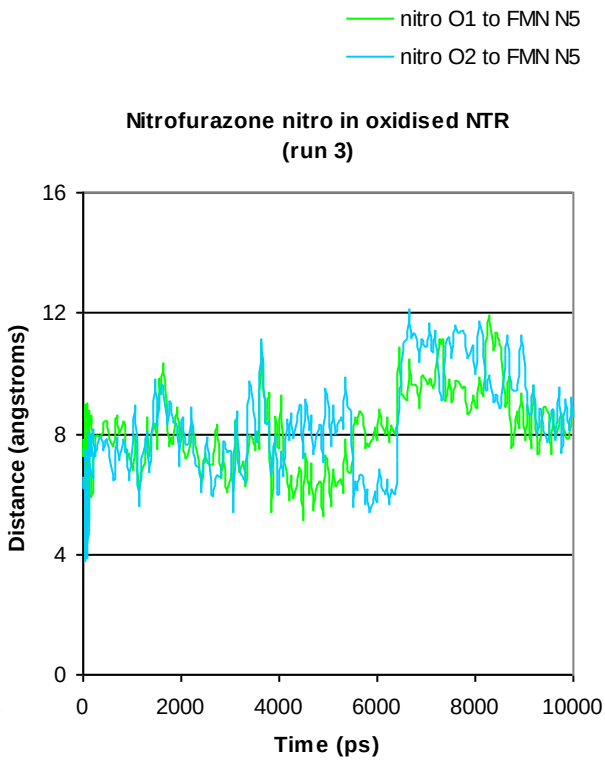
nitro O1 to FMN N5
nitro O2 to FMN N5
Nitrofurazone nitro in oxidised NTR
(run 3)
Distance (angstroms)
Time (ps)
0
4
8
12
16
0
2000
4000
6000
8000
10000

Nitrofurazone in reduced NTR (Section 5.2.5):

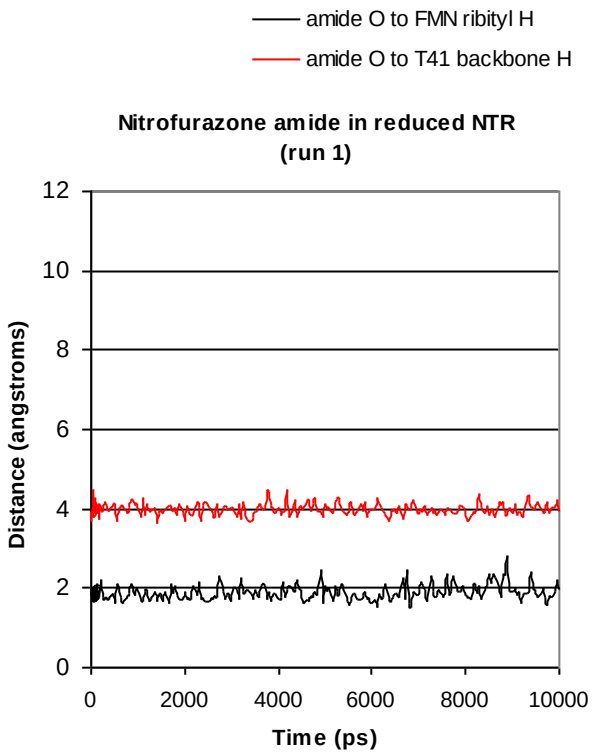

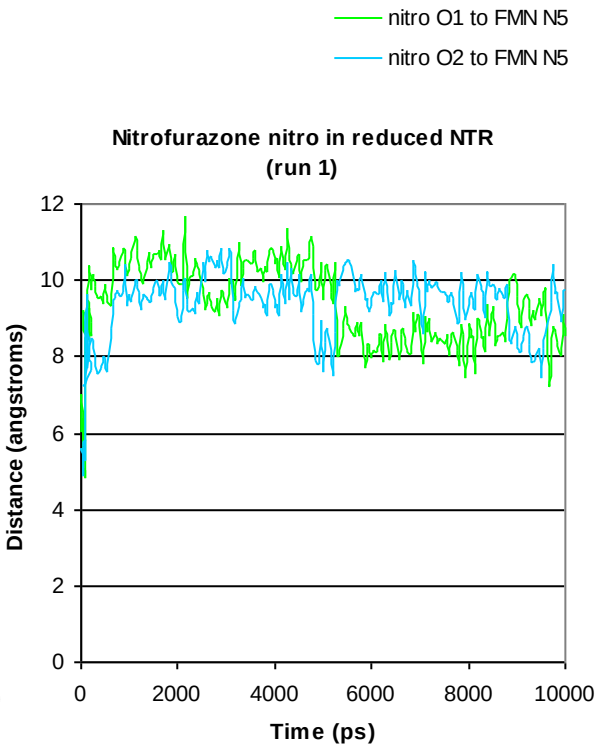

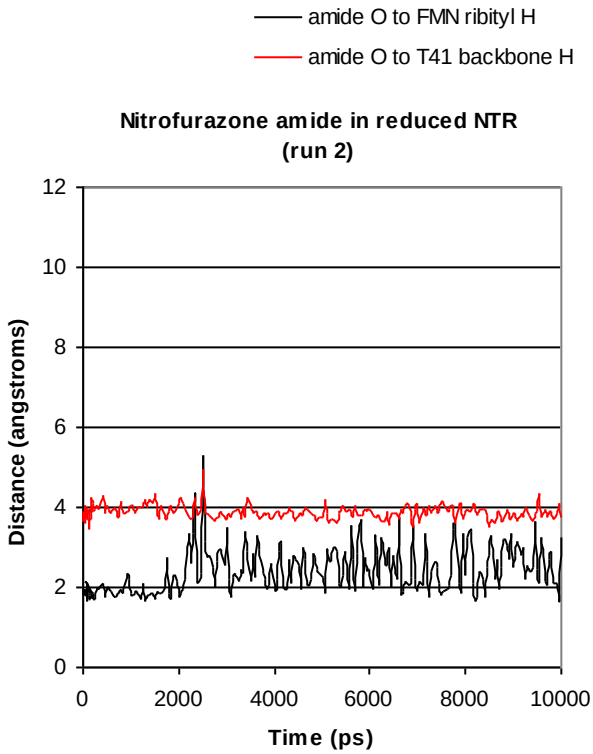

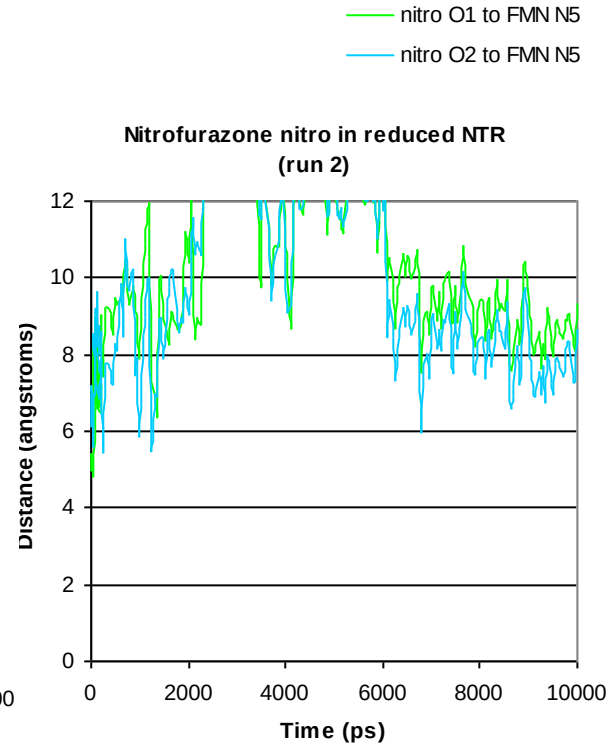

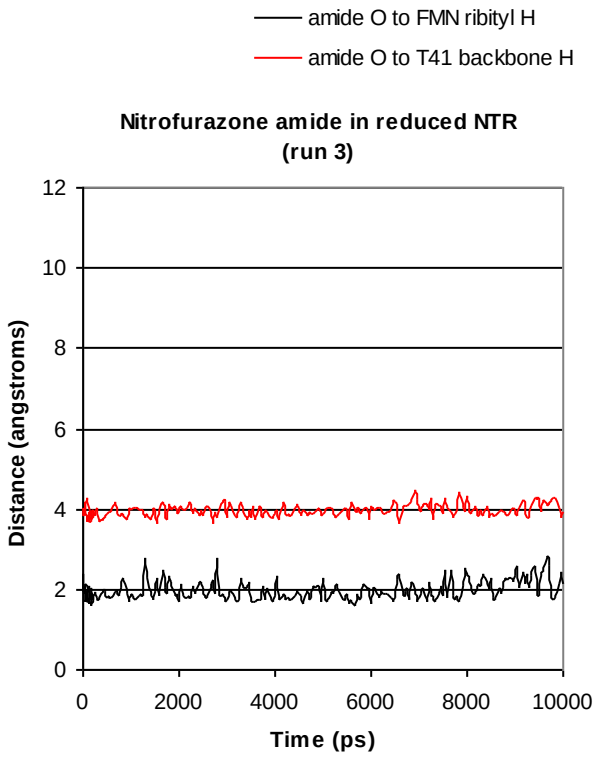

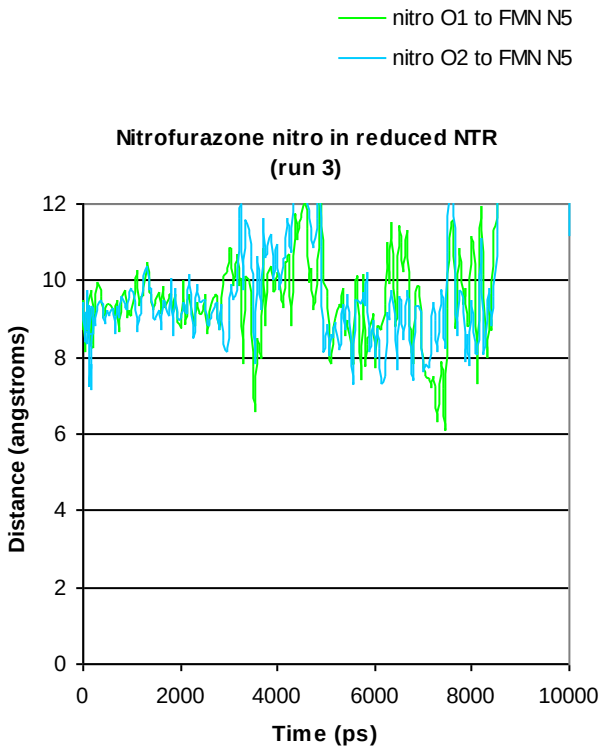

CB1954 in reduced nfsA (Section 5.2.6):

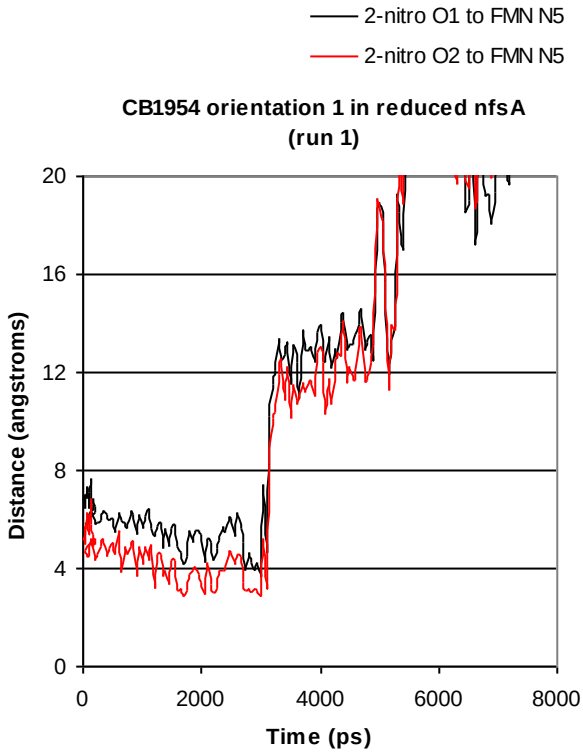

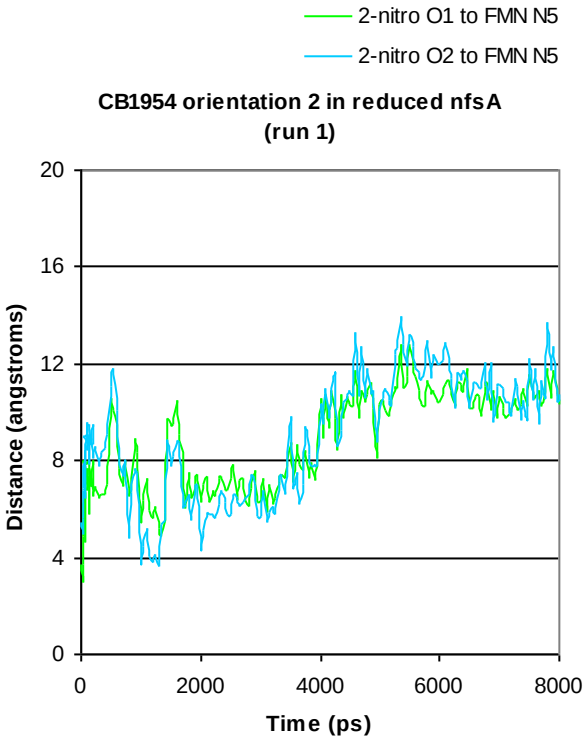

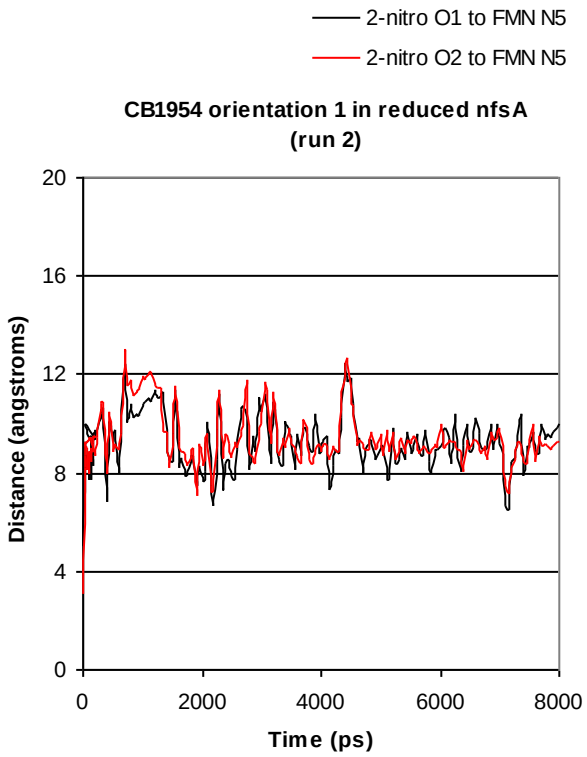
2-nitro O1 to FMN N5
2-nitro O2 to FMN N5
CB1954 orientation 1 in reduced nfsA (run 2)
Distance (angstroms)
Time (ps)
0
4
8
12
16
20
0
2000
4000
6000
8000

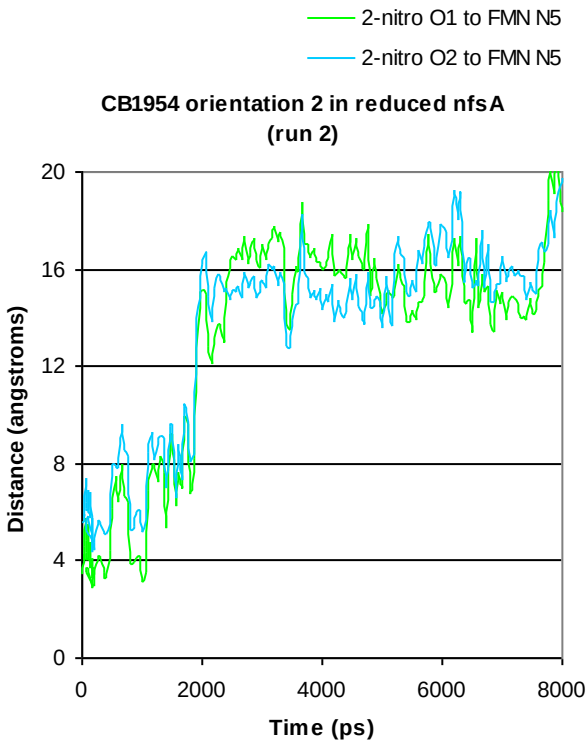
2-nitro O1 to FMN N5
2-nitro O2 to FMN N5
CB1954 orientation 2 in reduced nfsA (run 2)
Distance (angstroms)
Time (ps)
0
4
8
12
16
20
0
2000
4000
6000
8000

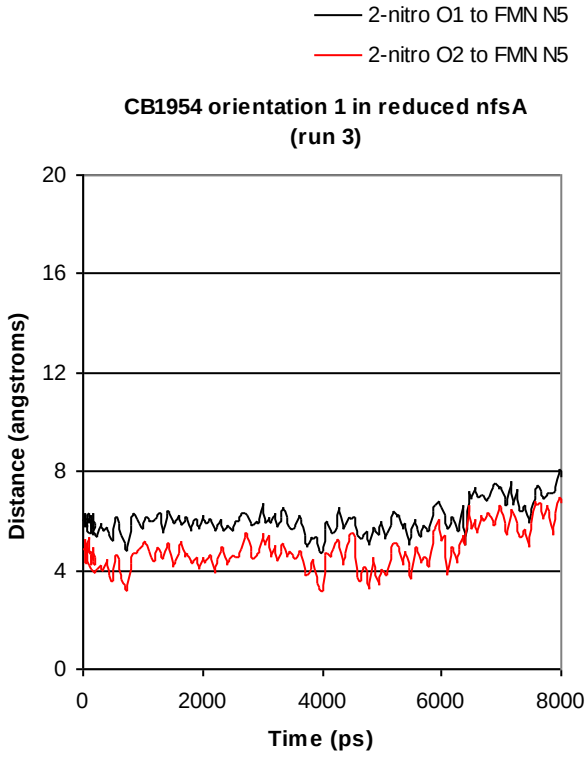
2-nitro O1 to FMN N5
2-nitro O2 to FMN N5
CB1954 orientation 1 in reduced nfsA (run 3)
Distance (angstroms)
Time (ps)
0
4
8
12
16
20
0
2000
4000
6000
8000

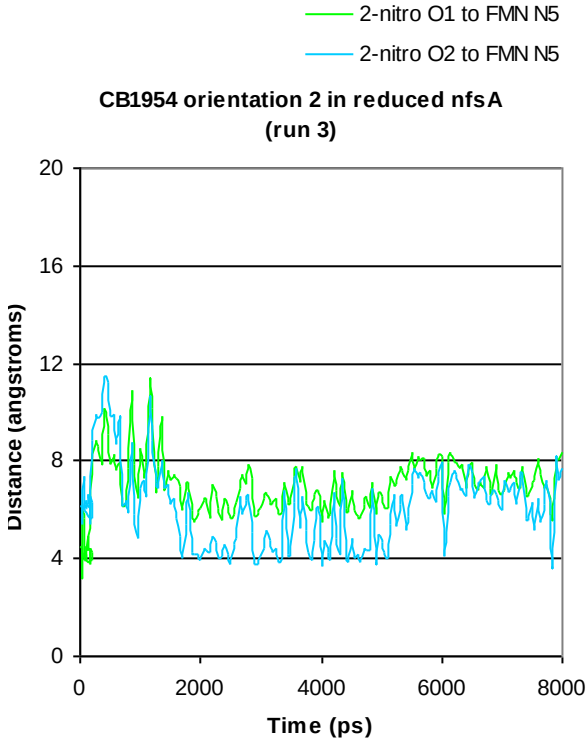
2-nitro O1 to FMN N5
2-nitro O2 to FMN N5
CB1954 orientation 2 in reduced nfsA (run 3)
Distance (angstroms)
Time (ps)
0
4
8
12
16
20
0
2000
4000
6000
8000

CB1954 in reduced NQO2 (Section 5.2.7):

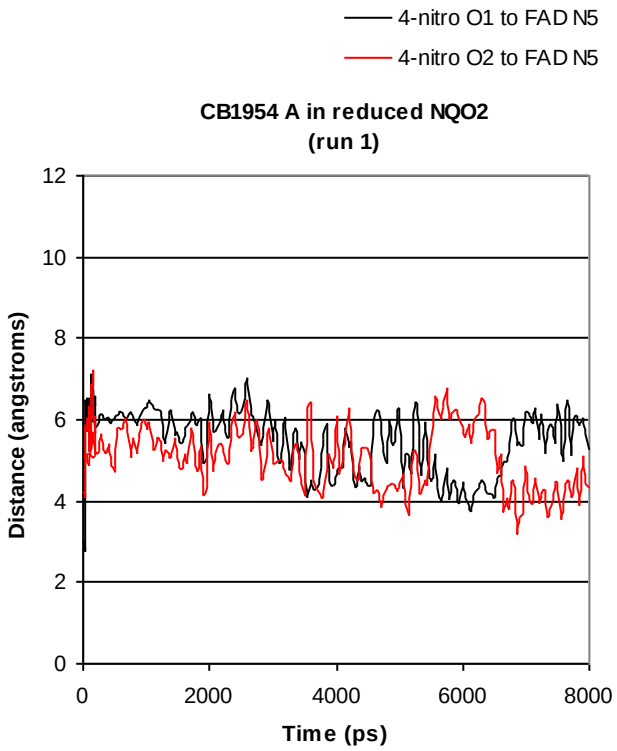

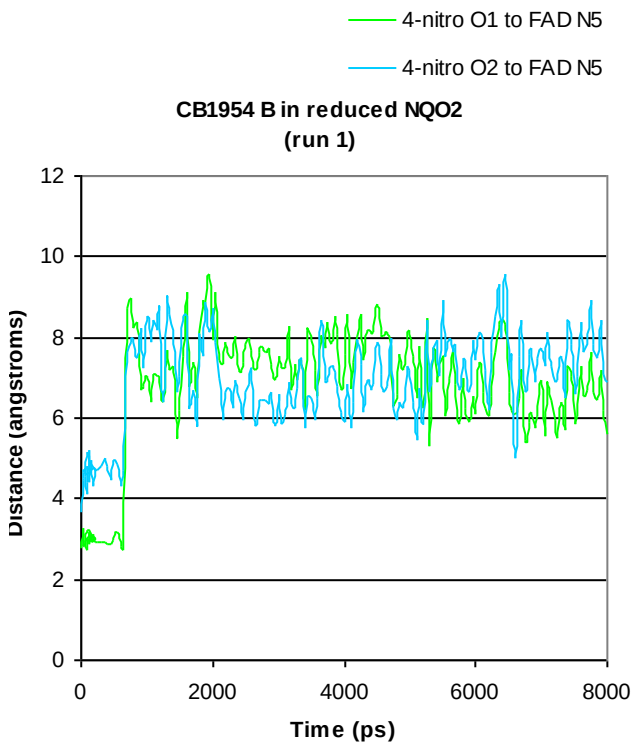

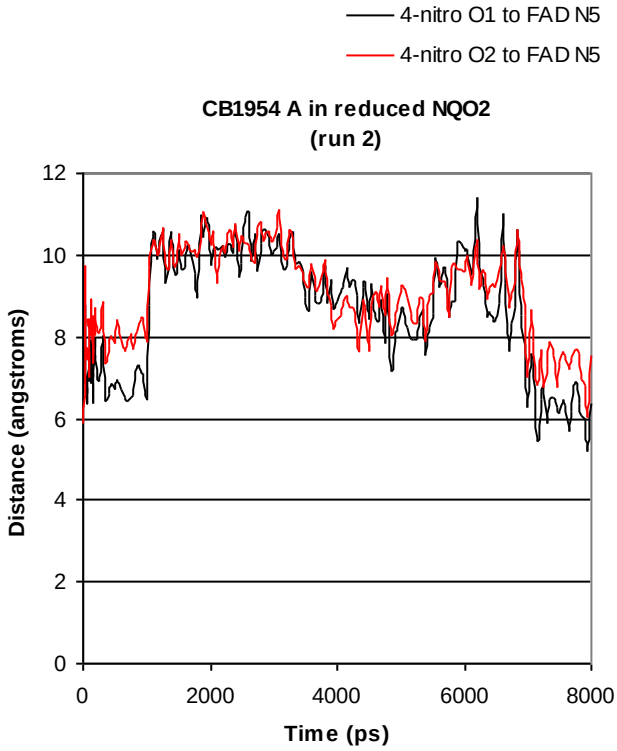

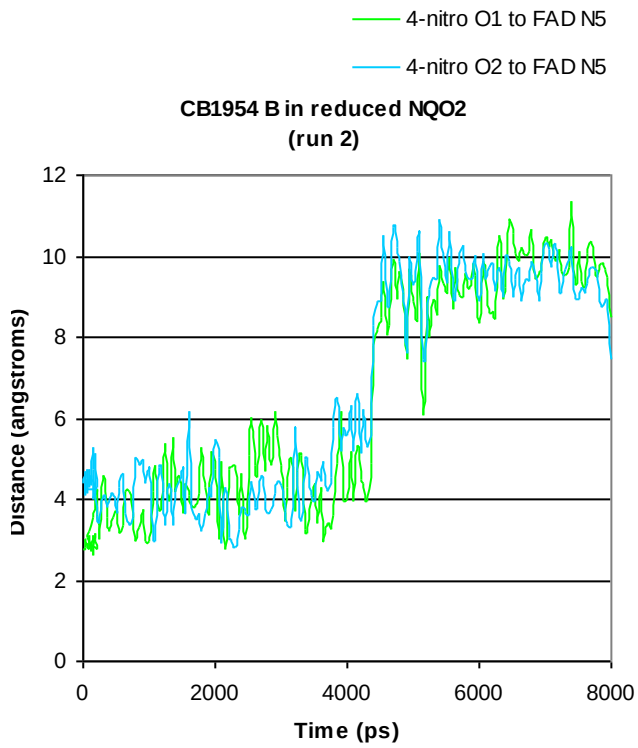

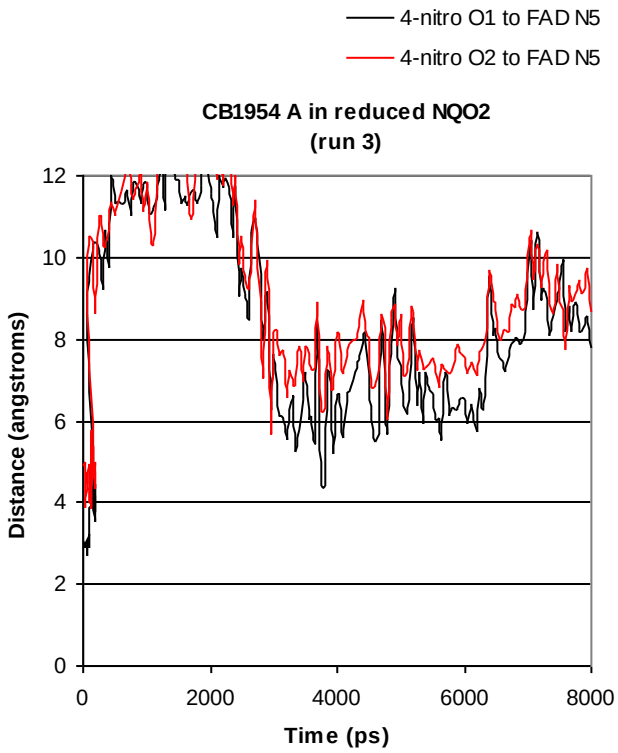

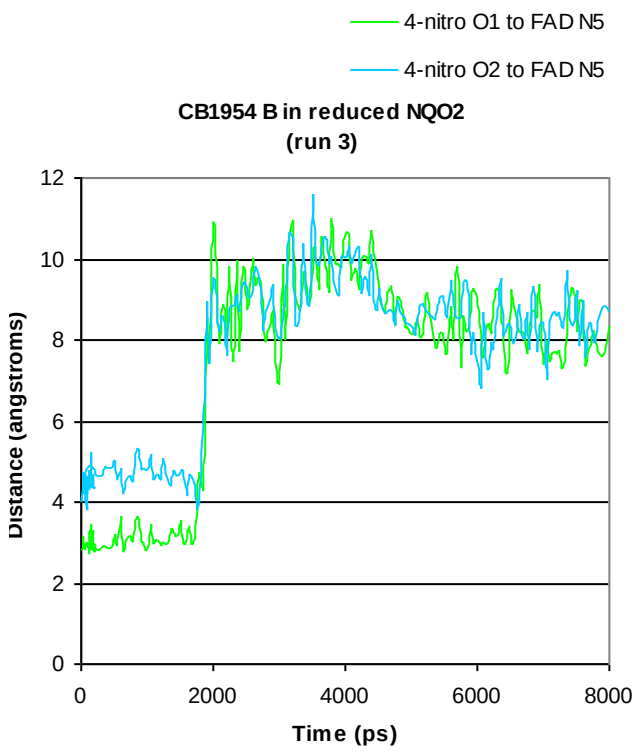

CB1954 with nitro groups in reduced NTR (Section 5.2.8):

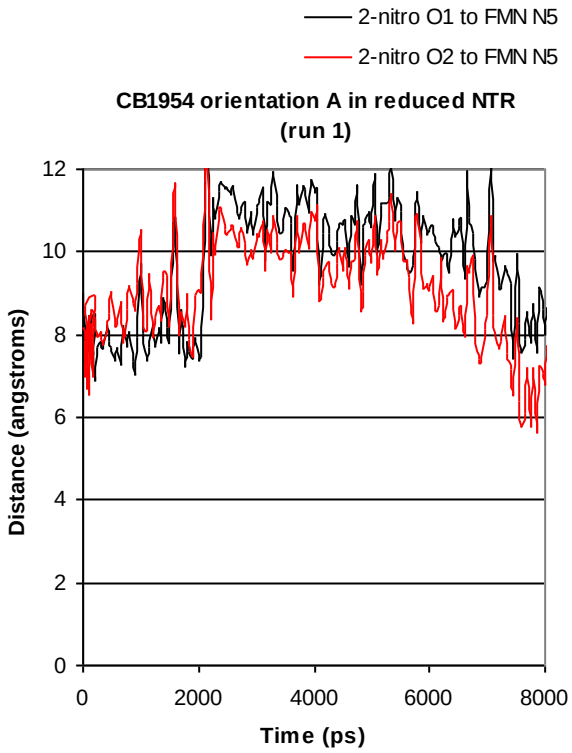

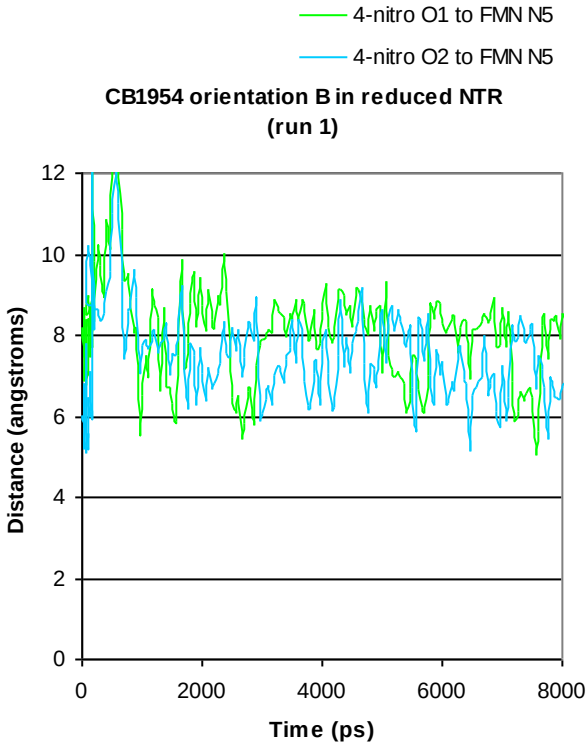

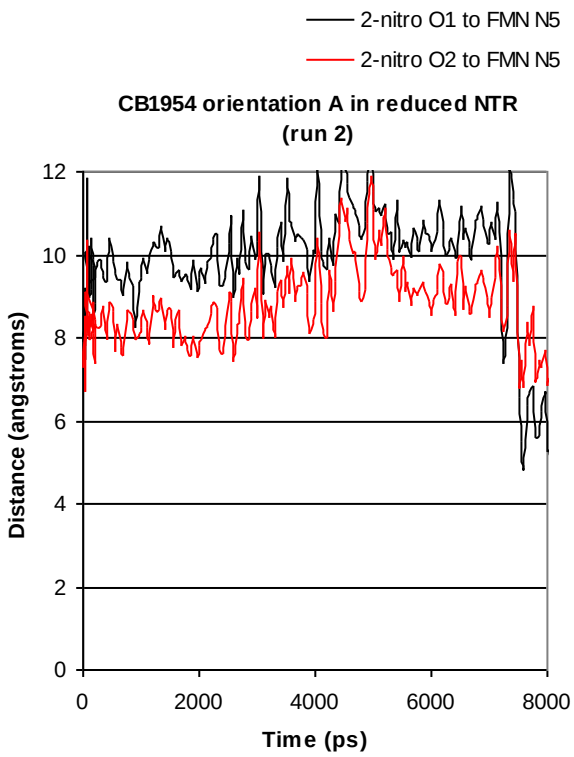
2-nitro O1 to FMN N5
2-nitro O2 to FMN N5
CB1954 orientation A in reduced NTR
(run 2)
Distance (angstroms)
Time (ps)
0
2
4
6
8
10
12
0
2000
4000
6000
8000

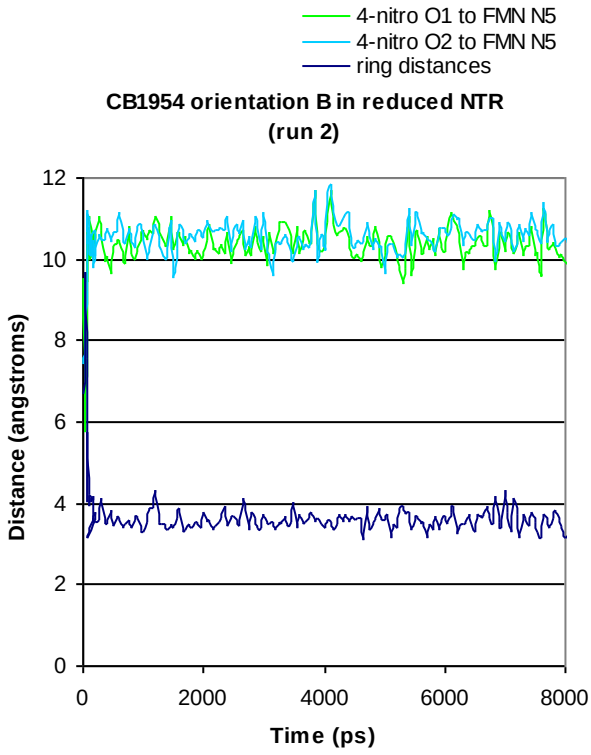
4-nitro O1 to FMN N5
4-nitro O2 to FMN N5
ring distances
CB1954 orientation B in reduced NTR
(run 2)
Distance (angstroms)
Time (ps)
0
2
4
6
8
10
12
0
2000
4000
6000
8000

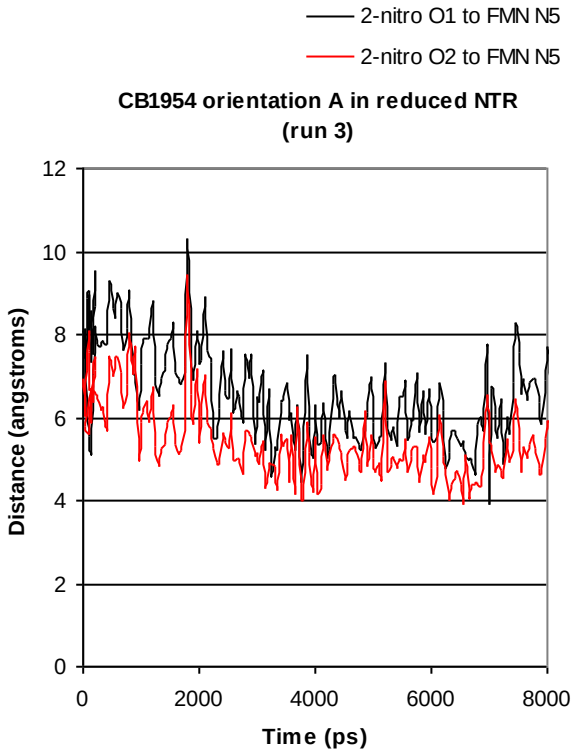
2-nitro O1 to FMN N5
2-nitro O2 to FMN N5
CB1954 orientation A in reduced NTR
(run 3)
Distance (angstroms)
Time (ps)
0
2
4
6
8
10
12
0
2000
4000
6000
8000

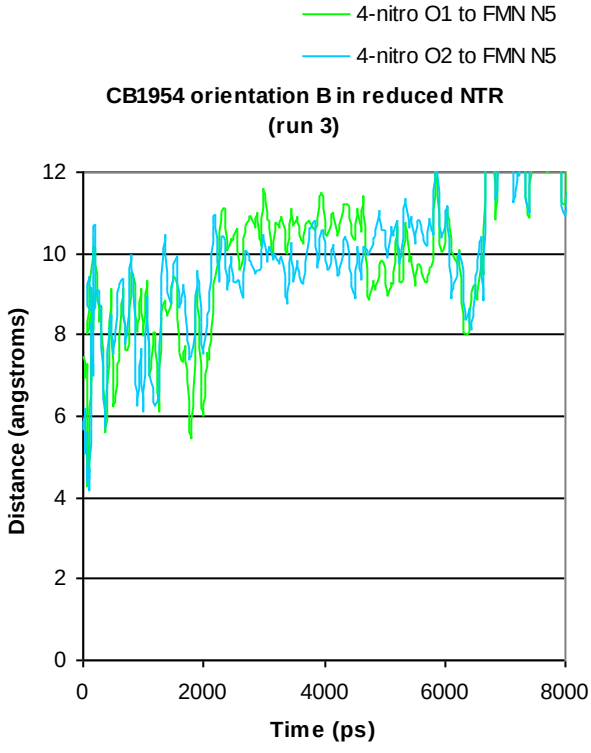
4-nitro O1 to FMN N5
4-nitro O2 to FMN N5
CB1954 orientation B in reduced NTR
(run 3)
Distance (angstroms)
Time (ps)
0
2
4
6
8
10
12
0
2000
4000
6000
8000

CB1954 with nitro groups in reduced NTR mutants (Section 5.2.9):

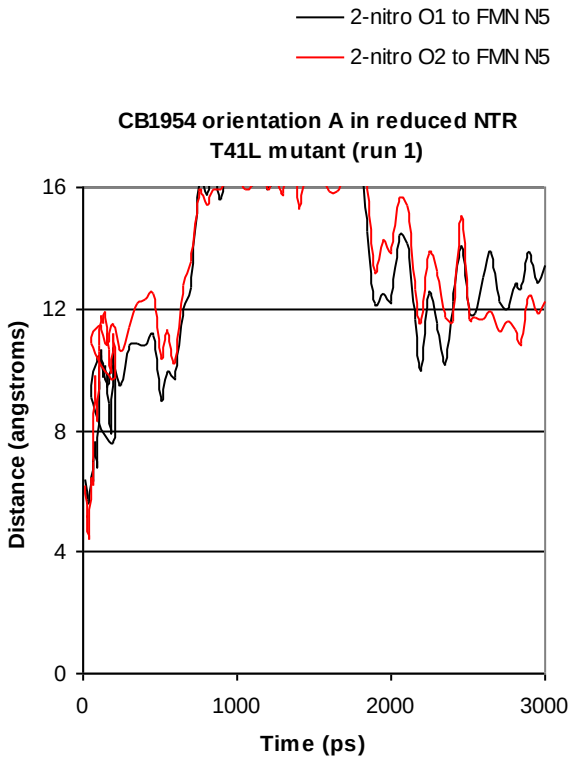

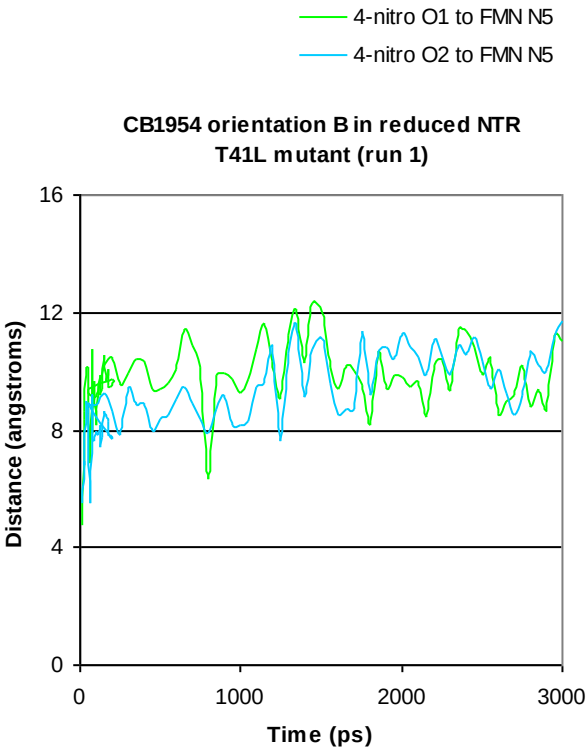

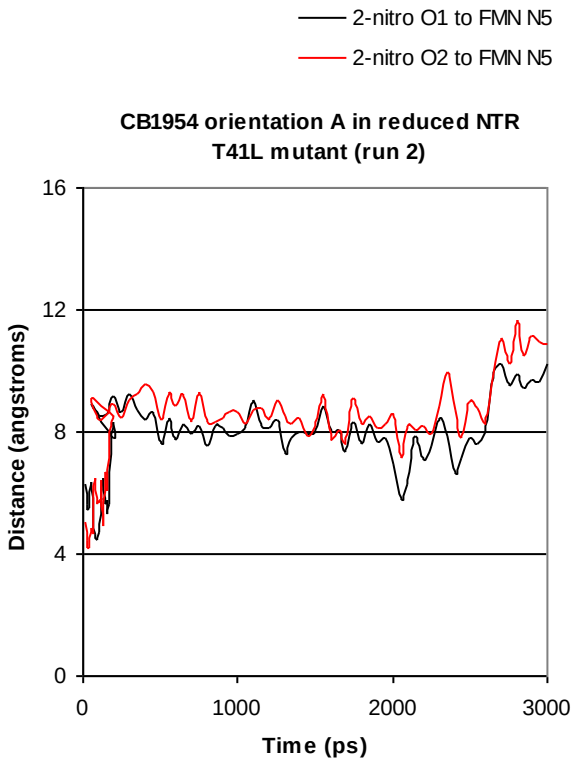

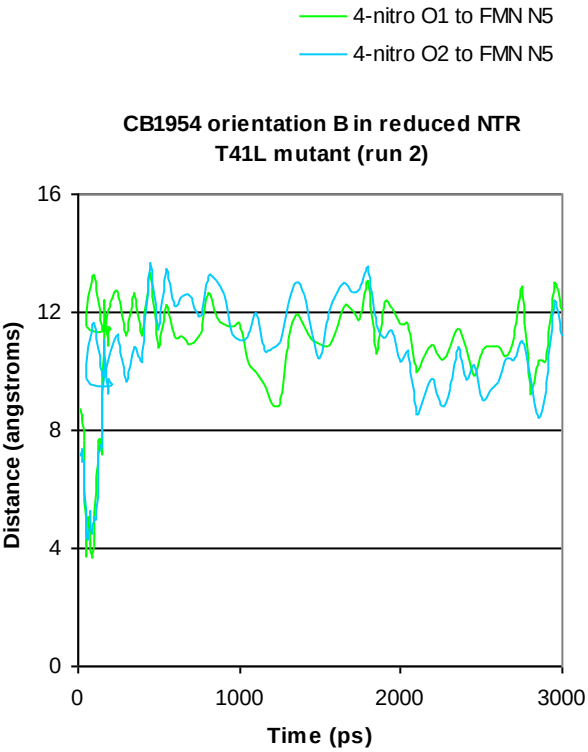

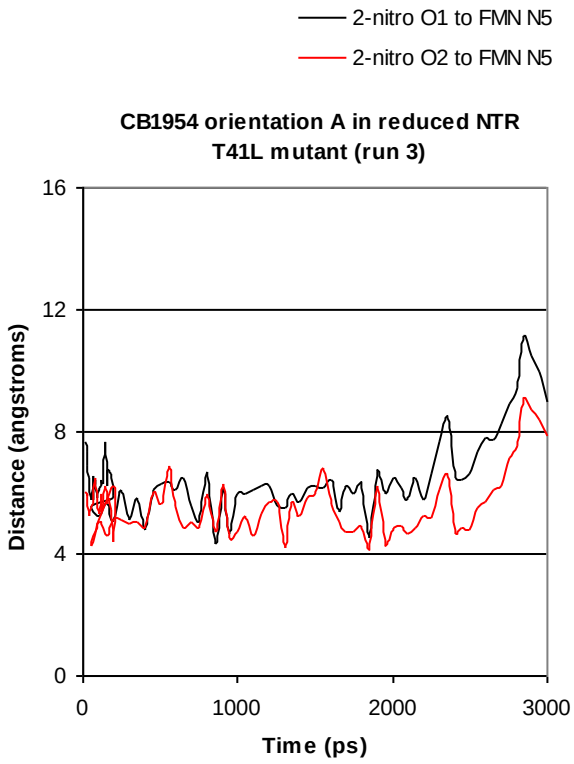
2-nitro O1 to FMN N5
2-nitro O2 to FMN N5
CB1954 orientation A in reduced NTR
T41L mutant (run 3)
Distance (angstroms)
Time (ps)
0
4
8
12
16
0
1000
2000
3000

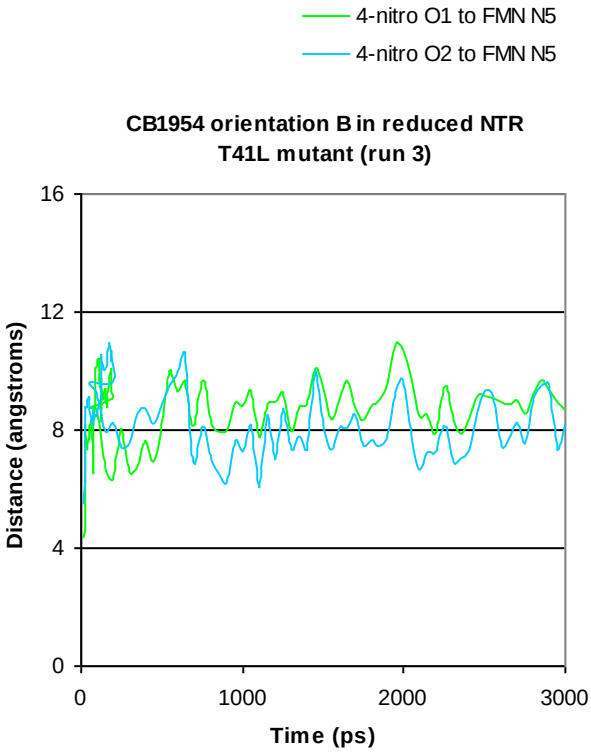
4-nitro O1 to FMN N5
4-nitro O2 to FMN N5
CB1954 orientation B in reduced NTR
T41L mutant (run 3)
Distance (angstroms)
Time (ps)
0
4
8
12
16
0
1000
2000
3000

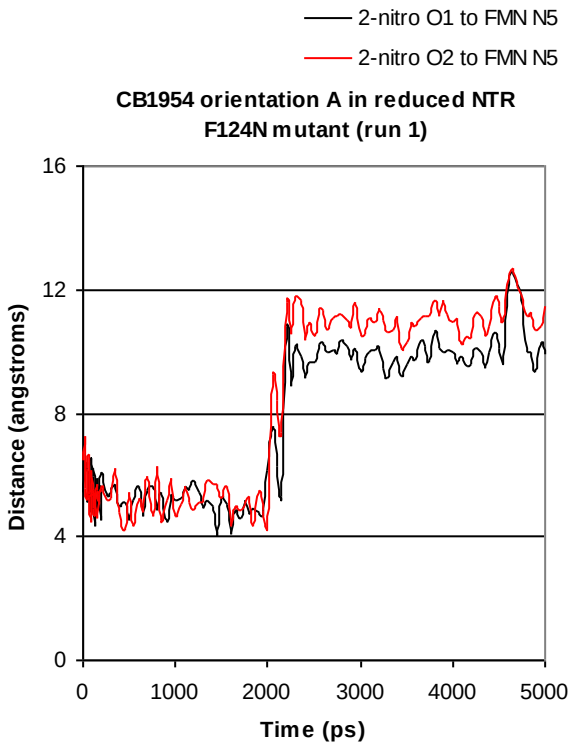
2-nitro O1 to FMN N5
2-nitro O2 to FMN N5
CB1954 orientation A in reduced NTR
F124N mutant (run 1)
Distance (angstroms)
Time (ps)
0
4
8
12
16
0
1000
2000
3000
4000
5000

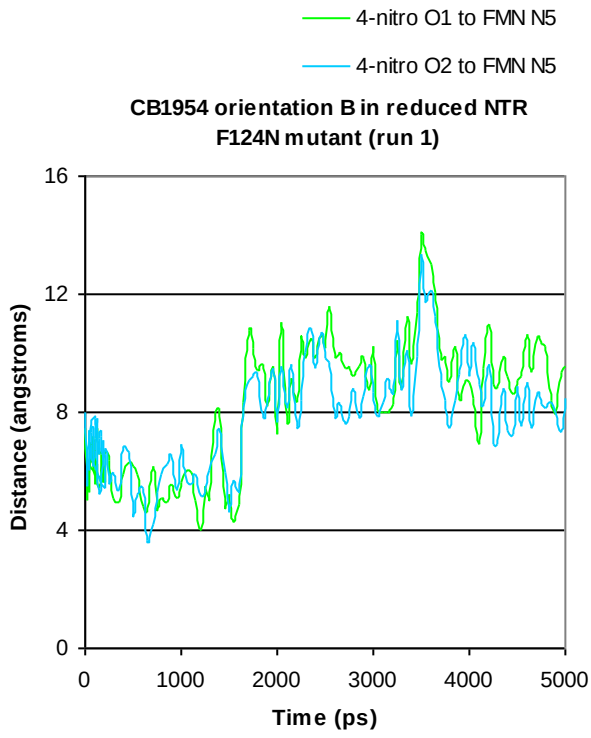
4-nitro O1 to FMN N5
4-nitro O2 to FMN N5
CB1954 orientation B in reduced NTR
F124N mutant (run 1)
Distance (angstroms)
Time (ps)
0
4
8
12
16
0
1000
2000
3000
4000
5000

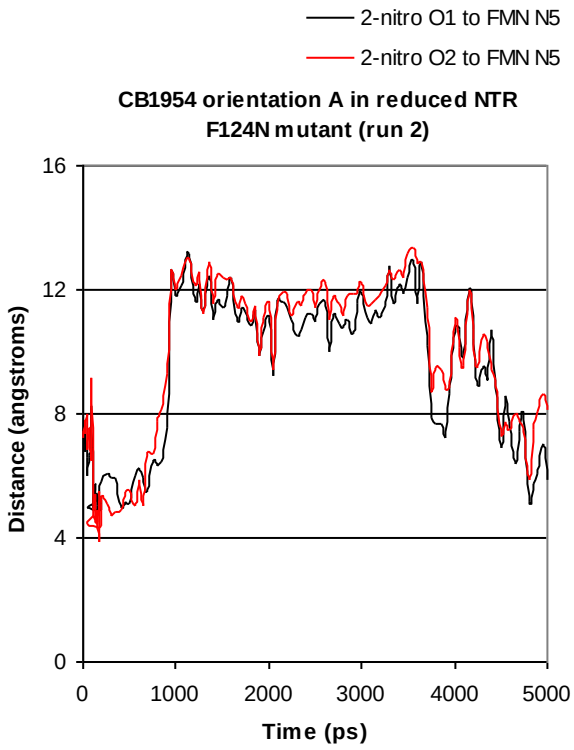
2-nitro O1 to FMN N5
2-nitro O2 to FMN N5
CB1954 orientation A in reduced NTR F124N mutant (run 2)
Distance (angstroms)
Time (ps)
0
4
8
12
16
0
1000
2000
3000
4000
5000

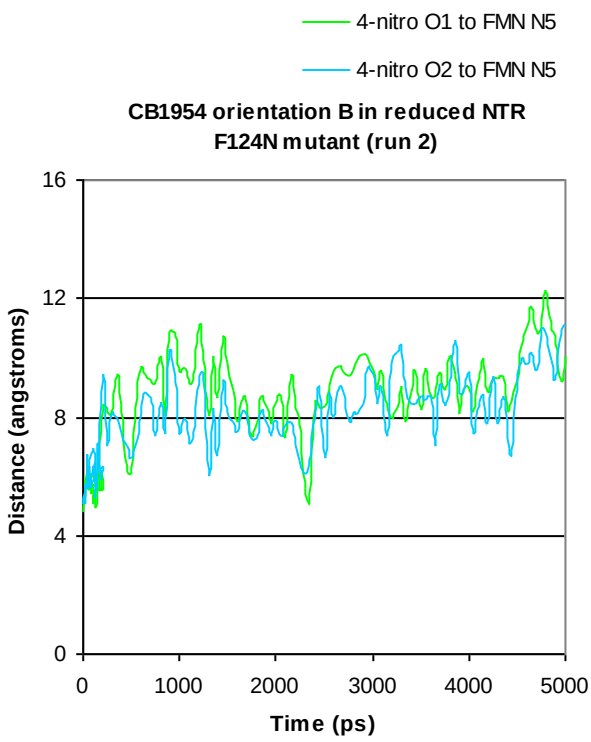
4-nitro O1 to FMN N5
4-nitro O2 to FMN N5
CB1954 orientation B in reduced NTR F124N mutant (run 2)
Distance (angstroms)
Time (ps)
0
4
8
12
16
0
1000
2000
3000
4000
5000

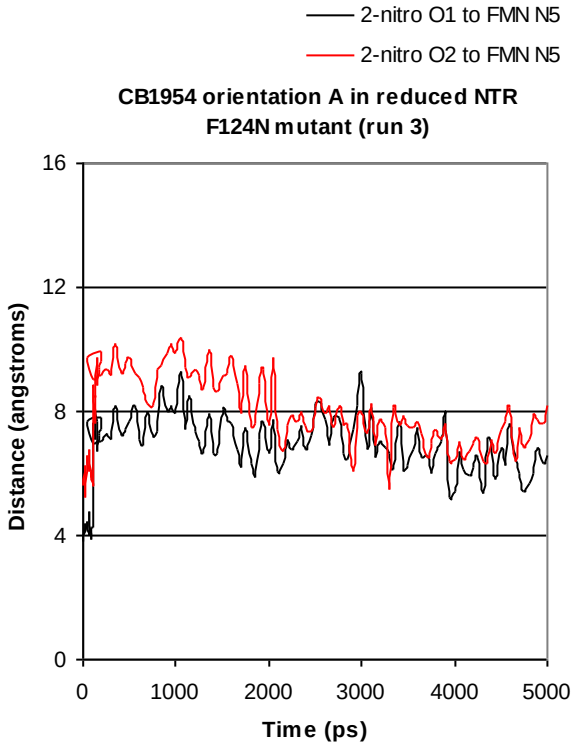
2-nitro O1 to FMN N5
2-nitro O2 to FMN N5
CB1954 orientation A in reduced NTR F124N mutant (run 3)
Distance (angstroms)
Time (ps)
0
4
8
12
16
0
1000
2000
3000
4000
5000

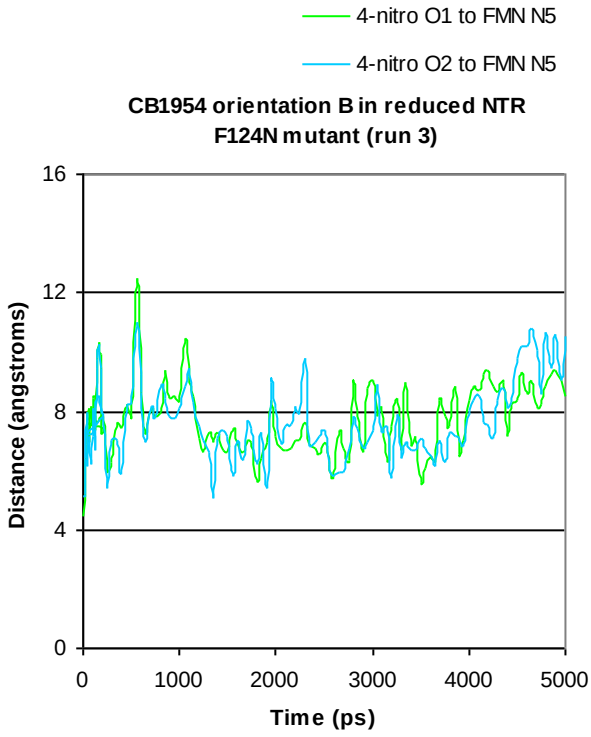
4-nitro O1 to FMN N5
4-nitro O2 to FMN N5
CB1954 orientation B in reduced NTR F124N mutant (run 3)
Distance (angstroms)
Time (ps)
0
4
8
12
16
0
1000
2000
3000
4000
5000

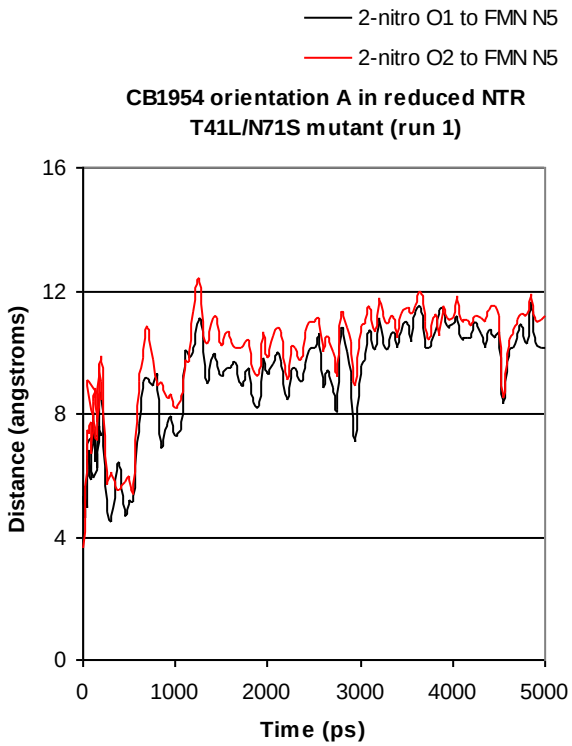
2-nitro O1 to FMN N5
2-nitro O2 to FMN N5
CB1954 orientation A in reduced NTR
T41L/N71S mutant (run 1)
Distance (angstroms)
Time (ps)
0
4
8
12
16
0
1000
2000
3000
4000
5000

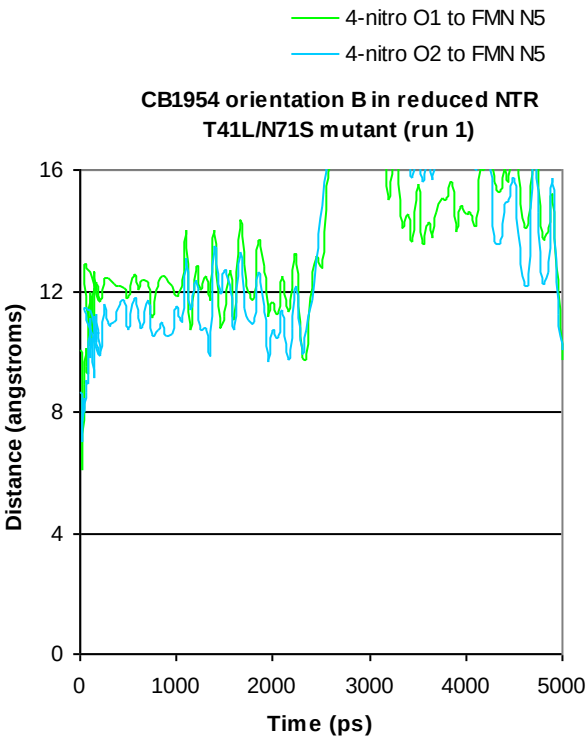
4-nitro O1 to FMN N5
4-nitro O2 to FMN N5
CB1954 orientation B in reduced NTR
T41L/N71S mutant (run 1)
Distance (angstroms)
Time (ps)
0
4
8
12
16
0
1000
2000
3000
4000
5000

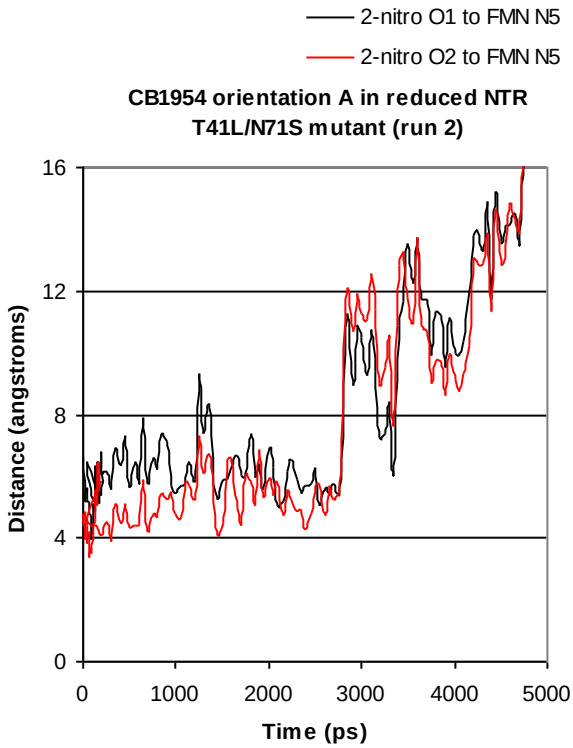
2-nitro O1 to FMN N5
2-nitro O2 to FMN N5
CB1954 orientation A in reduced NTR
T41L/N71S mutant (run 2)
Distance (angstroms)
Time (ps)
0
4
8
12
16
0
1000
2000
3000
4000
5000

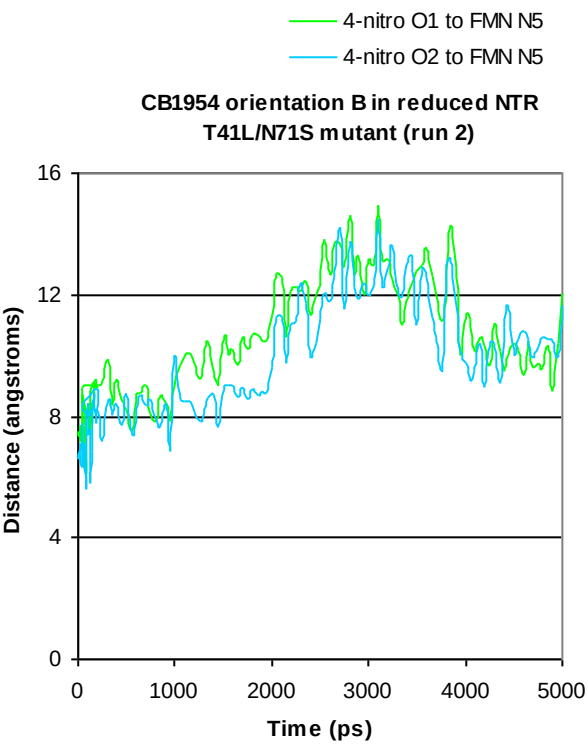
4-nitro O1 to FMN N5
4-nitro O2 to FMN N5
CB1954 orientation B in reduced NTR
T41L/N71S mutant (run 2)
Distance (angstroms)
Time (ps)
0
4
8
12
16
0
1000
2000
3000
4000
5000

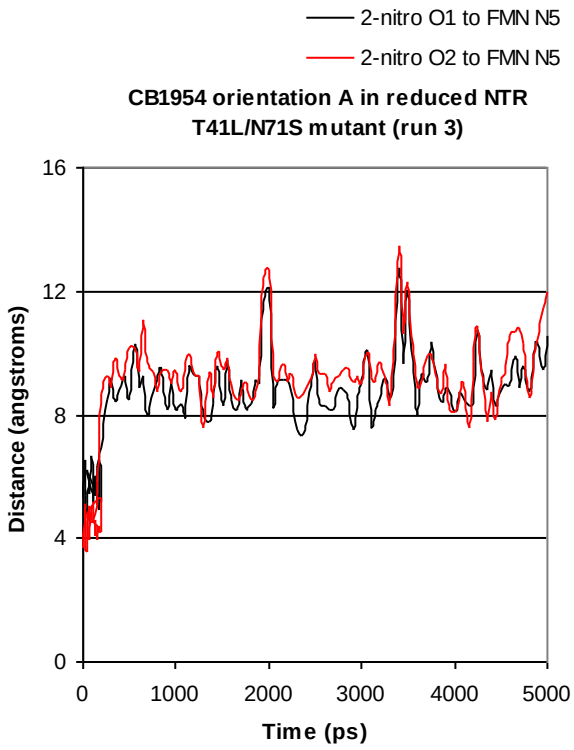
2-nitro O1 to FMN N5
2-nitro O2 to FMN N5
CB1954 orientation A in reduced NTR
T41L/N71S mutant (run 3)
Distance (angstroms)
Time (ps)
0
4
8
12
16
0
1000
2000
3000
4000
5000

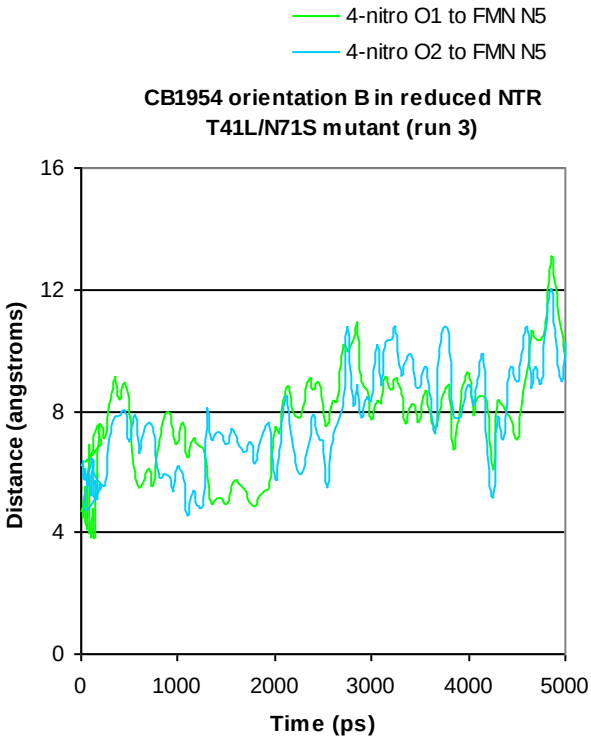
4-nitro O1 to FMN N5
4-nitro O2 to FMN N5
CB1954 orientation B in reduced NTR
T41L/N71S mutant (run 3)
Distance (angstroms)
Time (ps)
0
4
8
12
16
0
1000
2000
3000
4000
5000

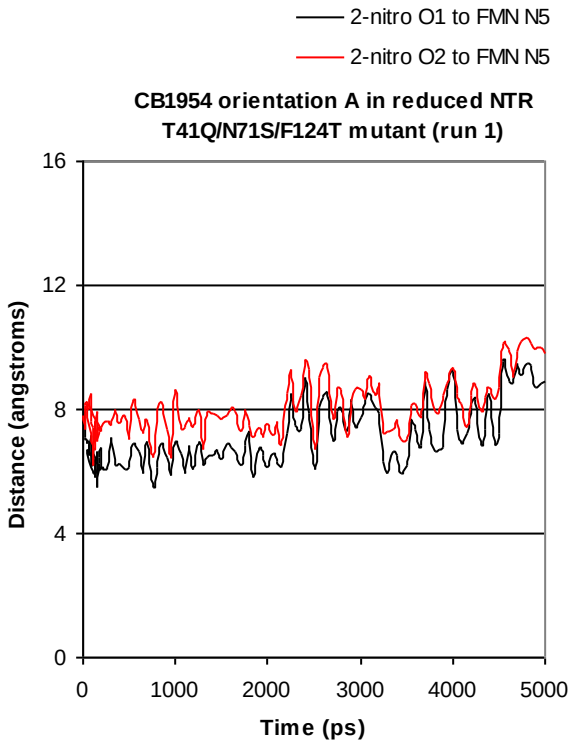
2-nitro O1 to FMN N5
2-nitro O2 to FMN N5
CB1954 orientation A in reduced NTR
T41Q/N71S/F124T mutant (run 1)
Distance (angstroms)
Time (ps)
0
4
8
12
16
0
1000
2000
3000
4000
5000

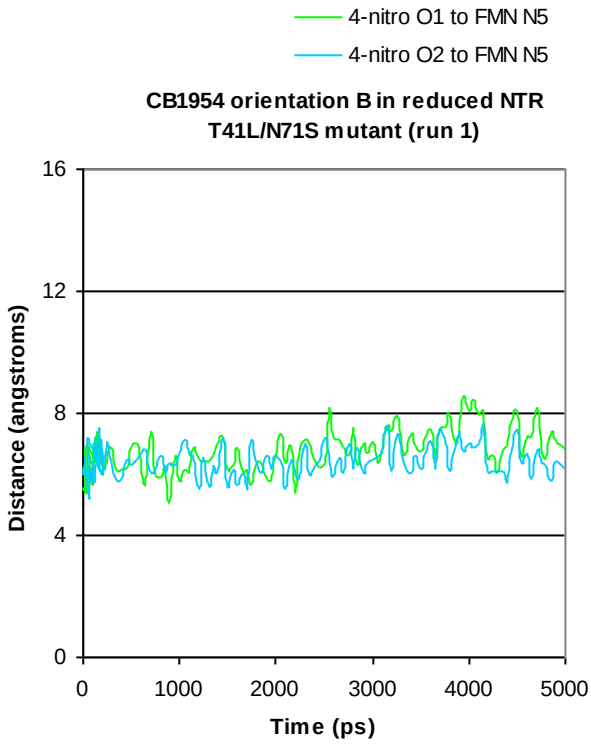
4-nitro O1 to FMN N5
4-nitro O2 to FMN N5
CB1954 orientation B in reduced NTR
T41L/N71S mutant (run 1)
Distance (angstroms)
Time (ps)
0
4
8
12
16
0
1000
2000
3000
4000
5000

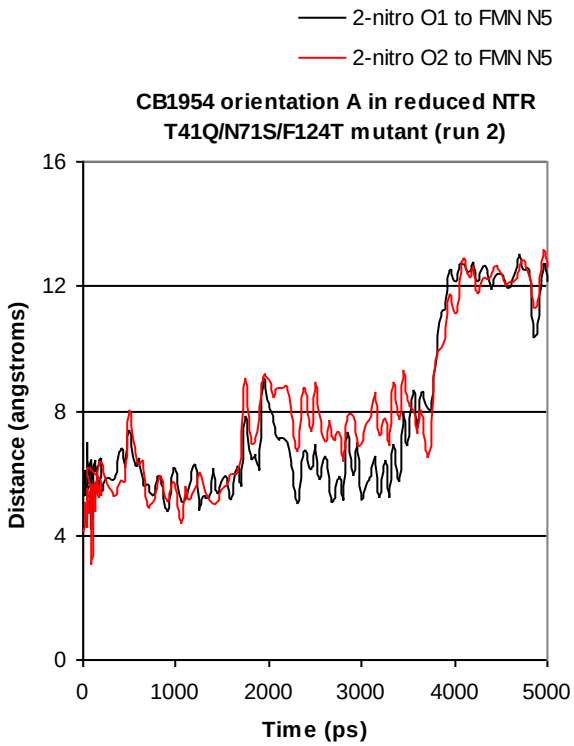
2-nitro O1 to FMN N5
2-nitro O2 to FMN N5
CB1954 orientation A in reduced NTR
T41Q/N71S/F124T mutant (run 2)
Distance (angstroms)
Time (ps)
0
4
8
12
16
0
1000
2000
3000
4000
5000

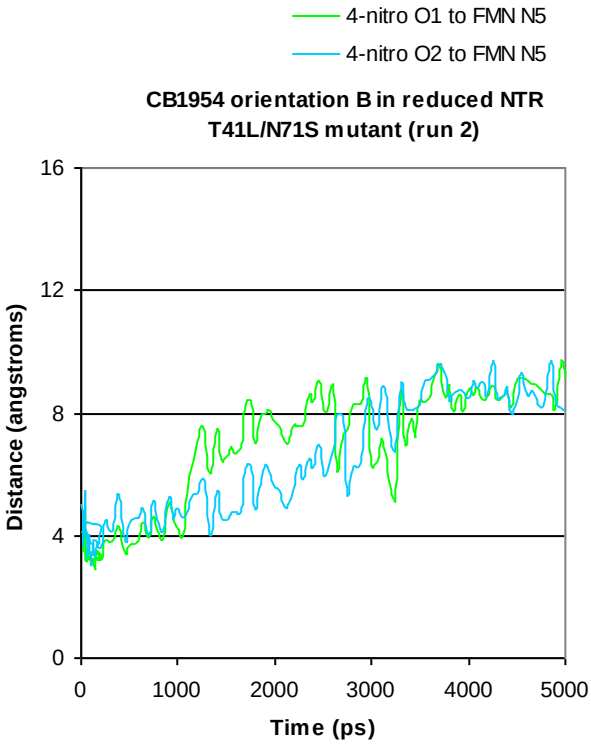
4-nitro O1 to FMN N5
4-nitro O2 to FMN N5
CB1954 orientation B in reduced NTR
T41L/N71S mutant (run 2)
Distance (angstroms)
Time (ps)
0
4
8
12
16
0
1000
2000
3000
4000
5000

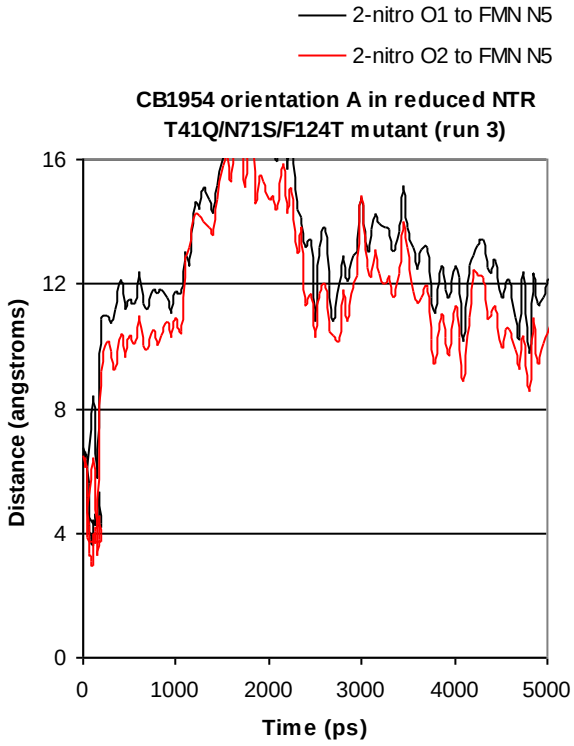
2-nitro O1 to FMN N5
2-nitro O2 to FMN N5
CB1954 orientation A in reduced NTR
T41Q/N71S/F124T mutant (run 3)
Distance (angstroms)
Time (ps)
0
4
8
12
16
0
1000
2000
3000
4000
5000

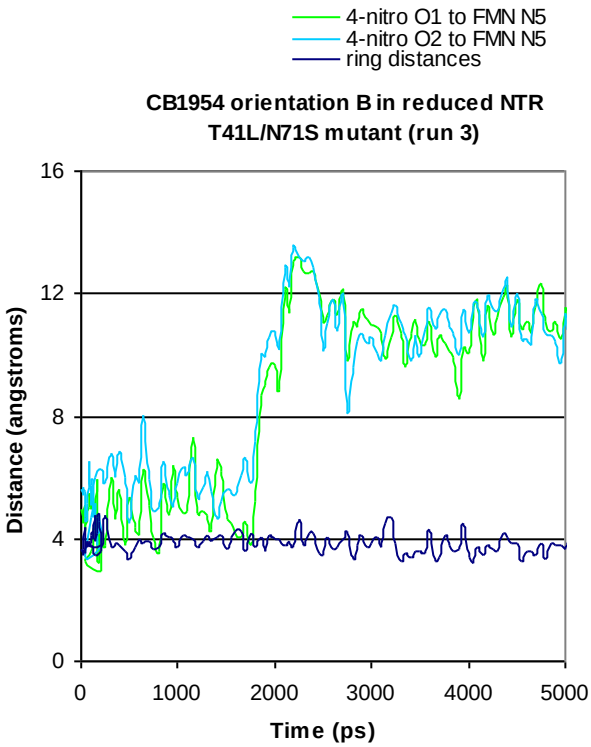
4-nitro O1 to FMN N5
4-nitro O2 to FMN N5
ring distances
CB1954 orientation B in reduced NTR
T41L/N71S mutant (run 3)
Distance (angstroms)
Time (ps)
0
4
8
12
16
0
1000
2000
3000
4000
5000

CB1954 with amide group in reduced NTR (Section 5.2.10):

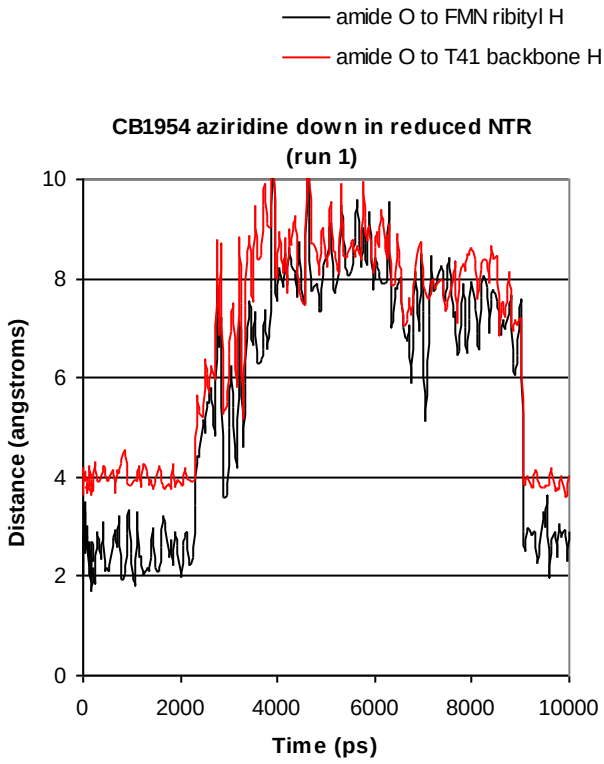

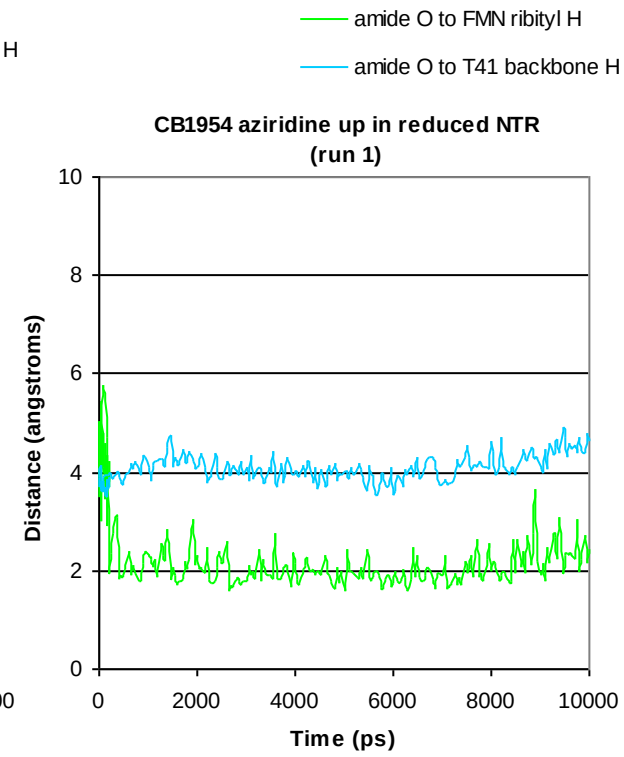

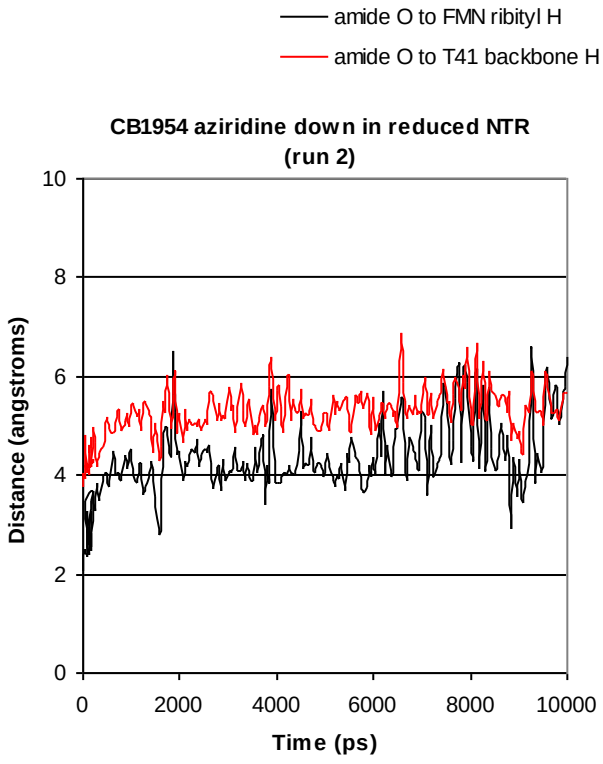

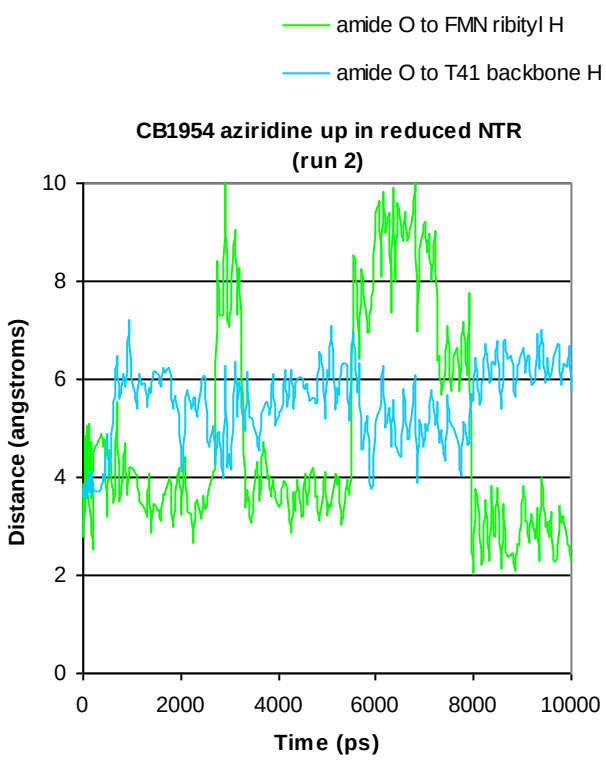

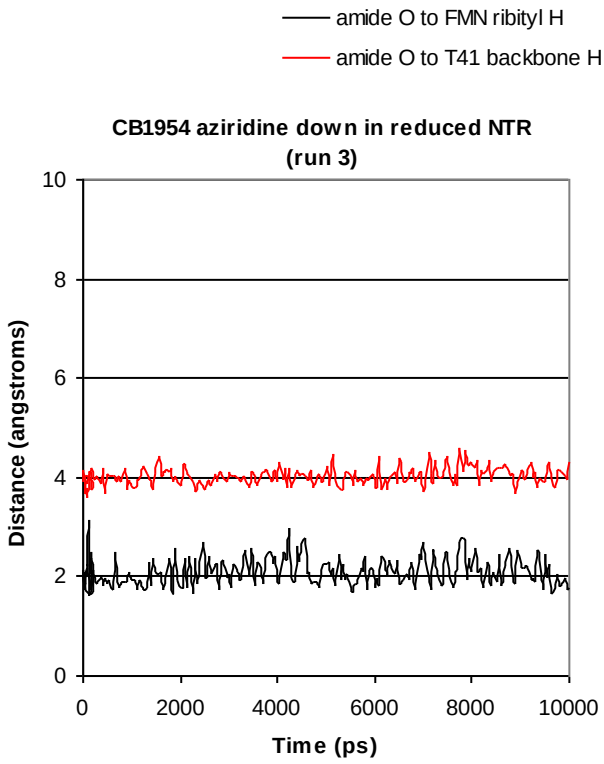

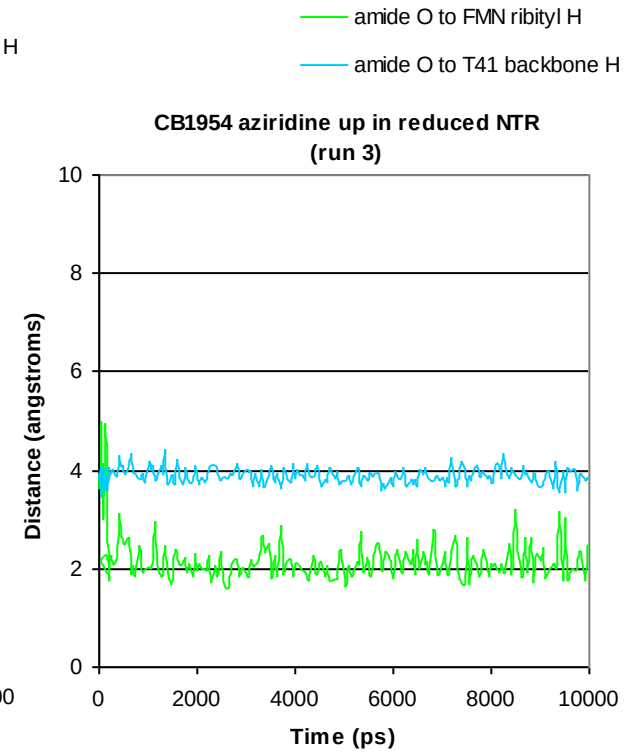

CB1954 with amide group in reduced NTR mutants (Section 5.2.11):

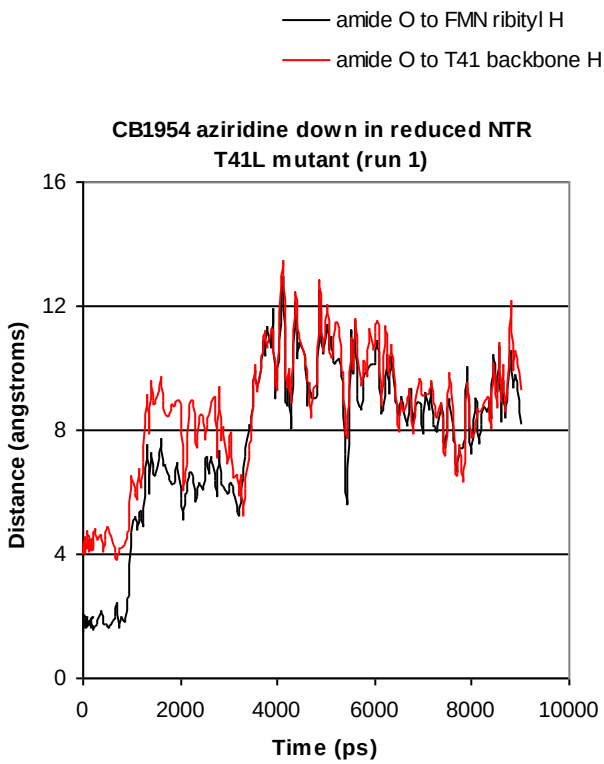

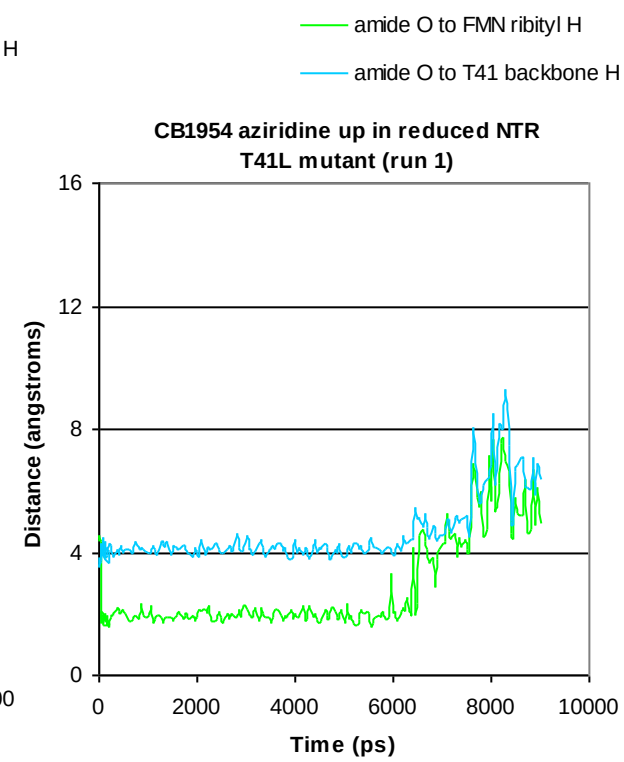

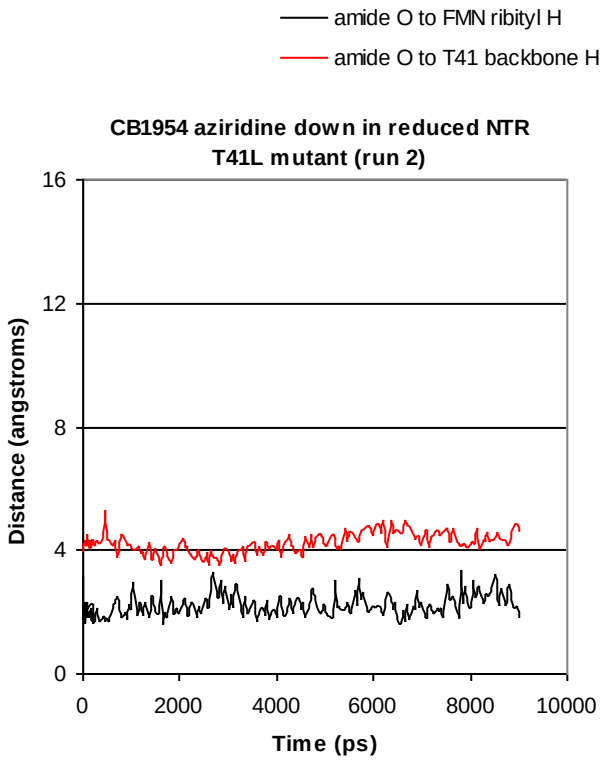
amide O to FMN ribityl H
amide O to T41 backbone H
CB1954 aziridine down in reduced NTR
T41L mutant (run 2)
Distance (angstroms)
Time (ps)
0
4
8
12
16
0
2000
4000
6000
8000
10000

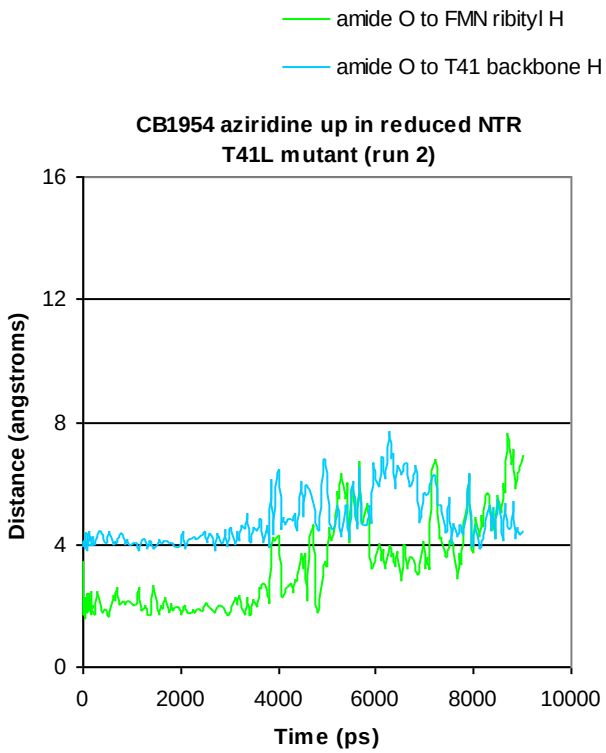
amide O to FMN ribityl H
amide O to T41 backbone H
CB1954 aziridine up in reduced NTR
T41L mutant (run 2)
Distance (angstroms)
Time (ps)
0
4
8
12
16
0
2000
4000
6000
8000
10000

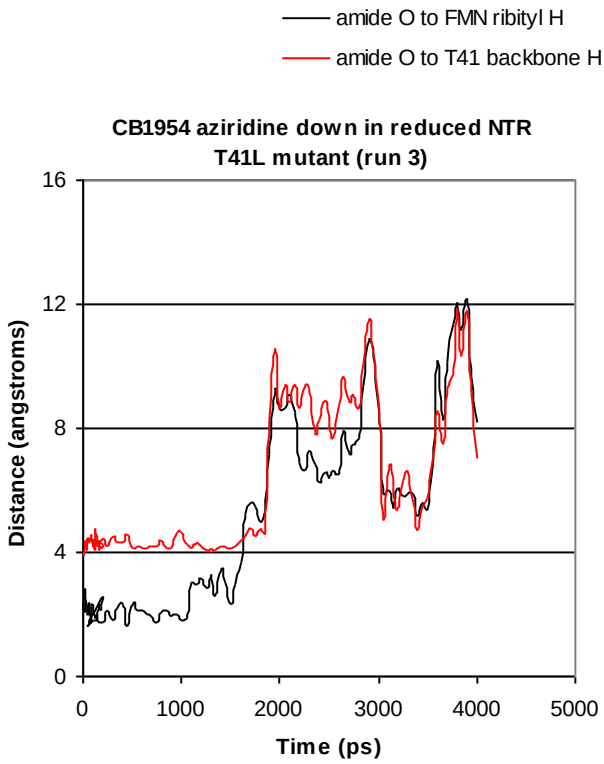
amide O to FMN ribityl H
amide O to T41 backbone H
CB1954 aziridine down in reduced NTR
T41L mutant (run 3)
Distance (angstroms)
Time (ps)
0
4
8
12
16
0
1000
2000
3000
4000
5000

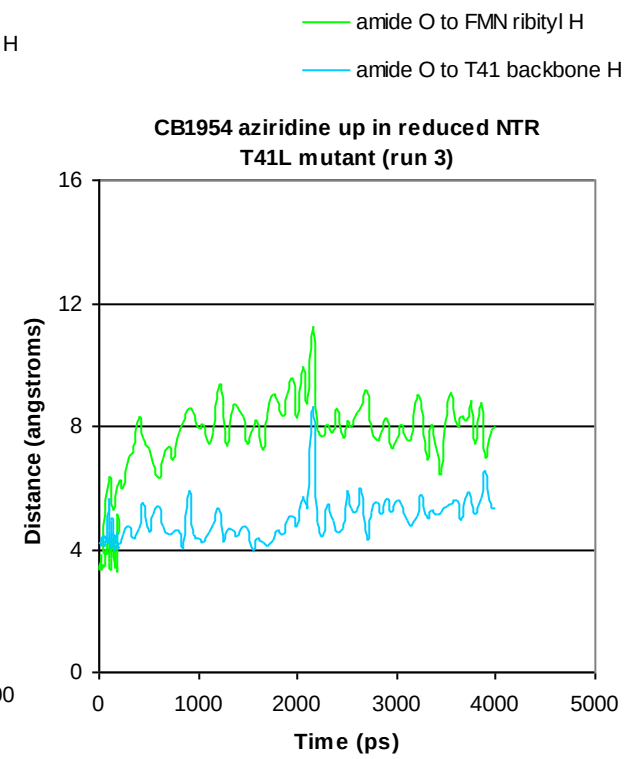
amide O to FMN ribityl H
amide O to T41 backbone H
CB1954 aziridine up in reduced NTR
T41L mutant (run 3)
Distance (angstroms)
Time (ps)
0
4
8
12
16
0
1000
2000
3000
4000
5000

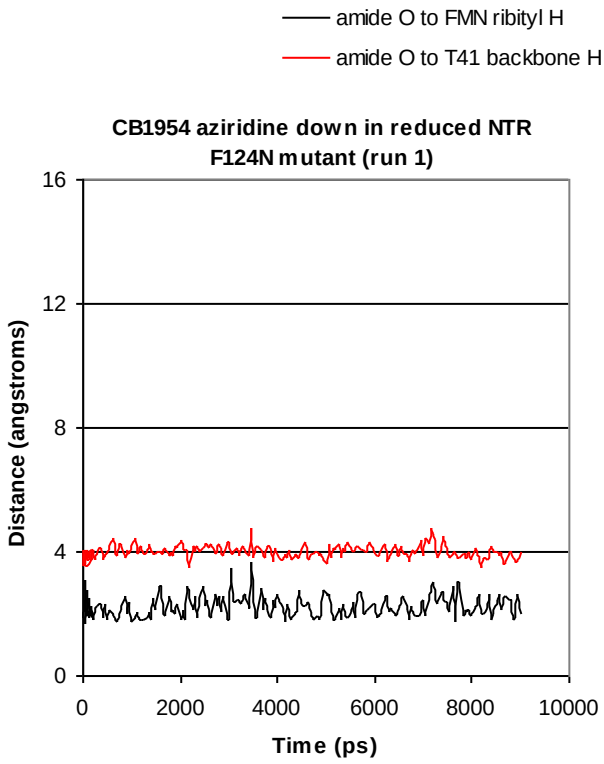
amide O to FMN ribityl H
amide O to T41 backbone H
CB1954 aziridine down in reduced NTR
F124N mutant (run 1)
Distance (angstroms)
Time (ps)
0
4
8
12
16
0
2000
4000
6000
8000
10000

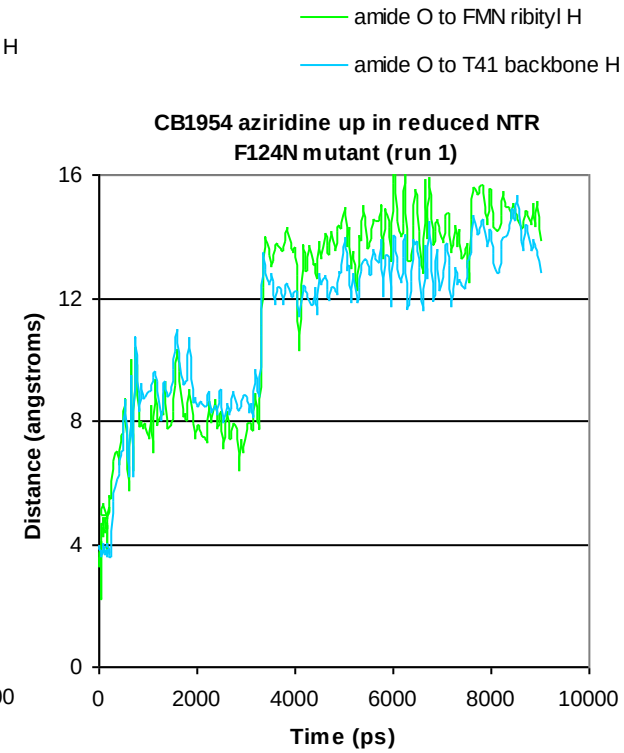
amide O to FMN ribityl H
amide O to T41 backbone H
CB1954 aziridine up in reduced NTR
F124N mutant (run 1)
Distance (angstroms)
Time (ps)
0
4
8
12
16
0
2000
4000
6000
8000
10000

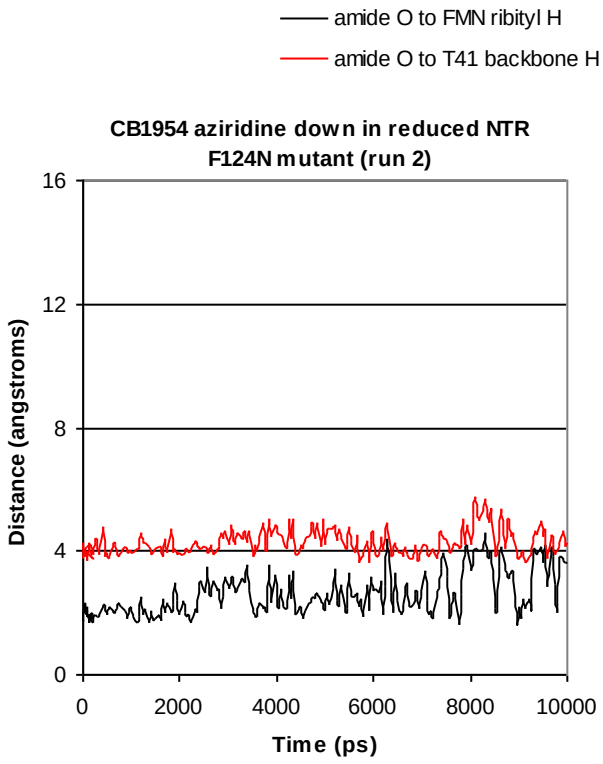
amide O to FMN ribityl H
amide O to T41 backbone H
CB1954 aziridine down in reduced NTR
F124N mutant (run 2)
Distance (angstroms)
Time (ps)
0
4
8
12
16
0
2000
4000
6000
8000
10000

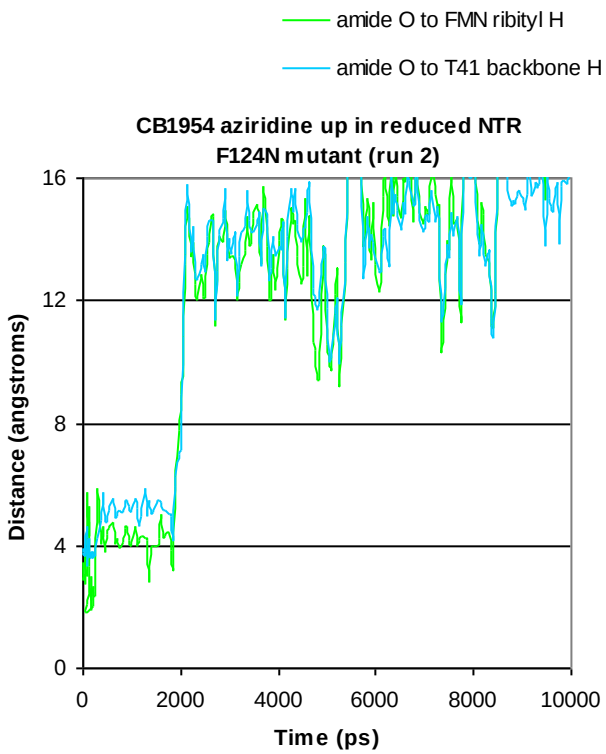
amide O to FMN ribityl H
amide O to T41 backbone H
CB1954 aziridine up in reduced NTR
F124N mutant (run 2)
Distance (angstroms)
Time (ps)
0
4
8
12
16
0
2000
4000
6000
8000
10000

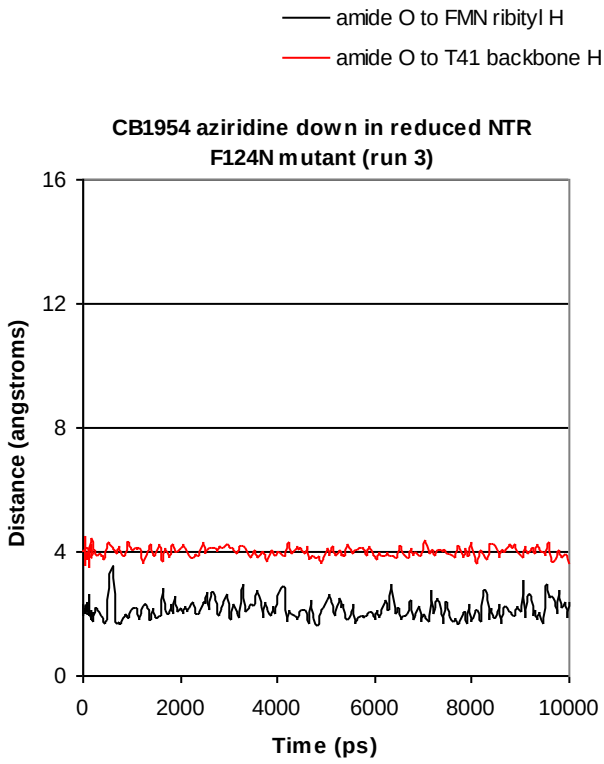
amide O to FMN ribityl H
amide O to T41 backbone H
CB1954 aziridine down in reduced NTR
F124N mutant (run 3)
Distance (angstroms)
Time (ps)
0
4
8
12
16
0
2000
4000
6000
8000
10000

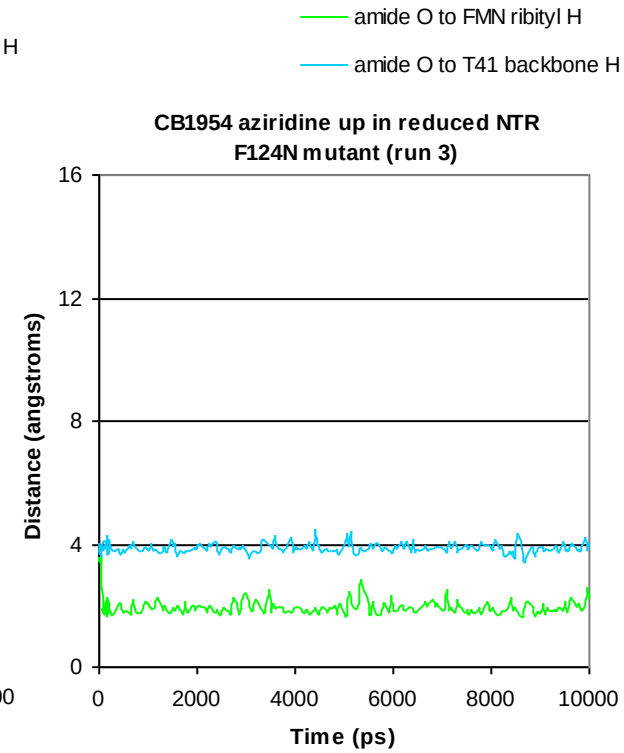
amide O to FMN ribityl H
amide O to T41 backbone H
CB1954 aziridine up in reduced NTR
F124N mutant (run 3)
Distance (angstroms)
Time (ps)
0
4
8
12
16
0
2000
4000
6000
8000
10000

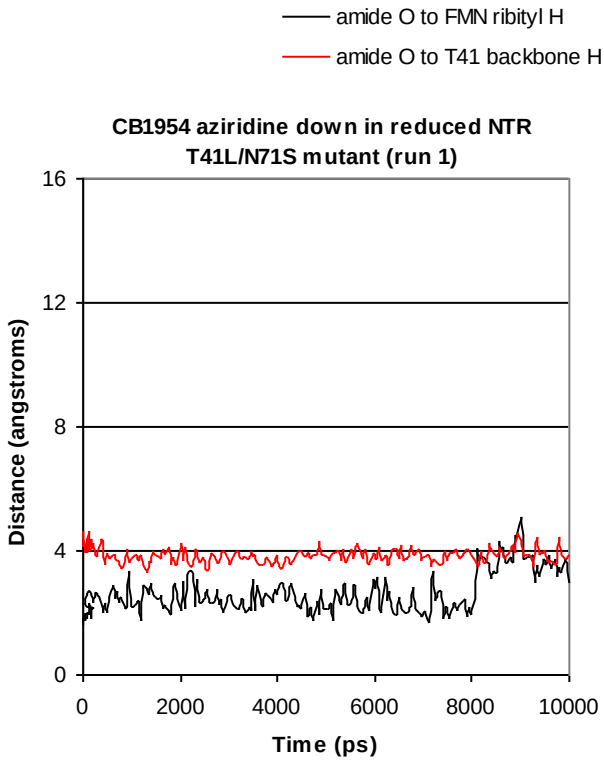
amide O to FMN ribityl H
amide O to T41 backbone H
CB1954 aziridine down in reduced NTR
T41L/N71S mutant (run 1)
Distance (angstroms)
Time (ps)
0
4
8
12
16
0
2000
4000
6000
8000
10000

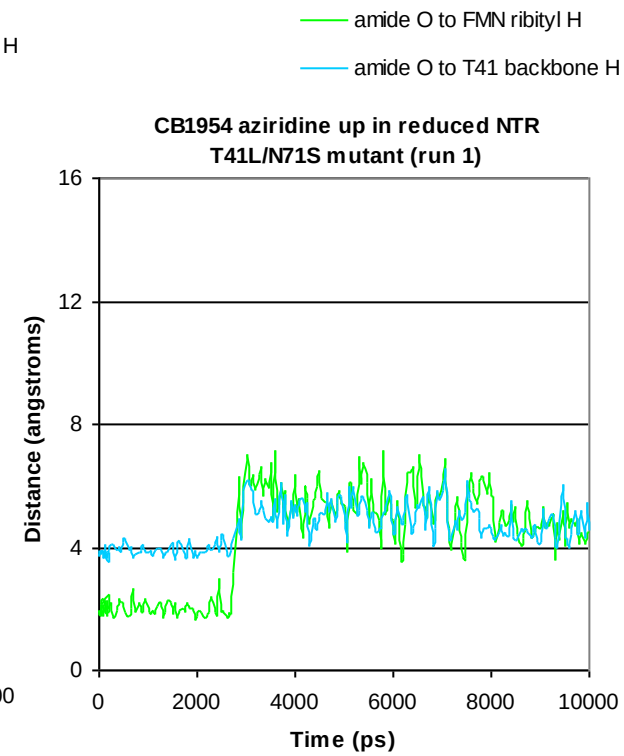
amide O to FMN ribityl H
amide O to T41 backbone H
CB1954 aziridine up in reduced NTR
T41L/N71S mutant (run 1)
Distance (angstroms)
Time (ps)
0
4
8
12
16
0
2000
4000
6000
8000
10000

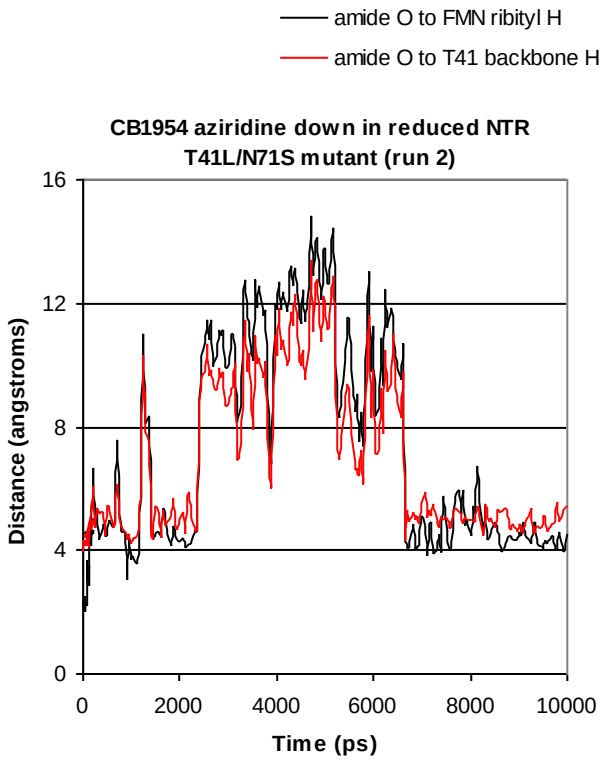
amide O to FMN ribityl H
amide O to T41 backbone H
CB1954 aziridine down in reduced NTR
T41L/N71S mutant (run 2)
Distance (angstroms)
Time (ps)
0
4
8
12
16
0
2000
4000
6000
8000
10000

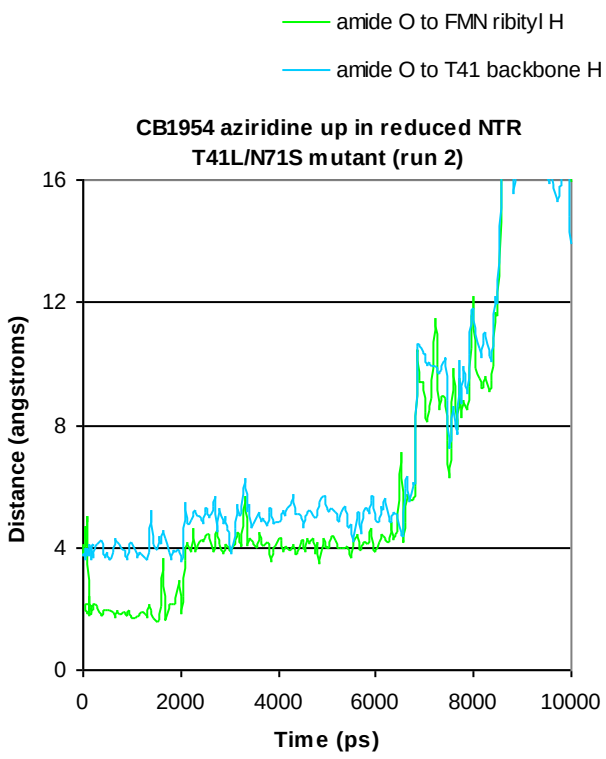
amide O to FMN ribityl H
amide O to T41 backbone H
CB1954 aziridine up in reduced NTR
T41L/N71S mutant (run 2)
Distance (angstroms)
Time (ps)
0
4
8
12
16
0
2000
4000
6000
8000
10000

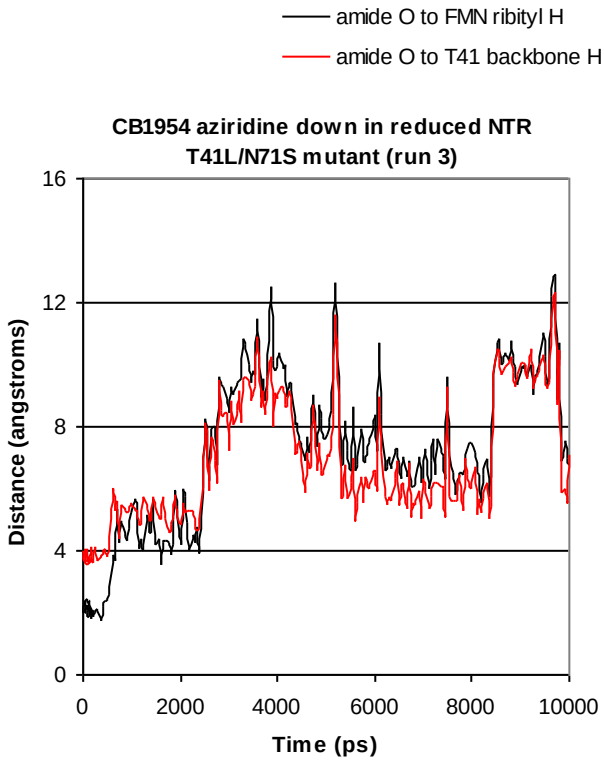
amide O to FMN ribityl H
amide O to T41 backbone H
CB1954 aziridine down in reduced NTR
T41L/N71S mutant (run 3)
Distance (angstroms)
Time (ps)
0
4
8
12
16
0
2000
4000
6000
8000
10000

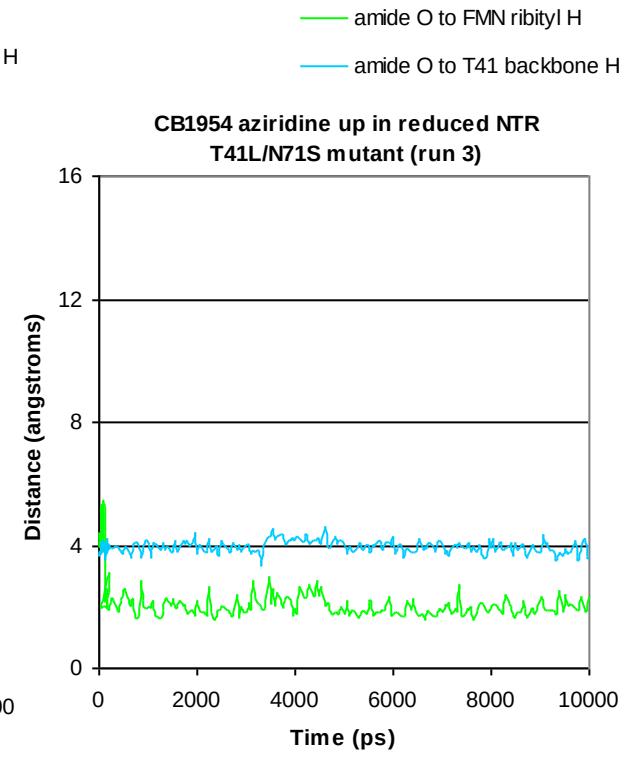
amide O to FMN ribityl H
amide O to T41 backbone H
CB1954 aziridine up in reduced NTR
T41L/N71S mutant (run 3)
Distance (angstroms)
Time (ps)
0
4
8
12
16
0
2000
4000
6000
8000
10000

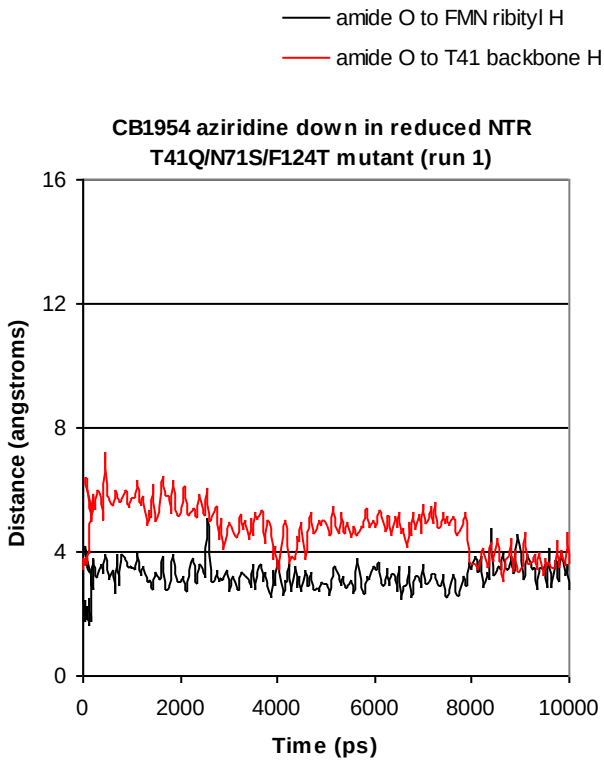
amide O to FMN ribityl H
amide O to T41 backbone H
CB1954 aziridine down in reduced NTR
T41Q/N71S/F124T mutant (run 1)
Distance (angstroms)
Time (ps)
0
4
8
12
16
0
2000
4000
6000
8000
10000

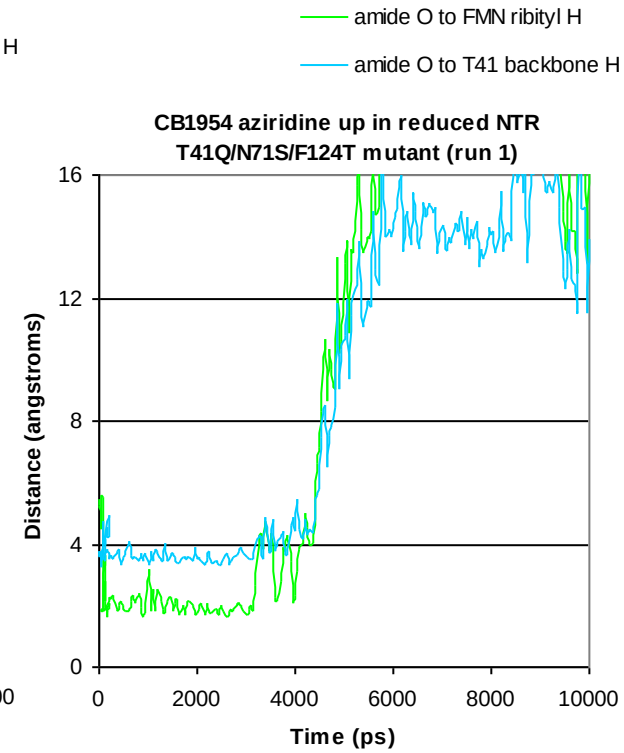
amide O to FMN ribityl H
amide O to T41 backbone H
CB1954 aziridine up in reduced NTR
T41Q/N71S/F124T mutant (run 1)
Distance (angstroms)
Time (ps)
0
4
8
12
16
0
2000
4000
6000
8000
10000

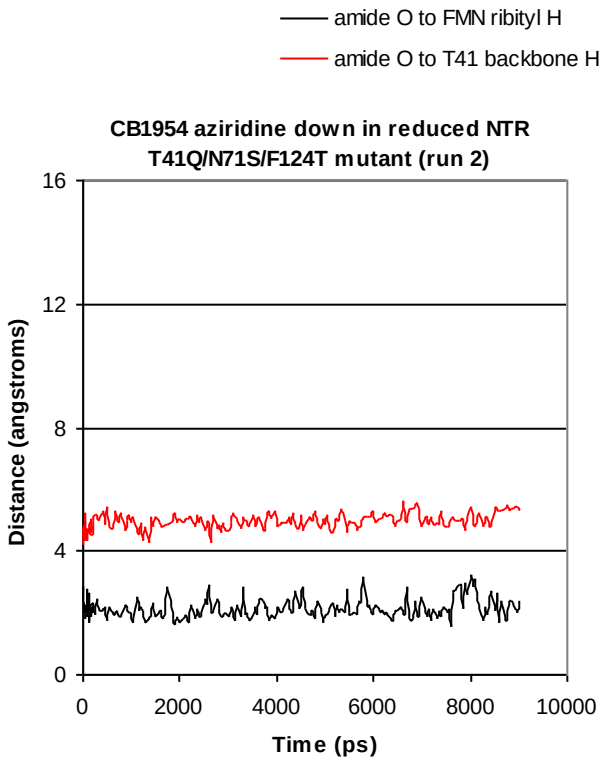
amide O to FMN ribityl H
amide O to T41 backbone H
CB1954 aziridine down in reduced NTR
T41Q/N71S/F124T mutant (run 2)
Distance (angstroms)
Time (ps)
0
4
8
12
16
0
2000
4000
6000
8000
10000

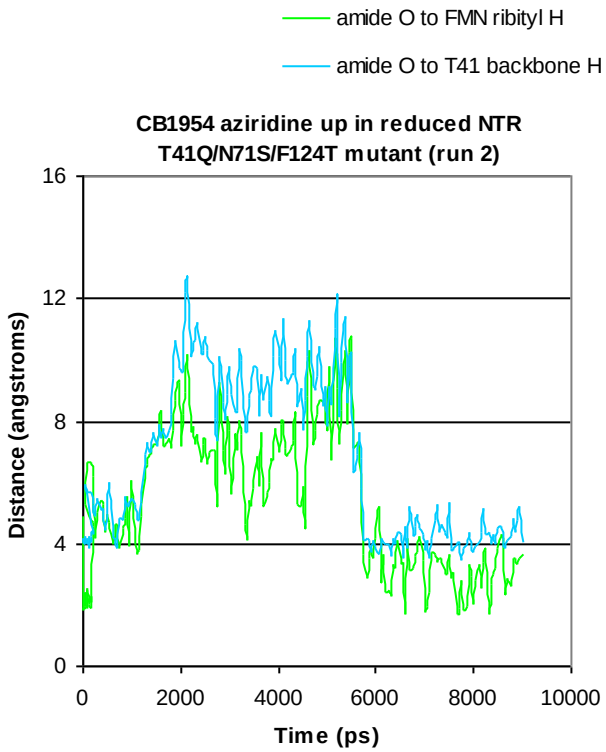
amide O to FMN ribityl H
amide O to T41 backbone H
CB1954 aziridine up in reduced NTR
T41Q/N71S/F124T mutant (run 2)
Distance (angstroms)
Time (ps)
0
4
8
12
16
0
2000
4000
6000
8000
10000

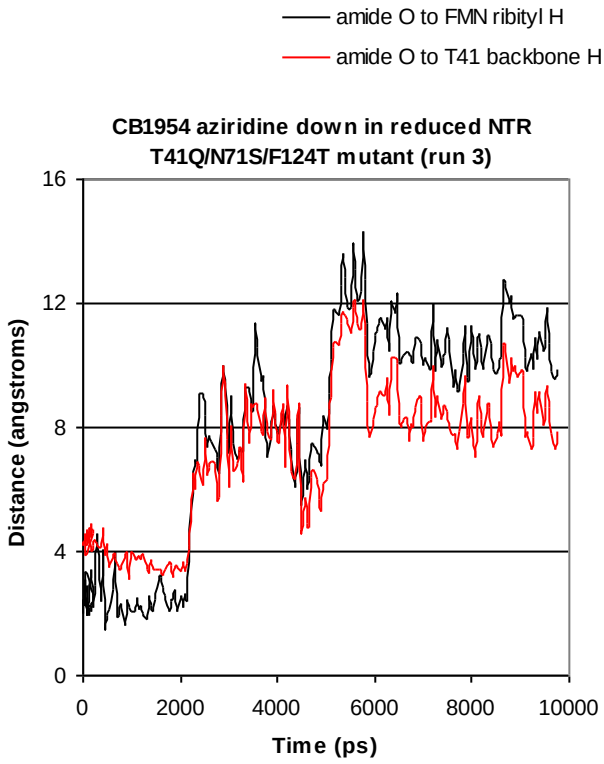
amide O to FMN ribityl H
amide O to T41 backbone H
CB1954 aziridine down in reduced NTR
T41Q/N71S/F124T mutant (run 3)
Distance (angstroms)
Time (ps)
0
4
8
12
16
0
2000
4000
6000
8000
10000

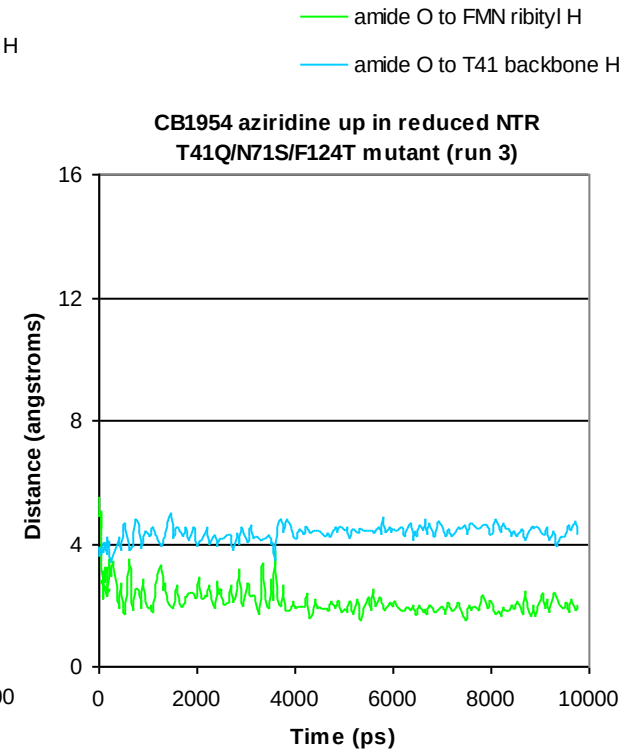
amide O to FMN ribityl H
amide O to T41 backbone H
CB1954 aziridine up in reduced NTR
T41Q/N71S/F124T mutant (run 3)
Distance (angstroms)
Time (ps)
0
4
8
12
16
0
2000
4000
6000
8000
10000

Appendix D

Mechanism of CB1954 reduction by *Escherichia coli* nitroreductase

Andrew Christofferson and John Wilkie

School of Chemistry, University of Birmingham, Edgbaston,

Birmingham B15 2TT, U.K.

Biochemical Society Transactions. (2009) 37, 413–418;

doi:10.1042/BST0370413